L-AMINO ACID BASED POLYESTER NANOCARRIERS FOR DRUG DELIVERY AND BIOIMAGING

A THESIS

SUBMITTED IN PARTIAL FULFILMENT OF THE REQUIREMENTS

OF THE DEGREE OF

DOCTOR OF PHILOSOPHY

BY

SONASHREE

Registration Number: 20123203

DEPARTMENT OF CHEMISTRY

INDIAN INSTITUTE OF SCIENCE EDUCATION AND RESEARCH (IISER), PUNE

PUNE 411 008, MAHARASTRA, INDIA

SEPTEMBER 2018

Dedicated to

My Mother

Dr. Kumudini

Who lives forever and ever

in our hearts...

भारतीय विज्ञान शिक्षा एवं अनुसंधान संस्थान पुणे
INDIAN INSTITUTE OF SCIENCE EDUCATION AND RESEARCH PUNE
(An Autonomous Institution of Ministry of Human Resource Development, Govt. of India)
Dr. Homi Bhabha Road, Pune - 411 008.

Prof. Manickam Jayakannan
Department of Chemistry

CERTIFICATE

Certified that the work done in the thesis entitled "***L-Amino acid Based Polyester Nanocarriers for Drug Delivery and Bioimaging***" submitted by ***Ms. Sonashree*** was carried out by the candidate under my supervision. The work presented here or any part of it has not been included in any other thesis submitted previously for the award of any degree or diploma from any other University or Institution.

Date: 18th September 2018
Pune, Maharashtra, India

Professor M. Jayakannan
(Thesis Supervisor)
18/9/2018

DECLARATION

I declare that this written submission corresponds to my ideas in my own words and where ever others' ideas have been taken account of; I have sufficiently cited and referenced the original sources. I declare that I have adhered to all principles of scientific honesty and integrity and have not misrepresented or fabricated or falsified any idea/data/fact/source in my submission. I understand that violation of the above will be cause for disciplinary action by the institute and can also evoke penal action from the sources which have thus not been properly cited or from whom proper permission has not been taken when needed.

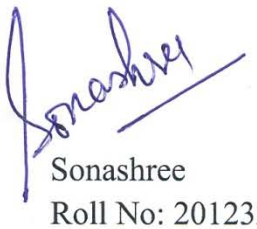

Date: 18th September 2018
Pune, Maharashtra, India

Sonashree
Roll No: 20123202

ACKNOWLEDGEMENTS

The tenure of my PhD would not have been possible without exclusive help and support of my supervisor **Prof. M. Jayakannan**. I would like to acknowledge him and thank him with great gratitude for his insights, exceptional suggestions, scientific discussions, constant encouragement, and faith and support to me during the tenure of my PhD. He helped shape the overall direction of my thesis and my research work. He always entertained my ideas and gave insights to me to think more scientifically and trained me into a better scientist. Discussions with him always generated energy and kept alive my passion for science. I faced difficulties in my PhD, but he always stood right next to me and smiling at the difficulties transformed me into more confident person who could face the challenges. Worth to mention he always had faith and gave me liberty to work on brain storming ideas and encouraged me to do same. I always tell him, that he is a very good supervisor who takes pain to mould all his students into capable scientists and I am fortunate enough to have worked with him for five years.

I would like to thank **Dr. S. Britto** and **Dr. Prakash Wadgaokar**, my research advisory committee (RAC) members and offered me valuable comments during RAC meetings, which made me realise shortcomings of work and make necessary improvements. I am extremely thankful to **HC** for giving me access instruments and culture room facilities.

I would like to express my sincere thanks to **Prof. K. N. Ganesh**, Former Director, IISER-Pune for providing world class research facility at IISER Pune carrying out this research work and **Prof. J. Udgaonkar,** current director for taking forward this institute to newer heights.

I am grateful to **Dr. Asha, S. K.** for her constant support and for extending research facilities in her laboratory.

I would like to thank all the faculty members in the Department of Chemistry, and Department of Biology, IISER Pune for interactive scientific discussions and teaching me various chemistry and biology courses.

Special thanks to my present and former lab mates for their support and cooperation which made my life memorable at IISER, Pune especially, Dr. Smita, Dr. Ananthraj, Dr. Pramod, Dr. Narsimha, Dr. Rajendra, Dr. Bapu Rao, my collegues Bhagyashree (and Sparsh), Nilesh, Mehak, Vikash, Thameez, Maithreyi, Lipi, Khushboo, Shraddha, Nithish, Hemlatha, Sharda, Mishika, Rasika, Khuddoos, Dheeraj, Ruma, Sharaffudin, Anu, Swetha, Caroline, Rekha, Nagesh, Chinmay, Shekar, Nisha, Senthil, Saibal, Prajitha, Swapnil, Sandeep, Moumita, and Sarabhjot .

Special thanks should be extended to **Mehak**, Nilesh and Anu for their support, help and beyond words contribution in my life.

I take this occasion to say my earnest thanks to Siddhi Inchankar for providing me experimental hands-on-training on different aspects of cell culture methods and MTT assays. I owe gratitude to **Dr. Nagaraj Subramaniam**.

I would like to thank all instruments' technicians of IISER Pune for their support: Pooja, Deepali (NMR), Swati (MALDI), Neetha (HRMS), Megha (AFM), Anil, Yatish (FE-SEM) and Vijay (CLSM). I thank National Chemical Laboratory (NCL) Pune for HR TEM.

I would like to thank many friends for providing an inspiring and fun filled environment in IISER Pune, and also the ones who walked the path of life and inspired me to start this beautiful journey and they are: Alisha, Yamini, Jyoti, Nishtha, Sudeshna, Lopa, Arya, Kalyanashish, Yashwant, Reman, Avdooth, Aditi, Hrithik, and all the IISM players in IISER. Other friends from outside IISER community for their unending support: Gautami, Simran, Nitin **T2**, Manish, Utkarsh, Ashish, specially Shilpi, Bonkita, Darshana, Vijay, Rohit Kumar, Benny, Saurabh Luthra, Raj Kumar Da, Vaibhav Durga,. I want take opportunity to thank my mentors Vikram Dutt, Kumar Abhishek Sir who inspired me to dream big and imbibed faith in life and created a beautiful outlook to life. I would like to thank from deep within Dr. Venkat Pachangula who has inspired me to heights that even I couldn't think of and in believing in me beyond. I would also like to thank my tennis partners Meenakshi and Shubham who made tennis much more than a game to me. I also thank all the staff members in administration, finance, accounts, stores, library, canteen (MDP CHAI) especially, Ms. Naina, Mr. Mayuresh, Mr. Tushar for their immediate help whenever I needed them. I thank

Dr. Amit Gupta, my husband, as my parterner in crime, and having shared the beautiful imagination of science and for being influential in my zeal for sceince.

I would like to acknowledge from deep within my heart and soul my mother **Dr. Kumudini**, without whom I wouldn't have been here and typing this. She was my mentor, my guru, my parents, my family and she meant the world to me and she taught me the meaning of self and self existence being a scholar herself. And there are no words to thank her for raising me and I would want to thank her by letting her know that I love her and always believed in her and would always cherish this life she has given me. To let her know she lives on forever in my thoughts and my heart. My sister, **Monika** who is reflection of my mother, has been a crucial person in the journey of my life, and is utmost important to me and I thank her for being their in my difficult times.She loves me beyond all the limits and has always supported me even when things are low. She is intelligent and organised and highly dependable person in actual times of need. She has been a source of inspiration to me since childhood and shall always remain close to me.

Financial support from IISER Pune and DST SERB is greatly acknowledged.

Sonashree

Synopsis

Design and development of multipurpose polymer nano-assemblies is an important area of research for delivering anticancer drugs and genes to improve the efficacies in cancer treatment. L-Amino acid based synthetic polypeptides and their well defined di- and tri-block copolymers were extensively explored for the above applications. In the last one decade, significant effort has been taken to design non-peptide polymer analogues for biomedical application owing to their structural diversity, biocompatibility and biodegradability. This thesis work is aimed to explore new classes of amphiphilic and biodegradable polyester and their fluorescent nano-assemblies based on natural L-aspartic acid resources for accomplishing anticancer drug delivery and intracellular bioimaging in cancer cells.

The thesis is divided into five chapters and their details are as follows:

Chapter-1: This introduction chapter provides the details on the importance of polymer nano-assemblies for drug delivery application, the literature update on the L-amino acid polymer nano-carriers, structural design aspects of the non-peptide polymer nano-carriers, and emphasize the need for the development of amphiphilic polyester with respect to the context of this thesis work.

Chapter 2: New classes of enzyme and pH responsive amphiphilic polyester based on L-aspartic acid was designed and developed through thermo-selective melt trans-esterification polymerization process. The amphiphilic polymers were self-assembled into nano-carriers and their multiple drug delivering capabilities were investigated in detail.

Chapter 3: π-Conjugate fluorophore-tagged amphiphilic L-aspatic acid polyester nano-assemblies were tailor-made using polymerizable oligo-phenylenevinylene (OPV) derivatives and their blue fluorescent nano-assemblies were explored for the construction of biodegradable FRET probe. The action of FRET probe was studied in details by photophysical techniques and their in vitro live cell bio-imaging was demonstrated in cervical and breast cancer cell lines.

Chapter 4: Aggregation induced emission (AIE) concept was introduced in the L-aspartic acid polymer nano-carriers by incorporating tetraphenylethylene (TPE) in the amphiphilic polyester backbone and the resultant blue-luminescent TPE-tagged nano-carriers were employed as multi-colour tunable FRET bio-probes from blue-to-green-to-red colour.

Chapter 5: New classes of hydroxyl and carboxylic functionalized polyesters were cleverly designed in L-aspartic acid polymer system for loading as well as delivering of anticancer drug as well as conjugating cisplatin drug in single polymer platform. TPE-tagged fluorescent nano-assemblies were also explored to build new theranostic FRET probe for simultaneous drug delivery and bio-imaging.

In chapter 2, L-aspartic acid resource was converted into multi-functional monomer and it was polymerized under melt conditions in the presence of hydrophilic and hydrophobic diols to yield amphiphilic copolymers. These polymers were designed in order to possess inbuilt

pH responsive BOC urethane hanging groups and esterase-responsive ester backbone making them dual stimuli containing amphiphilic polyesters. The BOC urethanes underwent cleavage and transformation into cationic moieties NH_3^+ in the highly acidic endosomal compartments of the intracellular regions (***trigger 1***). The ester containing backbone was susceptible to cleave under the presence of esterase enzyme present in the hydrolytic enzyme rich lysosomes which acts as the (**trigger-2**). Three different therapeutically active drugs curcumin (CUR), doxorubicin (DOX), and topotecan (TPT) were loaded into the polymer scaffolds and their cytotoxicity were studied in breast cancer (MCF 7) and cervical (HeLa) cancer cell lines. The uptake of these drugs was monitored using confocal microscopy.

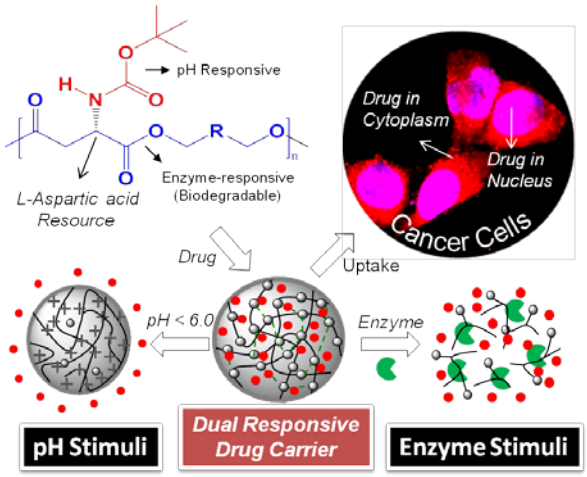

In chapter 3, L-amino acid based amphiphilic luminescent polyester was developed using π-conjugate luminescent materials and their FRET (fluorescence resonance energy transfer) probes for colour-tunable intracellular imaging were demonstrated. Highly luminescent oligo-phenylenevinylene (OPV) with π-conjugated cores were tailor made into melt polymerisable diols and were subjected to thermo-selective melt trans-esterification polymerization with modified multi-functional L-aspartic acid monomers along with hydrophilic triethylene glycols and hydrophobic dodecanediol to yield OPV-labelled luminescent amphiphilic polyesters. Comprehensive photo-physical analyses exhibited that the OPV and NR (a hydrophobic encapsulated dye) were constricted within close proximity and aligned at apt geometry within the nano-domains of polymer micelles for highly efficient excited energy transfer from OPV excited state to NR ground state. The OPV tagged nascent polymer nanoparticles and OPV-NR FRET probes were tested for their cytotoxicity in normal cell lines (wild-type MEF, WT-MEF), and cancer cells {breast cancer (MCF 7), cervical cancer (HeLa) cells} and were found to be biocompatible. The cellular uptake studies of these nanoparticles revealed that luminescent polymers and the FRET probes could be transported efficiently across the cell membrane and these could accumulate within the cytoplasm of the cells. Live cell imaging experiments manifested the co-localisation of donor and acceptor molecules in the lysosomal compartments of the cells which was supported by lyso-trackers, which provided direct evidence for endocytotic pathway as the mode of entry of these nanoparticles. The enzymes

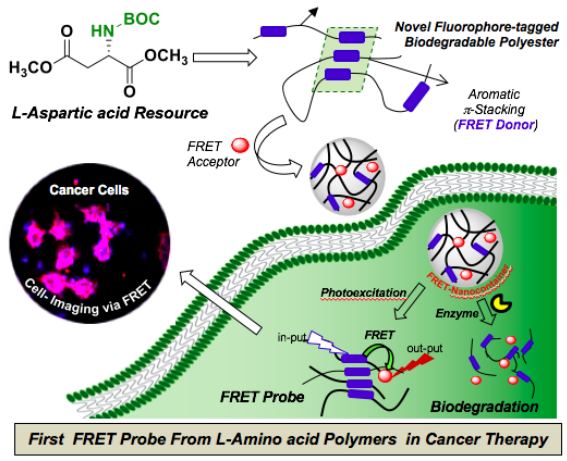

found in lysosomes of the cells such as esterase, chymotrypsin, trypsin, and GSH reducing agents were employed to study the bio-degradability of the polymeric micelles and were found to be efficient in degrading the polymers.

In chapter 4, aggregation induced emission (AIE) chromophore tagged L-amino acid based biodegradable polyester have been designed and their fluorescent nano-scaffolds were explored as multi-colour tunable FRET nano-probe for bio-imaging in cancer cells. AIE capable hydroxyl functionalized tetra-phenylethyelene (TPE) diol was tailor-made through multi-step reaction and it was subjected to melt transesterification with L-aspartic acid monomer to yield new blue-luminescent amphiphilic polyesters. These AIE polyesters self assembled into compact spherical nanoparticles and they were found to be capable of encapsulating water insoluble red-fluorophore Nile red (NR) and green-fluorophore drug Curcumin (CUR). Two FRET probes TPE-NR and TPE-CUR were constructed in the TPE conjugated polymer nano-system as donor and CUR and NR as acceptors. Third FRET probe was build between CUR-NR using non-TPE amphiphilic polyester scaffolds. Confocal and live cell imaging experiments threw light on the accumulation of these nanoparticles in the cytoplasm of the cells and demonstration of FRET within the cell lines showed the stability of the nanoparticles during the efficient uptake into the cells. The cleavage of these nanoparticles in the presence of lysosomal enzymes were demonstrated by using various enzymes and the FRET as probe was used to study the bio-degradation of these nanoparticles in *in vitro* experiments.

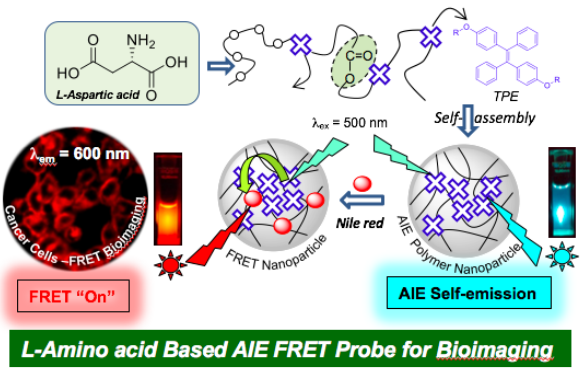

In chapter 5, enzyme-responsive hydroxyl and carboxylic acid dual functional polyesters were synthesized from natural L-amino acid residues. L-Aspartic acid was converted into di-ester functional monomer containing acetal protecting amine groups. The methyl esters of the aspartic acid monomer under-went melt trans-esterification with dodecane diols, an aliphatic hydrophobic di-functional alcohol to produce high molecular weight polyesters. The hydroxyl functionalised polyesters were synthesised by acid assisted deprotection of the acetal groups in each repeating units of the polymer. The free hydroxyl groups were further converted into carboxylic functional groups by ring opening of succinic anhydride. The hydrophilic hydroxyl and carboxylic groups along with the hydrophobic aliphatic backbone made these polymer amphiphilic in nature and enabled these to self-assemble into spherical nanoparticles in water. Successful and high amount of DOX loading was achieved and the cellular uptake

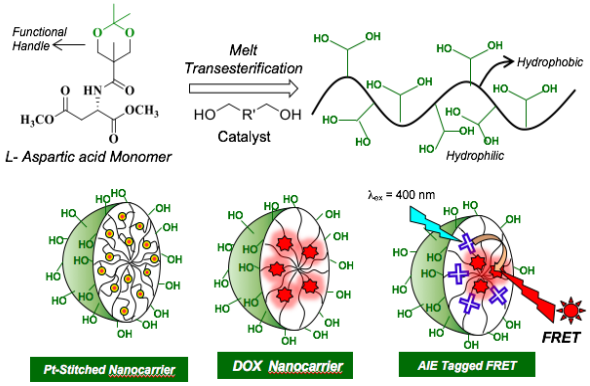

and killing were demonstrated in MCF 7 cells. The carboxylic polymers were further covalently stitched to a second anticancer drug cisplatin and their killing was demonstrated in the cancer cells. These polyesters were further tailor-made into AIE active polymers by introducing custom designed tetraphenylethene units in the backbone during melt condensation process making these polymers nanoscaffolds luminescent in nature. The DOX loaded AIE active polymers were used to demonstrate FRET at the cellular level where aggregated TPE acted as donor and DOX acted as an acceptor.

The last chapter summarizes the thesis work and put forward the direction for future research. The new classes of amphiphilic polyesters designed and developed based on L-aspartic acid residues in the thesis are new entries as enzymatic-biodegradable polymers in the literature; hence they would be expected to be very important nano-carriers for long-term application in the biomedical field. Further, the custom designed OPV-tagged and TPE-tagged fluorescent polymers are excellent nano-scaffolds for constructing wide range of FRET probes with drugs and fluorophores which could be employed for early diagnostics of cancer and other bio-imaging applications. Thus, the work described in the thesis opens up new platform of opportunities in biomaterials arena based on L-Amino acid polymers.

TABLE OF CONTENTS

Chapter 1

Introduction

1.1 Nano-carriers in Drug Delivery

Cancer is one of the leading causes of mortality all over the world and early detection and identification of cancer has only been able to extend the life of organisms. When the normal cells start dividing and growing uncontrollably, they stop dying and form cancerous cells. Some of these cancer cells form solid tumours (unlike leukemia which is blood cancer) and are difficult to treat. For the past few decades the most commonly used procedures to combat cancer include i) surgical removal of solid tumours, ii) chemotherapy aided radiotherapy, iii) hormonal therapy, iv) radiation (X-ray) therapy, v) adjuvant therapy (concomitant use of chemicals and surgery), vi) immunotherapy etc. However, the disease has not yet been fully understood and it's treatment now demands superior remedies which includes anti-angiogenic chemotherapy, advanced targeted treatments, nanotechnology, RNA expression profiling and proteomics etc.[1] Chemotherapeutic agents are mostly organic molecule drugs or large protein enzymes which often causes kink or cut to DNA chains present in nucleus and damage the cell. The ability to target therapeutics inside the complex and highly dynamic network of cellular machinery in multicellular organism is a challenging task. Some of these chemicals or enzymes alternatively cause cell death by interfering with essential pathways inside the cell network crucial for cell functioning. The metabolites needed for cell growth and cell functioning are also targeted by certain drug molecules called as anti-metabolites. Such organic drug molecules and enzyme molecules are often employed as active or passive therapeutic agents against cancer and related diseases. However, the poor bio-availability of free drugs administered to living organisms concomitant with decreased accessibility towards cancer cells generates major unwanted fate i.e. undesirable targeting of normal cells over cancer cells. The consequences of these outcomes include severe side effects of the organism such as low immunity, hair loss, nausea, reduced appetite etc. It's worth to mention that these form 'the immediate side-effects' on the organisms followed by major psychological traumas in long term faced by the patients. One of most common way increase bioavailability of drugs is that these anticancer agents are loaded in self assembled nanoparticles to cause desirable effects which can be developed and organised into aspiring assemblies. These drug loaded nanoparticles manifests advanced pharmacokinetics and pharmaco-dynamics

compared to their free loaded drugs because they provide better control over active intracellular delivery and protection of the loaded drug from the plasma conditions.

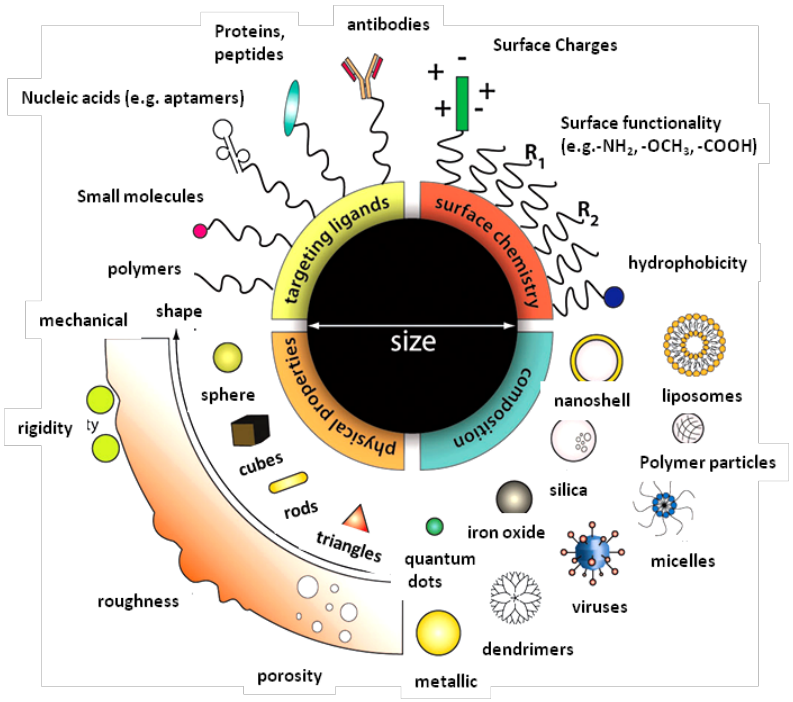

Figure 1.1: *Various nanoparticles known for bio-medical applications. (Adapted from Chou et al. Chem Soc. Rev.* **2011**, *40*,233-245*)*

The nanoparticles provide an edge over conventional drug carriers as these can be applied for molecular and cellular labelling and tracking, diagnosis, drug delivery, precise medical bio-imaging.[2,3] Nanoparticles are developed carefully keeping in mind the properties of drug meant for delivery (see figure 1.1). Highly hydrophobic drugs such as adriamycin, cisplatin, docetaxel, etoposide have been successfully stabilised in hydrophobic cavities of nano-scaffolds. The delivery of hydrophilic drugs on the other hand faces challenges due to limited options for loading water soluble drugs as well as elevated loss of drug molecules due to high solubility in blood. Nano-vesicles play major role in loading and delivering hydrophilic drugs such as: doxorubicin HCl, gemcitabine, L-asparginase etc, at target site. Therapeutic agents based on DNA and siRNA/miRNA are rather stabilised by cationic polymers or systems for efficient loading and formation of nanoparticles [4]. Cationic nano-hydrogels *PEO-cl-PEI* (crosslinked poly(ethylene oxide) and polyethyleneimine) were employed for immobilizing and delivery of retinoic acid, indomethacin, and

oiligonucleotides etc to cells.[5] Tumour marker mediated drug release has been performed by silica nanoparticles of size 100 nm for delivery of DOX to HL-60 and LO2 cells with efficient killing. [6] Therefore, the choice of chemical systems capable of forming nanoparticles highly depends upon the drug for delivering in question. PEGylated liposomal doxorubicin (Doxil/Caelyx), liposomal daunorubicin (daunoXome) and Abraxane (albumin- paclitexal conjugate) are the three FDA approved nanomedicines that have shown lower toxicity and better efficacy compared to the drugs alone against cancer [7]. Liposomes (LD: Liposomal doxorubicin and Myocet) are one of the first therapeutic nanoparticles approved for clinical trials for drug delivery.[8] The efficacy of the chemotherapeutic agents however are trimmed down due to various reasons including lack of appropriate drug delivery vehicles, the scarce targeted delivery (causing poor bio-availability), undesirable side effects to normal cells (due to non-specificity, example cardio diseases etc), and multi drug resistance acquired by cancer cells during several phases of drug administration, lack of large scale production of such nanoparticles, lack of well defined chemistry to built such nanoparticles[9] etc. Research and development of drug delivery vehicles are being carried out to subjugate these short comings of therapeutics drugs.

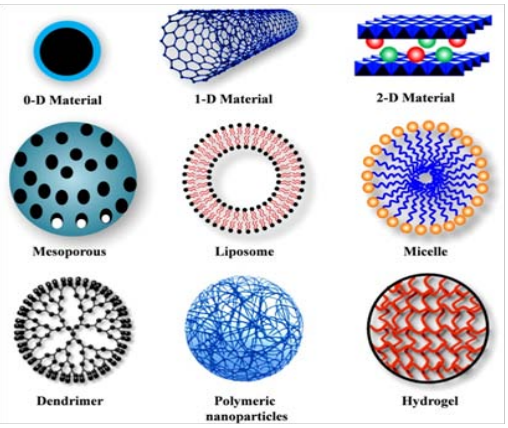

Figure 1.2: *Various nanoparticle structures employed for Drug delivery applications. (Adapted from Senapati et al, Signal Transduct and Targeted Ther. (2018) 3:7 and* Abdalla et al, *Theranostics* **2018**, *8*, 533-549*).*

Nano-technology is one of the most widely used science that has also been explored and studied for carrying out efficient drug delivery at cellular levels in living

organisms showing higher circulation periods in organism and reduced toxicity[9]. Nano-therapy comprises of advanced delivery of chemotherapeutic agents such as small molecule drugs, short length peptides, long chain proteins, lipids, synthetic polymers, and nucleic acid, metal, metal oxides etc which find potential role in combat against diseases like cancer [2,10,11]. The nanoparticle based therapeutics of various sizes from 1-1000 nm like polymer-drug conjugates, liposomes, albumin based nano-carriers, PLA nanoparticles, polymer based nanoparticles etc have been proposed for treatment of cancer.[1] A variety of structures from nano-materials have been made for developing stable nano-carriers for drug delivery applications including hydrogels, carbon nanotubes, mesoporous silica nanoparticles[6], quantum dots, hydrogels, polymeric micelles, polymeric vesicles, lipid nanoparticles, lipo proteins, plant virus nanoparticles (figure 1.2). The underlining strategies used in developing these materials involve their careful designing capable of undergoing self assembly into stable nano-carriers keeping the loaded cargoes intact till the point of delivery. Amongst the very first nano-carriers are liposome based nano-vescicles which are comprised of bilayer membranes and have been used in treatment of various diseases such as HIV-related Kaposi's sarcoma (FDA approved Doxil), fungal infections (liposomal amphotericin). The advantage of using liposomal drug-carriers lies in the versatility of encapsulating both hydrophilic and hydrophobic drugs, as a consequence of which, a vast span of anticancer drugs could be used for loading and delivery purposes [12]. Nanoparticle based cancer therapy provides a platform for enhanced tumoural delivery of water insoluble drugs, long circulation time, site specific targeted delivery, transfer of drug through epithelial and endothelial membrane barriers [12], enhanced delivery of large drug molecules, systematic delivery of more than one drugs to target site, bio-imaging of intracellular regions [13], reduce immunogenicity of drugs [12], early detection of cancerous tissues, etc [13]. A precise control of size of nanoparticles for therapeutics is an essential aspect which influences the pharmacokinetics, bio-distribution, accumulation and penetration in the tumour tissue [9,14,15].

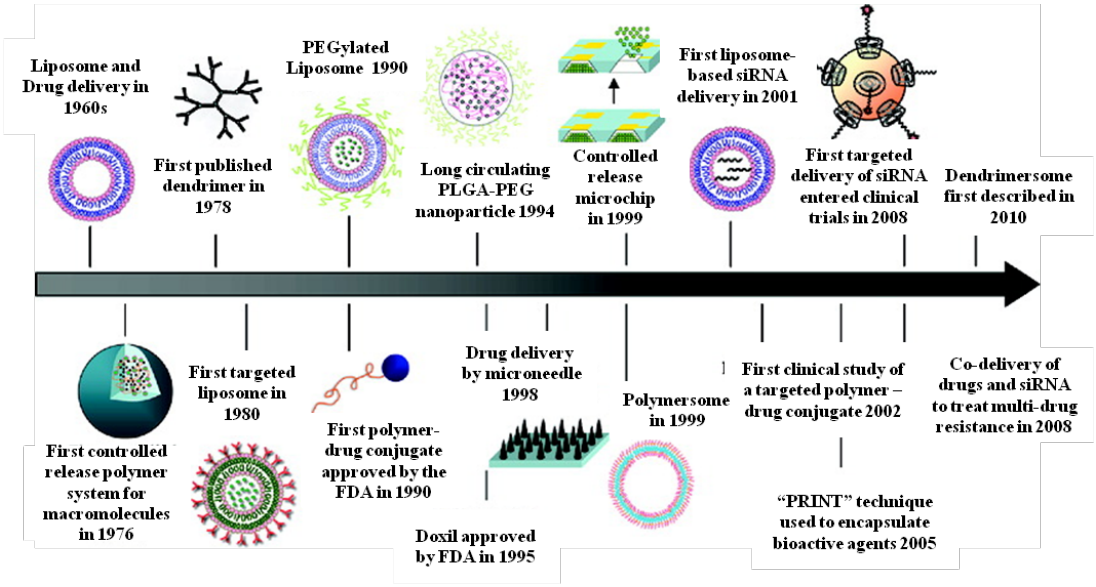

Figure 1.3*: A timeline showing various nano-particle based delivery systems as important milestones of history (figure adapted from Shi et al, Nano Lett.* **2010***, 10,* 3223-3230*).*

The Abraxane, nab paclitaxel and ABI-007 are one of the most prominent sub nano-meter sized FDA approved albumin-bound drug composites successfully used for treatment of metastatic breast cancer [16,17]. PEG modified proteins have been found to be an interesting class of nanoparticles having higher retention in blood and enhanced efficacy than free drugs [18]. For example, PEG based nanoparticles; Pegaspargase was proven to be highly efficient anti-leukemic chemotherapeutic agent [19]. Various classes of nano-materials used for drug delivery were engineered to develop high ordered structures for drug delivery purposes as shown in figure 1.3 [20]. In a nutshell, nanoparticles provide a platform for drug delivery vehicles that can be modified into better designs by tuning the chemistry behind their development and knowledge of more clinical data could further enhance the optimisation of nanoparticle structures as future medicine for drug delivery. However, having explored a huge number of nanoparticles that are finding their way to high standards of research and development yet unfortunately only 0.7 % of known nanoparticles are found to be effective in reaching the solid tumour and causing collateral damage to cancer tissue [21]. The individual profiling of patients with aid of genomic and proteomic informations of individuals have been proposed as future in medicines and targeetting proangiogenic signalling pathways and this form of advanced nano-

therapy has been quoted to bring a reform in the field of medicines and are anticipated to play a major role in enhanced efficacy [22,23].

1.2 Enhanced Permeability and Retention Effect (EPR Effect)

The enhanced permeability and retention effect (EPR effect) is related to the hyper permeability of cancer vasculature over normal cells which allow particles of size < 500 nm to extravasate passively from blood circulation and lead to accumulation in tumour vasculature. The tumour vasculature is known to be permeable by large sized molecules compared to normal vasculature [7]. This is due to an imbalance between the growth of tumour under uncontrolled pro-angiogenic signalling and the anti-angiogenic signalling [23] which renders the tumour vasculature immature and leaky in nature [7]. The resultant large intracellular aperture is created within the endothelial cells causing development of poor support (impaired pericytes) in the tumour vasculature [7]. The physical forces like pressure in the intracellular region in the tumour are high due to nearly collapsing intratumoural lymphatics. However, the clearance of the molecules occurs from the tumour environment at a sluggish rate. [7]

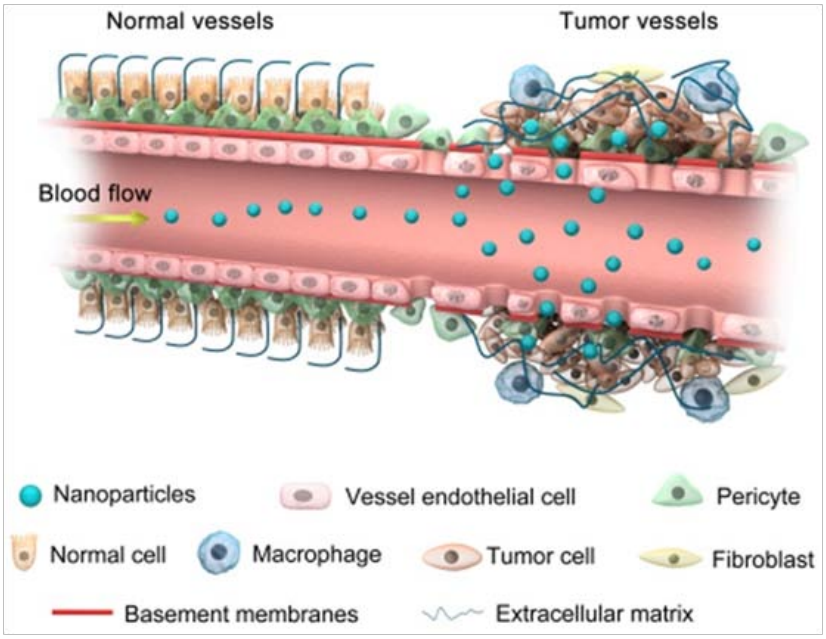

Figure 1.4: *Schematic representation of EPR effect (figure adapted from* Abdalla et al, *Theranostics* **2018**, *8*, 533-549).

EPR effect was one of the historic events in the field of cancer research and therapeutics and led to FDA approval of major anticancer drugs based on liposomal nano-particles such as Doxil[7,9] and daunorubicin[24] etc. Accumulation of an anticancer protein, neocarzinostatin, was studied in normal and tumour bearing mice by conjugating it to macromolecules of various chain lengths and these nanoparticles were found to accumulate more in the tumour induced sites of xenografted mice model compared to the normal tissues [25]. It is believed that the endothelial cells along the blood passage are loosely bound at the site of tumour growth and the endothelial cells at normal tissues on the other hand are highly intact and well ordered such that only small small molecules can diffuse through these to the internal organs. The loosely bound endothelial cells therfore offer free passage of the nanoparticles of large size into the highly complex growing tumour tissues which causes a gradient of large sized molecules accumulated at the tumour tissue sites. This offers a non-selective passive accumulation of nanoparticles at cancer sites due to the above mentioned leaky and poorly developed tumour vasculature. Tumour tissues also lack well define lymphatic drainage system which leads to the accumulation of nanoparticles for longer duration leads to poor clearance of the nanoparticles from the cancer tissue from lymphatic system [25, 26, 27] ,which adds the advantage of retention of the nanoparticles in the cancerous tissue regions. The high accumulation of drugs into tumour tissues and the retention due to dysfunctional lymphatic drainage gives rise to the “enhanced permeability and retention” effect (see figure 1.4)[7]. Having stated the role EPR in uptake and retention of annaopatrilces it is worth to consider that small sized particles undergo excretion via kidney from blood circulations and large sized particles are evaded by the macrophage phagocytic system (MPS) (also called reticulo-endothelial system (RES)) (figure 1.5).The MPS is a web of various organs of the body mostly liver and spleen which work together by targeting foreign particles through their phagocytotic cells network and cause the excretion of any object smaller than 5.5 nm in diameter via renal i.e., kidney system[20]. Therefore, a trade off is used to develop optimum sized nanoparticles that stay in the blood circulation overcoming these hurdles and are eventually taken up by the tumour tissues (this has been discussed in detail in section size of the nanoparticles). The bio-distribution of any nanoparticles used for bio-medical applications is one of the

underlying information required to begin to understand the mechanism of action by any therapeutic agents [28]. The RES system built on macrophages cells at liver and spleen organs forms the underlining principle behind bio-distribution studies of nanoparticles in animal models wherein prefential accumulation of nanoparticles in liver and spleen gives insight on the clearance of the nanoparticles by RES system. Experiments involved in understanding the fate of intravenously injected nanoparticles often include : i) hyper-vasculature of the tumour, ii) the presence of nanoparticles in the tumour vasculature, iii) low recovery of nanoparticles from the blood serum and iv) from the lymphatic system, which provides indirect information about uptake of the nanoparticles into the system.[26,27,28]

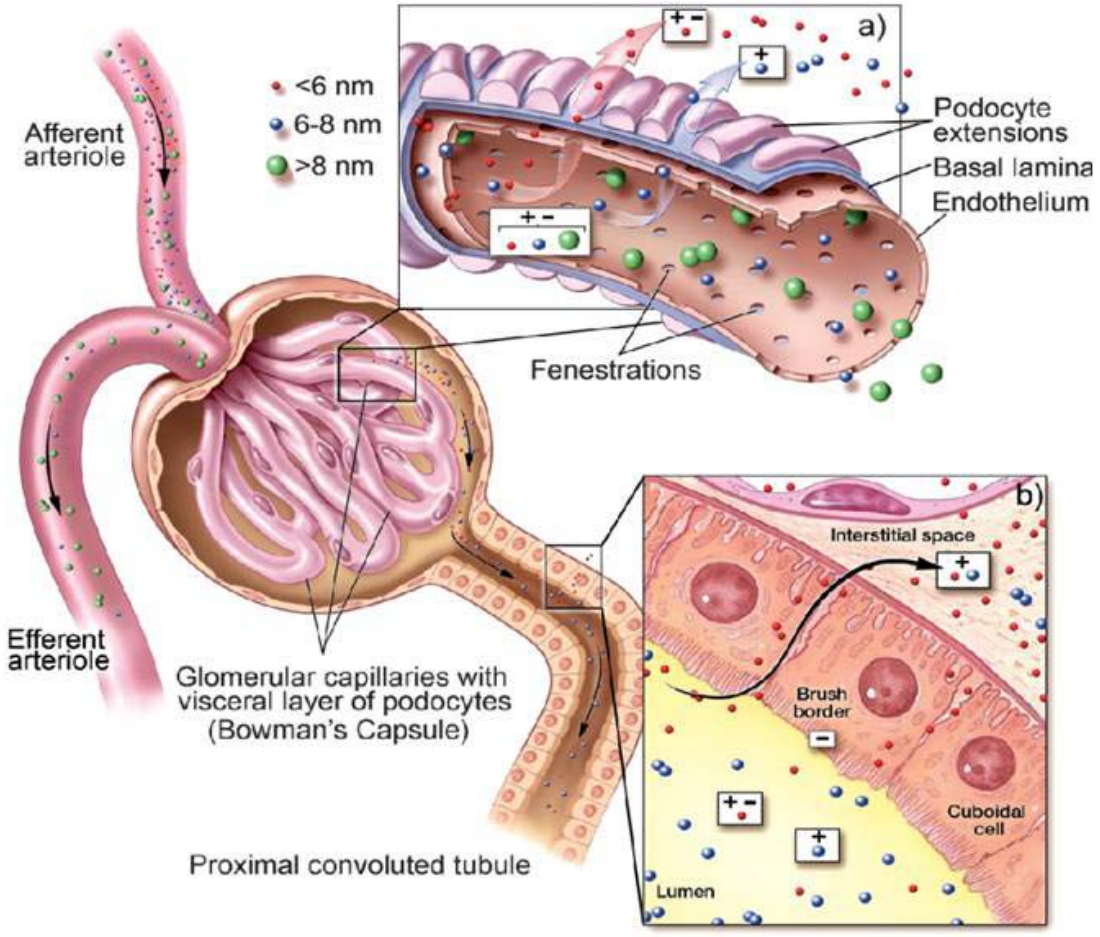

Figure 1.5*: Renal clearance of various sized nanoparticles from glomerular capillary wall of phagocytotic pore size <5nm showing phenomenon of renal clearance. (Figure adapted from Sun et al, Angew. Chem. Int. Ed.* **2014**, *53*, 12320-12364).

The EPR effect is one of the most sought passive approaches found behind designing of the nanoparticles for the drug delivery and has been known in general to accumulate macromolecules 20-30% higher compared to small molecular weight agents.[28] The size and shape of nano-therapeutics plays a vital role in their bio-distributions in living organisms and affects the action of killing.[29,30] The fate of nanoparticles injected intravenously is best described based on their mechanism of transport in the living systems. Having understood the EPR effect one must look towards the ideal characteristics nanoparticles must exhibit in order to act as successful drug delivery carrier. An assortment of nanoparticles encounter various fates upon injecting intravenously (shown in the figure 1.6) and are described as : i) particles larger than 5-7 nm trap and accumulate mostly in small capillaries of lungs; ii) particles of size around 4-5 nm are engulfed by phagocytic cells of RES of organs such as liver, spleen and lungs; iii) the particles less than sub-micrometer range (<500 nm) in size have been known to accumulate in tumour tissues via EPR effect and iv) even smaller sized carbon nano-tubes, Q-dots, gold nanoparticles were known to cross the tight endothelial junctions and are found to clear rapidly through kidneys[29].

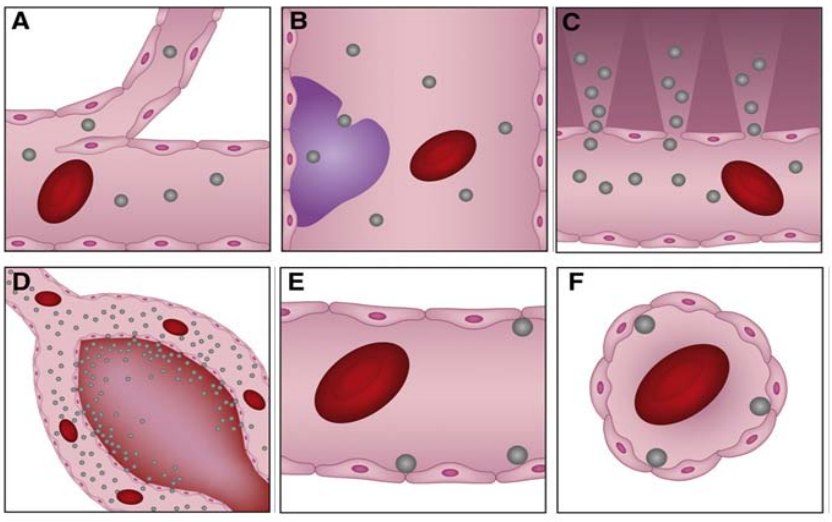

Figure 1.6: *Segregation of intravenously injected nanoparticles from the circulating blood trapped in small blood capillaries A), taken up by phagocytic cells B), extravasation through porous endothelial cell wall C), excretion from the kidneys D), E) , blood vessel wall adhesion F).*(Figure adapted from: P. Decuzzi et al. *J. Control. Release* **2010**,*141*, 320-327).

Apart from size, the charge on nanoparticles also affects their fate in living organism. For example, neutral and slightly negatively charged, sub-150 nm sized nanoparticles were mobile within the tumour tissues[31] and on the other hand cyclodextrin based polycation of size 50-100 nm with slight positive charge demonstrated deeper penetration in tumour [32] in animal model. Therefore optimisation of size of a nanoparticle with careful selection of charge on them becomes essential qualification for use as therapeutic agent. Material architecture plays a crucial role in efficacy of drug carrier and delivery, as it determines the folding and packing of the materials into various nano-shapes capable of loading a range of drugs etc. The drug ballasting, drug conjugating, drug release profiles etc can be tuned into single nanoparticles by engineering the material for use. Various polymer architectures including linear polymers, branched polymers, cross linked, dendrimers; hyperbranched polymers etc have been employed for the same applications [33]. A plethora of intra-vascularly injectable particles of various shapes like classical spherical to discoidal, cylindrical, hemispherical and conical etc were proposed for diagnostic and therapeutic purposes for treating diseases [29]. Julie et al. have reported the phagocytosis of polystyrene particles macrophages like continuous alveolar rat macrophage cells NR8383 [34].

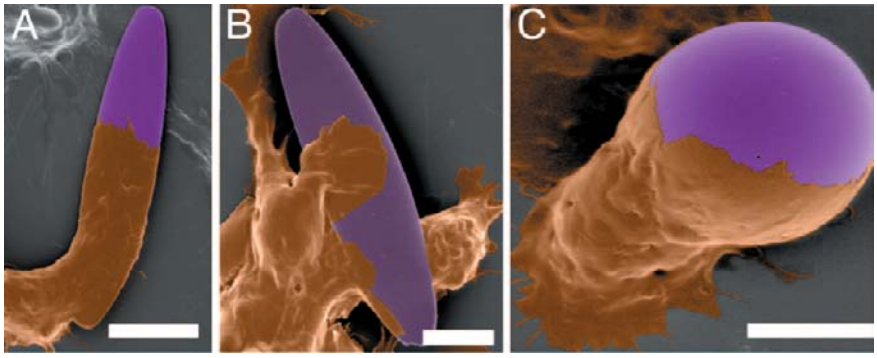

Figure 1.7: *The scanning electron micrographs and actin filaments stained time lapse vedio microscopy of polystyrene nanoparticles A) oval shaped nanoparticles interacting along the major axis B) oval shaped nanoparticles interacting along the lateral axis and C) uptake of a spherical nanoparticle into the macrophages. (Scale Bar: 10 μm).* (Picture adapted from Julie et al. *PNAS*, **2006**, *13*, 4930-4934.)

The polystyrene particles were modified into oval and spherical shaped nanoparticles and their uptake into the cells were monitored using time lapse video microscopy imaging. It was observed that the nanoparticles which hit the cells along their major axis were taken up by the cells within 3 min, however, the same

nanoparticles when came in contact with the cells along their minor axis were not taken up by the cells even up to 38 min. The spherical nanoparticles on the other hand being uniform in shape from all sides could be taken up effortlessly by the macrophages and has been shown in figure 1.7 c. Figure 1.7 shows that since the point of contact is uniform in case of spherical nanoparticles therefore they were taken up in < 6 mins into the cells characterised by actin polymerisation which is first step towards uptake of the particles into the cells[34]. P. Decuzzi et al. have reported a detailed analysis of uptake of silica spheres of various sizes (0.7 -5.0 μm) and non spherical particles (discoidal, cylindrical, and quasi-hemispherical) by subjecting them to nude mice after inducing tumour in them using MDA-MB-231 breast cancer cells. The bio-distribution of these particles was studied by analysing the silica content in various organs of the mice. It was observed that while discoidal particles were found to accumulate more (4 fold of spherical and 8 fold of cylindrical and quasi-hemispherical) in lungs. The cylindrical particles accumulated more in the liver (2 folds that of spherical & quasi-hemispherical; and 5 folds higher than discoidal particles). Discoidal particles also found their way into heart more than other particles, and discoidal along with quasi-hemispherical were found to accumulate more in spleen. The kidneys, brain and tumour were found to have lower amount of these particles (1.0 % overall) which reflected on poor uptake of these large sized particles. Clearly, the shape of the nanoparticles affects their fate of accumulation in the various parts of the mice system [29]. These data presented could form rationale behind designing of particle size and shape for desired applications.

1.3 Polymer Nano-carriers for Drug Delivery

Use of nano-structures architected into water soluble materials improves the bio-availability of drugs, improves their solubility, and reduces their toxicity [35]. Amongst many desirable features for drug delivery, a polymeric nanostructure offers: water solubility, low toxicity and low immune response, narrow poly-dispersity, and availability of multiple functional handles for drug conjugations [36]. The most essential advantage of a polymeric drug carrier and delivery system is the controlled release of drug to the target site. In order to act as an efficient drug carrier a nanoparticles has to strike a balance between clearance from the blood from the

organs such as kidney, liver, spleen, and the escaping and extravasation from the blood circulation and fenestrate through the wide gaps in the endothelial cells of the tumour tissues. Various structures have been summarised by Megan E Fox et al [37] and they have postulated the role of the structure on polymer nano-particle and these have been summarised in figure 1.8. They postulated that given the V_H (hydrodynamic Volume) similar for various polymers, the linear polymers can pass through the pores in the blood capillaries into the vasculature. A globular rigid structure needs to undergo shape deformation in order to pass pores (see figure 1.8 (b)). A cyclic polymer having no chain ends would also require shape transformation to enter pores; a rod like structure with similar dimensions would find it easier to pass through the pores if aligned precisely. And macromolecular structure originating from a centre or a core and protruding out via various chains would find their initial entry into the pores rapid, however the transport of the whole molecule through the pores maybe be time and energy dependent [37].

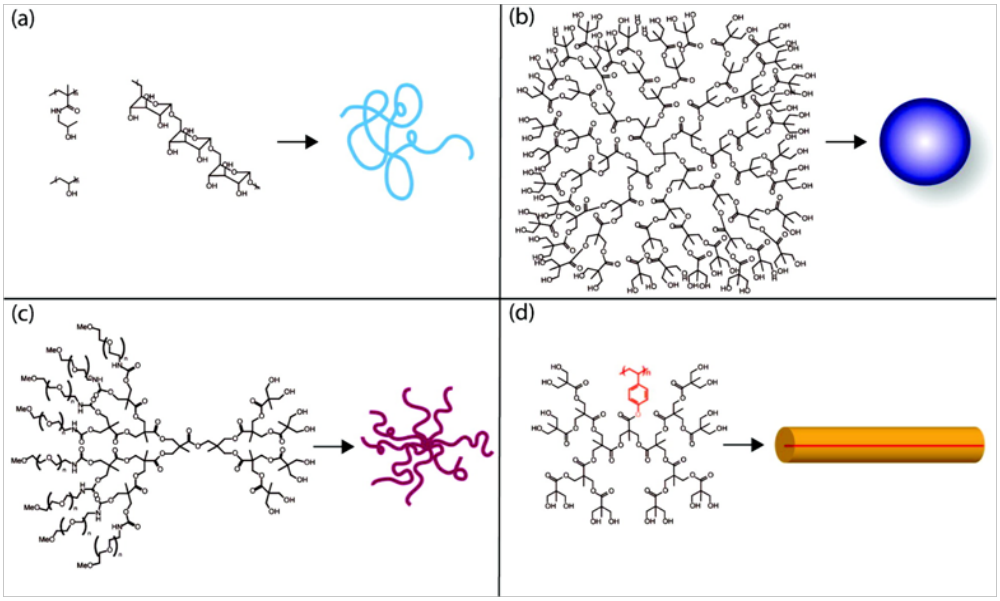

Figure 1.8: *Molecular conformations adopted by various macromolecular structures: linear (a), spherical (b), star-like (c), and rod-like (d). (Figure adopted Fox et al, Acc Chem Res.,* **2009**, *42,* 1141-1151*).*

Intelligent architectures were developed by Mariarosa Mazza et al. and demonstrated peptide epitopes tightly wrapped nanofibre core forming highly

advanced molecular structure which achieved high accumulation within the brain upon crossing the blood brain barrier [38]. Kai Li. et al have proposed the formation of Laponite Nanodisks for high loading (98.3%) and efficient delivery of doxorubicin to mice model with higher accumulation in tumour compared to free DOX, and had higher retention in the blood for 45 days which demonstrated the role of disk like nanoparticles in drug delivery [39]. A. G. Cheetham et al synthesised protein-drug conjugates from Tau-β-sheet proteins and CPT (camptothecin) drug and modulated the self assembled structure from fibres (23% CPT) to nanotubes (38 % CPT) and used these structure for drug delivery [40]. The effective drug delivery is based on precise combination of designing materials that can escape renal filtration, enhance blood accumulation, and uptake in higher amounts in the tumour tissues compared to healthy cells. The polydispersity of any polymer for developing nanocarriers should be low which brings in high reproducibility and helps in better control over pharmacokinetic behaviour of the polymer nanocariers [36].The size and structure of nanoparticles can be easily monitored and played with using polymer as underlining materials for developing these nanoparticles. An ideal polymer drug carrier should be able to clear from the system after it has released its loaded cargo at the desired place of action. Hydrophobic drugs that are ideally insoluble in water readily stabilize in the hydrophobic core of micelles and that is essentially desirable to load hydrophobic drugs [41].

Figure 1.9: *Polymeric micelles having hydrophobic core for loading hydrophobic guest molecules (a) (Schematic adapted from Sutton et al Pharm. Res.* **2007***, 24,* 1029-1046)*, Polymeric vescicle having hydrophilic watery core and hydrophobic layer for dual loading applications(b) (Schematic adapted from Meng et al, J. Phys. Chem. Lett.* **2011***, 2,* 1533-1539)*.*

In most of the copolymers the hydrophilic units are often provided by the polyethylene glycol units (PEG chains) of molecular weight 2-15kD. The hydrophilic portion of the amphiphilic polymers interacts with the aqueous surroundings and creates a tight shell around the hydrophobic core, thereby safe guarding the loaded cargo from the hydrolysis or enzymatic degradation abundant in aqueous environment. The advantages of using PEG as hydrophilic units include their water solubility, bio-compatibility, and reduction of electrostatic interactions with plasma proteins leading to drop in opsonisation and the clearance from the blood circulation [42]. Other hydrophilic polymers often used to impart water soluble segments to polymer include poly(N-isopropylacrylamide) (pNIPAM), and poly (N-vinyl pyrrolidone) PVP and examples of hydrophobic segments include hydrophobic polyesters, polypeptides, polyethers, poly (β-amino ester) etc[13,43] PEG-PPO-PEG is ternary copolymer named as pluronic made up of hydrophilic PEG and hydrophobic poly (propylene oxide), to yield amphiphilic polymers which self assemble into micelles where PPO forms the core while the PEG forms corona of the nanoparticles. Three polymeric micelles based on PEG have been reported which have been used in clinical trials and their clinical data are available. These are SP1049C (doxorubicin encapsulated Pluronic micelles), NK911 (doxorubicin encapsulated in micelles obtained from PEG and DOX conjugated poly (aspartic acid), and Genexol-PM (paclitexal encapsulated in PEG-PLA copolymer micelles) [9, 44, 45]. The pharmacokinetics of these drug loaded polymers were compared to that of the free drugs and it was observed that the half life of excretion of free DOX was 48 min whereas the SP1049C and NK911 increased the half life upto 45.9 h which was a predigious accomplishment in retention of doxorubicin within the system. This was due to prevention of opsonisation rendered due to the shealth effect of PEG chains to the nanoparticles. Liposomes are synthetic vescicles made up of biocompatible phospholipids and cholesterols used for delivery of cargoes specially gene delivery as these are known to possess bilayer like structure and these exhibit ability to pass through bilayers as well as cell membranes [3]. Vesicles or liposomes (liposomes are vesicles made up of lipid) are unique nano-scaffolds that are capable of loading hydrophobic as well as hydrophilic cargoes in their interiors. A vesicle is comprised of hydrophilic core surrounded by hydrophobic layer which is further protected by a

hydrophilic corona (see figure 1.9 (b))[46]. Liposomal drug delivery has been well employed for cancer therapy, because of extending the loading capabilities to hydrophilic drugs along with hydrophobic drugs (micelles can load only hydrophobic drugs) too, increasing the range of delivery of drugs for drug delivery applications. Other advantages of using vesicular liposomes are: their reduced size, better bio distribution and higher penetration into tumour tissues than free drugs etc. Liu and co-workers have reported multifunctional poly(ethylene oxide) (PEO) based vesicles constructed by using cetyl trimethyl ammonium bromide (CTAB)/sodium dodecyl benzene sulfonate surfactants (SDBS), fabricated via the electrospinning process. This vescicular system was demonstrated as dual anticancer model drug delivery system for hydrophilic 5-Fluorouracil and hydrophobic paeonolum [47]. PEG-liposome conjugated doxorubicin "Doxil" is approved in ovarian cancer and multiple myeloma and in treatment for sarcoma [10]. Tranferrin (Tf)-lipoplex have shown high efficiency delivery of tumor targeted *p53* gene, which is known to be involved in control of DNA-damage induced apoptosis. This liposome based non-viral drug carrier has been used in therapy for head, neck and prostate cancer in humans [48]. Other examples of liposomal nano-medicine approved by FDA are DaunoXome (Liposomal daunorubicin)[24], liposomal doxorubicin (Myocet)[49] and Mifamurtide (Mepact)[8] etc to name a few. Liposomal Cisplatin (Lipoplatin) [50], Thermo DOX[51], Liposomal Paclitaxel (EndoTAG-1)[52], and these are currently in various phases I, II, and III trials in cancer treatment.

1.4 Ligand targeted delivery

Apart from the rudimentary features of a nano-particle, they are decorated with specific cell targeting agents that are based on ligand receptor binding, which improvises the bio-distribution of nanoparticles in the living systems. The targeting of the nanoparticles can be either of passive nature or active nature. The passive targeting is the preferential accumulation of nanoparticles of certain sizes (50-200 nm) in cancer tissues compared to normal tissues and this effect has been discussed in detail in EPR effect [7]. The active targeting is more specific in nature and relies on the fact that certain receptors are over expressed on hastily growing cancer cells. Rapid proliferation in cancer cells is associated with high rate of metabolism which in turn

causes expression of various receptors on the cell surface depending on the biochemical properties of the surface of the cells, for example trasferrin, folate etc [30,36]. The strategy of targeting ligands relies on highly specific molecular recognition [20] and interactions between such ligands and their receptors. These receptors can bind to transferrin and folic acid ligands and this gives rise to a promising approach of engineering nanoparticles with these molecules [30, 36]. Nanoparticles are therefore engineered to modify their surfaces by attaching ligand which specifically bind to receptors over expressed in rapidly growing cancer cells (see figure 1.10)[53]. The potential of such nanoparticles as therapeutic agents are enhanced and these show promising reduction in side effects caused by conventional therapeutic agents [13].

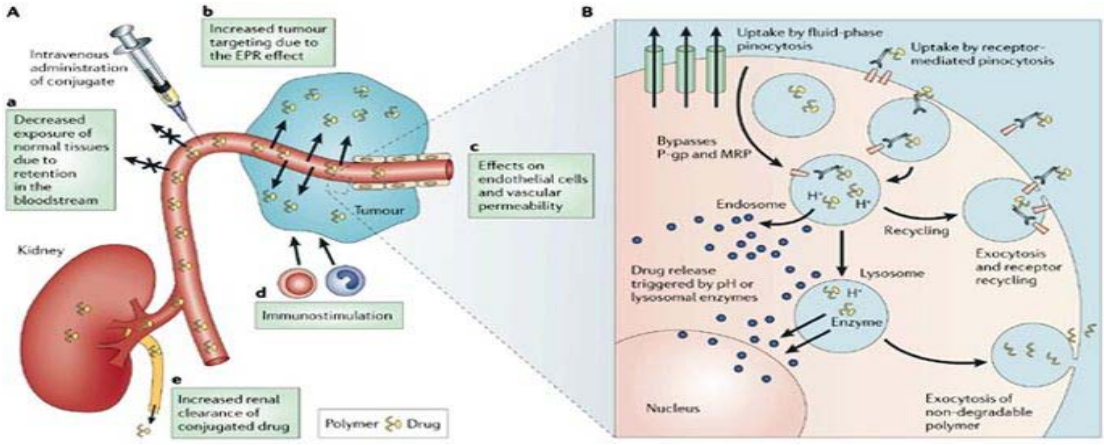

Figure 1.10: *Schematic representing various steps involved in receptor mediated targeted uptake of cells. (Figure adapted from Duncan etal, Nat.Rev.,* **2006**, *6,*688-700.

Eventually the ligand and receptor binding leads to endocytosis of the nanoparticles and this phenomenon is referred to as 'receptor mediated endocytosis' [54]. The major advantages of ligand assisted targeting of nanoparticles includes transcytosis of drugs across tight epithelial cells, and endothelial barriers such as blood brain barriers, and across the highly dense and complex network of solid tumour, overcoming mutli drug resistance (MDR), rendering long circulation periods to the nanoparticles, targeting the migrating cells in events of metastasis[13]. However, multi step synthesis involved in preparation of ligands, biomaterial self assembly, ligand conjugation, scalable manufacturing without batch to batch variations are few of the major disadvantages of receptor mediated targeting of nanoparticles [55]. Most importantly, the presence of

these receptors on other non specific cells cannot be ruled out, and therefore the toxicity caused by drug loaded nanoparticles or the askew toxicity are not completely eliminated. One of the ligand mediated polymeric nanoparticle which made it to the clinical trials is PK2 (FCE28069), a HPMA-polymer-Gly-Phe-Leu-Gly-DOX chemical conjugate containing galactosamine sugar which was used as target for the receptor asiaglycoprotein which is over expressed on hepatocytes of liver cells. Being expressed in normal hepatocytes too, the nanoparticles were found to be accumulated in normal tissue as well. However, in human trials it showed promising results [56]. Transferrin is known to be over expressed over many malignant cells due to severe requirement of iron for growth [57]. MBP-426 is a transferrin conjugated liposomal nanoaparticle used for delivery of cisplatin [9]. Monoclonal antibodies (mAB) are another class of targeting agents that are widely used as therapeutic agents, imaging materials and for radiotherapy applications in tumour. Prostate specific membrane antigen (PSMA) is a glycol protein selectively over expressed in all prostate cancers and nonprostatic tumourous neovasculature, in vascular endothelium of solid tumours (carcinoma and sarcoma) and not in normal vascular endothelium regions [58]. J591 antibody specific to PSMA were conjugated to dendrimers and were demonstrated as potential targeting agent for cellular internalisation [58]. Peptides are another class of targeting agents used for active targeting in cells, one of the most widely used being RGD peptide which have high molecular recognition toward integrin $\alpha_v\beta_3$ receptors overexpressed in human melanoma cells[59,60]. The multiple (24 mer) RGD ligands based Doxil delivery to mice model showed high affinity towards the neoplastic endothelial cells over expressed with $\alpha_v\beta_3$ receptors [61]. Phospholipid-anchored folate conjugates were used to target the folate receptor expressing tumours [62], activated macrophages [63], and has been used for delivery and bio-imaging applications. Very recently Jayakannan and co-workers developed biotin conjugated dextran based biodegradable nanoscaffoleds and showed their higher uptake in cancer cell lines [64]. Ligand conjugation has even enabled the organ specific targeting of nanocariers for delivery of loaded cargoes at specific organs in living organisms. Ligands comprising of cationic species triphenylphophonium moieties are very well known to target the mitochondrial surface in the cells [65, 66]. The nucleus targeting is a challenging task as the nucleus in eukaryotic cells are separated from cytosol via two membranes having

pores as small as 10 nm in size. Nucleoplasmin is the chemical entity often used for targeteing the nuclus in the cells [67, 68]. Poly-L-Lysine DNA conjugates have also been reported for nucleus specific delivery purposes [69]. The biocompatibility and quintessentially biodegradability of these nanostructures are desirable traits for use at clinical trials. The biodegradation of nano-scaffolds are unfortunately not addressed in majority of these scaffolds and it poses an elevated limitation to use of nano-vehicles for drug delivery purposes. Phenomenon such as pinocytosis and endocytosis are known to take up polymer nanocarriers into the cells and expose them to endosomal and lysosomal compartments where they face degradation. Certain non degradable polymers tend to accumulate inside the cell causing toxicity over a period of time [37]. The means of entry of nanoparticles inside the cells determine the efficacy of the polymer nanoparticles and can be analysed and used to engineering polymer designs to begin with. The most challenging task faced by any polymeric drug carrier is established on its ability to deliver the loaded cargo (like anti cancer drug or gene etc) to the region of interest. An ideal ligand targeted nanoparticle should have utmost specificity, and it should recognise in principle all the overexpressed receptors present on the cancer cells over normal cells [13].

1.5 Stimuli Responsive Polymers for drug delivery

The clatherin mediated endocytosis causes the nanoaprticle to end up in the lysosomal compartments of the cell. The lysosomes are abundaunt in hydrolytic enzymes and are highly acidic in nature and the nanoparticles are bound to degrade in such harsh conditions. An endosomal escape from the lysosomes is a must for nanoparticles to deliver the loaded cargoes to cytosol so that these can target mitochondria, nucleus etc. In the case of caveolin mediated endocytosis also the nanoparticles need to escape the endosomes before they are fused into lysosomes [30]. Macropinocytosis which is neither cavelion-mediated nor clatherin mediated endocytosis is an actin dependent process which is used for taking up of large molecules into the cells. These kinds of endocytosis are exploited by making use of cell penetrating peptides that are attached to the cells [30]. Apart from these it is noteworthy to address various dissimilarities in cancer and normal cells , for example i) high temperature of cancer tissues, ii) over-expression of reducing agents such as

GSH, iii) higher acidity of cancer tissues, iv) low oxygen content in the cancer tissues, v) over expression of receptors such as folic acid receptors, biotin receptors, peptides receptors, etc. The drugs molecules are linked to the polymeric systems via covalent bonds keeping the rationale behind the linkages that are affected or cleaved influenced by above mentioned dissimilarities, and these have been explained in details. The use of block copolymers having individual hydrophobic and hydrophilic segments offer an opportunity for these to self assemble into supra-molecular structures capable of loading hydrophobic drugs in their core via encapsulation. These polymers offer technological advancement in the area of drug delivery applications, as these are often imbibed with stimuli responsiveness with respect to internal cancer tissue regions. Improvising the drug carrier structure often the polymer molecules are engineered and developed having more than one stimulus so as to improve the efficacy of the drug delivery which occurs due to more systematic release of drug following controlled kinetics. The fine tuning of stimuli response in the polymeric structures offers a better control over release of drug and enhanced regulation of release profile of the drugs released. A polymer design strategy which included synthesis of self assembling amphiphilic polymers with stimuli responsiveness in built are sort after [70, 71].

pH responsive polymers

A marginal difference in pH exists between normal and cancerous cells, wherein the pH of a normal cell is around 7.4, the pH in the extracellular tumour region is found to be 6.5-7.2. The major reason for this difference arises due to fast rate and irregular angiogenesis in the uncontrollably growing tumour cells. Since the blood vessel in cancer tissue is not well developed there is a scarcity of nutrients as well oxygen in these tissues and thus cancer cells shifts towards glycolytic metabolism. Since the glycolytic metabolism creates acidic metabolites, there is a drop in the pH of tumour tissue environment causing it to be more acidic than the healthy tissues. The majorly used strategies for developing pH sensitive nancarriers for drug delivery include use ionisable acid or base containing polymers which can structurally change upon variaition in pH in surroundings or which shows difference in solubility in aqueous medium with change in pH. Also incorporating acid sensitive chemical linkages within the polymer scaffold or conjugating drugs or fluorophores

with similar chemical linkages can help in release of the loaded cargoes once the scaffolds reach the acidic tumour site [72]. Warbug effect also explains the development of acidic conditions at tumour sites due to formation of lactic acid as a by product of insufficient consumption of glucose molecules [73]. Acid cleavable or labile bonds such as imines bonds and hydrazones linkages are used to bind the drug molecule to the polymeric system such that these drugs are released only upon reaching the highly acidic cancer tissues regions while staying stable at normal tissue regions. The drop in the pH of cancerous tissue is often exploited to form such linkages, which are sensitive to slight change in pH of the surrounding environment [74]. The pH of the cancerous tissues is around 5-6 and the lysosomes have a pH of range of 4-5. Low pH can act as extracellular as well as intracellular stimuli to cause breakage of drug molecule and subsequently aid its delivery.

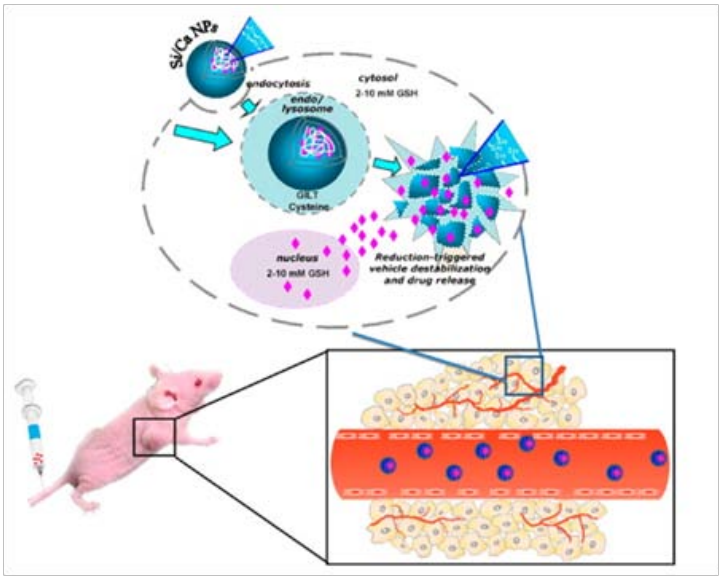

Figure 1.11: *The acidic conditions in cytosol causing disruption of pH responsive nanoparticles. (Adapted from Hao et al, ACS Nano,* **2015**, *9,* 9614-9625*).*

Upon reaching the highly acidic and hydrolytic enzyme rich lysosomes these bonds are cleaved and the drug molecules are released to the target sites. In an alternative approach, the pharmacological state of the drug is kept intact by the physical loading of the drug molecules in the polymeric nanostructures. The linkages discussed above are successfully incorporated in the polymeric backbone to bring about complete disassembly and degradation of the amphiphilic polymers in order to

disrupt the assembly leading to release in the loaded cargo. These include incorporating Ca^{2+} ions within Si/Ca NPs which are senstitive to acidic environment and causes a disruption of the NPs (see figure 1.11) [75]. Natural resources like L-amino acid have been carefully chosen to develop pH sensitive nano-carriers namely poly-L-Lysine, polyhistidine, poly(β-amino esters), etc which have buffering capabilities and often undergo structural changes with change in pH conditions [76,77]. Amphiphilic block copolymers of poly(polyethyleneglycol)-poly(aspartate-hydrazone-adriamycin) (PEG-p(Asp-Hyd-ADR) were developed and the anticancer drug adriamycin was carefully attached to the polymer via acid labile hydrazone linkages[78]. Acetal chemical linkages are another class of acid sensitive molecules which readily undergo hydrolysis in acidic conditions. PEG-block-acetalated-dextrans were developed and employed by Chen and co workers to efficiently delivery DOX for anticancer applications [79]. Acid labile Schiff bases were used by Cheng and co-workers to conjugate DOX and develop Polylactide-graft-doxorubicin nanoparticles and used them for DOX delivery [80]. Polyacetal urethane based polymers were synthesised having acetal linkages within the polymer backbone to synthsise PEG-PAU-PEG triblock copolymers [81]. The advantages of such systems are the lowering in the pH of the system causes disruption of the polymer backbone and disturbs the self assembly of the amphiphilic polymer causing a burst release of the loaded cargo [81]. Amine side chain containing pH sensitive PEG-Polypeptide diblock were synthesised and amine were further used as initiator for ring opening of N-carboxyanhydride (NCA) monomers and the self assembled nanovescicles of these diblocks were employed for delivery of DOX and these showed high killing towards triple negative breast cancer cell line, MDA-MB-468 at *in vitro* levels [82].

Thermo-responsive polymers

Temperature change between normal healthy tissues and cancerous tissues is one of the exogenous stimuli often exploited for polymeric drug delivery applications. The non linear sharp change in the characteristic properties of polymer or their components with temperature is basic fundamental of themo-responsiveness. In an ideal scenario nanocarriers retaining their loaded cargoes at 37 °C physiological

conditions, and releasing the loaded drugs/cargoes at locally heated tumour sites are used as thermoresponsive delivery agents against the strong blood circulation [83].

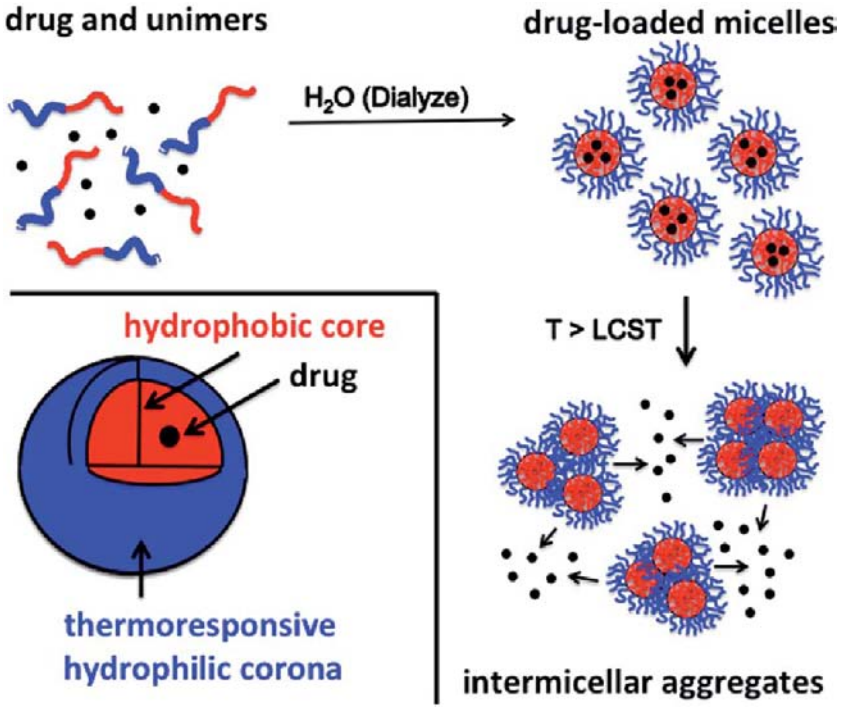

Figure 1.12: *Development of aggregated species of micelles above their LCST as thermoresponsive polymer (Schematic adapted from Sun et al, J. Mater. Chem. B,* **2015**, *3,* 814–823*).*

Sensitivity of polymers towards temperature has been long employed to synthesise thermoresponsive polymers. Poly(*N*-isopropylacrylamide) (PNIPAAm) is one of the most extensively studied thermoresponsive polymer which exhibits a lower critical solution temperature (LCST) at 33 °C when dispersed in aqueous solution. Below this temperature however, this polymer dissolves in aqueous solution and above this temperature it precipitates out (See figure 1.12 [84] for a schematic representation) [85]. The drug delivery is controlled temporally, as any slight change above or below the LCST would disrupt the self assembly of the nanoparticles or would force it to precipitate out leading to the burst release of the encapsulated loaded cargoes. During the micelle formation the PNIPAAm segment and hydrophobic component of the polymer forms core-shell nanoparticles structure with the hydrophilic PNIPAAm exposed to the aqueous environment and the hydorphobic component formed the core of the micelles [86]. The hydrophobic core loaded cargoes

are prevented from interacting with the biocomponents and the hydrophobic component gets exposed upon heating. The hydrophobicity induced into the system forces the nanoparticles to precipitate out and selective accumulation could be enhanced due to micelle adsorption into tumour tissues. The combined effect of EPR and thermo-responsive micellar accumulation can be exploited to deliver drugs at tumour sites making thermoresponsive polymers efficient for drug delivery [87]. Various polymer structures have been reported based on tuned LCST properties for their potential use for effective drug delivery at tumour tissue environment. Use of oligoethylene units to induce thermo-resposiveness into polymers were demonstrated by Stefan and co-worker, who prepared copolymer poly(γ-2-(2-(2-methoxyethoxy)ethoxy)ethoxy-ε-caprolactone which self assembled into micelles and showed thermoresponsiveness at 47.5 °C. A slight modification in the structure of the polymer by adding hydrophobic poly(γ-octyloxy- ε-caprolactone), the resultant block copolymer poly(γ-2-(2-(2-methoxyethoxy)ethoxy)ethoxy-ε-caprolactone-*b*- poly(γ-octyloxy- ε-caprolactone) showed thermoresponsive behaviour at 37.5 °C which is closer to physiological temperature and can be used for bio-applicaions [88]. Jayakannan and co-workers reported the development of amphiphilic molecules from ethylene glycols and PDP molecules that formed shape transformable and thermoresponsive scaffolds which exhibited core shell nature at ambient temperatures but were transformed to rod like structure at temperature close to cancer tissues. High and stable loading of DOX and CPT were demonstrated and these nano-scaffolds were found to be ideal shape transforming nano-materials for drug loading applications [89]. Futher these small molecule amphiphiles were translated into polymeric amphiphiles diblock with PDP and PEG using amide bonds. These polymers formed super LCST thermo-responsive core-shell nanoparticles because they formed high temperature LCST > 90 °C. These nanoparticles preferentially bound to ATP compared to ADP, AMP, P_i at cancer tissue temperature i.e., at 42-44 °C. Stefan and co-workers reported a thermo-responsive, fluorescent as well as biocompatible poly{γ-2-[2-(2-methoxyethoxy)- ethoxy]ethoxy-ε-caprolactone}-b-poly(γ-octyloxy-ε-caprolactone) (PMEEECL-b-POCTCL) diblock copolymer were reported and these showed a lower critical solution temperature (LCST) of 38 °C and were demonstrated as thermally responsive micelles. Nile Red and Doxorubicin

(DOX) were loaded and were stable in FBS and BSA conditions exhibited thermo-responsive *in vitro* drug release. These also showed higher killing in the MCF 7 human breast cancer cell at incubation temperature above the LCST. The DOX-loaded micelles were found to internalize into the cells via endocytosis which was monitored using confocal imaging [88]. The thermo-responsive nano-scaffolds were promising candidate for drug delivery at cancer sites [90]. Jayakannan and co-workers have reported a completely biodegradable polyester urethane based on L-Tyrosine natural resources by grafting PEG chains on the side chains of the polymer using the tyrosine phenolic groups [91]. Many other polymers are known for their thermoresponsive structural changes and have been employed for their temperature sensitivity for example Poly(N-vinylcaprolactam) (PVCa) [92], Poly (N-vinylpyrrolidone) (PVPy)[93], Poly(N-n-propylacrylamide) (PNNPAM), Poly(N-cyclopropylacrylamide) (PNCPAM), Poly(N,N-diethylacrylamide)(PDEAM), oligo(ethyleneoxide)-grafted polylactide, P(Val-Pro-Gly-Val-Gly)[83] etc to name a few. The research in the field of thermoresponsive polymers are limited to only *in vitro* experiments and utilisation of hypo/hyperthermia conditions of cells *in vivo* are still untapped and remains a critical challenge for further use of thermoresponsive polymers in drug delivery applications.

Enzyme responsive polymers

Enzymes are one of most essential components of the cellular machinery and are highly specific in nature and they exhibit outstanding bio-recognition abilities and act as excellent catalytic molecules. Designing of conjugated nanoparticles for clinical testing are generally based on hydrolysis assisted cleavage of chemical bond between the polymer and drug or the drug-nanoparticle conjugates by enzymes that are specifically present either outside or inside cellular compartments of the cells. These enzymes include mostly lysozymes, esterases, or intracellular enzymes such as cathepsin B [94]. Conjugates of poly-L-Glutamic acid (PG) with paclitaxel have been developed with high loading content of paclitexal (37% wt/wt) and these polymer drug conjugates were found to be biodegradable and have been used in clinical trials [9]. Enzyme-responsive nanoparticles can be designed and developed based on the chemical linkages towards which these enzymes can possess molecular recognition to,

for gene therapy (figure 1.13) [95] . Enzymes that are mainly used for drug delivery applications include proteases, phospholipases, oxidoreductases, esterases, trypsin (serine protease in the mammalian small intestine), Pepsin A (aspartic protease in stomach), dextranase in the colon and protease hepsin overexpressed in prostate carcinoma. For example, Gly-Phe-Phe-OEt (GFF-OEt) is a shortest peptide cleaved by pepsin [96]. Hydrophilic poly(γ-glutamic acid) (γ-PGA) and hydrophobic L-phenylalanine ethylester (L-PAE) were used to develop amphiphilic graft copolymers which self assembled into 200 nm-sized nanoparticles. The backbone γ-PGA was sensititve towards γ-glutamyl transpeptidase (γ-GTP), Pronase E, protease, cathepsin B and lipase and their enzyme aided hydrolytic degradation was demonstrated [97]. *β*A*β*AKLVFF-PEG_{3000} peptide- polymer conjugate were developed, and were found to be sensitive to α-chymotrypsin and their self assembled spherical micelles were disrupted using this enzyme [98]. Gly-Phe-Phe (GFF) peptide was conjugated to copolymer of styrene and acrylic acid and their nanoparticles were studied for their biodegradability in presence of pepsin and trypsin as model enzymes specific to this peptide sequence [99]. α-Chymotrypsin assisted cleavage of biodegradable poly(ether ester amide)s (PEEAs) made up of triblock of L-phenylalanine, oligo-ethylene glycol, and aliphatic acid dichlorides were demonstrated as unique polymer-peptide conjugates for drug delivery applications [100]. Multifunctional theranostic molecular probes have been developed having DOX as FRET donor covalently linked to a black hole quencher (BHQ-2) via lysine junction having an inbuilt cell-penetrating peptide (octa-arginine (R8)) to enhance cellular internalization[101].

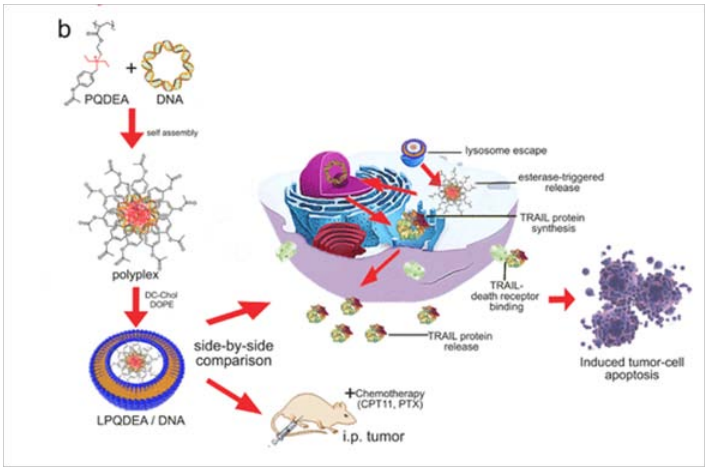

Figure 1.13: *Enzyme responsive polymers for gene therapy (Schematic adapted from Qui et al, Biomacromolecules,* **2018**, *19,* 2308–2319*).*

Cathepsin B (CatB), a lysosomal protease was employed to cleave the molecular probe and it was monitored by retention of self emission of the DOX molecules and has been used for sensing of DNA, RNA etc. The tetrapeptide (GFLG) was used for the specific cleavage by the cathepsin B substrate. The lysosomal protease Cathepsin B was chosen for these studies because it is over expressed in many cancers [101]. Enzyme responsive hybrid PEG-hybrids were synthesised with hydrophobic cleavable end groups and these self assembled into compact polymeric micelles and were employed to encapsulate small hydrophobic guests for biomedical applications [102].

GSH responsive polymers

GSH is a tripeptide found in living organisms capable of reducing disulphide bonds for cellular functioning. L-cysteine-based poly(disulfide amide) (Cys-PDSA) were developed from two non-toxic repeating units as biodegradable and biocompatible, having a disulfide part (L-cystine ester) making these redox-responsive thereby making them sensitive to the presence of lysosomal GSH and diacid part (aliphatic dicarboxylic acid). DTT degradation of these nanoparticles was shown by release of NR dye from the nanoparticles. Doxetal loaded nanoparticles (Dtxl-loaded NPs) showed antitumor efficacy in A549 xenograft mouse model wherein 5 $mgkg^{-1}$ of Dtxl loaded in NPs suppressed tumor growth and 10 $mgkg^{-1}$ enhanced tumor inhibitions after 48 days [103]. Guanidinylated bioreducible polyplexes (GBP) were reported for gene delivery application, which were found to biodegrade due to reducible disulfide bonds. The guanidine groups enhanced their cell-penetrating ability [104]. Mouse model studies showed 7-fold higher gene delivery efficiency in 2-month-old male C57BL/6 mice and were found to be non toxic to A7r5 cells and mouse cavernous endothelial cells [105]. Core shell polymeric nanoparticles were developed with cross-linked shell loaded with Paclitaxel and poly(lactic acid) core. The poly(lactic acid) core was enzymatically and hydrolytically degradable where as the cross-linked poly(oligoethylene glycol)-containing corona had glutathione-responsive disulfide units. These nanoparticles were stable in PBS buffer however paclitaxel released from the core rapidly in the presence of glutathione at both pH 5.5 and pH 7.4.

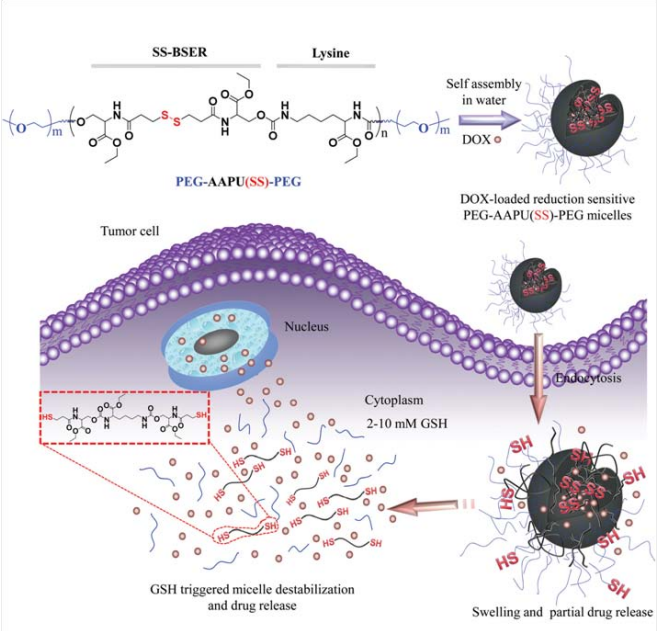

Figure 1.14: *Triblock copolymer PEG-AAPU(SS)-PEG nanoparticles disrupting in intracellular GSH rich environment. (Illustration adapted from Lu et al, Polym. Chem.,* **2015***, 6,* 6001–6010*).*

Hydrolysis of the nanoparticle poly(lactic acid) core catalyzed by enzyme showed 30% degradation within 12 h which corroborated well with 37% release of GSH triggered paclitaxel release of the nanoparticles. The paclitaxel-loaded nanoparticles showed 11-fold lower IC_{50} than a Taxol-mimicking formulation against human ovarian adenocarcinoma cells making these nanoparticles promising for delivery of paclitaxel to tumor tissues [106]. Biodegradable α-amino acid-based poly(disulfide urethane)s {AAPU(SS)s} were reported and their amphiphilic triblock copolymer micelles PEG-AAPU(SS)-PEG were synthesized for DOX release triggered by redox reduction (figure 1.14) [107]. Disulfide-linked bis(ethyl L-serinate) (SS-BSER) and L-lysine ethyl ester diisocyanate (LDI). AAPU(SS)s degraded into low molecular weight fragments under 10 mM glutathione (GSH), a reductive condition and exhibited effective growth inhibition of both RAW 264.7 and corresponding nascent micelles were found to be non-cytotoxic at high concentration of 1.0 $mgmL^{-1}$ [108]. Other major examples of reduction-responsive polymers are methoxypoly(ethyleneglycol)-block-poly(S-tert-butylmercapto-L-cysteine) copolymers (i.e., $mPEG_{113}$-*b*-$PBMLC_4$ and $mPEG_{113}$-*b*-$PBMLC_9$) have been used for DOX delivery to MCF-7 breast tumor-bearing BALB/c nude mouse model and this

was studied using histopathological and immunohistochemical experiments [107]. The prodrug OEG-2S-SN38 connecting oligoethylene glycol to SN38 drug via disulphide bonds was found to release the parent drug SN38 by thiolysis because of GSH giving rise to enhanced *in vitro* cytotoxicity and *in vivo* anticancer therapeutic activity. Combination of two or more above mentioned stimulus has been exploited to make polymer nanoparticles highly efficient drug carriers and delivery agents [109].

Figure 1.15: *Multi-stimuli responsive amphiphilic block copolymer nanoscaffolds. (Illustration adapted from Klaikherd et al, JACS,* **2009***, 131,* 4830–4838*).*

Klaikherd. A. et al have reported a multi-stimuli responsive amphiphilic polymer where in PNIPAM, poly (*N*-isopropylacrylamide), was used as hydrophilic segment having temperature responsiveness, tetrahydropyran protected HEMA (2-hydroxy ethyl methacrylate) was used as hydrophobic segment with inbuilt acetal groups with pH responsiveness and these hydrophilic and hydrophobic segments were linked via disulphide bonds that are very well known redox responsive bonds (figure 1.15) [110]. Atom transfer radical polymerisation (ATRP) was employed to synthesise the hydrophobic and hydrophilic polymer segments using 2-(pyridine-2-yldisulfanyl) ethyl 2-bromo-2-methylpropanote as initiator. The hydrophobic and hydrophilic pre-amphiphilic polymer were reduced by DTT to yield the respective thiols as end groups and further the two segments were linked together to form the disulphide containing amphiphilic polymer. The release of polymer nanoparticles as response to pH changes were studied using Nile red as loaded cargo and its release was studied as function of DLS size change which was observed to increase with time suggesting

the disassembly caused to acid sensitive acetal groups. The release of Nile red was further studied at pH 4.0, 5.0 and 6.0 and it was observed that more acidic environment lead to higher release of the Nile red. The disappearance of acetal protons were further proven by disappearance in proton NMR. The presence of PNIPAM thermoresponsive segment made these amphiphilic block polymers responsive to temperature change and the micelles obtained from these polymers were subjected to temperature ranging from 20-50 °C and the LCST of the polymers were found to be 35 °C. The redox responsiveness of these polymers were studied using DTT and the resultant polymers were monitored using GPC analysis which showed the presence of the intrinsic peaks of PNIPAM and HEMA counter polymers separately showing the cleavage of the disulphide containing polymer. The GSH based cleavage of the polymers was studied by monitoring the turbidity of the polymers as a function of time (due to cleavage of the hydrophobic polymer segments which are expected to preicipitate out of the solution). The increasing turbidity in the solution further confirmed the cleavage of the amphiphilic polymer under redox environment. The GSH based release studies were performed on nile red loaded nanoparticles, and it was observed that at high concentration of 16mM of GSH, a complete release of nile red in three days occurred indirectly indicating towards the redox responsiveness of the polymers. Further combinations of these stimuli were employed to mimic intracellular cancer conditions and it was found that use of combination of these stimuli further enhanced the release of the loaded cargoes and these polymer structures were found to be highly responsive to stimuli such as temperature, pH change and redox conditions [110]. The multistimuli responsive polymers are used for enhanced therapy; however the multifunctional polymers having targeting as well as inherent fluorescence nanocarriers are also gaining importance. Lee et al have reported theranostic cores having CPT (camptothecin drug-disulphide-conjugates of RGD peptides which act as theranostic applicants for targeted pharmaceutical results, fluorescent imaging as well as thiol repsonsive nanomaterials in A549 cells, KB cellsand enhanced killing in tumour in xenografted mouse model , HeLa cells [111].

1.6 Amino acid based polymer nanocarriers

L-Amino acids are naturally occurring chiral molecules having tetrahedralcarbon atom attached to a carboxylic acid group (-COOH) and amine group ($-NH_2$) and a functional R group as side chain. These R group vary from carboxylic acid, thiols, hydroxyl, aromatic groups, alkyl chains etc and play crucial role in the functioning of proteins which are made up of amino acids. There are twenty major naturally occurring amino acids which constitutes majority of animal kingdom. Amino acids are extensively used, biomedical, food additives, polymers, cosmetics, pharmaceuticals fields etc., and are produced over 2 million tons annually [112]. Amino acids are produced via i) extraction (from Meat extracts and plant hydrosylates), ii) chemical synthesis (Strecker amino acid synthesis) [113-115], iii) fermentation (Corynebacterium glutamicium microbe used for synthesising L-glutamic acid) and, iv) enzymatic catalysis (amidocarbonylation reaction in presence of a transition metal catalyst) [116-117]. α-amino nitriles produced from ammonia and aldyhyde or ketone, and H_2S, are hydrolysed to produce amino acids chemically. For ex L-aspartic acid was synthesized from fumaric acid and ammonia enzymatically using L-aspartate ammonia lyase enzyme (figure 1.16) [118]. The amine unit and carboxylic group of two individual amino acids can be coupled to form and amine bond with loss of water. Oligopeptides are small chain polymers of amino acid made via amide bonds and are synthesised by liquid phase synthesis and solid phase synthesis (figure 1.17). Liquid phase synthesis involves multistep syntheses, and is highly tedious, and solid phase synthesis is more commonly used due to their ease of preparation and minimal need of purification [119-121]. However, both the processes involve loss of reaction yields to large extent. The amide bonds capable of forming hydrogen bonding interactions, give rise to various morphologies like micelles, vesicles, nano-rods, fibres at nano-dimensions which encourage their use as drug delivery, gene carrier, antimicrobial agents etc.

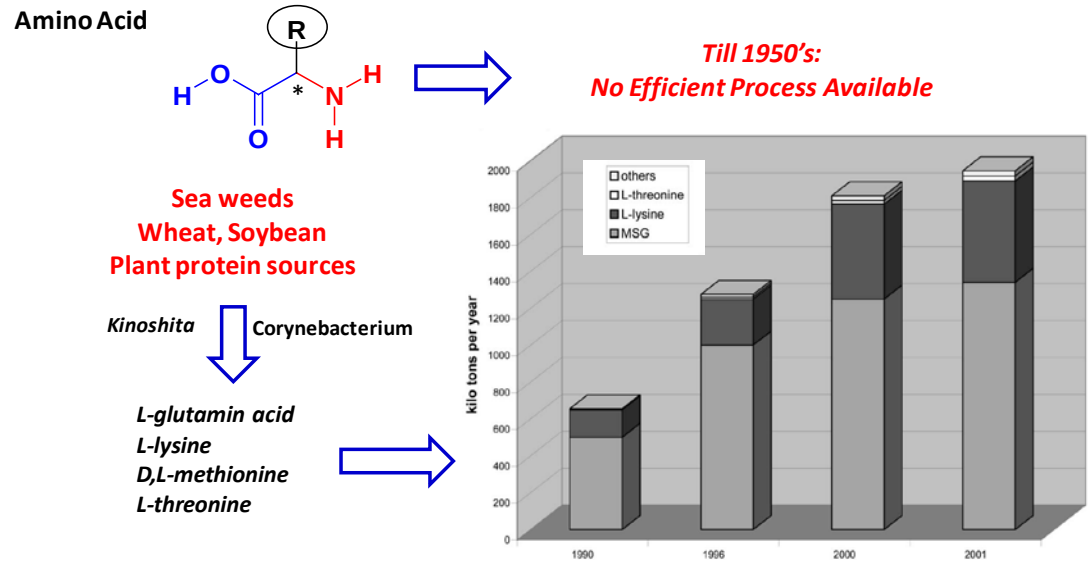

Figure 1.16: *The yearly production of L-amino acid. (Data adapted from Hermann et al, J. Biotech*, **2003**, *104*, 155-172, and from *Breuer et al. Angew. Chem. Int. Edn. (Review)*, **2004**, *43*, 788-824).

Peptide ampiphiles (PA), are a subclass of peptides, that can be tuned into various similar high defined nano-structures [122-124]. Highly developed architectures of peptides like βAβAKLVFF and C14-KKFFVLK were found to form short proto-filaments which twist into ribbons and nano-tubes with time [125]. Dehsorkhi et al. reported that bilayer peptides like KLVFFAE form high defined nanotubes and the structural features have been shown in figure 1.18. Collagen based PA assembles into poly-proline II triple helix structure and alkyl chain substituted peptides gave rise to formation of helical ribbons and nano-tapes and these transformations were thermally reversible in nature.The added advantage of some peptides was found to be responsive to certain stimuli such as light, heat and pH. Presice conjugation of nitrobenzoyl group to Ac-Lys-Thr-Val-ILe-ILe-Glu-NH2 fragment resulted in formation of UV light sensitive amyloid [126]. UV cleaving of nitrobenzoyl moieties transformed the β-sheet to a random coil. Hydrogels based on alkylated Arg-Gly-Asp-Ser peptide were reported by Stupp's group and were found to be responsive to light using nitrobenzoyl bound units.

Figure 1.17: *Essential segments of any oligopeptide for forming higher order structures. (Structure adapted from Dehsorkhi et al. J. Pept. Sci.* **2014**, *20,* 453–467).

Figure 1.18: *Self assembly model for hydrogen bond assisted helical coiling of flat rectangular bilayer peptide KLVFFAE into nanotubes and their top view (Structure adapted from Dehsorkhi et al. J. Pept. Sci*. **2014**, *20*, 453–467*).*

Synthetic polypeptides are prepared by ring opening polymerization of activated carboxylic group of amino acid and amine units in presence of base. The esterified acid chloride, p-nitrophenyl ester are mostly used to activate the carboxylic units of amino acids [127]. It was reported that poly-condensation of N-carboxy anhydride monomer which self condense to form polyamides [128]. The NCA monomer was developed in situ by converting the amine group of the amino acid to phenyl carbamate using diphenyl carbonate. Ring opening polymerization (ROP) approach was employed with monomers having built in strained rings topology, which undergoes polymerization by opening of the rings using appropriate initiator yielding consistently high molecular mass, narrow dispersity and monodispersed polymers. Effective modulation in the monomer/initiator ratio gave a control over the molecular weight built up of these polymers. Fuchs-Farthing method can be employed to syntheisis polypeptides from amino acids which are based on formation of optically active NCA monomer from α-amino acid and triphosgene [129-130]. Primary amines and alkoxide anions are major initiators used routinely for ROP of NCA. Deming demonstrated the living NCA polymerization in presence of Ni(COD)bipy metal

catalyst using eight member cyclic NCA monomer yielding high molecular weight polymers with low polydispersity due to formation of highly reactive metallocyclic complex [131]. pH responsive poly(l-glutamic acid sandwiched between hydrophobic poly(l-alanine) from each side made triple block poly peptide which was pH responsive and underwent structural changes from short tapes to spherical aggreages upon increasing the pH of the system [132]**.** Amine functionalised polypeptides were developed by polymer side chain protected lycine NCA followed by post polymerisation de-protection. Similarly carboxylic, imidazole, thiol, hydroxyl functionalised polypeptides could be developed by using corresponding protected NCA monomers of L-aspartic acid (or Glutamic acid), histidine monomer, S-tert-butylmercapto-L-cysteine NCA monomer, L-serine (or L-dihydroxy phenyl alanine) NCA monomers using ROP respectively. Xing et al reported copolymerization of cystine NCA monomer with benzyl protected glutamic using PEG-NH_2 initiator to yield disulfide based cross-linked polymers [133]. Post polymerization approach was suggested for L-methionine based polypeptide by Deming et al [134]. Here stable sulfonium ion derivative substituted poly-L-methionine was prepared by alkylation from various alkyl halides and triflates containing functional groups. Poly (L-methionine)$_{65}$-b-poly(L-leucine$_{0.5}$-stat-L-phenylalanine$_{0.5}$)$_{20}$, a diblock co-polypeptide, was prepared by Deming et al. This polymer self assembled into vesicles on oxidation reaction showed enzyme responsive release of loaded cargoes.

Polymers with alternating α-amino acids and α-hydroxy acid containing aliphatic ester linkages, are called poly depsipeptides often synthesised by ROP of morpholine-2,5-dione (derivatives of α-hydroxy acid and α-amino acid) in presence of a tin octanoate catalyst and alcohol as initiator. Efforts were made to polymerize glycine and D,L-lactic acid based on morpholine-2,5-dione (by Feijen et al) [135]. This polymerization was further broadened to include morpholine-2,5-dione derivatives of various amino acids (alanine, glycine or valine) and α-hydroxy acids (lactic acid, glycolic acid) [136]. ROP of depsipeptide with glycolic acid and O-benzyl-L-serine was carried out by John et al resulting in the formation of benzyl protected polydepsidpeptides which were subsequently were de-protected to yield hydroxyl functionalized polymer [137]. Enzymatically degradable L-phenyl alanine based poly (ester-amide) polymers, were developed by Arabuli et al. from bis (p-nitrophenyl)

adipate and its reaction with di-p-toluenesulfonic acid salts of several diol diesters (1,2-ethanediol, 1,3-propanediol, or 1,4-butanediol bis L-phenyl alanine diesters) [138]. By varying the amino acid ratios (L-lysine Boc and L-phenylanine, from 0:100 to 20:80).

Figure 1.19: *L-Amino acid building blocks (Adapted from Biomacromolecules* **2011**, *12,* 1937–1955*).*

Gillies et al. synthesized range of amino functional poly (ester-amide) which showed increased hydrolytic and enzymatic degradation due to the L-lysine content (obtained from deprotection of L-lysine BOC) [139-140]. Guo et al. synthesized poly (ester-amides) using solution polycondensation approach on unsaturated diols diacids or diacid chlorides [141]. Here two unsaturated monomers, di-p-nitrophenyl fumarate and L-phenyl alanine 2-butene-1,4-diol diester p-toluene sulfonate along with four saturated monomers (based on 1,4-butanediol, 1,6-hexanediol, adipoyl chloride and sebacocyl chloride) were used in varying ratio for polymerization. These unsaturated poly (ester-amides) showed slower degradation in α-chymotrypsin. Partially unsaturated poly (ester-amide) were also reported by Chu and Guo synthesized using mixture of saturated and unsaturated monomers (e.g. using L-phenyl alanine, aliphatic diacid chlorides, 1,4-butanediol) [142]. This ratio of saturated to unsaturated monomers provided for a way to tune the polymers' biodegradability. Major disadvantages of these reactions included the fact that i) it produced a racemic product, and ii) due to higher temperature of reaction, it leads to lot of undesirable side products.

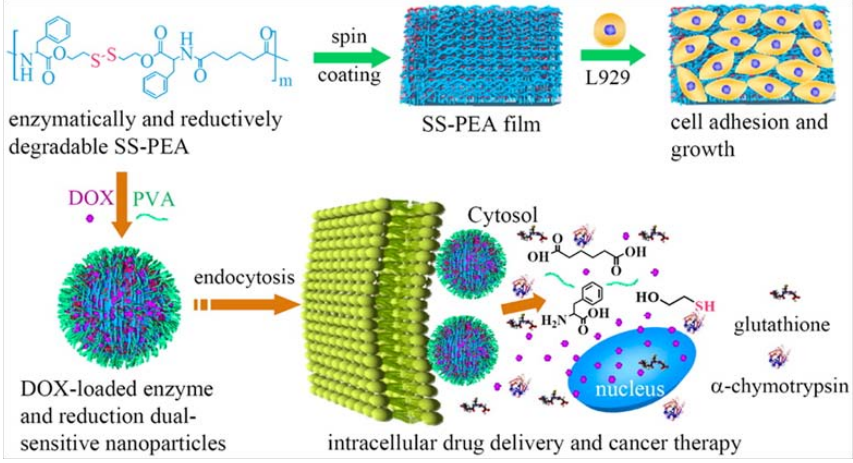

Figure 1.20: *Enzyme and DTT responsive disulphide based polyester(amides) for enhanced cell killing in DOX resistant cells(schematc adapted from Sun et al. Biomacromolecules* **2015**, *16*, 597-605*).*

Sun et al. reported the synthesis of enzymatically and reductively degradable and amorphous α-amino acid-based poly(ester amide)s (SS-PEAs) from solution polycondensation of di-p-toluenesulfonic acid salts of bis-Lphenylalanine di-esters having disulphide units (SS-Phe-2TsOH) and with di-p-nitrophenyl adipate (NA) in DMF with high molecular weight ranging from M_n 16.6 to 23.6 kg/mol [143]. The SSPEA films were subjected and found to dergrade in the presence of 0.1 mg/mL α-chymotrypsin and were sensitive to bulk degradation in presence of 10 mM dithiothreitol (DTT). These were non toxic to proliferating of L929 fibroblast cells and supported their adhesion in culture plates. There DOX loaded nanoparticles were futher studied for their therapeutic efficacies and it was found that DOX realeased in resence of 0.1 mg/mL α-chymotrypsin or 10 mM DTT. Confocal microscopy revealed the efficient delivery of DOX in the cytoplasm of the cells into both drug sensitive and resistant MCF 7 cells. DOX-loaded SS-PEA nanoparticles exhibited high antitumor activity in drug-sensitive MCF 7 cells, and 10 folds higher killing in drug-resistant MCF 7/ADR cells compared to free DOX in (see figure 1.20). Hence these non peptide polymers were shown to be effective bio-degradable materials that could be developed into nano scaffolds for bio-medical applications.

α-amino acid reacted with sodium nitrite under acidic condition resulting diazotization reaction to form α-hydroxy acids (with preservation of the stereochemistry), where α-amino acid amine group gets converted into hydroxyl

group [144]. α-hydroxy acid self-condenses in presence of p-toluene sulfonic acid, to yield dilactide monomer. Other ways to produce same monomer include coupling of α-halo carboxylic acid or α-halo acyl halide and α-hydroxy acid. Obtained dilactide monomers undergo ROP using $Sn(Oct)_2$ catalyst to produce polyester. Benzyl protected dilactide were subjected to ROP followed by deprotection to yield carboxylic functional polyester, whereas ROP and deprotection of hydroxyl protected dilactide, in presence of $Sn(Oct)_2$ catalyst, hydroxyl functional polyester with α-hydroxy acid [144]. Water soluble OEG/PEG functionalized polyester was synthesized by Jiang et al using ROP of dilactide monomers. They also synthesized alkene and alkyne functional polyester from post polymerization of thiol-ene and thiol-yne respectively. Solvent free poly-condensation reaction for α-hydroxy acid was demonstrated by Farokhzad, Langer and et al.[145-146] They employed p-toluene sulfonic acid as a catalyst and removed of water which formed as a byproduct in reaction. Polyurethane is synthesized by a catalysis mediated reaction between diisocyanide and diol. Polyurethane are mechanically stable because of the hydrogen bonding in the -NH groups of urethane functional group (-NHCOO). An A-B type urethane monomer was synthesized by Endo et al. by reacting L-phenyl alanine sodium salt with five membered carbonate in ethylene glycol medium and was self-condensed with the help of dicyclohexylcarbodiimide (DCC) coupling agent resulting in polyurethane polymers with low molecular mass [147]. Endo et al. reported L-tyrosine based polyurethane where in L-tyrosine methyl ester amine salt was reacted with ditertbutyltricarbonate to yield L-tyrosine isocyanide monomer [148]. Its self-condensensation in basic media led to the formation of polyurethanes. Hydroxyl functional polyurethane synthesized from bifunctional cyclic carbonate's reaction with L-lysine hydrochloride was also prepared. Polymers synthesized with half ester and half urea functional group are called poly (ester-urea)s, and can be prepared by both solution polycondensation as well as interfacial polycondensation process. Reaction between α-amino and diol group, with PTSA medium produces di-p-toluenesulfonic acid salts of bis-(α-amino acid) α,ω-alkylenediesters (BAAD). Phenyl alanine or tyrosine's BAAD p-toluene sulfonic acid salt, on reaction with triphosgene gives poly (ester-urea) (Becker et al.) [149-154]. This reaction occurs in presence of sodium carbonate, and takes the interfacial polycondensation route. These polymers are

biodegradable, and urea group provides mechanical stability along with water stability making these polymers useful in wide ranging applications. Polycarbonates are obtained when bisphenol is reacted with phosgene or activated esters and is often aided by an appropriate catalyst. Non-toxic tyrosine based bisphenol have been used for the poly carbonate synthesis. Kohn et al. used 3 (4-hydroxylphenyl) propionic acid and reacted it with tyrosine alkyl ester to produce tyrosine bisphenol monomer in DCC [155]. Obtained tyrosine bisphenol monomer yields polycarbonate on reaction with phosgene or triphosgene. Tyrosine based polycarbonates are often prepared with substitutes, such as alkyl, polyethylene glycol etc [156].

1.7 Melt polycondensation for L-amino acid polymers

From our laboratory, new eco-friendly high temperature solvent-free condensation chemistry for the natural amino acids under solvent free melt process was developed to make diverse polymer structures as shown in figure 1.21. Natural L-amino acids were converted into ester-urethane monomer where firstly carboxylic acid was converted into corresponding methyl ester and then amine part was converted into corresponding urethane (or carbamate) functional group. Equimolar amounts of amino acid monomer and diols were poly condensed using $Ti(OBu)_4$ as catalyst (1 mole %) under nitrogen purge and high vaccum (0.01 mm of Hg). During this process, the viscosity of the melt increased very rapidly and the stirring stopped at the end of the polycondensation [157].

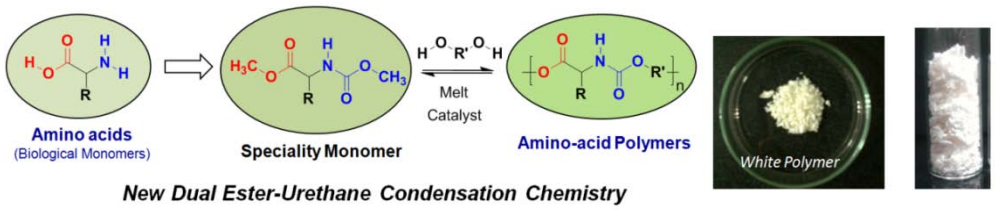

Figure 1.21: *One-pot high temperature condensation chemsitry for L-amino acid polymer.*

The polymer mass was purified by precipitation method and dried in vacuum oven (0.1 mm of Hg) prior to further analysis. In the current process, the diol reacted with both methyl ester and methyl urethane units in the amino acid monomers; as a result the new class of polymers named as poly(ester-urethane)s were deveoped. The

new poly-condensation process was tested for various diols of di-, tri- and tetraethylene glycols, 1,12-dodecandiol (linear aliphatic diols) and 1,4-cyclohexanedimethanol (cycloaliphatic diols) and for various amino acid monomers. The occurrence of dual ester-urethane process and the structure of the new poly (ester-urethane)s were confirmed by NMR spectroscopy. The different types of the protons and carbon atoms in the monomer and polymer structure were assigned by alphabets [157].

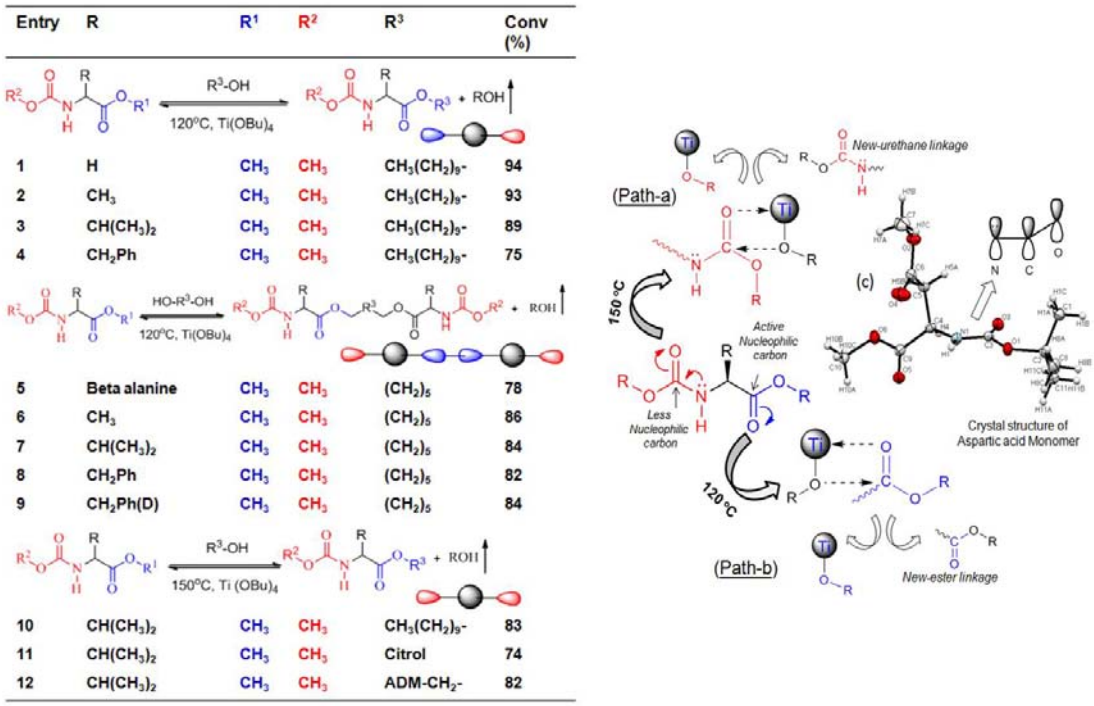

Figure 1.22: *Table shows the synthesis of small molecules at 120 ℃ and 150 ℃. Mechanism of ester (a) and urethane (b) melt condensation. Single crystal structure of aspartic acid monomer (c).*

The mechanism for high temperature selective condensation has been shown in figure 1.22. The hydroxyl of R-OH interacts with $Ti(OBu)_4$ to form active species Ti-O-R which attack the electrophilic carbonyl C of the monomer forming a 4 membered active transition state. Table 1 show that ester carbon is more susceptible to undergo ester-exchange at 120 °C. The urethane carbonyl and ester carbonyl both differ in their electrophilicity. :N-C=O bond existed in the same plane in the crystal structure for aspartic acid monomer which facilitated the overlap of the nitrogen lone

pair with the p-orbitals on the carbon and oxygen atom. This resonance caused the lone pair electron of N on the carbonyl caorbon to thereby decreasing its electrophilicity. The calculation of electron densities at each carbonyl carbon atom by Gaussian programme revealed lower electron density at the ester carbonyl carbon compared to urethane carbonyl carbon. Both single crystal structure and DFT calculation, confirmed that the electron rich urethane carbonyl carbon and therefore it was less susceptible for attack by Ti-O-R active species at 120 °C [160].

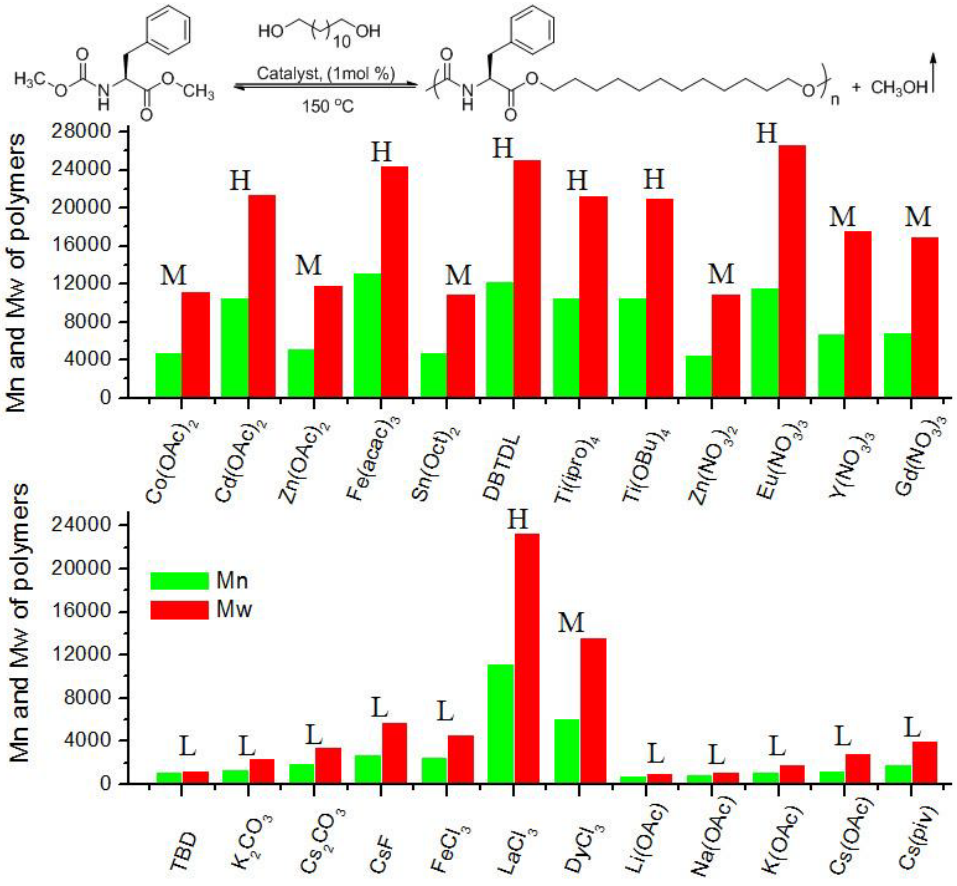

Figure 1.23: *Molecular weights (M_n and M_w) of linear poly (ester-urethane)s made by various catalysts at 150 ℃. The molecular weights of the polymers were classified into L-low (< M_n = 3000 g/mol), M-moderate (M_n = 3000 to 9000 g/mol) and H-high (M_n> 9000 g/mol) for comparison purpose.*

However at higher temperatures, the N-C bond in the urethane became more rotationally active; and the resonance vanished and increased the electrophilicity of the urethane carbonyl thereby causing attack at urethane carbonyl carbon at higher temperature. This difference in the carbonyl carbon electrophilicity enabled to expand

this chemistry to wide range of amino acids. Variuos catalysts and salts were scanned to optimise this chemistry and it was observed that metal carbonate such as K_2CO_3 and Cs_2CO_3 were poor choices for the reaction as they did not produce high molecular weight polymers (see figure 1.23). Metal halides $LaCl_3$ produced higher molecular weight polymers in poly (ester-urethane) synthesis,. $Co(OAc)_2$, $Zn(OAc)_2$ and $Cd(OAc)_2$ afforded high molecular weight polymers compared to other metal acetates. Among metal nitrate, $Eu(NO_3)_3$ produced higher molecular weight polymers whereas other metal nitrate $Zn(NO_3)_2$, $Y(NO_3)_3$ and $Gd(NO_3)_3$ produced moderate molecular weight polymers. The molecular weight of functional polymers produced by K(OAc), Cs_2CO_3, $FeCl_3$ and K_2CO_3 catalysts were found to be very low. As per Carrothers equation for step-growth polymerization approach, X_n= 1/(1-p), where p= extent of the reaction; an ideal catalyst should facilitate more than 98% conversion of ester to produce at least 50-mers on laboratory scale. Among all these catalyst, Ti $(OBu)_4$, Ti $(iOpr)_4$, $Fe(acac)_3$, $LaCl_3$, $Eu(NO_3)_3$, Cd(OAc) and DBTDL model compound resulted in more than 99 % of the ester conversion; forming high molecular weight polymers. The amino acid based functional monomers were synthesized from natural L-aspartic and L-glutamic acid containing two carboxylic acid and one amine functional groups. The carboxylic acids were converted into corresponding methyl esters and the amine group was converted into urethane (or carbamate) functional group using Boc anhydride (see Figure 1.24). The variation in the selectivity in reaction ester and urethane towards aliphatic alcohol developed the roots of development of the temperature selective melt polycondensation reaction. Monomers (**1a** or **1b** shown in figure scheme 1) and diols were subjected to melt condensation in 1: 1 mole ratio using $Ti(OBu)_4$ (1 mole %) as a catalyst at 120 °C in presence nitrogen purging for 4 h followed by application of vaccum (0.01 bar) for 2 h. The end gropus methoxy proton in the polymer and the new ester peaks were compared to yield the the high number repeating units of the polymers which was further supported by GPC molecular weights in DMF as M_n=2.5x10^4 to 8.2x10^4 and M_w = 3.0x10^4 to 1.1x10^5. Also increasing the spacer length increased molecular weight of the polymers for both L-aspartic and L-glutamic series. The increase in the molecular weight with increase in the spacer length was attributed to the reduction in the steric effect in the chain backbone by the bulky Boc functional groups [158].

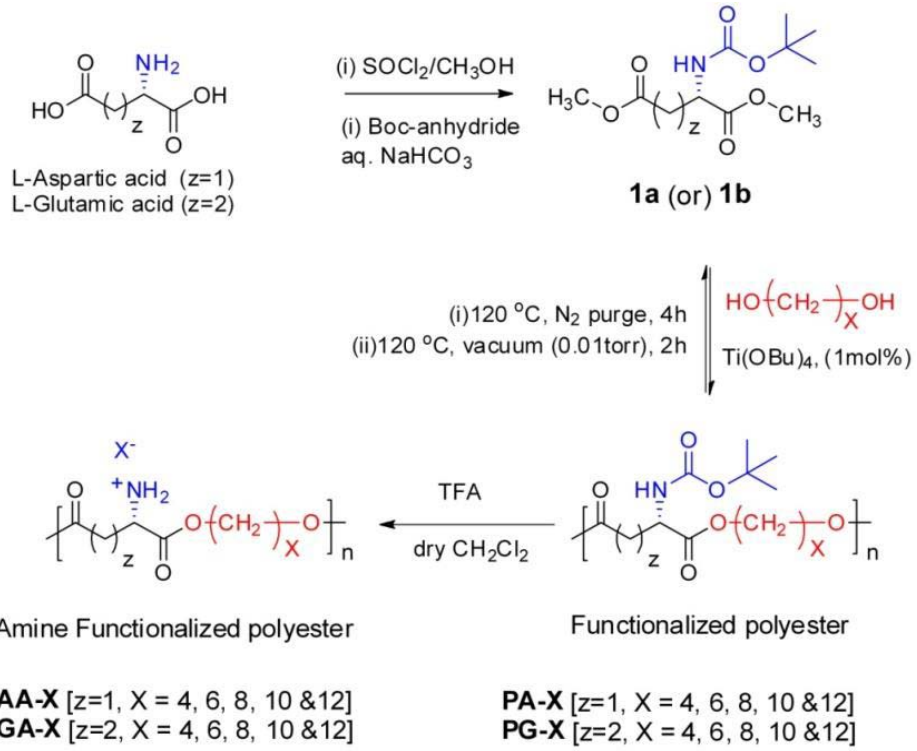

Scheme 1.1: *Functional polyesters from Synthesis of L-aspartic and L-glutamic acid monomers.*

Melt polycondensation approach was extended to disulfide based functional poly-esters based on L-cystine amino acid resources making them redox-responsive in nature. L-Cystine amino acid was transformed to multi-functional ester-urethane thermally stable monomer and subjected to thermo-selective transesterification at 120 °C with aliphatic diols in the presence of $Ti(OBu)_4$ with urethane side chains [161]. The two carboxylic acid of L-cystine amino acid were converted into methyl ester and the amine was converted to BOC urethane (see scheme 2). Under the melt conditions at 120 °C the ester functional group of the monomer underwent thermo-selective polymerization with diol in presence of $Ti(OBu)_4$ (1 mole %) to produce linear polyester with urethane pendant in each repeating unit which were completely inert at 120 °C. High molecular weight polymers were successfully obtained for these polyesters. To avoid the radical cleavage of disulfide linkages in the melt condensation a pinch of hydroquinone was added as radical quencher to the polymerization mixture.

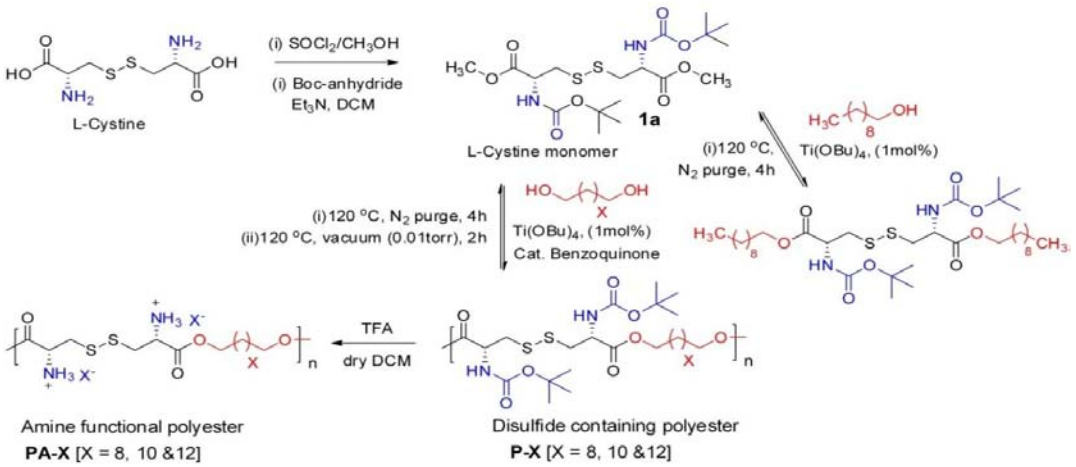

Scheme 1.2: *Synthesis of disulfide based functional monomer **1**, model compound and polymers P-X.*

Hyperbranched polymers based on melt condensation approach were made for the first time from L (or) D-serine and L–threonine with primary and secondary hydroxyl functionality. These monomers were converted into corresponding ABB' monomers, with A, B and B' as the hydroxyl, carboxylic ester and urethane functional groups, respectively. One-pot polycondensation of these monomers produced linear polyester and hyperbanched poly(ester-urethane)s depending on thermoselection (see figure 1.24 and scheme 3) [159]. A and B reacted to produced A-B linear polyester (with B' pendent in each repeating unit). A reacted with B and B' to produced hyperbranched poly(ester-urethane)s. L-Serine was transformed to di-methyl ester and methyl urethane functional monomer and was represented as ABB' type monomer with A as hydroxyl unit which could react with both ester (B) and urethane (B') functionalities. Similarly L-threonine (**2**) and D-serine (**3**) monomers were prepared and were demonstrated for their temperature selective polymerisation. The ABB' monomer underwent melt condensation two different temperatures: (i) at 120 °C alcohol (A) reacted with ester units (B) to produce linear polyester and (ii) at 150 °C alcohol (A) reacted with both ester (B) and urethane (B') for dual ester-urethane polycondensation to yield new classes of hyperbranched poly(ester-urethane).

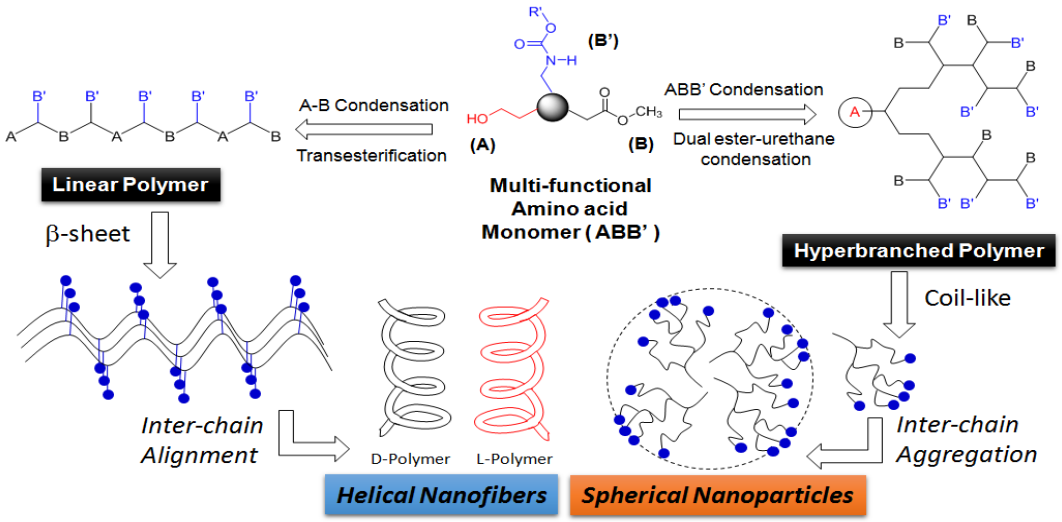

Figure 1.24. *A novel one-pot temperature selective polycondensation approach for linear and hyperbranched polymers based on L-amino acids and their self-assembled nano-structures*

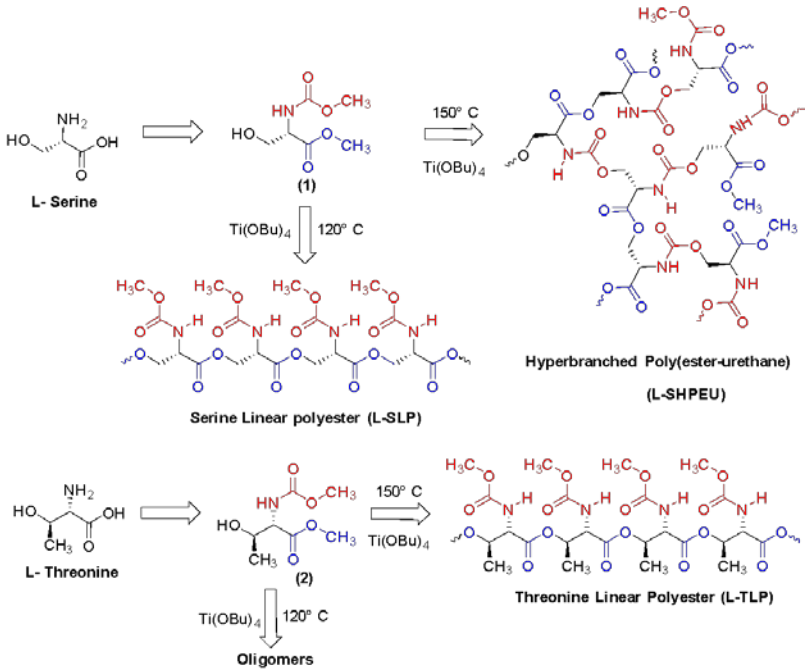

Scheme 1.3: Synthesis of *linear and hyperbranched polymers based on L-serine and L-Threonine monomers*

L-Tyrosine is a unique L-amino acid with three different functional groups which are carboxylic acid, amine and phenolic-OH. L-Tyrosine was converted to methyl ester and methyl urethane respectively (compound **1**, in scheme 4). The phenolic group was conjugated to two different types of alkyl chains C_4 and C_{16}. The

functional L-tyrosine monomer was reacted with 1:1 mole ratios with aliphatic oligoethylene diols (PEG 400, PEG 600, triethylene glycol) for polymerisation under melt conditions with $Ti(OBu)_4$ catalyst (1 mol %) at 150 °C to produce linear amphiphilic poly(ester-urethane)s **P-1** to **P-6** (see Scheme-4a). The polymerization performed in one-pot and two stages: (i) polymerization at 150 °C for 4 h under N_2 purge to produce oligomers and (ii) further polycondensed under vacuum for 2 h to yeild high viscous polymer. The molecular weights of the polymers were obtained in the range of M_n = 4.0 to 13.0 × 10^3 g/mol, and M_w = 9.0 to 27.0 ×10^3 g/mol with PDI 1.9 to 2.2 [162].

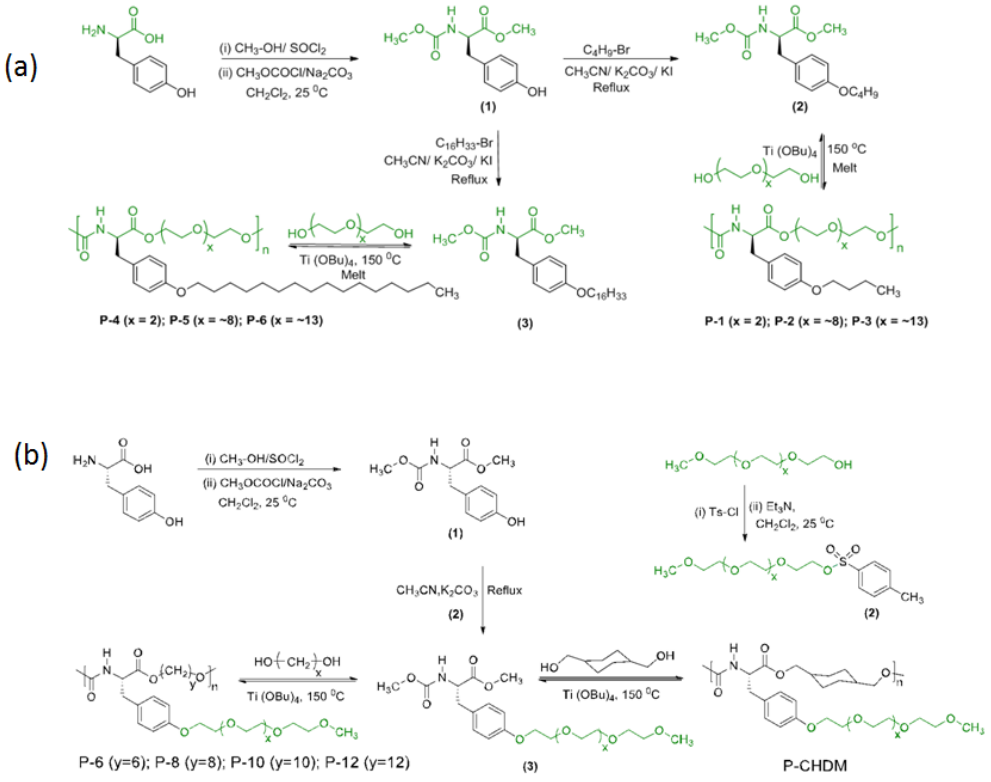

Scheme 1.4: Synthesis of L-tyrosine monomers and new classes of amphiphilic poly(ester-urethane)s.

The amphilic polester urethanes were synthesised by mofiying the L-tyrosine monmer by using polyethylene glycol monomethyl ether (Mn =350) corresponding tosylate (**2**) (see scheme 1b). The phenolic group of L-Tyrosine in compound **1** was substituted with **2** to get PEG-lated L-Tyrosine monomer (**3**). The monomer (**3**) was subjected to melt polymerization with aliphatic diols such as 1,6- hexane diol; 1,8-octane diol; 1,10-decane diol; 1,12-dodecane diol and 1,4-cyclohexane dimethanol

(CHDM) (which provided enough structural diversity to tune hydrophobicity of the backbone) to yield polymers as shown in scheme-4b. The polymer synthesis in one-pot reaction at 150°C was performed involving two step produce 3-8 oligomeric chains (in N_2 purge state) which further polycondensed to yield L-tyrosine based poly(ester-urethane)s under high vacuum. The occurrence of the melt polymerization was confirmed by NMR spectroscopy. And the gel permeation chromatograms showed mono-modal distributions and the polymers were produced in moderate molecular weights in the range of M_n = 4.0 to 14.4 × 10^3 g/mol and M_w = 7.5 to 24.8 × 10^3 g/mol. It is observed that there is a linear increment in the molecular weights of the polymers with increase in the carbon atoms in diols employed in polymerization reaction.[163] Confocal laser scanning microscope (CLSM) was employed to visualize cellular internalization of DOX in MCF 7 cells after staining the nucleus with DAPI. The DOX was imaged in the red channel and DAPI was stained in the blue channel. The CSLM images are shown in figure 1.25 a. It was observed that DOX was predominantly internalized into the cell throughout the cytoplasm and within the nucleus of the cells and this was confirmed by the merged image of the DOX and DAPI. This direct evidence supported the endocytosis process involved in uptake of these DOX loaded polymer nanoparticles from L-tyrosine amino acid are compatible to the cells and excellent vehicles for delivering the anti cancer drugs. The L-tyrosine based nanoparticles made the present approach open new opportunity for structural engineering in L-amino acid polymer for the development of biodegradable thermo-responsive nano-carriers.

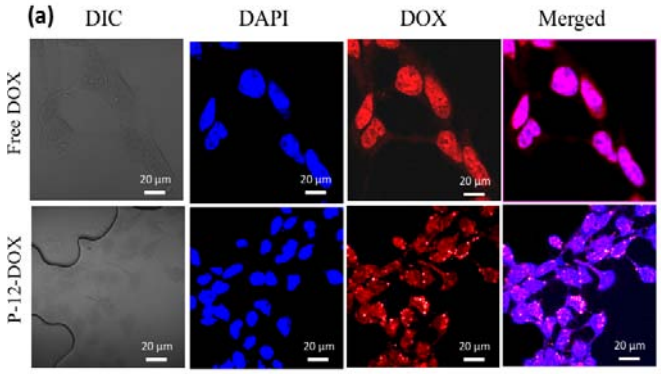

Figure 1.25: *(a) CLSM images of free DOX and DOX loaded* tyrosine polymer *nanoparticles in MCF 7 (9 h incubation).*

1.8. Aim of the thesis

The above literature survey envisages that the development of amphiphilic polymer nano-carriers based on L-amino acid is one of the emerging areas in the drug delivery research. The potential of L-amino acid based biodegradable polymers are still untapped to maximize their application in biomedical filed and new polymers structures are required to be designed and developed. In this thesis, new amphiphilic polyester nano-carriers were designed through the thermo selective melt polycondensation approach developed in our group for L-amino acids. Efforts were also taken to study the molecular self-assembly of the polymer carriers and explored their potential for drug delivery applications. Two new melt polymerizable fluorophore diols were designed based on oligo-phenylenevinylene (OPV) and tetraphenylethylene (TPE) to introduce aromatic π-stack induced aggregates and aggregation induced emission (AIE), respectively inthe L-Amino backbone. These photophysical phenomena were further exploited to constructed multi-color tunable FRET probes and their bio-imaging application was demonstrated in cancer cell lines. The over all achievements of the thesis work in schematically shown below in figure 1.26.

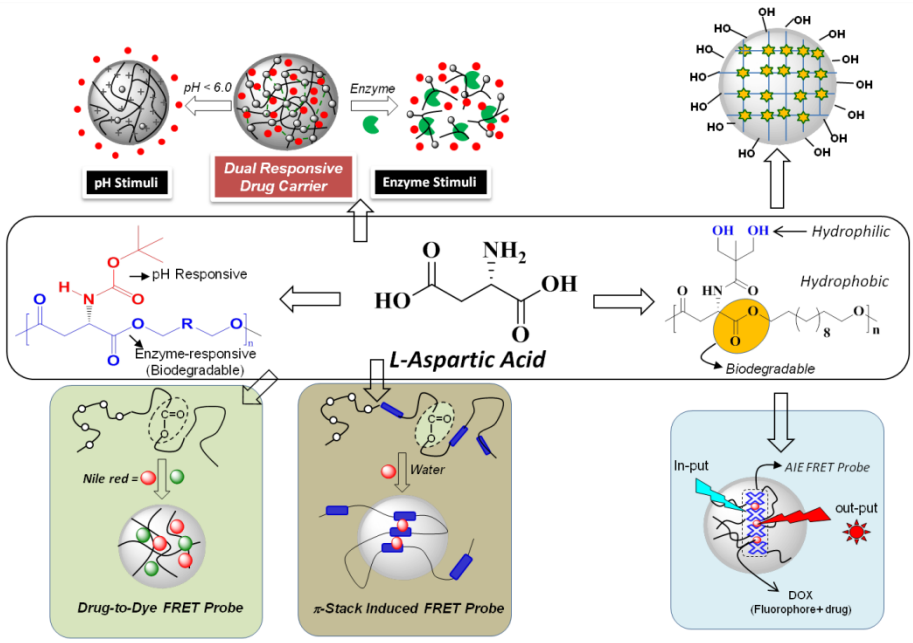

Figure 1.26: *L-Aspartic acid based polymer nano-carriers developed in this thesis work.*

The thesis work is described in the subsequent four chapters. In chapter 2, new classes of enzyme and pH responsive amphiphilic polyester based on L-aspartic acid was deign and developed through thermo-selective melt tranesterification polymerization process. The amphiphilic polymers were self-assembled to nano-carriers and their multiple drug

delivering capabilities were investigated in detail. In chapter 3, π-conjugated fluorophore-tagged amphiphilic L-aspartic acid polyester nano-assemblies were tailor-made using polymerizable oligo-phenylenevinylene (OPV) derivatives and their blue fluorescent nano-assemblies were explored for the contraction of biodegradable FRET probe. The action of FRET probe was studied in detail by photophysical techniques and their in vitro live cell bio-imaging was demonstrated in cervical and breast cancer cell lines. In chapter 4, aggregation induced emission (AIE) concept was introduced in the L-aspartic acid polymer nano-carriers by incorporating tetraphenylethylene (TPE) in the amphiphilic polyester backbone and the resultant blue-luminescent TPE-tagged nano-carriers were employed as multi-colour tunable FRET bio-probes for the entire visible light imaging from blue-to-green-to-red. In chapter 5, new classes of hydroxyl and carboxylic functionalized polyesters were cleverly deigned in L-aspartic acid polymer system for both loading and delivering of anticancer drug as well as conjugating cisplatin drug in single polymer platform. TPE-tagged fluorcenet nano-assemblies were also explored to build new theranostic FRET probe for simultaneous drug delivery and bio-imaging. The last chapter summerizes the thesis work and put forward the direction for future research. The new classes of amphiphilic polyesters designed and developed based on L-aspartic acid residues in the thesis are new entries as enzymatic-biodegradable polymers in the literature; hence they would be expected to be very important nano-carriers for long-term application in the biomedical field.

References

1. A. Sudhakar *J. Cancer Sci Ther.* **2009**, *1*, 1-7.
2. L. Y. T. Chou; K. Ming; W. C. W. Chan *Chem. Soc. Rev.* **2011**, *40*, 233-245.
3. S. K. Sahoo; S. Parveen; J. J. Panda *Nanomedicine: Nanotechnology, Biology, and Medicine*, **2007**, *3*, 20-31.
4. R. Kanasty; J. R. Dorkin; A. Vegas; D. Anderson *Nat. Mater.* **2013**, *12*, 967-977.
5. S. V. Vinogradov; T. K. Bronich; A. V. Kabanaov *Adv. Drug. Deliv. Rev.* **2002**, *54*, 135-147.
6. X-L. Li; N. Hao; H-Y. Chen; J-J. Xu *Anal.Chem.* **2014**, *86*, 10239-10245.
7. V. P. Chauhan; R. K. Jain Nat. Mater. 2013, 12, 958-962.
8. J. Shi; P. W. Kantoff; R. Wooster; O. C. Farokzhad *Nat. Rev. Cancer* **2017**, *17*, 20-37.
9. M. E. Davis; Z. G. Chen; D. M. Shin *Nat. Rev. Drug Discov.* **2008**, *7*, 771-782.
10. S. Senapati; A. K. Mahanta; S. Kumar; P. Maiti *Signal Transduct. Target Ther.* **2018**, *3*, 1-19.
11. A. M. E. Abdalla; L. Xiao; M. W. Ullah; M. Yu; C. Ouyang; G. Yang *Theranostics* **2018**, *8*, 533-548.
12. K. M. Skubitz *Cancer Investigation* **2003**, *2*, 167-176.
13. J. Shi; A. R. Votruba; O. C. Farokhzad; R. Langer *Nano Lett.* **2010**, *10*, 3223-3230.
14. Y. Tabata; Y. Murakami; Y. Ikade *J.Control. Release* **1998**, *50*, 123-133.
15. H. Maeda; Y. Matsumura *Crit. Rev. Ther. Drug. Carrier Syst.* **1989**, *6*, 193-210.
16. W. J. Gradishar *Expert Opin. Pharmacother.* **2006**, *7*, 1041-1053.
17. W. J. Gradishar, S. Tjulandin, N. Davidson, H. Shaw, N. Desai, P. Bhar, M. Hawkins, J. O. Shaughnessy *J. Clin. Oncol.* **2005**, *23*, 7794-7803.
18. F. Fuertges, A. Abuchowski *J. Control. Release* **1990**, *11*, 139-148.
19. M. L. Graham *Adv. Drug Deliv. Rev.* **2003**, *55*, 1293-1302.
20. T. Sun, S. Zhang, B. Pang, D. C. Hyun, M. Yang, Y. Xia *Angew. Chem. Int. Ed.* **2014**, *53*, 12320-12364.
21. S. Wilhelm; A.J. Tavares; Q. Dai; S. Ohta; J. Audet; H. F. Dvorak; W. C. W. Chan *Nat. Rev. Mater.* **2016**, *14*, 1-12.
22. K. Riehemann; S. W. Schneider; T. A. Luger; B. Godin; M. Ferrari; H. Fuchs *Angew. Chem. Int. Ed.* **2009**,*48*, 872-897.
23. S. W. Tas; C. X. Maracle; E. Balogh; Z. Szekanecz *Nat. Rev. Rheumatol.* **2015**, *164*, 1-12.
24. C. E. Petre; D. P. Dittmer *Int. J. Nanomedicine* **2007**, *2*, 277-288.
25. Y. Matsumura, H. Maeda *Cancer Res.* **1986**, *46*, 6387-6392.
26. A.S. Narang; S. Varia *Adv. Drug. Deliv. Rev.* **2011**, *63*, 640-658.

27. J. Fang; H. Nakamura; H. Maeda *Adv. Drug. Deliv. Rev.* **2011**, *63*, 136-151.
28. H. Kobayashi; B. Turkbey; R. Watanabe; P. L. Choyke *Bioconjugate Chem.* **2014**, *25*, 2093-2100.
29. P. Decuzzi; B. Godin; T. Tanaka; S-Y. Lee; C. Chiappini; X. Liu; M. Ferrari *J. Control. Release* **2010**, *141*, 320-327.
30. R. A. Petros; J. M. DeSimone *Nat. Rev. Drug. Discov.* **2010**, *9*, 615-627.
31. T. Nomura; N. Koreeda; F. Yamashita; Y. Takakura; M. Hashida *Pharm. Res.* **1998**, *15*, 128-132.
32. S. Hu-Lieskovan; J. D. Heidel; D. W. Bartlett; M. E. Davis; T. J. Triche *Cancer Res.* **2005**, *65*, 8984-8992.
33. L. Y. Qiu; Y. H. Bae *Pharm. Res.* **2006**, *23*, 1-30.
34. J. A. Champion; S. Mitragotri *PNAS*, **2006**,*103*, 4930-4934.
35. M. W. Tibbitt; J. E. Dahlman; R. Langer *J. Am. Chem. Soc.* **2016**, *138*, 704-717.
36. D. Rosenblum; N. Joshi; W. Tao; J. M. Karp; D. Peer *Nat. Commun.* **2018**, *9*, 1-12.
37. M. E. Fox; F. C. Szoka; J.M. J. Frechet *Acc. Chem. Res.* **2009**,*42*, 1141-1151.
38. M. Mazza; R. Notman; J. Anwar; A. Rodger; M. Hicks; G. Parkinson; D. McCarthy; T. Daviter; J. Moger; N. Garrett; T. Mead; M. Briggs; A. G. Schatzlein; I. F. Uchegbu *ACS Nano* **2013**, *7*, 1016-1026.
39. K. Li; S. Wang; S. Wen; Y. Tang; J. Li; X. Shi; Q. Zhao *ACS Appl. Mater. Interfaces* **2014**, *6*, 12328-12334.
40. A. G. Cheetham; P. Zhang; Yi-an Lin; L. L. Lock; H. Cui *J. Am. Chem. Soc.* **2013**, *135*, 2907-2910.
41. N. Larson; H. Ghandehari *Chem. Mater.* **2012**, *24*, 840-853.
42. K. Knop; R. Hoogenboom; D. Fischer;U. S. Schubert *Angew. Chem. Int. Ed.* **2010**, *49*, 6288-6308.
43. D. Sutton; N. Nasongkla; E. Blanco; J. Gao *Pharm. Res.* **2007**, *24*, 1029-1046.
44. A. Pitto-Barry; N. P. E. Darry *Polym. Chem.* **2014**, *5*, 3291-3297.
45. Y. Zhang; Y. Huang; S. Li *AAPS PharmSciTech* **2014**, *15*, 862-871.
46. F. Meng; Z. Zhong *Phys. Chem. Lett.* **2011**, *2*, 1533-1539.
47. W. Li; T. Luo; Y. Yang; X. Tan; L. Liu *Langmuir* **2015**, *31*, 5141-5146.
48. L. Xu; K. F. Pirollo; E. H. Chang *J. Control. Release* **2001**,*74*, 115-128.
49. M. Marty *The Breast* **2001**, *2*,28-33
50. C. F. Jehn; T. Boulikas; A. Kourvtaris; K. Possinger; D. Lufitner *Anticancer Realease* **2007**, *27*,471-476.
51. P. C. Lyon; L.F. Griffiths; J. Lee; D. Chung; R. Carlisle; F. Wu; M. R. Middleton; F. V. Gleeson; C. C. Coussios *J. Ther. Ultrasound* **2017**, *5*, 28-35.
52. J. M. Löhr; S. L. Haas; W.-O. Bechstein; G. Bodoky; K. Cwiertka; W. Fischbach;U. R. Fölsch; D. Jäger; D. Osinsky; J. Prausova; W. E. Schmidt; M. P. Lutz *Annals of Oncology* **2012**, *23*, 1214-1222.
53. R. Duncan *Nat. Rev. Cancer* **2006**, *6*, 688-700

54. A. Nori; K. D. Jensen; M. Tijerina; P. Kopeckova; J. Kopecek *Bioconjugate Chem* **2003**, *14*, 44-50.
55. F. Gu; L. Zhang; B. A. Teply; N. Mann; A. Wang; A. F. Radovi-Moreno; R. Langer, O. C. Farokhzad *PNAS* **2008**, *105*, 2586-2591.
56. L. W. Seymour; D. R. Ferry; D. Anderson; S. Hesslewood; P. J. Julyan; R. Poyner; J. Doran; A. M. Young; S. Burtles; D. J. Kerr *J. Clin. Oncol.* **2002**, *20*, 1668-1676.
57. T. Kakudo; S. Chaki; S. Futaki; I. Nakase; K. Akaji; T. Kawakami; K. Maruyama; H. Kamiya; H. Harashima *Biochemistry* **2004**, *43*, 5618-5628.
58. A. K. Patri; A. Myc; J. Beals; T. P. Thomas, N. H. Bander; J. R. Baker, Jr. *Bioconjugate Chem.* **2004**, *15*, 1174-1181.
59. D. A. Cheresh *Cancer Metastasis Rev.* **1991**, *10*, 3-10.
60. M. Oba; K. Aoyagi;K. Miyata; Y. Matsumoto; K. Itaka; N. Nishiyama; Y. Yamasaki; H. Koyama; K. Kataoka *Mol. Pharm.* **2008**, *5*, 1080-1092.
61. N. Nasongkla; E. Bey; J. Ren; H. Ai; C. Khemtong; J. S. Guthi; S. F. Chin; A. D. Sherry; D. A. Boothman; J. Gao *Nano Lett.* **2006**, *6*, 2427-2430.
62. A. Gabizon; H. Shmeeda; A. T. Horwitz; S. Zalopsky *Adv. Drug Deliv. Rev.* **2004**, *56*,1177-1192.
63. P. S. low; W. A. Henne; D. D. Doorneweerd *Acc. Chem. Res.* **2007**,*41*,120-129.
64. N. U. Deshpande; M. Jaykannan, *Biomacromolcules* **2018,** *19*, 3572-3585.
65. S. V. Boddapati; G. G. M. D'Souza; S. Erdogan; V. P. Torchilin; V. Weissing *Nano Lett.* **2008,** *8*,2559-2563.
66. J. Callahan; J. Kopecek *Biomacromolecules* **2006**, *7*, 2347-2356.
67. N. Pante; M. Kann *Mol. Bio. Cell* **2002,** *13*, 425-434.
68. C. W. Pounton; K. M. Wagstaff; D. M. Roth; G. W. Moseley; D. A. Jans *Adv. Drug Deliv. Rev.* **2007,** *59*, 698-717.
69. C-K. Chan; T. Senden; D. A Jans *Gene Ther.* **2000**, *7*,1690-1697.
70. K. T. Oh; H. Yin; E. S. Lee; Y. H. Bae *J. Mater. Chem.* **2007**, *17*, 3987-4001.
71. M. A.C. Stuart; W. T. S. Huck; J. Genzer; M. Muller; C. Ober; M. Stamm; G. B. Sukhorukov; I. Szleifer; V. V. Tsukruk; M. Urban; F. Winnik; S. Zauscher; I. Luzinov; S. Minko *Nature Mater.* **2010**, *9*, 101-113.
72. L. E. Gerweck; K. Seetharaman *Cancer Res.* **1996**, *56*, 1194-1198.
73. M. DAmaghi; Z. W. Wojtkowiak; R. J. Gillies *Front Psychol.* **2013**, *4*, 1-9.
74. S. Mura; J. Nicolas; P. Couvreur *Nature Mater.* **2013**, *12*, 991-1003.
75. X. Hao; X. Hu; C. Zang; S. Chen; Z. Li; X. Yang; H. Liu; G. Jia; D. Liu; K. Ge; X-J. Liang; J. Zhang *ACS Nano* **2015**, *9*, 9614-9625.
76. J. Liu; Y. Huang; A. Kumar; A. Tan; S. Jin; A. Mozhi; X-J. Liang *Biotechnol. Adv.***2014**, *32*, 693-710.
77. D. W. Pack; A. S. Hoffman; S. Pun; P. S. Stayton *Nature Rev. Drug Discov.* **2005**, *4*, 581-593.

78. Y. Bae; S. Fukushima; A. Harada; K. Kataoka *Angew.Chem. Int. Ed.* **2003**, *42*, 4640-4643.
79. Z. Zhang; X. Chen; L. Chen; S. Yu; Y. Cao; C. He; X. Chen *ACS Appl.Mater.Interfaces* **2013**, *5*, 10760-10766.
80. Y. Yu; C-K. Chen; W-C. Law; E. Weinheimer; S. Sengupta; P. N. Prasad; C. Cheng *Biomacromolecules* **2014**, *15*, 524-532.
81. F. Huang; R. Cheng; F. Meng; C. Deng; Z. Zhong *Biomacromolecules* **2015**, *16*, 2228-2236.
82. M. A. Quadir; S. W. Mortan; Z. J. Deng; K. E. Shopsowitz; R. P. Murphy; T.H. Epps, III; P. T. Hammond *Mol. Pharm.* **2014**, *11*, 2420-2430.
83. D. Roy; W. L. A. Brooks; B. S. Sumerlin *Chem. Soc. Rev.* **2013**, *42*, 7214-7243.
84. X-L. Sun; P-C. Tsai; R. Bhat; E. M. Bonder; B. Michnik-Khon; A. Pietrangelo *J. Mater. Chem. B* **2015**, *3*, 814-823.
85. N. M. Matsumoto; P. Prabhakaran; L. H. Rome; H. D. Maynard *ACS Nano* **2013**, *7*, 867-874.
86. H. Wei, S-X. Cheng; X-Z. Zhang; R-X. Zhuo *Prog. Polym. Sci.* **2009**, *34*, 893-910.
87. E. A. Rainbolt; J. B. Miller; K. E. Washington; S. A. Senevirathne; M.C. Biewer; D. J. Siegwart; M. C. Stefan *J.Mater. Chem. B* **2015**, *3*, 1779-1787.
88. Y. Cheng; J. Hao; L. A. Lee; M. C. Biewer, Q. Wang; M. C. Stefan *Biomacromolecules* **2012**, *13*, 2163-2173.
89. S. Kashyap; M. Jayakannan *J.Mater. Chem. B* **2014**, *2*, 4142-4152.
90. S. Kashyap; M. Jayakannan *J.Mater. Chem. B* **2015**, *3*, 1957-1967.
91. R. Aluri; M. Jayakannan *Biomacromolecules* **2017**, *18*, 189-200.
92. A. C. W. Lau; C. Wu *Macromolecules* **1999**, *32*, 581-584.
93. Y. Maeda; T. Nakamura; I. Ikeda *Macromolecules* **2002**, *35*, 217-222.
94. R. D. L. Rica; D. Aili; M. M. Stevens *Adv. Drug Deliv.Rev.* **2012**, *64*, 967-968.
95. N. Qiu; J. Gau; Q. Liu; J. Wang; Y. Shen *Biomacromolecules* **2018**, *19*, 2308-2319.
96. M. Maier; N. Kotman; C. Friedrichs; J. Andrieu; M. Wagner; R. Graf, W. S. L. Strauss; V. Mailander; C. K. Weiss; K. Landfester *Macromolecules* **2011**, *44*, 6258-6267.
97. T. Akagi; M. Higashi; T. Kaneko; T. Kida; M. Akashi *Biomacromolecules* **2006**, *7*, 297-303.
98. V. Castelletto; J. E. McKendrick; I. W. Hamley *Lagmuir* **2010**, *26*, 11624-11627.
99. A. V. Fuchs; N. Kotman; J. Andrieu; V. Mailander; C. K. Weiss; K. Landfester *Nanoscale* **2013**, *5*, 4829-4839.
100. K. Guo; C. C. Chu *Biomacromolecules* **2007**, *8*, 2851-2861.

101. L. L. Lock; Z. Tang; D. Keith; C. Reyes; H. Cui *ACS Macro Lett.* **2015**, *4*, 552-555.
102. A. J. Harnoy; M. Buzhor; E. Tirosh; R. Shaharabani; R. Beck; R. J. Amir *Biomacromolecules* **2017**, *18*, 1218-1228.
103. J. Wu; L. Zhao; X. Xu; N. Bertrand; W II Choi; B. Yameen; J. Shi; V. Shah; M. Mulvale; J. L. MacLean; O. C. Farokhzad *Angew. Chem. Int. Ed.* **2015**, *54*, 9218-9223.
104. J-K. Ryu; M. J. Choi; T-I. Kim; H-R. Jin; K-D. Kwon; D. Batbold; K-M. Song; M-H. Kwon; G. N. Yin; M. Lee; S. W. Kin; J-K. Suh *Andrology **2013**, 1*, 216-222.
105. S. Samarajeewa; R. Shrestha; M. Elsabahy; M. Karwa; A. Li; R. P. Zentay; J. G. Kostelc; R. B. Dorshow; K. L. Wooley *Mol. Pharm.* **2013**, *10*, 1092-1099.
106. M. J. Heffernan; N. Murthy *Anal Bio. Eng.* **2009**, *37*, 1993-2002.
107. W. Lu; X. Wang; R. Cheng; C. Deng; F. Meng; Z. Zhong *Polym. Chem.* **2015**, *6*, 6001-6010.
108. W. Xu; J. Ding; X. Chen *Biomacrmolecules* **2017**, *18*, 3291-3301.
109. J. Wang; X. Sun; W. Mao; W. Sun; J. Tang; M. Sui; Y. Shen; Z. Gu *Adv.Mater.* **2013**, *25*, 3670-3676.
110. A. Klaikherd; C. Nagamani; C. Thayumanavan *J. Am.Chem. Soc.* **2009**, *131*, 4830-4838.
111. M. H. Lee; J. L. Sessler; J. S. Kim *Acc. Chem. Res.* **2015**, *48*, 2935-2946.
112. M. Ikeda *Adv Biochem Eng Biotechnol* **2003**, *79*, 1-35.
113. A. Strecker; J. Liebigs *Ann. Chem.***1850**, *75*, 27.
114. H. T. Bucherer; H. T. Fischbeck, *J. Prakt. Chem.***1934**, *140*, 69.
115. H. T. Bucherer; W. Steiner *J. Prakt. Chem.***1934**, *140*, 291.
116. M. Beller; M. Eckert *Angew. Chem.* **2000**, *112*, 1026.
117. M. Beller,; M. Eckert *Angew. Chem. Int. Ed.***2000**, *39*, 1010.
118. M. Breuer; K. Ditrich; T. Habicher; B. Hauer; M. Kebeler; R. Sturmer; T. Zelinski *Angew. Chem. Int. Ed.* **2004**, *43*, 788-824.
119. S. B. H. Kent *Chem. Soc. Rev.* **2009**, *38*, 338-351.
120. S. Chandrudu; P. Simerska; I. Toth *Molecules* **2013**, *18*, 4373-4378.
121. B. Bacsa; K. Horvati; S. Bosze; F. Andreae; C. O. Kappe *J Org Chem.* **2008**, *73*, 7532-7542.
122. I. W. Hamley *Soft Matter*. **2011**, *7*, 4122-4138.
123. A. Trent; R. Marullo; B. Lin; M. Black; M. Tirrell *Soft Matter*. **2011**, *7*, 9572-9582.
124. V. Castelletto; I. W. Hamley; J. Perez; L. Abezgauz; D. Danino *Chem. Commun*. **2010**, *46*, 9185-9187.
125. J. J. Panda; V. S. Chauhan *Polym. Chem.***2014**, *5*, 4418-4436.
126. C. Tang; F. Qiu; X. Zhao *J. Nano Mat.* **2013**, *2013*, 1-9.
127. S. Yamada; K. Koga; A. Sudo; M. Goto; T. Endo *J. Polym. Sci. Polym. Chem.***2013**, *51*, 3726-3731.

128. C. Deng; J. Wu; R. Cheng; F. Meng; H-A. Klok; Z. Zhong *Prog Polym Sci.* **2014**, *39*, 330-364.
129. A. C. Farthing; R. J. W. Reynolds *Nature* **1950**, *165*, 647-657.
130. D. Coleman; A. C. Farthing *J Chem Soc***1950,** 3218-3222.
131. T. J. Deming, *J. Polym. Sci. Polym. Chem.***2000**, *38*, 3011-3018.
132. M-T. Popescu; G. Liontos; A. Avgeropoulosc; C.Tsitsilianis *Soft Matter* **2015**, *11*, 331-342.
133. T. Xing; B. Lai; X. Ye; L. Yan *Macromol Biosci* **2011**, *11*, 962.
134. J. R. Kramer; T. J. Deming *Biomacromolecules* **2012**, *13*, 1719-1723.
135. J. Helder; F. E. Kohn; S. Sato; J. W. van den Berg; J. Feijen, *Makromol. Chem. Rapid Commum.***1985**, *6*, 9-14.
136. P. J. A. in 't Veld; P. J. Dijkstra; J. Feijen *Makromol. Chem.***1992**, *193*, 2713-2730.
137. G. John; M. Morita *Macromol. Rapid Comm.* **1999**, *20*, 265-268.
138. N. Arabuli; G. Tsitlanadze; L. Edilashvili; D. Kharadze; T. Goguadze; V. Beridze; Z. Gomurashvili; R. Katsarava *Macromol. Chem. Phys.***1994**, *195*, 2279-2289.
139. M. A. De Wit; Z. X. Wang; K. M. Atkins; K. Mequanint; E. R. Gillies *J. Polym. Sci. Pol. Chem.***2008**, *46*, 6376-6392.
140. K. M. Atkins; D. Lopez; D. K. Knight; K. Mequanint; E. R. Gillies *J. Polym. Sci. Pol. Chem.***2009**, *47*, 3757-3772.
141. K. Guo; C. C. Chu; E. Chkhaidze; R. Katsarava *J. Polym. Sci. Pol. Chem.* **2005**, *43*, 1463-1477.
142. K. Guo; C. C. Chu *J. Polym. Sci. Pol. Chem.* **2007**, *45*, 1595-1606.
143. H. Sun; R. Cheng; C. Deng; F. Meng; A. A. Dias; M. Hendriks;J.Feijen;Z. Zhong *Biomacromolecules* **2015**, *16*, 597-605.
144. Y. Yu; J. Zou; C. Cheng *Polym. Chem.*, **2014**, *5*, 5854
145. Y.B. Lim; C-H. Kim; K. Kim; S. W. Kim; J.-S. Park *J. Am. Chem. Soc.*,**2000**, *122*, 6524-6525.
146. N. Kolishetti; S. Dhar; P. M. Valencia; L. Q. Lin; R. Karnik; S. J. Lippard; R. Langer; O. C. Farokhzad *PNAS* **2010**, *107*, 17939-17944.
147. N. Kihara; K. Makabe; T. Endo *J. Polym. Sci., Part A: Polym. Chem.***1996**, *34*, 1819.
148. A. Nagai; J. Ishikawa; H. Kudo; T. Endo *J. Polym. Sci., Part A: Polym. Chem.***2004**, *42*, 1143.
149. J. Yu; F. Lin; P. Lin; Y. Gao; M. L. Becker *Macromolecules*, **2014**, *47*, 121-129.
150. F. Lin; J. Yu; W. Tang; J. Zheng; S. Xie; M. L. Becker *Macromolecules*, **2013**, *46*, 9515-9525.
151. J. Zhou; A. P. Defante; F. Lin; Y. Xu; J. Yu; Y. Gao; E. Childers; A. Dhinojwala; M. L. Becker *Biomacromolecules*, **2015**, *16*, 266-274.

152. S. Li; J. Yu; M-B. Wade; G. M. Policastro; M. L. Becker *Biomacromolecules*, **2015**, *16*, 615-624.
153. G. M. Policastro; F. Lin; L.A. Smith Callahan; A. Esterle; M. Graham; K. S. Stakleff; M. L. Becker *Biomacromolecules*, **2015**, *16*, 1358-1371.
154. J. Yu; F. Lin; M. L. Becker *Macromolecules*, **2015**, *48*, 2916-2924.
155. S. I. Ertel; J. Kohn *J. Biomed. Mater. Res.***1994**, *28*, 919-930.
156. M. H. R. Magno; J. Kim; A. Srinivasan; S. McBride; D. Bolikal; A. Darr; J. O. Hollinger; J. Kohn *J. Mater. Chem.*, **2010**, *20*, 8885-8893.
157. S. Anantharaj; M. Jayakannan *Biomacromolecules,* **2012**, *13*, 2446- 2455.
158. S. Anantharaj; M. Jayakannan *Biomacromolecules,* **2015**, *16*, 1009- 1020.
159. R. Aluri; M. Jayakannan *Polym. Chem.*, **2015**, *6*, 4641-4649.
160. S. Anantharaj; M. Jayakannan *J. Polymer Sci., Part A: Polym. Chem***, 2016,** *54***,** 1065-1077.
161. S. Anantharaj; M. Jayakannan *J. Polymer Sci., Part A: Polym. Chem***, 2016,** *54***,** 2864-2875.
162. R. Aluri; M. Jayakannan *Biomacromolecules* **2017**, *18*, 189-200.
163. R. Aluri; S. Saxena; D. C. Joshi; M. Jayakannan *Biomacromolecules* **2018**, *19*, 2166-2181.

Chapter 2

Enzyme and pH Dual Responsive L-Amino acid Based Biodegradable Polyester Nano-carrier for Multi-drug Delivery to Cancer Cells

Abstract

We report a new pH and enzyme dual responsive biodegradable polymer nano-carrier to deliver multiple anticancer drugs at the intracellular compartment in cancer cells. Natural L-aspartic acid was converted into multi-functional monomer and polymerized to yield new classes of biodegradable aliphatic polyester in-build with pH responsiveness. The transformation of side chain BOC urethanes into cationic NH_3^+ in the acidic endosomal environment disassembled the polymers nanoparticles (pH trigger-1). The biodegradation of aliphatic polyester backbone by esterase enzyme ruptured the nano-assemblies and released the drugs in the cytoplasm (trigger-2). The polymer scaffolds were capable of delivering multiple drugs such as doxorubicin (DOX), topotecan (TPT), and curcumin (CUR). The cytotoxicity of the nascent and drug loaded nanoparticles were tested in cervical (HeLa) and breast cancer (MCF 7) cell lines. The nascent polymer nano-scaffolds were found to be non-toxic to cells whereas their drug loaded nano-particles exhibited excellent killing. Confocal microscopic images revealed that the drug loaded polymer nanoparticles were taken up by the cells and the dual degradation process delivered the drugs to the nucleus and established the proof-of-concept. The present investigation opens up new platform for L-amino acid based polyester scaffolds, for the first time, in the intracellular drug delivery in cancer treatment.

2.1. Introduction

Polymer nano-assemblies responsive to intracellular stimuli are emerging as important class of nano-carriers for delivering anticancer drugs and genes in cancer therapy.[1-2] Polymer nano-carriers are typically taken up by the cells through endocytosis process and they are internalization by acidic early and late endosomes (6.0 – pH = 5.0) at cellular level (see Figure 2.1).[3] Subsequent disassembly or degradation of polymer assemblies at the lysosomal compartments by enzymes delivered the drugs/genes in the cytoplasm for apoptosis or cell death.[4] Therefore, the development of intracellular multi-stimuli polymers provide excellent opportunity to enhance the drug delivering capabilities of polymer nano-assemblies.[5] In the last few years, polymer scaffolds having intracellular responsiveness to enzyme,[6-11] pH [12-19] or combination of these triggers together [20-23] were reported for drug delivery. In most of these examples pH and enzyme were employed to disassemble the polymer scaffold; unfortunately, the fate of the digestion (or biodegradation) of the remaining long polymer chains were not clearly understood. This is partially associated with the non-biodegradation of majority of the synthetic polymer carriers and also the selection of their monomer constituents from un-natural resources (see figure 2.1). Hence, it would be more appropriate to design biodegradable polymer nano-carriers based on biological monomer resources for cancer treatment and biomedical applications.

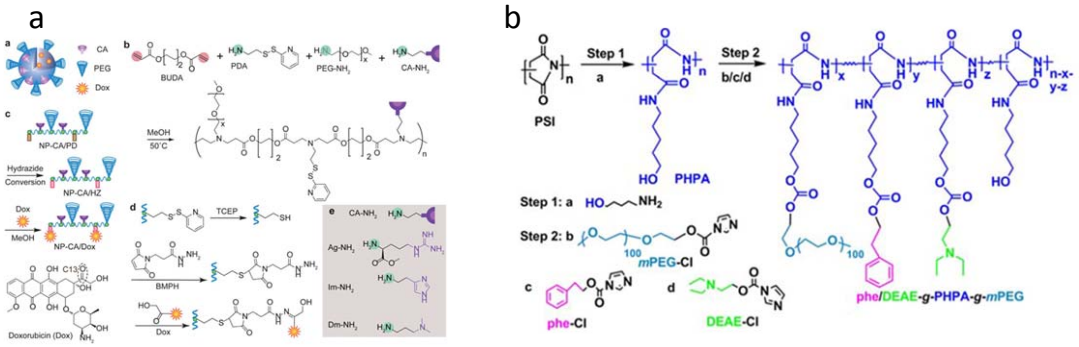

Figure 2.1: *Figure: DOX conjugated cationic poly(b-amino ester) with disulphide linkages in the side chains (Adapted from Fang et al, Nanoscale* **2012**, *4,* 7012-7020*) (a), Polyaspartamide based dual thermo- and pHsensitive phe/DEAE-g-PHPA-g-mPEG (b) (adappted from Ma et al, Polym. Sci., Part A: Polym. Chem.* **2016**, *54,* 879-888*).*

Among the natural resources, L-amino acids are particularly interesting since their sequence and structure control the three dimensional assemblies of proteins and their enzymatic action in biological system.[24-25] L-Amino acid based synthetic amphiphilic oligo-peptides[26] and diblock polypeptides[27-30] were tailor-made and their supramolecular nano-scaffolds were employed for tissue engineering,[31-32] drug and gene delivery,[33-34] etc. These higher secondary structures and well defined architectures were obtained due to spefic molecular interactions between the amino acid residues as well as the strong hydrogen bonding amongst the amide bonds of the polypeptides. These well defined architectures can be further sued for drug loading and delivery applications (see figure 2.2).

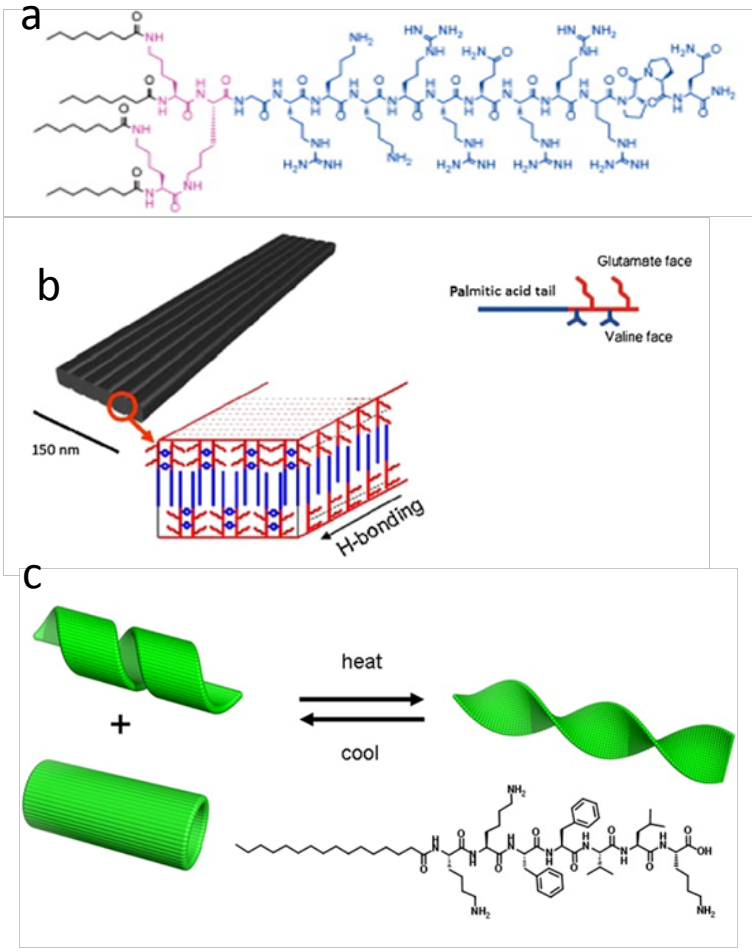

Figure 2.2: *Self assembled nanotubes conjugated TAT peptide as drug (PTX) delivery agents. (Adapted from Zhang et al, ACS Nano,* **2013**, *7,* 5965-5977*) (a), Grooves on surface of nanobelts of the self-assembled peptide amphiphile (b), twisted fibres and nanotubes from the amyloid-β peptide KLVFF (C16-KKFFVLK) (both b and c adapted from Dehsorkhi et al, J. Pept. Sci.***2014**, *20*, 453-467*).*

Unfortunately, these synthetic peptides were known to encounter difficulty for biodegradation at the intracellular level [35]. Digestive enzymes such as α-chymotrypsin and trypsin (available in intestine) were found to be highly specific in action to cleave peptide sequences in proteins. For example, α-chymotrypsin-enzyme selectively cleaves C-terminal of phenyl alanine, tyrosine and tryptophan peptide linkages [36-38] whereas trypsin-enzyme cleaves the C-terminal of arginine and lysine in peptides [7]. It is rather difficult to predict or programme the enzymatic biodegradation of synthetic polypeptides. GSH responsive polymers were succefully developed for drug delivery as shown in Figure 2.3.

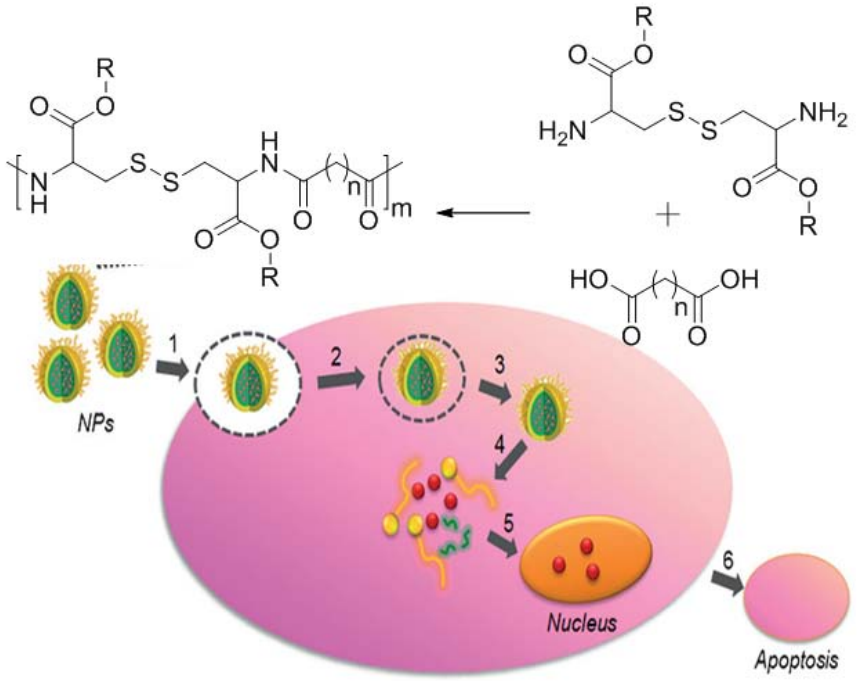

Figure 2.3: *S-S and amide bond containing enzymatic and Reduction sensitive and degradable SS- Polymer for biomedical applications (Adapted from Sun et al, Biomacromolecules,* **2015***, 16,* 597-605*).*

Almost 45 % of the pro-drugs in the market are based on aliphatic ester chemical linkages; thus, the design and development of new enzyme biodegradable polyester from L-amino acid resources in combination with pH responsiveness would provide new classes of polymer nano-carriers that are cleavable in endosome-lysosome compartments (see figure 2.4) [39]. Polymers with aliphatic ester chemical linkages (or polyesters) are excellent biodegradable systems under physiological

conditions [40-41]. Unfortunately, aliphatic polyesters based on L-amino acid natural resources with appropriate amphiphilicity for drug delivery at the intracellular compartmentsare not reported till date. This is associated with the lack of availability of appropriate synthetic methodology to design aliphatic polyester nano-scaffolds from L-amino acids.

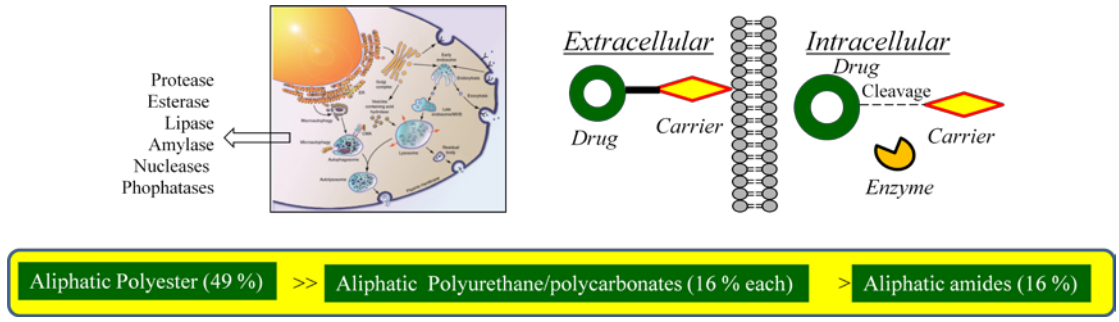

Figure 2.4: *Chemical linkages present in pro drugs based on the intracellular enzymes in living oragnanisms, with more than 49% pro drugs based on ester chemical linkages (Concept adapted from Rautio et al Nat. Reviews,***2008**, *7*, 255-270 *).*

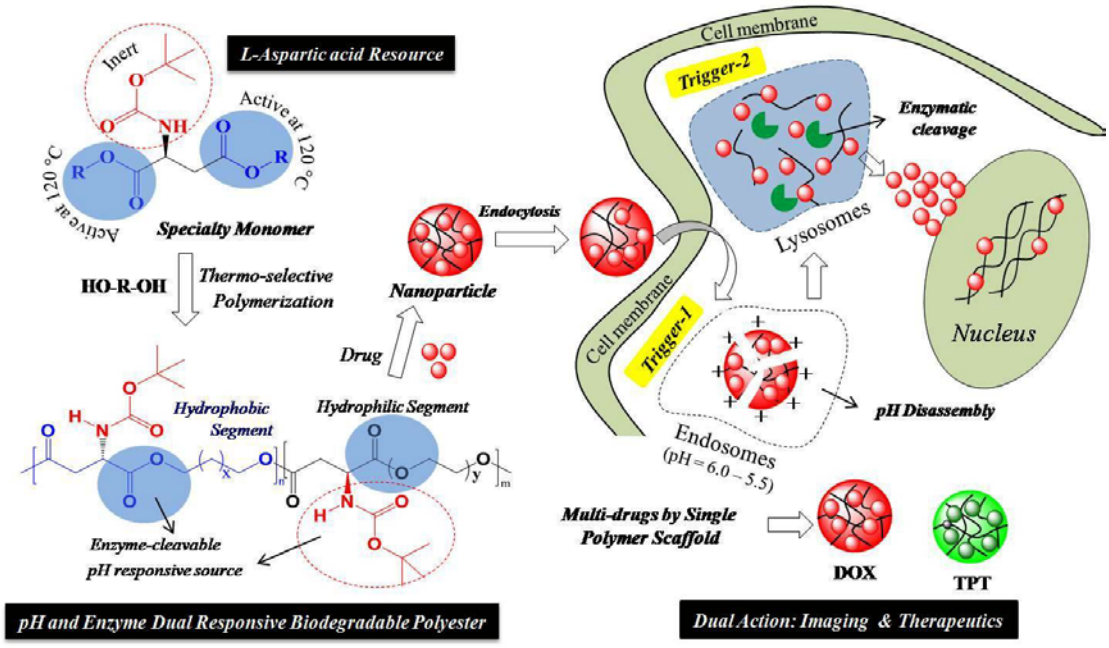

Figure 2.5: *pH Responsive and enzyme biodegradable polymer nano-assemblies from L-amino acid is developed for multiple-drug delivery at the intracellular compartments to cancer cells.*

To accomplish this goal, here we propose a new lysosome enzyme biodegradable amphiphilic polyester nano-carriers having pH responsiveness from L-

amino acid resources (see figure 2.5). For this purpose, thermo-selective melt polycondensation strategies earlier developed from our laboratory for L-amino acid resources[42-46] were employed to make new classes of amphiphilic biodegradable polymer nano-assemblies. New classes of amphiphilic biodegradable polyester having side chain BOC urethane were designed from L-aspartic acid by thermo-selective melt polymerization approach. These amphiphilic polyesters were self-assembled into stable nanoparticles and they also exhibited excellent nano-scaffold capabilities for loading a wide range of fluorescent anticancer drugs. At low pH = 6.0 to 4.0; the BOC urethane pendants in the polyesters were transformed into cationic species and in this process the nanoparticle disassembled to deliver the loaded drugs *(trigger-1).* The aliphatic polyester backbone was stable at extracellular condition (pH = 7.4) but readily underwent biodegradation in the presence of lysosomal-enzymes to deliver drugs (*trigger-2*). The amphiphilicity of the polyester backbone was fine-tuned carefully by varying the composition of hydrophilic and hydrophobic diolsin the polymer synthesis (see Figure **2.5**). *In vitro* drug release studies were performed at different pH (2.0 to 7.4) and in the presence of esterase-enzyme to ascertain the disassembly and biodegradation processes, respectively. Multiple anti-cancer drugs such as doxorubicin (DOX), topotecan (TPT) and curcumin (CUR) were loaded in the polymer scaffold and their cytotoxicty were tested in both cervical (HeLa) and breast cancer (MCF 7) cell lines.

2.2 Experimental Section

Materials: L-Aspartic acid, 1,12-dodecandiol, triethylene glycol (TEG), titanium tetrabutoxide ($Ti(OBu)_4$), triethyl amine (Et_3N), trifluoro acetic acid (TFA), sodium acetate, glacial acetic acid, phosphate buffer saline (PBS), Nile red (NR), topotecan hydrochloride (TPT), curcumin (CUR), horse liver esterase enzyme, tetrazolium salt: 3-4,5 dimethylthiazol-2,5diphenyltetrazolium bromide (MTT), DMSO, hoechst and 4% paraformaldehyde were purchased from Sigma Aldrich Chemicals and were used without further purification. Di-tert-butyl dicarbonate (BOC anhydride, referred in paper as BOC) was purchased from Spectrochem. Doxorubicin hydrochloride (DOX. HCl) was purchased from Alfa Aesar. Thionyl chloride, methanol, THF, DMSO, toluene, ethyl acetate, pet ether and other solvents were

purchased locally and purified before use. Cervical cancer (HeLa) cells, breast cancer (MCF 7) cells were maintained in DMEM (phenol red containing, Gibco) containing 10% (v/v) fetal bovine serum (FBS) and 1% (v/v) penicillin–streptomycin at 37°C under a 5% CO_2 atmosphere. For all the assays, cells were rinsed with 40 % DPBS (Gibco), trypsinized using 0.05 % trypsin (Gibco) and seeded in 96 well or 6 well (as per experiment) flat bottomed plastic plates (Costar). Fluoromount was obtained from Southern Biotech.

General Procedure: ^{1}H-NMR and ^{13}C-NMR spectra were recorded using 400-MHz JEOL NMR Spectrophotometer. The spectra were recorded in $CDCl_3$ containing TMS as internal standard. The mass analysis of monomers was done by using high resolution mass spectrometry-electro spray ionization-quantitative time-of-flight liquid chromatography-mass spectrometry (HRMS-ESI-Q-time-of-flight LCMS (SynaptG2, Waters)). The mass of degraded polymer intermediates were analyzed using Applied Biosystem 4800 PLUS matrix-assisted laser desorption/ionization (MALDI) TOF/TOF analyzer. Gel permeation chromatography (GPC) analysis was performed using Viscotek VE 1122 pump, Viscotek VE 3580 RI detector and Viscotek VE 3210 UV/Vis detector in tetrahydrofuran (THF) using polystyrene as standards**.** Thermal decomposition and thereby, the stability of polymers were determined using Perkin Elmer Thermal Analyzer STA 6000 model at a heating rate of 10 °C min^{-1} in inert atmosphere. Thermal analysis was done using TAQ20 differential scanning calorimeter (DSC) and the instrument was calibrated with Indium Standards, before carrying out the measurements. Polymer samples were heated to melt before recording their thermograms to remove any prior thermal history of samples. Polymers were heated and cooled at the rate of 10° C/min under nitrogen purge to record their thermograms. Dynamic Light Scattering (DLS) and Zeta potential were done using a Nano ZS-90 apparatus by 633nm red laser (at right angle) from Malvern Instruments. Field emission scanning electron microscopy (FE-SEM) images were obtained using Zeiss Ultra Plus scanning electron microscope. The samples were prepared by dissolving polymers in THF and dispersing in water and further drop casting them on silicon wafers followed by drying and gold coating. Atomic Force Microscopy (AFM) images were obtained in tapping mode using VeecoNanoscope IV instrument and samples were drop casted on freshly cleaved

mica sheets. High Resolution-Transmission Electron Microscopy (HR-TEM) images were recorded using Technai-300 instrument by drop casting aqueous sample on Formvar coated copper grids. LSM confocal microscope was used for cellular uptake images.The absorption spectra were recorded using Perkin Elmer Lambda 45 UV-vis spectrophotometer. The emissions studies were done using SPEX Fluorolog HORIBA JOBINVYON fluorescence spectrophotometer. The steady state emission spectra were recorded using 450 W Xe lamp excitation source. FT-IR spectra of polymers were recorded using BrukeralphaT Fourier transform infrared spectrophotometer.

Synthesis of dimethyl(tert-butoxy carbonyl)-L-aspartate (Monomer 1): Thionyl chloride (16.0 mL, 0.228 mol) was added dropwise into L-aspartic acid (10.1 g, 0.076 mol) in dry methanol (60.0 mL) at 0 °C under nitrogen atmosphere. The reaction mixture was stirred for 24 h at 25 °C under nitrogen atmosphere. The solvent and excess thionyl chloride were distilled off. To this mixture, sodium carbonate (16.0 g, 0.150 mol) in distilled water (160.0 mL) and tetrahydrofuran (80.0 mL) were added with vigorous stirring. This reaction mixture was kept in ice bath (< 5 °C) and BOC anhydride (18.0 mL, 0.082 mol) in THF (80.0 mL) was added dropwise at 0 °C. The content was slowly warmed to 25 °C and the stirring was continued for 12 h under nitrogen atmosphere. THF was distilled off and the product was extracted into ethyl acetate. The organic layer was isolated and dried over anhydrous Na_2SO_4. The solvent was evaporated to obtain the product as white solid mass. It was purified by passing through silica gel column using ethyl acetate and pet ether (1: 6 v/v). Yield =13.2 g (67 %). ^{1}H-NMR (400MHz, $CDCl_3$) δ ppm: 5.47 (s, 1H, -N**H**), 4.56 (s, 1H, -C**H**), 3.74 (s, 3H, COOC**H$_3$**), 3.68 (s, 3H,COOC**H$_3$**), 3.01-2.96 (dd, 1H, C**H$_2$**), 2.84-2.78 (dd, 1H, C**H$_2$**) and 1.43 (s,9H,NHCOO(C**H**$_3$)$_3$). ^{13}C-NMR (100MHz, $CDCl_3$)δ ppm: 171.48, 171.34, 155.33, 80.12, 52.65, 51.95, 49.94, 36.67 and 28.27. HRMS (ESI+): m/z (M+Na)+ calculated for $C_{11}H_{19}NO_6Na$ [M+]: 284.10 ; found: 284.1109.

Synthesis of Homopolyesters: The polymer synthesis is described in detail for P-TEG. Monomer **1** (0.64 g, 0.002 mol) was taken along with triethylene glycol (0.38 g, 0.002 mol) in a test tube shaped polymerization vessel and the content was melted at 100 °C under constant nitrogen purge. Titanium tetrabutoxide (0.01 g, 0.96 mol%) was added as a catalyst and he melt was evacuated under vacuum (0.01 mbar)

and purged with nitrogen to remove the moisture (the procedure was repeated at least thrice). The temperature of the polymerization reactor was increased to 120 °C and stirred for 4 h under nitrogen purge. Subsequently, the melt was subjected to condensation under vacuum (0.01 mbar) for 2 h. At the end of the process, the polymer was obtained as pale yellow viscous solid. It was purified by dissolving in minimum amount of THF, filtered and precipitated in water-methanol mixture (4:1 v/v). Yield= 0.8 g (95%). ^{1}H-NMR (400MHz, $CDCl_3$) δ ppm: 5.57 (bs, 1H, N**H**), 4.57 (bs, 1H, C**H**),4.31-4.19 region (m, 4H, (COOC**H$_2$)$_2$**), 3.73-3.59 (m, 8H, (OCH_2-C**H$_2$-)$_2$**), 3.07-2.96 (dd, 1H, C**H**$_2$), 2.90-2.75 (dd, 1H, C**H**$_2$) and 1.42 (s, 9H, BOC protons). ^{13}C-NMR (100MHz, $CDCl_3$)δ ppm: 171.07, 170.85, 155.42, 80.12, 70.58, 68.89, 64.71, 64.02, 52.77, 52.07, 50.02, 36.85, 28.35 and 28.44. A similar procedure was adopted to make polymer P-DD using 1,12-dodecanol as described above for P-TEG. Monomer 1 (0.65 g, 0.002 mol) and triethylene glycol (0.38 g, 0.002 mol) were weighed in a test tube shaped set up for melt condensation polymerisation and same procedure was followed as mentioned for synthesis of P-DD. Yield: 0.81 g (82 %). ^{1}H NMR (400MHz, $CDCl_3$) δ ppm: 5.48 (bs, 1H-N**H**), 4.53 (bs, 1H-C**H**), 4.14- 4.05 (m, 4H-(NHCOOC**H$_2$**), 3.00-2.77 (m, 2H, NH-C**H$_2$**) , 1.59 and 1.26 (aliphatic DD protons), 1.43 (s, 9H, BOC protons). ^{13}C-NMR (100MHz, $CDCl_3$) δ ppm: 171.25, 171.11, 155.51, 80.06, 65.95, 65.25, 50.10, 36.87, 30.39, 29.62, 29.32, 28.57, 28.37, 25.91.

Synthesis of Amphiphilic Copolyesters: The procedure is described in detail for the copolymer with 50:50 mole ratio of 1,12-dodecandiol and triethylene glycol (for polymer **P-40**). Monomer **1**(0.60 g, 0.002 mol) and triethylene glycol (0.18 g, 0.001 mol) and 1,12-dodecanediol (0.23 g, 0.001 mol), titanium tetrabutoxide (0.01 g, 0.96 mol%) were taken and melt polymerisation was carried out as descibed for P-TEG. Yield: 0.54 g (63 %). ^{1}H-NMR (400MHz, $CDCl_3$) δ ppm: 5.49 (bs, 1H, N**H**), 4.56 (bs, 1H, C**H**), 4.30-4.22 (m, 4H, COO-C**H**$_2$$CH_2O$), 4.16-4.03 (m, 4H-, COO-C**H**$_2$$CH_2CH_2$-), 3.77-3.61 (m, 8H, -C**H**$_2$C**H**$_2$O), 3.07-2.75 (m, 2H, NH-C**H$_2$**), 1.63 and 1.26 (aliphatic protons) and 1.44 (s, 9H, BOC protons). ^{13}C-NMR (100MHz, $CDCl_3$) δ ppm: 171.14, 155.50, 80.07, 70.61, 70.40, 68.96, 65.97, 65.26, 64.73, 64.02, 50.08, 36.89, 29.62, 29.31, 28.57, 28.38 and 25.09. FT-IR (cm^{-1}): 3376 (involved in H-

bond), 2931, 2849, 1709 (ester H-bond), 1506, 1463, 1369, 1281, 1251, 1158, 1051, 854, 777.

Synthesis of Copoplymer P-7: L-Aspartic acid monomer (1) 0.60 g (0.002 mol) used with 0.04 g (0.0002 mol) TEG and 0.42 g (0.002 mol) were used. $Ti(BuO_4)$ used 0.008 g (0.96 mol %) was used as catalyst. Yield: 0.46 g (50.7 %). ^{1}H NMR (400MHz, $CDCl_3$) δ ppm: 5.49 (bs, 1H, N**H**), 4.56 (bs, 1H, C**H**), 4.16-4.03 (m, 4H, COO-C**H**$_2$CH$_2$O) and 4H- COO-C**H**$_2$CH$_2$CH$_2$) , 3.75-3.63 (m, 8H, -C**H**$_2$C**H**$_2$O), 3.04-2.74 (m, 2H, NH-C**H$_2$**), 1.61 and 1.27 (aliphatic protons), 1.44 (s, 9H, BOC protons). ^{13}C-NMR (100MHz, $CDCl_3$) δ ppm: 171.14, 155.50, 80.07, 70.61, 70.40, 68.96, 65.97, 65.26, 64.73, 64.02, 50.08, 36.89, 29.62, 29.31, 28.57, 28.38, 25.09. ^{13}C NMR (100MHz, $CDCl_3$): 171.20, 155.26, 79.90, 65.8, 65.74, 50.07, 36.82, 32.76, 29.53, 29.49, 29.20, 28.52, 28.47, 28.29, 25.78.

Synthesis of Copolymer P-18: L-Aspartic acid monomer (1) 0.60 g (0.002 mol) used with 0.08 g (0.0005 mol) TEG and 0.35 g (0.002 mol) were used. $Ti(BuO_4)$ used 0.011 g (1.4 mol %) was used as catalyst. Yield: 0.72 g (68 %). ^{1}H NMR (400MHz, $CDCl_3$) δ ppm: 5.48 (bs, 1H, N**H**), 4.53 (bs, 1H, C**H**),), 4.26-4.21 (m, 4H, COO-C**H**$_2$CH$_2$O), 4.15-4.02 (m, 4H- COO-C**H**$_2$CH$_2$CH$_2$), 3.74-3.61 (m, 8H, -C**H**$_2$C**H**$_2$O), 3.05-2.73 (m, 2H, NH-C**H$_2$**), 1.61 and 1.26 (aliphatic protons), 1.44 (s, 9H, BOC protons). ^{13}C-NMR (100MHz, $CDCl_3$) δ ppm: 170.86, 155.28, 79.96, 70.63, 68.88, 65.84, 65.14, 64.63, 63.79, 50.30, 36.76, 29.54, 29.24, 28.52, 28.30, 25.85.

Synthesis of Copolymer P-30: L-Aspartic acid monomer (1) 0.6 g (0.002 mol) used with 0.14 g (0.001 mol) TEG and 0.28 g (0.001 mol) were used. $Ti(BuO_4)$ used 0.013 g (1.6 mol %) was used as catalyst. Yield: 0.89 g (69 %). ^{1}H NMR (400MHz, $CDCl_3$) δ ppm: 5.47 (bs, 1H, N**H**), 4.56 (bs, 1H, C**H**),), 4.33-4.22 (m, 4H, COO-C**H**$_2$CH$_2$O), 4.15-4.02 (m, 4H- COO-C**H**$_2$CH$_2$CH$_2$), 3.74-3.61 (m, 8H, -C**H**$_2$C**H**$_2$O), 3.05-2.73 (m, 2H, NH-C**H$_2$**), 1.61 and 1.26 (aliphatic protons), 1.44 (s, 9H, BOC protons). ^{13}C-NMR (100MHz, $CDCl_3$) δ ppm: 171.22, 155.50, 79.86, 70.42, 68.94, 67.92, 66.02, 65.40, 64.76, 64.34, 53.48, 51.96, 50.07, 36.48, 29.79, 29.35, 28.52, 26.0.

Synthesis of Copolymer P-69: L-Aspartic acid monomer (1) 0.60 g (0.002 mol) used with 0.28 g (0.001 mol) TEG and 0.12 g (0.0006 mol) were used. $Ti(BuO_4)$ used 0.012 g (1.4 mol %) was used as catalyst. Yield: 0.69 g (73 %). ^{1}H NMR (400MHz, $CDCl_3$) δ ppm: 5.55 (bs, 1H, N**H**), 4.55 (bs, 1H, C**H**),), 4.31-4.22 (m, 4H, COO-C**H**$_2$CH$_2$O), 4.14-4.01 (m, 4H- COO-C**H**$_2$CH$_2$CH$_2$), 3.73-3.59 (m, 8H, -C**H**$_2$C**H**$_2$O), 3.06-2.74 (m, 2H, NH-C**H$_2$**), 1.59 and 1.24 (aliphatic protons), 1.42 (s, 9H, BOC protons). ^{13}C-NMR (100MHz, $CDCl_3$) δ ppm: 171.01, 155.53, 80.06, 72.55, 70.50, 70.30, 70.24, 69.25, 68.8, 68.62, 64.62, 63.93, 61.59, 51.93, 50.0, 36.78, 29.5, 28.8.

Synthesis of Copolymer P-82: L-Aspartic acid monomer (1) 0.59 g (0.002 mol) used with 0.32 g (0.002 mol) TEG and 0.04 g (0.0002 mol) were used. $Ti(BuO_4)$ used 0.012 g (1.4 mol %) was used as catalyst. Yield: 0.8 g (74 %). ^{1}H NMR (400MHz, $CDCl_3$) δ ppm: 5.56 (bs, 1H, N**H**), 4.54 (bs, 1H, C**H**),), 4.28-4.26 (m, 4H, COO-C**H**$_2$CH$_2$O), 4.12-4.01 (m, 4H- COO-C**H**$_2$CH$_2$CH$_2$), 3.72-3.59 (m, 8H, -C**H**$_2$C**H**$_2$O), 3.05-2.78 (m, 2H, NH-C**H$_2$**), 1.58 and 1.24 (aliphatic protons), 1.41 (s, 9H, BOC protons). ^{13}C-NMR (100MHz, $CDCl_3$) δ ppm: 171.26, 155.27, 79.85, 72.35, 70.50, 68.87, 64.57, 63.93, 61.47, 52.76, 52.14, 50.03, 36.55, 29.67, 28.78, 28.15, and 25.59.

Deprotection of P-40: P-40 polymer (0.26 g, 0.697 mmol) was dissolved in 5 mL dry DCM and trifluoroacetic acid (0.54 mL, 7.0 mmol) was added drop wise under at 4°C under nitrogen environment. This was stirred for 15 minutes and the reaction mixture was brought to room temperature and stirred for another 2 h. After the completion of the reaction the DCM and TFA were removed by rotary evaporator. Yield= 0.22 g, (89 %). ^{1}H-NMR (400MHz, CD_3OD) δ ppm: 4.43 (m, 1H, -C**H**), 4.34-4.30 (m, 4H,COO-C**H**$_2$CH$_2$O), 4.26-4.18 (m, 4H,COO-C**H**$_2$CH$_2$CH$_2$-), 3.79-3.69 (m, 8H, - C**H$_2$**C**H$_2$**O), 3.17-3.08 (m, 2H, alkyl, -C**H$_2$**NH), 1.71 & 1.36 (m, -C**H$_2$**C**H$_2$** alkyl chain protons) .^{13}C-NMR (100MHz, CD_3OD) δ ppm: 168.73, 169.56, 167.95, 161.65, 70.05, 68.44, 68.23, 66.55, 65.47, 64.32, 49.05, 47.64, 47.43, 47.21, 47.00, 33.60, 29.35, 29.29, 28.98, 28.23, 28.20, 25.58, 25.43. FT-IR (cm^{-1}): 2924, 2857, 1740, 1665, 1518, 1403, 1192, 1129, 823, 795, 730.

Encapsulation of Drug or Dye in polymer nanoparticles: The drug/dye loading has been described in details for Nile red. To a mixture of 5 mg of amphiphilic polymer (in 1.0 mL DMSO) and 0.5 mg of Nile red (in 1.0 mL DMSO), Milli Q water was added drop wise (2.0 mL). The solution was stirred overnight and further transferred to a semi-permeable membrane dialysis tube with MWCO = 3500 (Spetropor). This solution was dialyzed against Milli Q water for 24 h while the reservoir was changed at regular interval with fresh water in order to remove DMSO and un-encapsulated dye molecules. The resultant solution was filtered through Whatmann filter paper prior to further analyses. By following the above procedure, curcumin, doxorubicin and topotecan were also loaded in the copolymer. In case of DOX and TPT, 0.5 mg of doxorubicin hydrochloride and topotecan hydrochloride were neutralized by Et_3N prior to loading. The dialyzed solution of DOX, TPT and CUR were lyophilized and stored at 4 °C for biology studies. In order to calculate the drug loading efficiency (DLE) and drug loading content (DLC) by the aid of absorption spectra of each drug and dye, the following equations were used:

Drug Loading Content (DLC) $= \left(\frac{mass\ of\ loaded\ \ drug\ or\ dye}{mass\ of drug\ or\ dye\ in\ feed}\right) \times 100$ ..... (1)

Drug Loading Effeciency (DLE)$=\left(\frac{total\ \ mass\ of\ loaded\ \ drug\ or\ dye}{total\ \ mass\ of\ polymer\ \ taken}\right) \times 100$ .....(2)

DLE for DOX, TPT, CUR, NR were found to be 2.0 %, 4.0 %, 14.7 %, and 8.0 % respectively. DLC for DOX, TPT, CUR, and NR were found to be 1.0 %, 2.2 %, 7.4 %, and 4.0 % respectively.

Esterase Stimulated *in-vitro* dye/drug release: P-40 nanoparticles loaded with Nile red and curcuminwere used in order to study the action of esterase enzyme on the polymeric scaffold and thereby their release from the nano-assembly. For this purpose 2.0 mL of dialyzed sample of Nile red loaded nanoparticles were taken in a 5.0 mL vial in PBS buffer and it was incubated at 37 °C in the presence of 10 units of esterase enzyme. At specific intervals of time 1.0 mL aliquots of the solutions were taken and their respective absorbance were recorded. Same procedure was followed for the curcumin loaded nanoparticles. The cumulative release of Nile red and curcumin with time were calculated using: Cumulative Release (%) = $(C_o\text{-}C_n/C_o)$ X

100, where C_o is the amount of Nile red loaded in 1.0 mL of polymer at time 0 h and C_n is the amount of Nile red loaded at n^{th} h. A controlled experiment was carried out in absence of esterase enzyme by incubating the Nile red and CUR loaded polymer nanoparticles in PBS at 37 °C for cumulative drug release studies.

pH Stimulated *in-vitro* dye/drug release: Nile red loaded **P-40** was subjected to various PBS buffers of pH = 4.0, 6.0, 6.5, and 7.4 in order to understand the release behaviour of the Nile red under different pH conditions.These pH were chosen to mimic the acidic environment gradient dwelling in normal and cancer cells. The tissue comprising of cancerous cells have pH of around 6.0-5.0 and highly acidic conditions were required to study the affect of environment provided by endosomes and lysosomes. For this 2.0 mL of dialysed sample of Nile red loaded **P-40** were taken in a 5.0 mL vial in PBS buffer of pH as mentioned above and it were incubated at 37 °C for 12 h. Similar procedure was followed as that of esterase enzyme release and a plot between cumulative releases of Nile red with time (upto 12h) were plotted. The curcumin loaded nanoparticles were subjected to pH= 5.5 to study its release pattern too.

Cell Viability Assay: P-40 nascent nanoscaffold and corresponding drug loaded nanoparticles were exposed to HeLa cell lines and MCF 7 cell lines independently in order to determine the cell viability in cancer cells, using quantification of tetrazolium bromide, 3-4,5 dimethylthiazol-2,5-diphenyl tetrazolium bromide (MTT), based on the metabolic activity of viable cells. For this assay a 96-well plate (Corning, U.S.A.) having 1000 cells per well in 100 μL of DMEM with 10 % FBS was taken and cells were allowed to adhere for 16 h. Media from each well was aspirated and various concentrations of **P-40**, free DOX, free TPT, free CUR and corresponding amount of DOX in **P-40**, TPT in **P-40**, and CUR in **P-40** were fed to each well in triplicates in individual experiments. As a blank control, DMEM with FBS in the absence of cells was also maintained in triplicates. After administering the nanoparticles and free drugs, the cells were incubated for 72 h without changing the media. After 72 h, medium was aspirated from each well and 100 μL of MTT solution (a freshly prepared stock of MTT in sterile PBS (5 mg/mL) diluted to 50 μg/mL in DMEM was added to each well. Cells were further incubated with MTT for 4 h at 37

°C. After this the media containing MTT was aspirated from each well and to the purple formazan crystals thus obtained in each well, (formed due to reduction of MTT by mitochondrial dehydrogenase enzyme from viable cells), 100 μL of DMSO was added. The absorbance from formazan crystals was immediately recorded using micro plate reader at 570 nm (Varioskan Flash). This gave a representative of the number of viable cells per well. Values corresponding to each triplicates (of control and polymer treated cells) were determined and their mean were used for calculations. Out of the triplicate, any value that deviated significantly from the other two values, were omitted during calculations. The mean of blank control was taken as 100% viable and relative percentage values for scaffold and drug loaded scaffold were calculated with respect to this. This procedure was followed for both the cell lines.

Cellular Uptake Studies by Confocal Microscopy: Flame dried coverslips in DMEM medium containing 10 % FBS were taken in 6 well plate and to this HeLa cells were seeded at a density of 1×10^5 cells and were incubated at 37 °C for 16 h. The cells were further exposed to required amount of polymer **P-40** loaded with DOX, TPT, CUR respectively, and correspondingly to the free dye and drugs and were incubated at 37 °C for 4 h under CO_2 environment. After incubation, drug or dye containing medium was aspirated from each well, and cells were washed twice with PBS (2×1 mL) and fixed with 4% paraformaldehyde solution in PBS for 10 min at room temperature. The cells were washed twice with PBS (2×1 mL) and stained with Hoechst solution in PBS. These were incubated for 2 min, at room temperature in dark conditions, and then the excess dye was washed from the plate and the cells were gently rinsed with PBS. The cover slips were mounted on slides using Fluoromount^{TM} mounting medium (Southern Biotech) and were left for drying overnight at room temperature in dark. The cells were imaged using a confocal microscope using the λ **405** nm (blue channel) and λ **560** nm (red channel) lasers, λ **488** nm (green channel) lasers. Images thus obtained were analyzed using Image J analysis software and the image for each channel was separated and merged.

2.3. Results and Discussion

2.3.1. Synthesis and Characterization of Amphiphilic Polyester

The carboxylic acid and amine functional groups in the L-aspartic acid were converted into their corresponding methyl esters and BOC urethane (or carbamate), respectively (see monomer 1 in scheme 2.1**)**. At 120 °C, in the presence of $Ti(OBu)_4$ catalyst; the bis carboxylic esters in monomer 1 underwent thermo-selective trans-esterification with diols to produce polyesters.[43] Under this polymerization condition, the BOC urethane functionality in monomer 1 was retainedand undisturbed as pendant in each repeating unit.[44] The polymers were synthesized using hydrophobic 1,12-dodecane diol (DD) and hydrophilic triethyleneglycol (TEG) to fine-tune the hydrophilic/hydrophobic balance in the polymer. The compositions of the diols DD and TEG were varied from 10 to 90 % to make a series of amphiphilic polyesters, P-X.

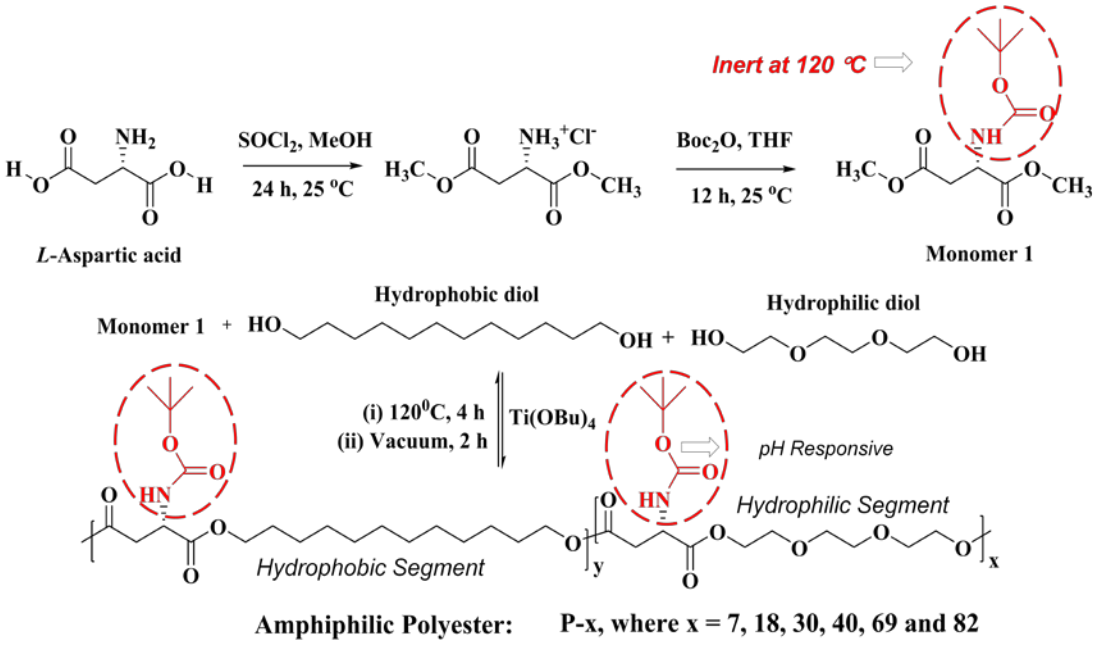

Scheme 2.1: *Synthesis of L-aspartic acid multi functional monomer-1 and its thermo-selective polymerization with diols to produce BOC urethane pendant amphiphilic biodegradable polyester.*

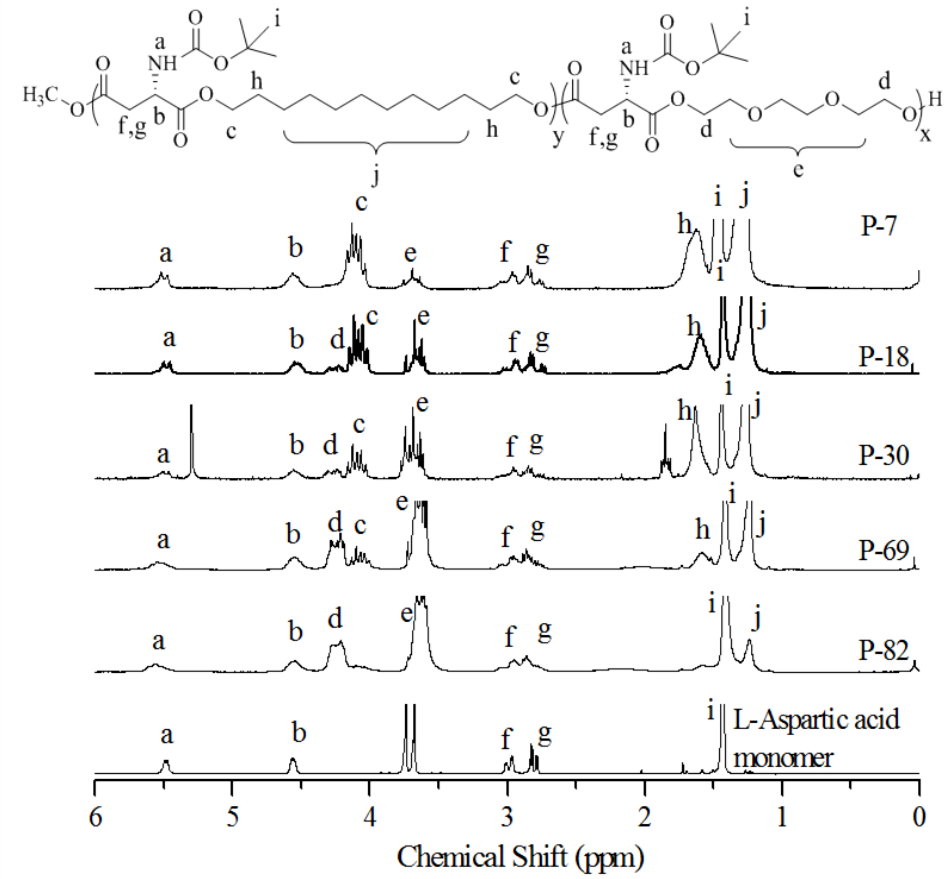

Figure 2.6: *Stack plot of 1H-NMR of L-aspartic acid monomer, and copolymers P-X: P-82, P-69, P-30, P-18, P-7.*

The structures of the polymers were characterized by ^{1}H- NMR and ^{13}C-NMR and the details are given in figure 2.6 and figure 2.7. The ^{1}H-NMR spectra of the representative amphiphilic polymer P-40 is given in figure 2.8 a and the different protons have been assigned various alphabets in the chemical structure (for other copolymers, figure 2.6). The disappearance of L-aspartic methyl ester protons -COOC**H**$_3$ at 3.74 and 3.68 ppm (figure 2.7 a) and the appearance of the new ester linkage at 4.12 and 4.06 ppm (for proton-**c** and d) confirmed the formation of the polyesters. The high intense peak at 1.44 ppm with respect to BOC urethane protons (protons-**i)** were found to be intact, which confirmed the occurrence of the thermo-selective transesterification process among the carboxylic esters and diols without disturbing the BOC urethane pendant. A similar observation was made from the ^{13}C-NMR spectra and the details are given in the figure 2.7).

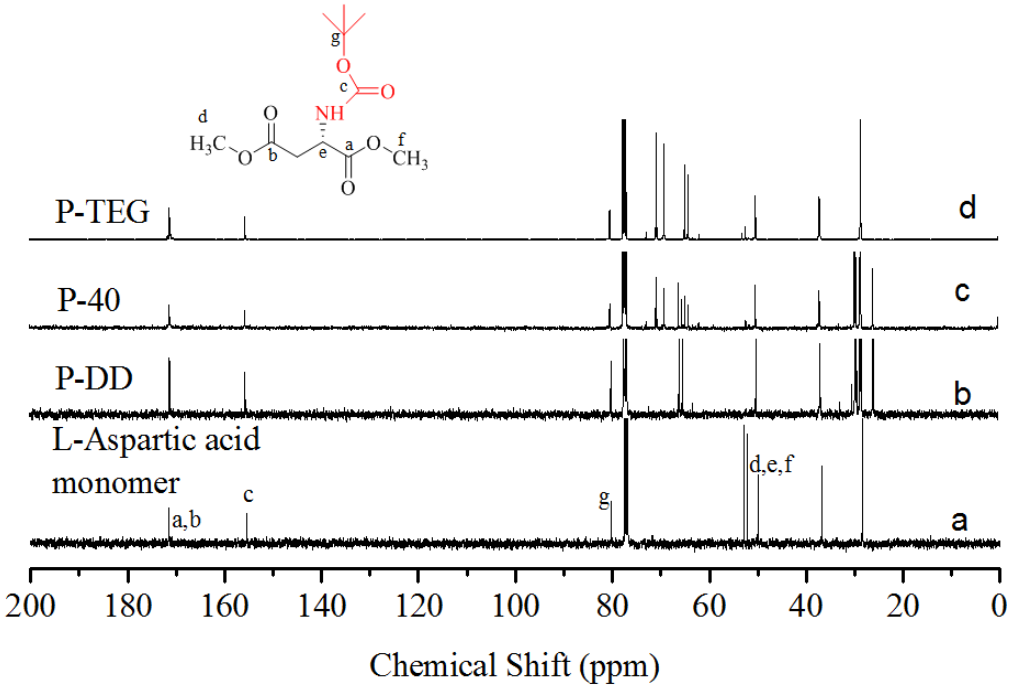

Figure 2.7: *Stack plot of ^{1}H-NMR of L-aspartic acid monomer (a), P-DD (b), P-40 (c) and P-TEG (d).*

Interestingly, the protons corresponding to –COOC**H**$_2$(CH$_2$)$_X$ (from DD hydrophobic part) and the –COOC**H**$_2$CH$_2$O- (from TEG hydrophilic part) segments were well separated as multiplets at 4.34- 4.28 ppm and 4.24- 4.22 ppm (see proton **c** and d in figure 2.8 a), respectively. This facilitated the determination of exact composition of the hydrophilic and hydrophobic segments in the polyester backbone by ^{1}H-NMR. Based on this, the actual incorporation of the copolymers, the TEG units were determined to be 7, 18, 30, 40, 69, and 82 for their feed molar ratios of 10, 25, 40, 50, 75, and 90, respectively. The polymers were designated as P-X, where X represents the actual incorporation of the hydrophilic segments (TEG units). The plot of copolymer composition against their feed ratio shown in figure 2.8 b exhibited a linear trend with respect to the complete random distribution of the hydrophilic and hydrophobic segments for the entire composition range. The incorporated Tri-ethylene glycol is less than the feed amount in melt condensation, because of the difference in the thermal properties of the diols used in the system. Initial boiling point and boiling range of triethylene glycol is 125 - 127 °C at 0.1 mbar/lt and that of dodecane diol 189 °C at 16 mbar/ lt. Since the melt-polycondensation in the system

was carried out at 120 °C under vacuum (0.1 – 0.05 mbar) some amount of triethylene glycol could escape the reaction vessel and it causes a slight reduction in the actual amount of alcohol available for the reaction. Therefore, the incorporated amount of triethylene glycol within the polymer backbone was found to be less than the feed; however, it followed a linear trend of incorporation vs feed in the entire composition (10 to 90 % TEG content), confirming the homogeneous reactivity during the polymerisation. The molecular weights of the polymers were determined by gel permeation chromatography (GPC) and their GPC plots are shown in figure 2.8 c (see table 2.1 for molecular weights). The molecular weights of the polymers were obtained as moderate to high M_n = 3.0-8.0 x 10^3 g/mol and M_w = 6.5-21.5 x 10^3 g/mol with polydispersity index of ~2.0 (see table 2.1). Thermo gravimetric analysis of the polymers confirmed the thermal stability of the polymers up to 285°C (see figure 2.9 a). Differential scanning calorimetry analysis revealed that all the polymers were amorphous. The DSC thermograms showed variation in the glass transition temperature from -15 to -1°C with change in the composition of DD and TEG contents in the random copolymer (fig 2.9 b).

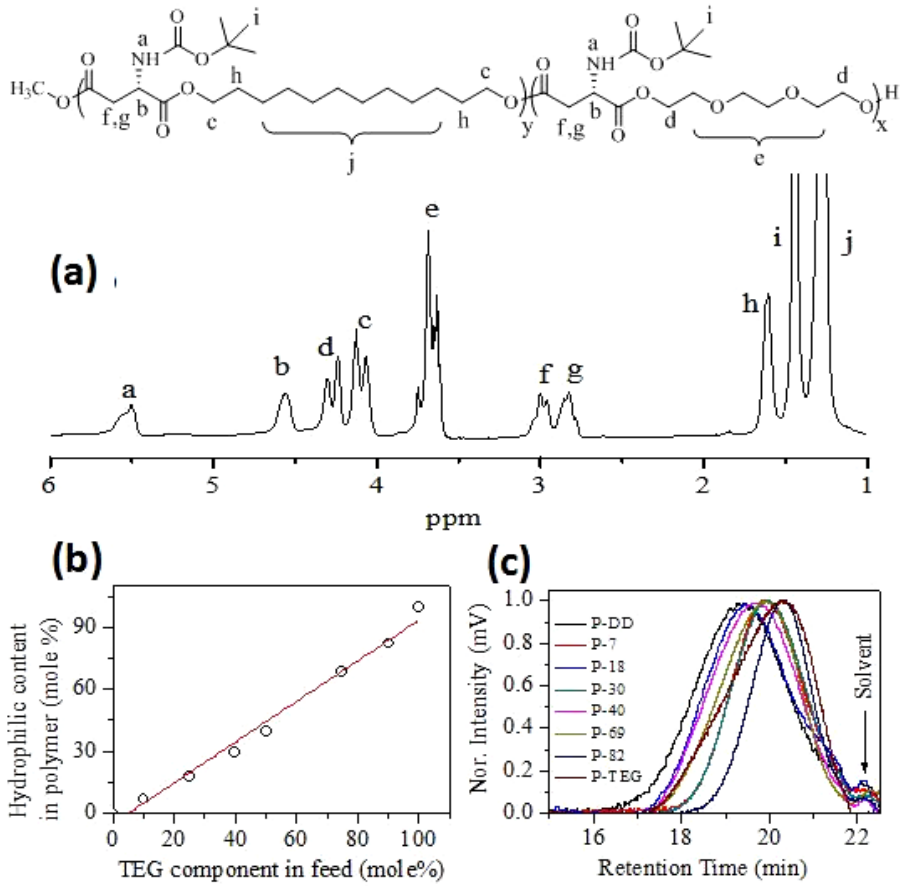

Figure 2.8: *(a)[1]H-NMR spectra of **P-40** in $CDCl_3$. Only the expanded spectrumfrom 1.0 to 6.0 ppm is shown for simplicity. (b) The plot of percentage incorporation of TEG content in the copolymer determined by [1]H-NMR versus TEG diol in the feed. (c) GPC chromatograms of P-DD, P-TEG and random copolyesters P-X.*

Table 2.1: *Summary of molecular weights of homo-polymers and copolymers*

Polymer	Feed TEG (mole %)	Incorporated TEG[a] (mole %)	M_n[b] (g/mol)	M_w[b] (g/mol)	M_w/M_n	T_g[c] (°C)	T_D[d] (°C)
P-DD	0	0	7900	21500	2.7	-10.9	302
P-7	10	7	5400	19600	3.6	-14.9	308
P-18	25	18	8600	17000	2.0	-10.5	300
P-30	40	30	4600	9700	2.1	-14.5	285
P-40	50	40	6000	16200	2.7	-9.5	316
P-69	75	69	6400	15000	2.3	-1.8	320
P-82	90	82	3700	6600	1.8	-1.6	316
P-TEG	100	100	3000	6500	2.2	-5.4	298

a. *Determined from ^1H NMR*
b. *Molecular weights M_n and M_w are determined from GPC with polystyrene as standards and THF as solvents at 25 ℃*
c. *Glass transition temperature (T_g) obtained from DSC analysis at 10 ℃/min heating rate.*
d. *Decomposition temperature (T_D) obtained for 10% weight loss determined by TGA under N_2 atmosphere.*

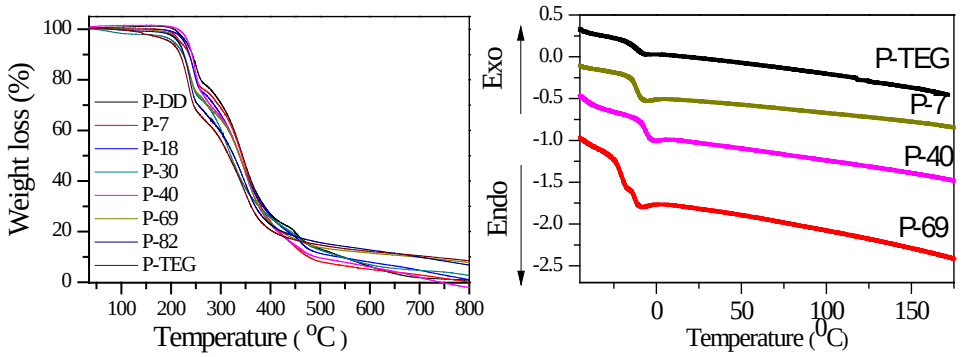

Figure 2.9: *(a) TGA plots of Copolymers composition P-X, X= 7, 18, 40, 82, and homopolymers P-DD and P-TEG. Inset showing the mechanism of cleavage of BOC group from the polymer backbone giving rise to first decomposition step in the TGA curve.(b) Differential scanning calorimetry (DSC) plot showing glass transition temperature of amorphous copolymers with composition P-X, X= 7, 40, 69, and homopolymer P-TEG.*

2.3.2. Aqueous Self-assemblies of Amphiphilic Polyesters

To study the self-assembly of the amphiphilic polymers; they were dialyzed using semi-permeable membrane and the photographs of the samples are shown in figure 2.10a. Dynamic light scattering (DLS) showed mono-modal distribution with respect to the formation of homogeneous nano-aggregates in water (see figure 2.10 b and 2.11 for other polymers). The average sizes of these nano-aggregates were plotted against the hydrophilic segment content in P-X (see 2.12 a). The sizes of the polymer nano-aggregates decreased from 550 nm to 250 nm with increase in the hydrophilic content up to 40% of TEG (for P-40). This trend indicated that the P-40 polymer possessed optimum hydrophilic- balance in the polymer backbone to produce tightly packed self-assembled nanostructures. To visualize the size and the shape of the aqueous polymer self-assemblies, the samples were subjected to electron microscopes (FE-SEM and HR-TEM) and atomic force microscope (AFM) analysis. AFM image of P-40 polymer in figure 2.10c showed the formation of spherical nano-particles of 200 ± 30 nm in size. FE-SEM and HR-TEM images (see 2.12 b and figure 2.10 d) also confirmed the existence of spherical nano-particles of ~250 nm in size.

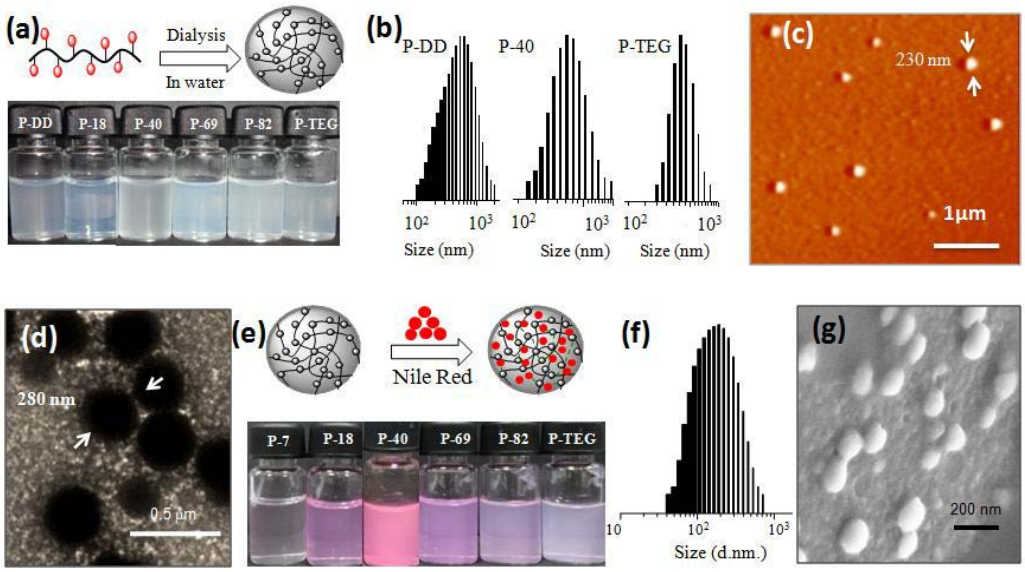

Figure 2.10: *(a) Representation of polymer nanoparticle formation and the photographs of vials containing the dialysed polymer samples. (b) DLS histograms of dialysed polymer samples(P-DD, P-40, P-TEG). (c) AFM image of P-40 nanoparticles.(d) HR-TEM image of P-40. (e)Nile red loaded nanoparticles and their photographs. (f) DLS of NR loaded P-40.(g) FE-SEM of NR loaded P-40.Concentration of P-40 = 1.0 mg/mL.*

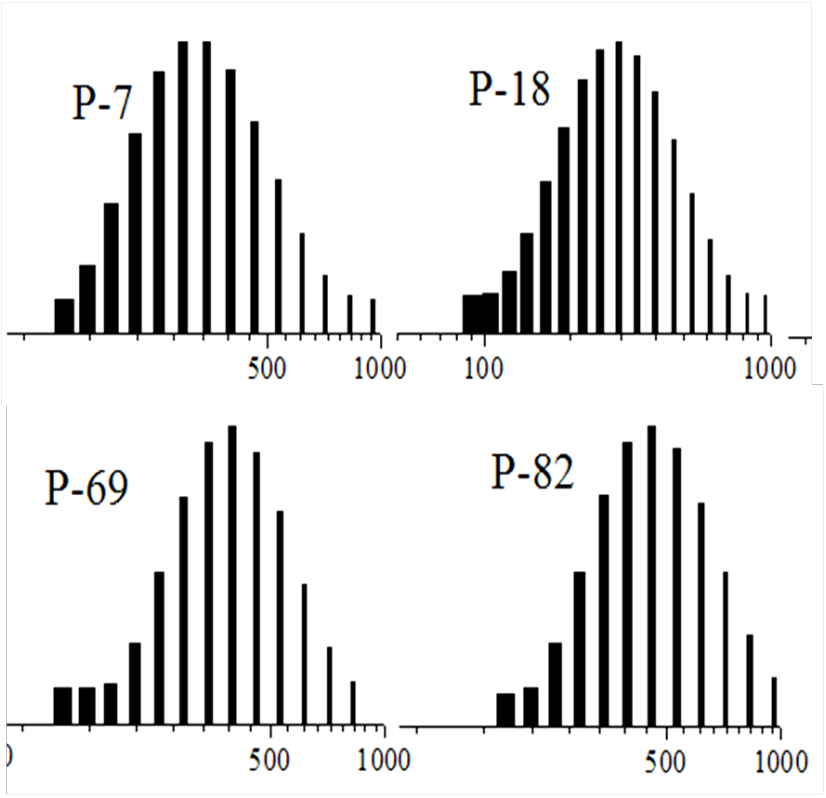

Figure 2.11: *DLS plots for copolymers with composition P-X, X= 7, 18, 69, 82 showing monomodel distribution of the particles formed.*

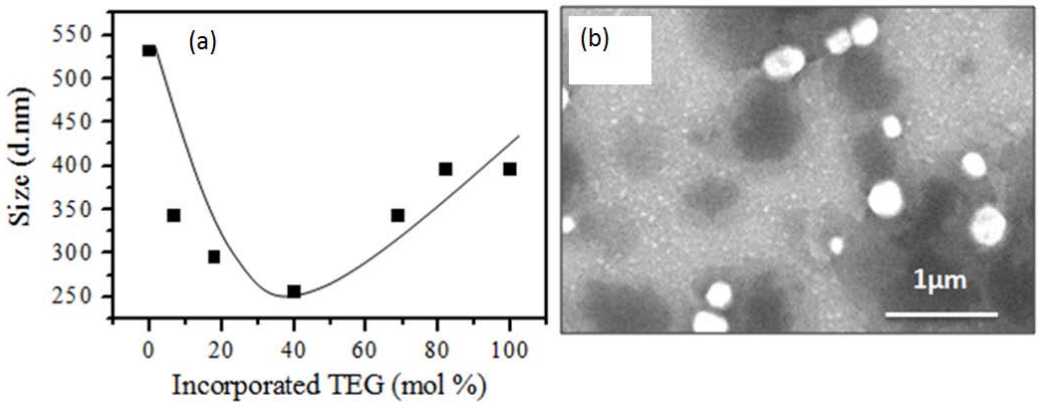

Figure 2.12: *A plot of average sizes of copolymers P-X, X= 0, 7, 18, 30, 40, 69, 82, 100 vs incorporated TEG(a) FE-SEM image of P40-in water(b)*

The encapsulation capabilities of the polymers were tested for fluorophoreNile red (NR) dye (see figure 2.10d). Being a highly luminescent fluorophore, Nile red has a large aromatic core similar to many polyaromatic anticancer drugs, and it is also water insoluble. Most often NR loaded polymer scaffolds readily load doxorubicin,

etc; thus, the NR loading studies would provide more information for the drug encapsulation capabilities of new polymer scaffold.[47-49] Typically, the polymer and NR were dissolved in DMSO+ Milli Q water and dialyzed against fresh water using semi-permeable membrane (MWCO = 3500) for 24 h at 37 °C. The photographs of the amphiphilic polymer P-X encapsulated with NR and schematic diagrams to exemplify the loading are shown in figure 2.10 b. Both the fully hydrophobic homopolymer P-DD and hydrophilic homopolymer P-TEG did not encapsulate the NR. The photographs clearly revealed that the encapsulation of NR increased with the increase in the hydrophilic content in the amphiphilic polymer and maximum loading was obtained for P-40. DLS of the NR loaded P-40 sample showed the formation of 250 nm nanoparticles (see figure 2.10 f) which was matching with that of its nascent polymer scaffold (see figure 2.10 b). The stability of the NR loaded P-40 was studied by DLS in PBS, pH = 7.4 at 37 °C (see Figure 2.13).NR loaded nanoparticles exhibited excellent stability in PBS at 37 °C and their DLS histograms showed mono-modal distribution for more than 48 h. FE-SEM images of the NR loaded P-40 sample (see figure 2.10 g) exhibited spherical nanoparticle features. The shape of the P-40 polymer scaffold was retained even after the loading of the NR in their hydrophobic core.

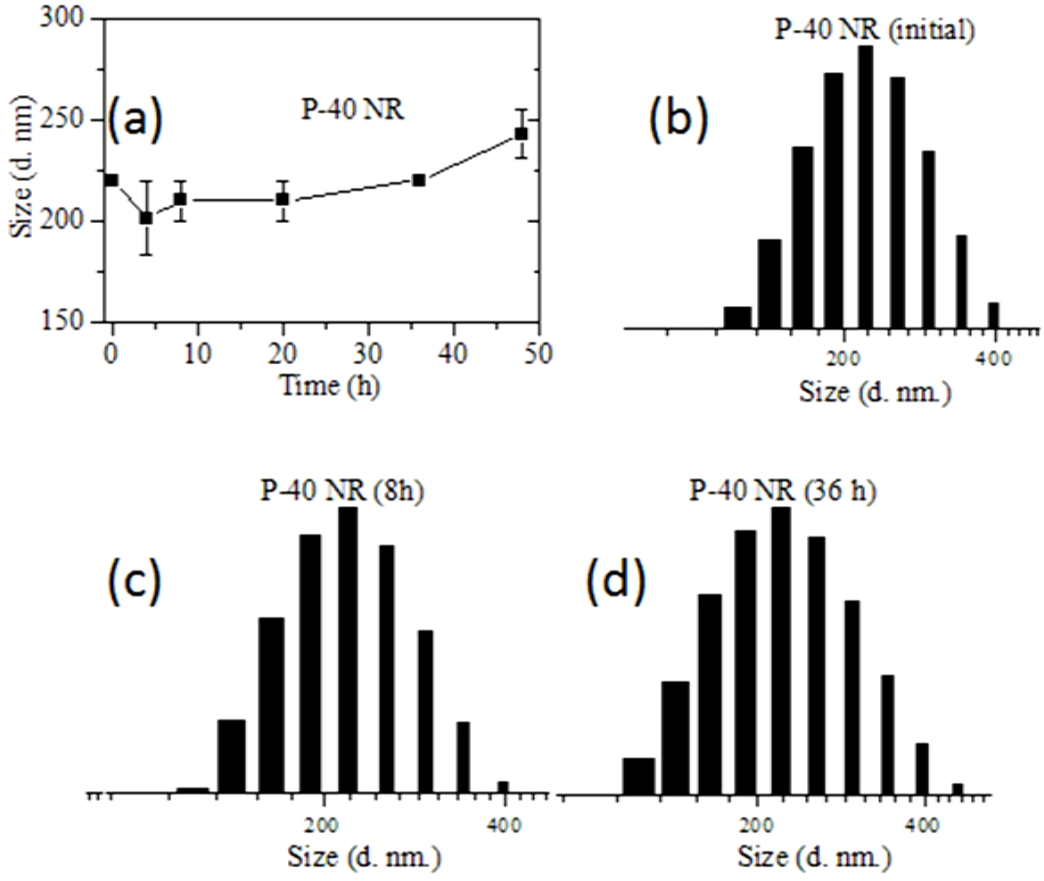

Figure 2.13: *Plot of size of P-40 loaded NR vs time (a). Representative DLS histograms of P-40 loaded NR at time 0 h (b), at time 8 h (c), and at time 36 h (d), showing stable mono-modal distribution.*

2.3.3 Transformation into Cationic Polyester

The custom designed amphiphilic polyesters have BOC urethane units in each of its repeating unit and these are typically susceptible to functional group transformation under acidic environment (see figure 2.14a). The aqueous P-40 nanoparticles dispersed in water were incubated at 37 °C at various pH = 7.4, 6.0, 4.0, and 2.0 for 12 h and the resultant nanoparticles were subjected to zeta-potential measurement. The zeta-potential curves for P-40 nanoparticles at various pH are shown in figure 2.14b. At pH= 7.4, the polymer nanoparticles showed +0.01 mV charge indicating their neutral behaviour. Interestingly, the zeta potential of the P-40 nanoparticles increased as + 8.43, + 12.6, and + 32.0 mV at pH = 6.0, 4.0, and 2.0, respectively. This study suggests that the neutral polymer chains systematically transformed into cationic $-NH_3^+$ species with the increase in the acidity. Independent experiments were carried out to completely de-protect the P-40 polymer into cationic species (see details

in fig 2.15). This de-protected polyester showed zeta potential as + 54.0 mV. The self-assembled nanoparticles exhibited + 32.0 mV in pH= 2.0 which is much lower than that of the zeta-potential of completely de-protected polymer (+ 54.0 mV). It may be assumed that some BOC urethane groups may be still not accessible for conversion in to $–NH_3^+$ species at pH= 2.0 during the zeta potential measurements. This observation supports the slow and controlled transformation of cationic species from the neutral polymer nanoparticles upon subjecting to acidic pH environment.

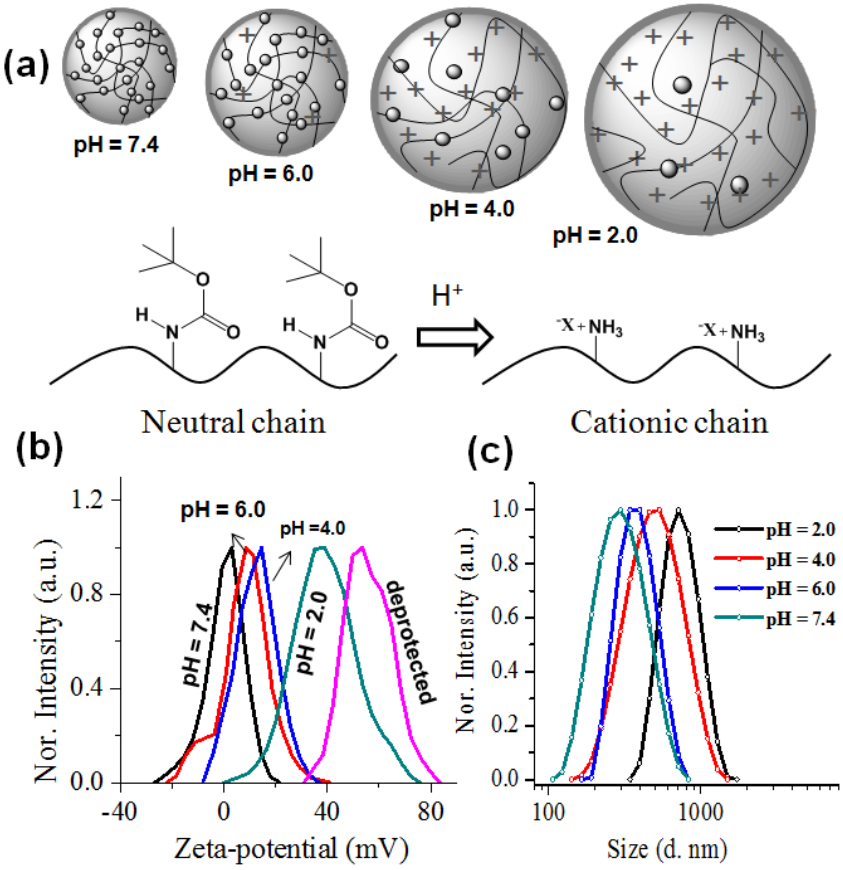

Figure 2.14: *(a) Schematic representation of polymer nanoparticle under various at pH = 7.4, 6.0, 4.0 and 2.0. (b) Zeta-potential plots of P-40 nanoparticle at pH = 7.4, 6.0, 4.0, 2.0 and deprotected P-40 afetr 12 h incubation at 37℃.(c) DLS histograms of P-40 incubated at pH = 7.4, 6.0, 4.0 and 2.0 afetr 12 h incubation at 37℃ . Concentration = 1.0 mg/mL.*

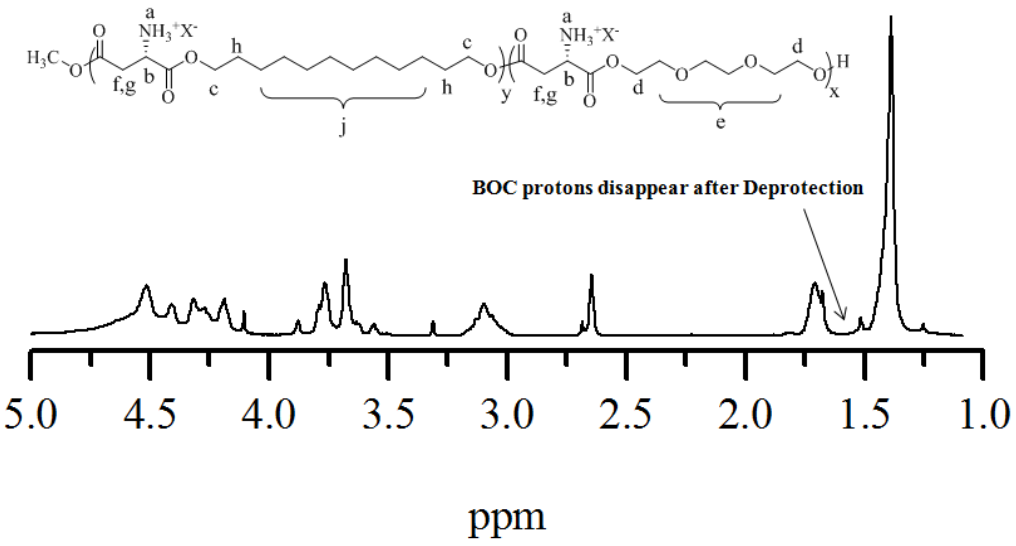

Figure 2.15: *^{1}H-NMR in CD_3OD for deprotected P-40 showing disappearance of BOC porotns yielding cationic polymer.*

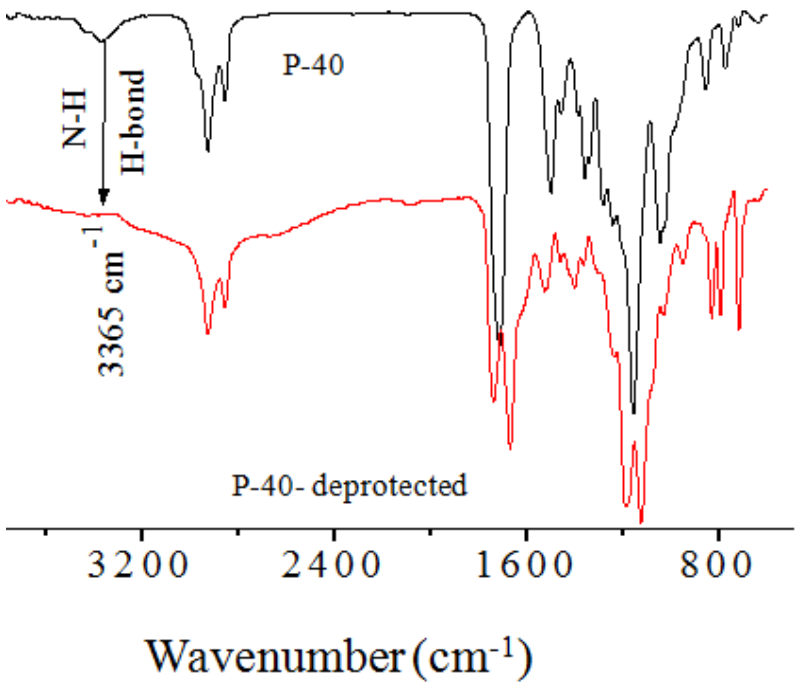

Figure 2.16: *FT-IR spectrum of P-40 (black) and deprotected P-40 (red).*

FT-IR spectra of neutral and cationic P-40 were recorded to study the hydrogen bonding interaction in these polymers (see figure 2.16). A vibrational band at 3365

cm^{-1} was observed in the neutral polymer which was assigned to the NH stretching frequency from the hydrogen bonded BOC urethane pendant groups. This was further supported by the stretching frequency of the C=O at 1715 cm^{-1} with respect to the hydrogen bonding interaction. In the cationic species, the amine salt (of P-40) did not show any peaks above the region of 3200 cm^{-1} indicating the lack of the hydrogen bonded interaction in the absence of the BOC pendant.[50-51,43] To further confirm this trend, DLS histograms of the neutral P-40 nanoparticles that were incubated at pH = 7.4, 6.0, 4.0 and 2.0 for 12 h were recorded and are shown in figure 2.14c. The size of the nanoparticle was observed to increase gradually from ~350 nm (in pH = 7.4) to 750 nm (in pH = 2.0) with increase in the acidic environment (see figure 2.14c). This trend supported the possibility that the self assembled neutral nanoparticle gradually disassembled into larger nano-aggregates. The increase in the particle size is attributed to the repulsion induced by the cationic charges in the polymer chains. Based on the zeta potential, DLS studies and FTIR studies; it may be concluded that the hydrogen bond stabilized amphiphilic nanoparticles were disassembled upon exposure to acidic environment.

2.3.4 pH and Enzyme Responsive Delivery

In order to study their delivering capabilities, the NR loaded P-40 nanoparticles were subjected to release studies at various pH. The pH responsive release profiles are shown in figure 2.17a. At extracellular conditions (in PBS, pH = 7.4, 37°C), the polymer nano-assemblies were stable and only< 12 % of the NR was found to be released. At pH = 6.5, it was observed that there was slight release of NR and up to 35% to 40 %. At pH = 6.0 similar to endosomal pH, the nanoparticles disassembled at a higher rate and attained 65 to 70 % NR release in 12 h. At much lower acidic pH = 4.0, the nanoparticles experienced drastic disassembly and almost 90 % loaded cargoes were released within a period of 4 to 5 h (see figure 2.17a**)**. This drug release profiles were indirectly confirmed by the DLS analysis of the P-40 nanoparticles at pH= 6.0 and 4.0 after incubating for 24 h (see figure 2.17b). The polymer nanoparticles exhibited monomodal distribution at 0 h (see figure 2.14c) and showed multi-modal distribution with respect to the disassembly of at longer exposure

(24 h). Thus, the complete release of NR from the nanoparticle at acidic pH (< 4.0) may occur by the disassembly mechanism as schematically shown in figure 2.17 b.

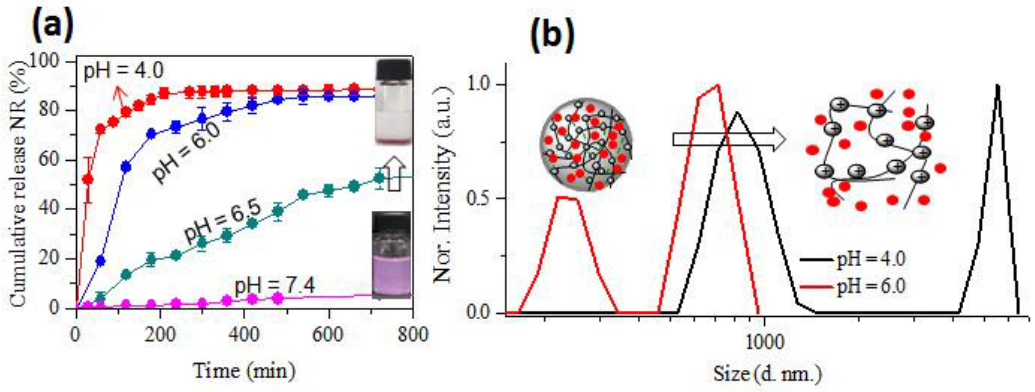

Figure 2.17: *(a) Cumulative release of Nile red encapsulated in P-40 nanoparticle at pH = 7.4, 6.5, 6.0, and 4.0 in PBS at 37℃. (b) DLS of P-40incubated at pH= 4.0 and 6.0 at 37 ℃ for 24 h. Concentration = 1.0 mg/mL in PBS.*

To study the enzyme responsive delivery via aliphatic polyester backbone cleavage; the release studies were conducted in the presence of esterase enzyme (from horse liver, 10 U) in PBS buffer (pH = 7.4) at 37 °C.[8,16] The cumulative release profiles of NR loaded nanoparticle in figure 2.18a revealed that the polymer nanoparticles were stable in PBS at extracellular conditions and susceptible to biodegradation in the presence of the esterase enzyme to release more than 80 % of the loaded cargoes in 12 h. In this process, the high molecular weight polyester chains were hydrolysed into smaller species which is essential for the clearance of the long polymer chains from intracellular to extracellular medium. An additional experiment was performed *in vitro* to confirm the cleavage of the ester bond in the polymer backbone by lysosomal esterase enzyme. The P-40 polymer was incubated with esterase enzyme (from horse liver, 10 U) at 37 °C and was subjected to DLS studies over a period of 48 h. DLS was employed previously to study the polymer disassembly of biodegradable polymer nano-assemblies.[52] The polymer nano-scaffolds initially swelled in the physiological conditions and subsequently disassembled from tightly packed nano-objects into loosely packed aggregates. As result, the sizes of the disassembled nanoparticles are expected to increase from nano-meter to micro-meter size. Upon de-protection of the BOC units in the polyester

backbone, the oligomer species lost the appropriate hydrophilic and hydrophobic balance in the aqueous medium and thus they would produce large size aggregates. The DLS histograms in figure 2.18b revealed that the tightly packed spherical nano-particles of 250 nm were gradually increased to micrometer size distribution with advent of time. The size of the enzyme cleaved species by the esterase enzyme was plotted (see fig 2.19) and it showed a pattern similar to that of cumulative release profile as seen in figure 2.18a. This trend was attributed to the action of esterase which degraded the polymers chains by hydrolysing the ester bonds and disassembled the polymer nano-assembly (see figure 2.18c). The enzyme-degraded polymers were analyzed by MALDI-TOF mass spectra analysis (figure 2.20). Based on the mass analysis, the biodegraded species were identified to be dimer and trimers. These *in-vitro* studies confirmed that the new polyester nano-assemblies are enzyme degradable (i.e., biodegradable) at the lysosomal enzymes at the intracellular environment to release drugs. Hence, the enzymatic degradation of the newly designed polyesters was directly proved by both MALDI-TOF and GPC analysis.

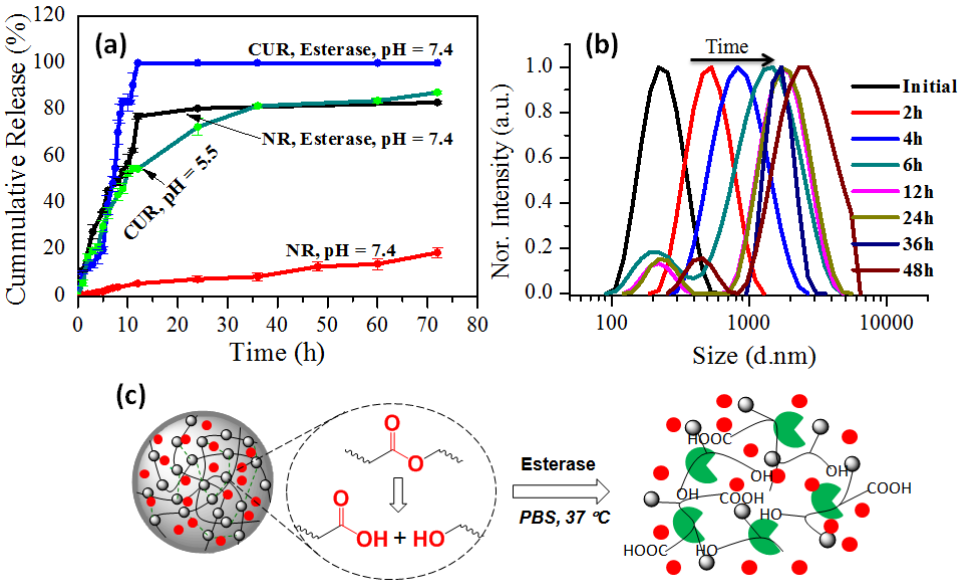

Figure 2.18: *(a) Cumulative release of NR and CUR loaded P-40 at pH= 7.4 in presence and absence of esterase enzyme in PBS at 37 ℃ and also the cumulative release of CUR at pH = 5.5 in PBS at 37℃ (b) DLS histograms of* ***P-40*** *in presence of esterase enzyme at 37℃ in PBS. (c) Schematic representation of release of cargoes from* ***P-40*** *in presence of esterase enzyme.*

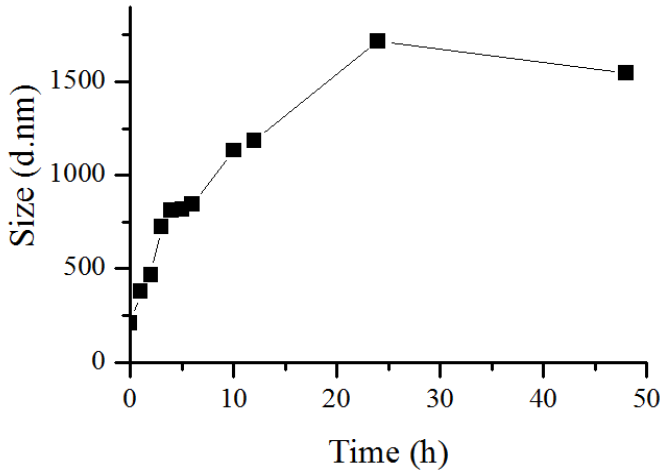

Figure 2.19: *Degradation of P-40 in presence of Esterase enzyme using DLS (a).*

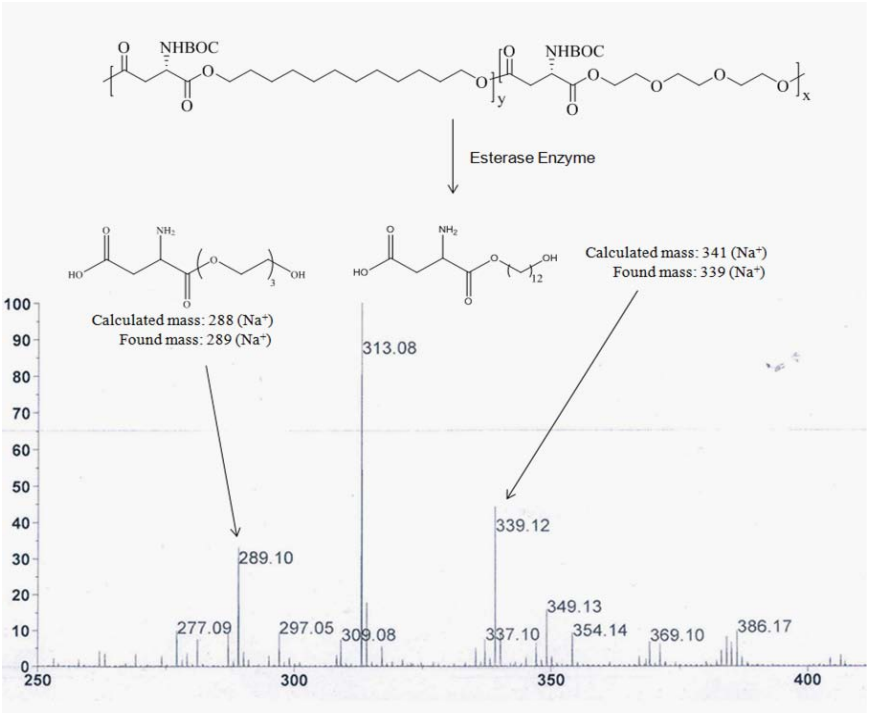

Figure 2.20: *MALDI- TOF of P-40 polymer treated with Esterase enzyme after 24 h.*

2.3.5 Multi- Drug Administration and Cytotoxicity Analysis

Anticancer drugs with different functionality and pharmo-kinetic action such as doxorubicin (DOX, topoisomerase inhibitor I as well as DNA intercalating agent), topotecan (TPT, topoisomerase inhibitor I) and curcumin (CUR, anti-metabolite) were chosen for the encapsulation in the P-40 and the chemical structures of the drugs and their drug loaded vials are shown in figure 2.21a. The entire drug loaded nano-assemblies exhibited good stability in water for administrating into cells. DLS histograms of the drug loaded polymers were obtained around 220 nm as shown in (see figures 2.21b and 2.21c, for P-40 loaded with TPT and CUR respectively). The stability of the curcumin (CUR) drug loaded nanoparticle P-40 and NR loaded P-40 were also studied by DLS in PBS, pH = 7.4 at 37 °C (see Figure 2.22).

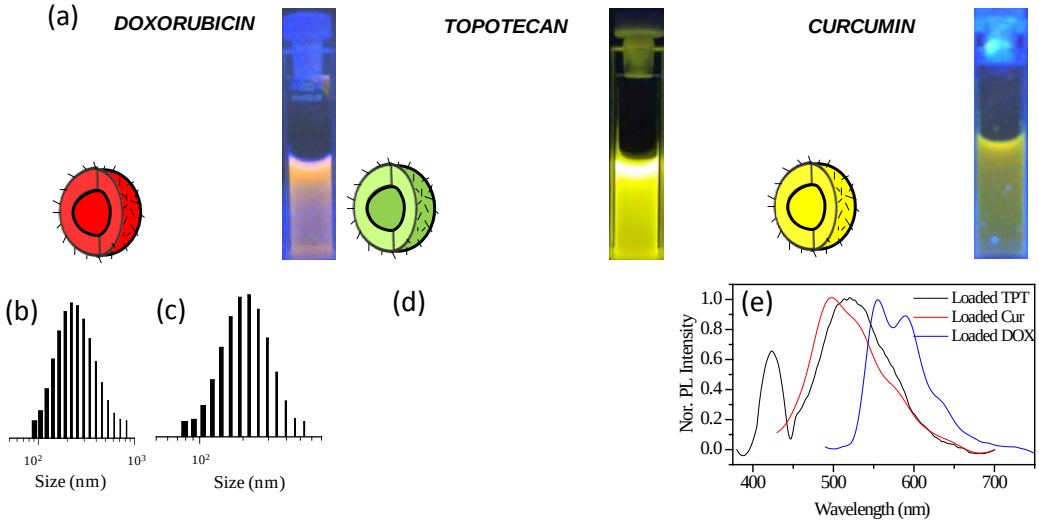

Figure 2.21: *Chemical structures of drugs and the photographs of vials containing their drug loaded nanopartciles for doxorubicin, topotecan and curcumin. DLS histograms of TPT (b) and CUR (c) loaded P-40 nanoparticles. Absorbance (d) and emission (e) spectra of drug loaded P-40 nanoparticles.*

Both NR and CUR loaded nanoparticles exhibited excellent stability in PBS at 37 °C and their DLS histograms showed mono-modal distribution for more than 48 h. This confirmed that the custom designed amphiphilic polymer based on L-aspartic polyesters are very good candidates for stabilizing the drugs at the extracellular level under physiological conditions.The absorbance spectra of the polymer showed peak maxima at 370 nm, 427 nm, and 493 nm for TPT, CUR, and DOX respectively (see figure 2.21d). The emission spectra of TPT and CUR loaded nanoparticles showed almost identical maxima whereas the DOX loaded nanoparticles exhibited higher wavelength red emission (see figure 2.21e).

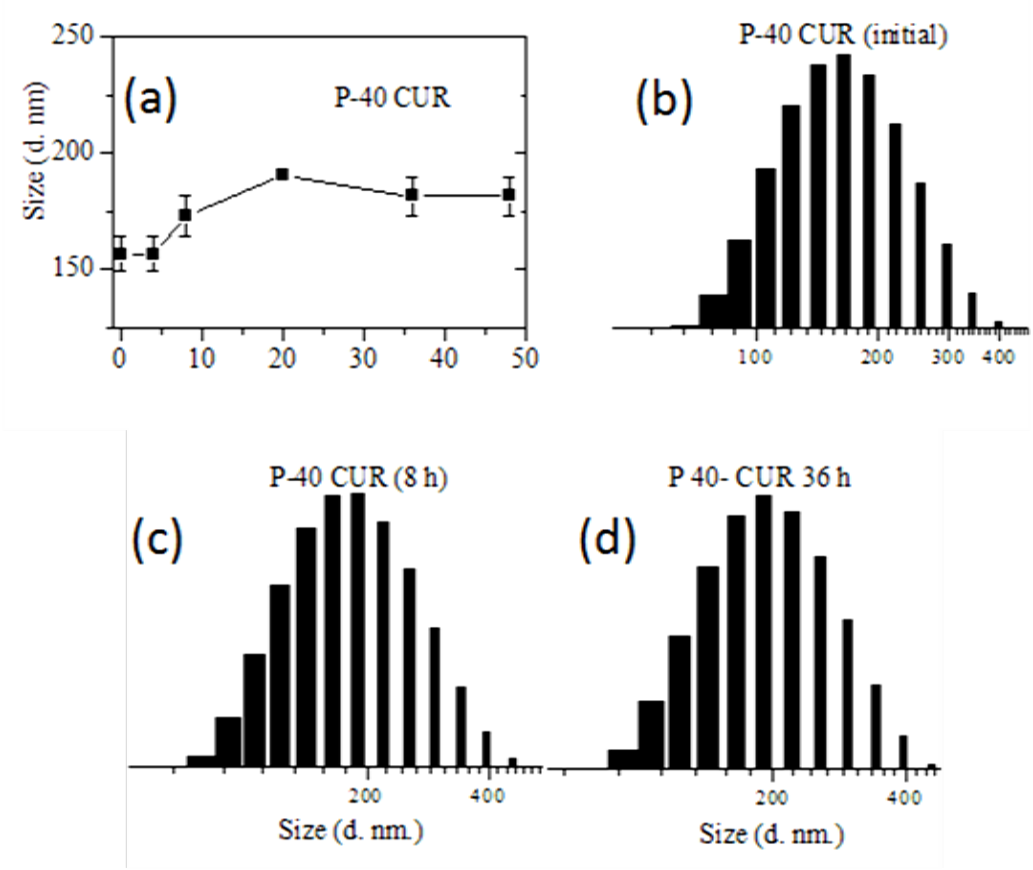

Figure 2.22: *Plot of size of P-40 loaded CUR vs time (a). Representative DLS histograms of P-40 loaded NR at time 0 h (b), at time 8 h (c), and at time 36 h (d), showing stable mono-modal distribution.*

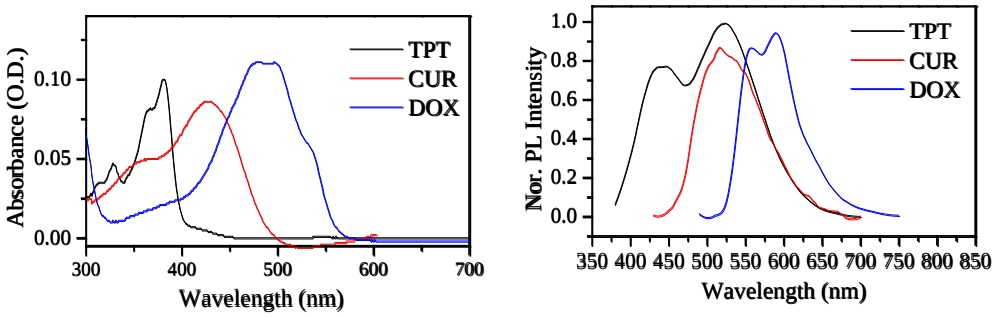

Figure 2.23: *Absorption and emission spectra of free drug in water.*

The absorption and emission spectrum for the respective free drugs (see fig 2.23) were found to be retained in encapsulated form. Among all the three anticancer drugs encapsulated in P-40, the curcumin loaded nanoparticle exhibited higher DLC; thus, it was examined for both enzyme and pH dual responsiveness. The drug releasestudies for curcumin loaded polymer nano-scaffold were carried out in the presence of esterase enzyme and their cumulative release was plotted along with NR release data in figure 2.18a. The CUR was found to release> 95 % in the presence of esterase in pH = 7.4 at 37 °C. At lower pH = 5.5, the CUR release was much slowercompared to the enzymatic process (see figure 2.18a). Interestingly, the pH responsive disassembly trend in the CUR loaded nanoparticle was found to be similar to that of NR loaded nanoparticle observed in figure 2.17a. Thus, pH and enzyme responsiveness of the newly designed polymer scaffold to load multiple anticancer drugs with different luminescence colours enabled the studies of the fluorescent polymer drug loaded nano-particles uptake in cancer cells as well as their cell killing ability. Thus, the newly designed pH and enzyme responsive biodegradable polyester nanoparticles based on L-aspartic acid could be employed as fluorescent biomarkers (diagnostics) as well as for cell killing (therapeutics).

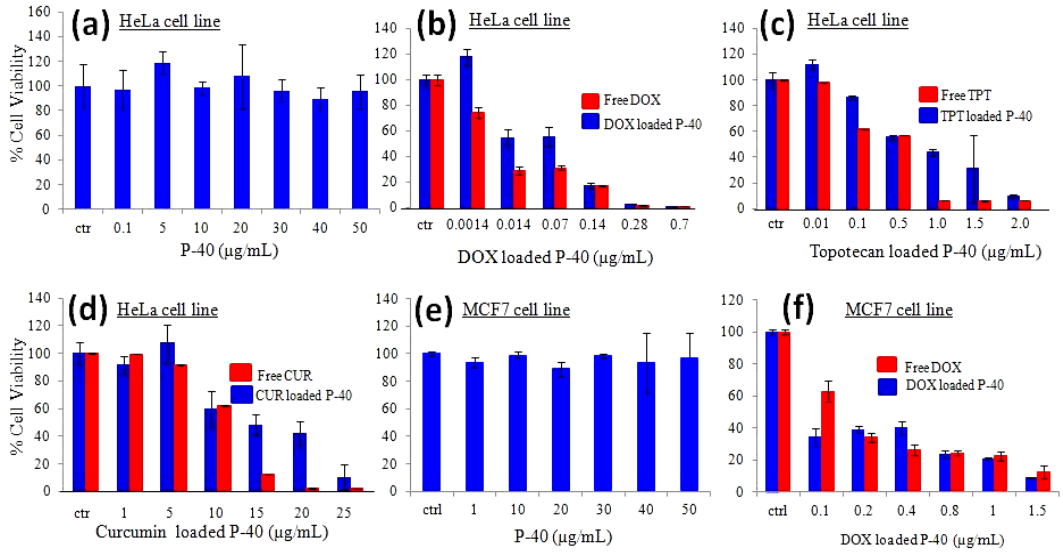

Figure 2.24: *(a) Cytotoxicity of P-40 nascent nanoparticles in HeLa Cells. (b) Cytotxicity of P-40 loaded with DOX and free DOX in HeLa cells. (c)* ***P-40*** *loaded with TPT and free TPT in HeLa cells. (d) P-40 loaded with CUR and free CUR in HeLa Cells. (e) Cytotoxicity of P-40 nascent nanoparticlesMCF 7 cells. (f)* ***P-40*** *loaded with DOX and free DOX in MCF 7 cells. (Incubation time= 72 h).*

The cytotoxicity of the nascent polymer and drug loaded polymer nanoparticles were investigated in cervical cancer cell (HeLa) line and breast cancer (MCF 7) cell lines. The cytotoxicity data for polymer nanoparticles in figure 2.24a (for higher concentrations see fig 2.25) showed that the amino acid based polymer were found to be non-toxic to cancer cells even at high concentrations of 300 μg/mL with upto 70 % cell viability. This high concentration biocompatibility makes the amphiphilic P-40 polymer attractive material for biological applications. The cytotoxicity of the free drug (DOX, TPT, and CUR) and drug loaded to P-40 were tested on HeLa cell lines. The concentration of DOX was varied from 0.0014 to 0.7 μg/mL in both free and drug loaded form (see figure 2.24b). Increasing the concentration of DOX showed higher killing in the HeLa cells. The IC_{50} value for free DOX and DOX loaded polymer were found to be 0.014 μg/mL and ~0.10 μg/mL, respectively. The TPT loaded P-40 was administered to the HeLa cells at various concentration from 0.01 to 2.0 μg/mL (see figure 2.24c). Free TPT and polymer loaded TPT showed IC_{50} ~ 0.50 μg/mL which suggested that newly designed scaffold is very good candidate for TPT delivery. A similar trend was observed for CUR and CUR loaded P-40(see figure 2.24c) and their IC_{50} values was found to be 10.0 μg/mL. The cytotoxicity analysis for the P-40 polymer scaffold was further expanded to breast cancer cell line i.e., MCF 7 cells. The MCF 7 cells were found to be viable up to a concentration of 50 μg/mL (see figure 2.24d). Free DOX and DOX loaded P-40 showed IC_{50} was around 0.10 μg/mL and IC_{50} = 0.20 μg/mL (figure 2.24f). Based on these cytotoxicity data, the following trend of the drugs could be drawn for their cell killing ability DOX > TPT >> CUR. As expected, the cytotoxicity was predominantly controlled by the nature of the drugs. For DOX and TPT, the DLC values were obtained little low compared to CUR; however, the amount was found to be sufficient enough to accomplish > 95 % cytotoxicity in both HeLa and MCF 7 cancer cells. Further efforts are required to optimize the scaffold with new design strategies to improve the amphiphilic nature of the polymer structure for higher DLCs. The effect of polymer carrier is expected to be more visible in the *in-vitro* experiments as EPR effect would facilitate better uptake in the cancer tissues over normal ones. Neverthless, the newly designed scaffold was found to be non-toxic to cells and

showed ability to carry multiple drug loads and exhibited excellent cell killing capabilities.

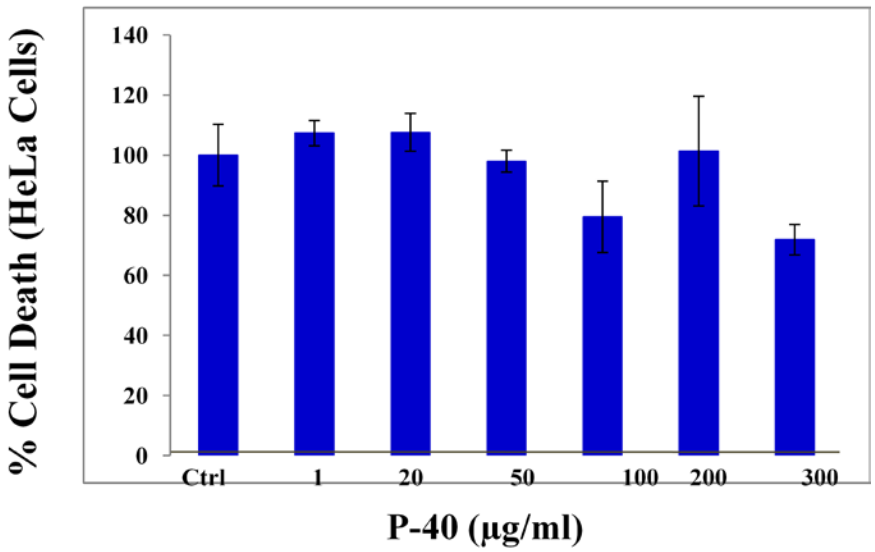

Figure 2.25: *Cytotoxicity of nascent P-40 nanoparticles in HeLa cell lines.*

2.3.6 Cellular Uptake and Drug Internalization

DOX, TPT, and CUR are luminescent drugs and hence free drugs and drug loaded to P-40 were administered to the HeLa cells (at a concentration of 2.0 µg/mL) and incubated for 4h before fixing them to study their uptake and localization inside the cells. DOX was excited at 560 nm and visualized through red channel. The nuclei of the cells were stained with Hoescht and visualized through blue channel upon excitation with 405 nm laser. In the case of free DOX administered cells, the drug was seen only at the nucleus and it superimposed to give magenta colour emission (see figure 2.26, first row). On the other hand, the uptake of the DOX loaded polymer nano-assemblies exhibited red emission at cytoplasm and magenta at the nucleus. This is another indication that the polymer nano-assemblies are initially taken up by the cells and they ruptured in acidic endosomes and esterase rich lysosomes in the cytoplasm. The merged images for DOX loaded nanoparticles clearly showed two different fluorescent region (see the second row in figure 2.26). Similar features were

observed for free TPT and TPT loaded P-40 uptake in cells.The comparison of the fluorescent intensities revealed that the free TPT was taken up much less compared to that of TPT loaded in P-40.

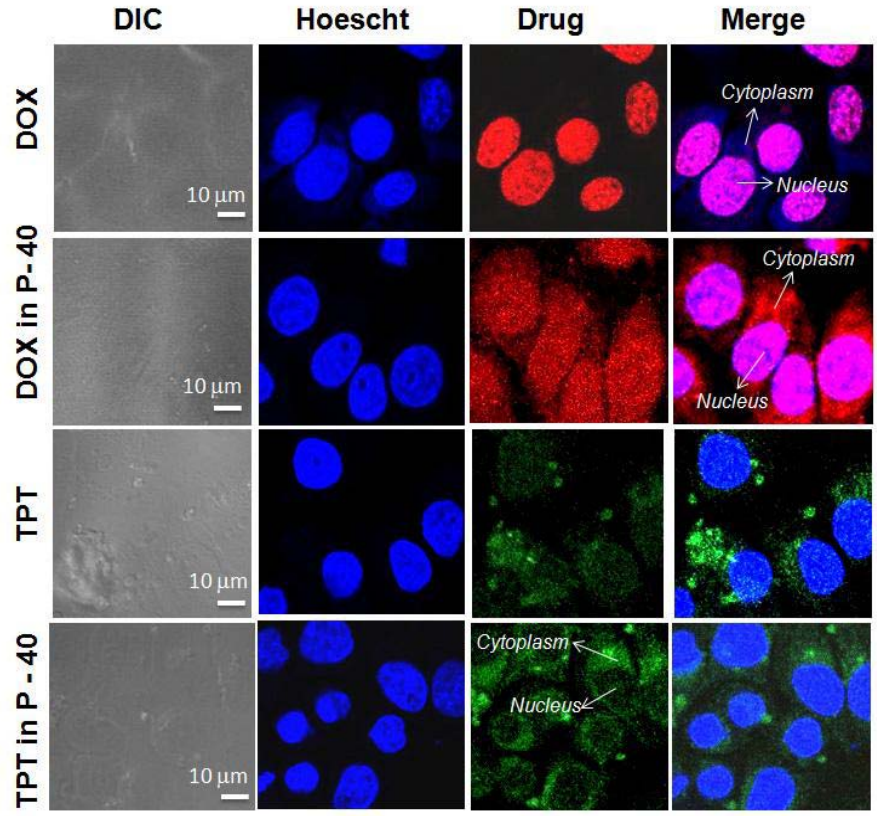

Figure 2.26: *CLSM images of Hela cells incubated with free drugs and drug loaded P-40 scaffold for 4 h at 37° C.*

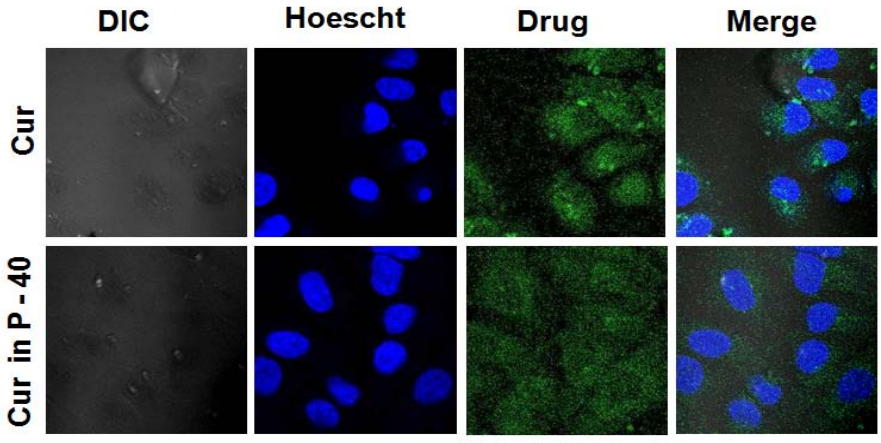

Figure 2.27: *Confocal images of P-40 loaded with CUR and free CUR in HeLa cell lines.*

A similar trend was observed in case of water insoluble CUR where a more intensity of CUR was observed from the cytoplasm and the nucleus of the cells (see fig 2.27). The cellular uptake of free DOX and TPT and their respective analogues with **P-40** loaded drugs were also studied in the breast cancer MCF-7 cell lines.

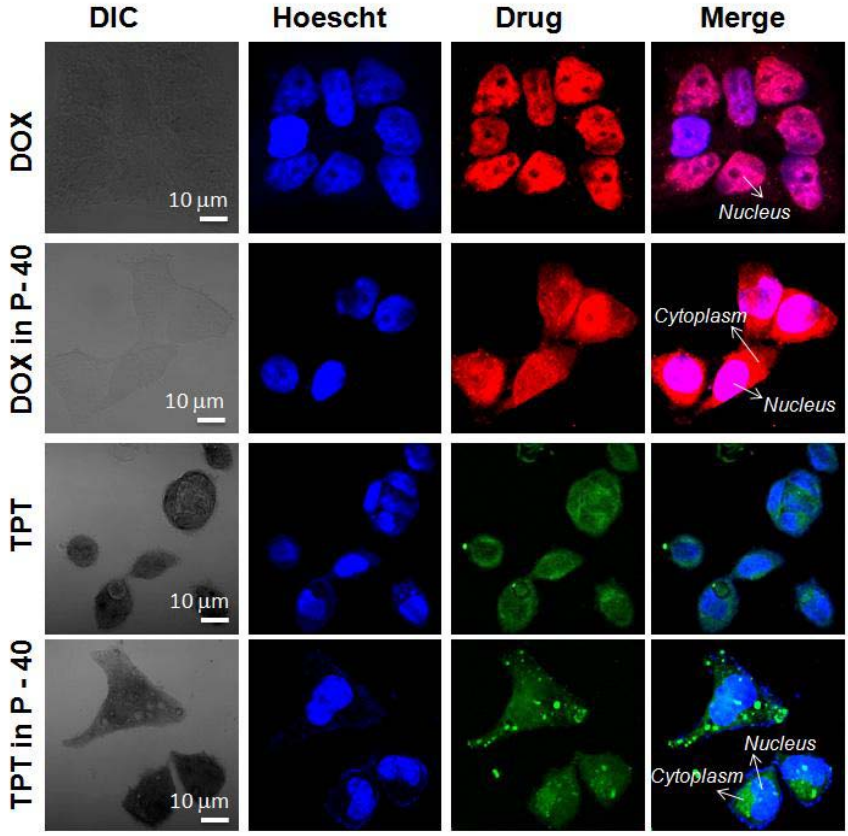

Figure 2.28: *CLSM images of MCF 7 cells incubated with free drugs and drug loaded P-40 scaffold for 4 h at 37° C.*

The corresponding images of P-40 nanoparticles loaded with DOX and TPT (and respective free DOX, and free TPT), with Hoechst stained nuclei are shown in figure 2.28. It can be observed that the free DOX showed red fluorescence only at the nucleus and this merges perfectly with the Hoescht stained nucleus. When the same concentration of DOX loaded in P-40 nanoparticles were administered to the cells, the strong red fluorescence from the nucleus and the cytoplasm were observed as earlier seen in HeLa cells (see figure 2.26). This indicated that the DOX loaded P-40 was also taken up by the breast cancer cells and delivered at the cytoplasm. The presence

of DOX in the nucleus also indicated the release of the DOX from the nanoparticles scaffold inside the cell and further inclusion in the nucleus. Similar observation was made in case of TPT cellular uptake where in the free TPT was distributed evenly in the cytoplasm and the nucleus of the cells as seen in figure 2.28. The enhanced green fluorescence from the cytoplasm and the nucleus by the corresponding P-40 loaded scaffolds showed clearly a better uptake of TPT by the cell compared to its free counterpart. The merged images as seen in figure 2.28 clearly indicated the release of TPT in the cytoplasm and eventual accumulation inside the nucleus. From the uptake studies of the anticancer drugs in both the HeLa cells and MCF 7 cell lines, a conclusion was drawn that drug loaded nanoparticles of P-40 were capable of releasing the respective drugs in the cytoplasm which was further substantiated by a gradual accumulation of majority drugs inside the nucleus without being excreted out of the cell via exocytosis or other clearance mechanism of the cells. Amphiphilic copolymer P-40 was seen to be capable of delivering multiple anticancer drugs to the nucleus and the cytoplasm of the cells. Both imaging the cells and also good cell killing was accomplished in cancer cells (HeLa cells and MCF 7 cells). Further studies with respect to the entry mechanism of uptake of these newly designed nano-carriers in cell membranes and their *in vivo* experiments are yet to be carried out. The advantages of the current polymer design is that the BOC units can be further utilized for drug conjugation, anchoring targeting units or for its NH_3^+ ions for deliverying of DNA or RNA through electrostatic interactions. This new pH and enzyme dual responsive approach is not restricted to L-aspartic acid based polymer scaffold alone; in general, this concept can be expanded to other polymer scaffolds for achieving better efficacies in cancer treatment.

2.4 Conclusion

In summary, the present investigation demonstrates one of the first example for L-amino acid based biodegradable polyesters nano-carriers as unique pH and enzyme dual responsive intracellular scaffold for delivering multiple anticancer drugs from single polymer scaffold. Thermo-responsive polymerization methodology was developed to make amphiphiic polyesterstructure from L-amino acid resources. The polymers nano-particles were in-built with polyester backbone for enzymatic biodegradation and acid-labile BOC urethane pendant for transformation into cationic species. In the neutral form; the BOC urethane units induced hydrogen bonding secondary structures and stabilize the nanoparticles. In acidic environment (pH < 6.0), the BOC unit was transformed in to NH_3^+ cationic species facilitating disassembly. FT-IR and Zeta potential measurements provided direct evidence for the transformation of BOC urethane unit into cationic species. Enzyme responsiveness of the polymer nanoparticles were tested in the presence of esterase enzymes (at 37 °C in PBS) and it was found that the polymer nanoparticles were completely biodegraded by enzymes to release > 80 % drugs in 12 h. The cytotoxicity studies revealed that the nascent polymer nanoparticles were non-toxic whereas the drug loaded nanoparticles exhibited 100 % cell death in cervical (HeLa) and breast cancer (MCF-7) cell lines. The drug internalization at the cytoplasm and nucleus seemed to be identical for all three drugs DOX, TPT and CUR in both HeLa and MCF 7 cells. This marks as the advantage of these polymer nanoparticles with high affinity to deliver the loaded cargoes to cancer cells. In a nut shell, the present investigation demonstated one of the first example for L-amino acid based aliphatic polyesters as potential nano-carriers for anticancer drugs and exploited their unique dual pH and enzyme-responsiveness for delivering multiple anticancer drugs from single polymer scaffold in cancer treatment.

References

1. S. Mura, J. Nicolas, P. Couvreur, *Nat. Mater.* **2013**, *12*, 991-1003.
2. O. Gok, I. Kosif, T. Dispinar, T. N. Gevrek, R. Sanyal, A. Sanyal, *Bioconjugate Chem* **2015**, *26*, 1550-1560.
3. J.-Z. Du, T.-M. Sun, W.-J. Song, J. Wu ,J. Wang, *Angew. Chem. Int. Ed.***2010**, *49*, 3621-3626.
4. Q. Hu, P. S. Katti, Z. Gu, *Nanoscale* **2014**, *6*, 12273-12286.
5. M. A. C. Stuart, W. T. S. Huck, J. Genzer, M. Muller, C. Ober, M. Stamm, G. B. Sukhorukov, I. Szleifer, V.V. Tsukruk, M. Urban, F. Winnik, S. Zauscher, I. Luzinov, S. Minko, *Nat. Mater.* **2010**, 9, 101-113.
6. J. Liu, B. Zhang, Z. Luo, X. Ding, J. Li, L. Dai, J. Zhou, X. Zhao, J. Ye, K. Cai, *Nanoscale* **2015**, *7*, 3614-3626.
7. A. V. Fuchs, N. Kotman, J. Andrieu, V. Mailänder, C. K. Weiss, K. Landfester, *Nanoscale***2013**, *5*, 4829-4839.
8. P. S. Pramod, R. Shah, S. Chaphekar, N. Balasubramanian, M. Jayakannan, *Nanoscale* **2014**, *6*, 11841-11855.
9. P. S. Pramod, K. Takamura, S. Chaphekar, N. Balasubramanian, M. Jayakannan, *Biomacromolecules* **2012**, *13* , 3627–3640.
10. B. Surnar, K. Sharma, M. Jayakannan, *Nanoscale* **2015**, *7*, 17964-17969.
11. C. Pottier, G. Morandi, V. Dulong, Z. Souguir, L. Picton, D. L. Cerf *J. Polym. Sci., Part A: Polym. Chem.* **2015**, *53*, 2606-2616.
12. M. A. Boerman, H. L. V. Der Laan, J. C. M. E. Bender, R. Hoogenboom, J. A. Jansen, S. C. Leeuwenburgh, J. C. M. V. Hest, *J. Polym. Sci., Part A: Polym. Chem.* **2016**, *54*, 1573-1582.
13. Y. Chu, H. Yu, Y. Ma, Y. Zhang, W. Chen, G. Zhang, H. Wei, X. Zhang, R. Zhuo, X. Jiang, *J. Polym. Sci., Part A: Polym. Chem.* **2014**, *52*, 1771-1780.
14. S. G. Roy, P. De, *J. Polym. Sci., Part A: Polym. Chem.* **2014**, *131*, 41084-41096.
15. Y. Ma, G. Zhang, L. Li, H. Yu, J. Liu, C. Wang, Y. Chu, R. Zhuo, X. Jiang,*J. Polym. Sci., Part A: Polym. Chem.* **2016**, *54*, 879-888.
16. P. S. Pramod, R. Shah, M. Jayakannan, *Nanoscale* **2015**, *7*, 6366-6652.

17. C. Fang, F. M. Kievit, Y-C. Cho, H. Mok, O. W. Press, M. Zhang, *Nanoscale* **2012**, *4*, 7012-7020.
18. I. R. Fernando, D. P. Ferris, M. Frasconi, D. Malin, E. Strekalova, M. D. Yilmaz, M. W. Ambrogio, M. M. Algaradah, M. P. Hong, X. Chen, M. S. Nassar, Y. Y. Botros, V. L. Cryns, J. F. Stoddart, *Nanoscale* **2015**, *7*, 7178-7183.
19. B. Surnar, M. Jayakannan, *Biomacromolecules***2013**,*14*, 4377-4387.
20. Y. Ma, X. Jiang, R. Zhuo, *J. Polym. Sci., Part A: Polym. Chem.* **2013**, *51*, 3917-3924.
21. J. Bian, Y. Hao, J. He, W. Zhang, M. Zhang, P. Ni,*J. Polym. Sci., Part A: Polym. Chem.* **2014**, *52*, 3005-3016.
22. M. Deng, S. G. Kumbar, L. S. Nair, A. L. Weikel, H. R. Allcock, C. T. Laurencin, *Adv. Funct. Mater.* **2011**, *14*, 2641-2651.
23. M. Deng, L. S. Nair, S. P. Nukavarapu, S. G. Kumbar, T. Jiang, A. L. Weilkel, N. R. Krogman, H. R. Allcock, C. T. Laurencin, *Adv. Funct. Mater*. **2010**, *17*, 2743-2957.
24. H. Sun, F. Meng, A. A. Dias, M. Hendriks, J. Feijen, Z.Zhong, *Biomacromolecules***2011**,*12*, 1937-1955.
25. A. Lalatsa, A. G. Schätzlein, M. Mazza, T. B. H. Le, I. F. Uchegbu, *J. Controlled Release* **2012**, *161*, 523-536.
26. A. Dehsorkhi, V. Castelletto, I. W. Hamley, *J. Pept. Sci.***2014**, *20*, 453-467.
27. T. J. Deming, *Prog. Polym. Sci*. **2007**, *32*, 858-875.
28. A. Carlsen and S. Lecommandoux, *Curr. Opin. Colloid Interface Sci.*,**2009**, ***14***, 329-339.
29. K. Osada and K. Kataoka, Adv. *Polym. Sci*., **2006**,*202*, 113-153.
30. C. Cai, L. Wang and J. Lin, *Chem. Commun.*, **2011**, *47*, 11189-11203.
31. R. N. Shah, N. A. Shah, M. M. D. R. Lim, C. Hsieh, G. Nuber and S. I.,Stupp, *Proc. Natl. Acad. Sci. USA*,**2010, *107***, 3293-3298.
32. P. Zhang, A. G. Cheetham, Y-a. Lin and H. Cui, *ACS Nano*,**2013**, *7*, 5965-5977.
33. H. Xu, Q. Yao, C. Cai, J. Gou, Y. Zhang, H. Zhong and X. Tang, *J. Controlled Release*, **2015**, *199*, 84-97.

34. L. Yin, Z. Song, K. H. Kim, N. Zheng, H. Tang, H. Lu, N. Gabrielson and J. Cheng, *Biomaterials*, **2013**,*34*, 2340-2349.
35. A. Ghaffar, G.J.J. Draaisma, G. Mihov, A. A. Dias, P.J. Schoenmakers and S. Van der Wal, *Biomacromolecules*,**2011**,*12*, 3243-3251.
36. T. Akagi, M. Higashi, T. Kaneko, T. Kida and M. Akashi, *Biomacromolecules*, **2006**, *7*, 297-303.
37. K. Guo and C. C. Chu, *Biomacromolecules*, **2007**,*8*, 2851-2861.
38. H. Sun, R. Cheng, C. Deng, F. Meng, A. A. Dias, M. Hendriks, J. Feijen and Z. Zhong, *Biomacromolecules*,**2015**, *16*, 597-605.
39. J. Rautio, H. Kumpulainen, T. Heimbach, R. Oliyai, D. Oh, T. Järvinen and J. Savolainen, *Nat. Reviews*, **2008**, *7*, 255-270.
40. Y. Ikada and H. Tsuujf, *Macromol. Rapid. Commun*. **2000**, *21*, 117-132.
41. M. Vert, *Biomacromolecules*, 2005, **6**, 538-546.
42. S. Anantharaj and M. Jayakannan, *Biomacromolecules*, **2012**, *13*, 2446-2455.
43. S. Anantharaj and M. Jayakannan, *Biomacromolecules*, **2015**, *16*, 1009-1020.
44. S. Anantharaj and M. Jayakannan, *J. Polym. Sci., Polym Chem.***2016**, *54*, 1065-1077.
45. R. Aluri and M. Jayakannan, *Polym. Chem*. 2015, **6,** 4641-4649.
46. S. Anantharaj and M. Jayakannan, *J. Polym. Sci.,Polym Chem.***2016**, *54*, POLA 28172 (in press)
47. S. Kashyap, N. Singh, B. Surnar and M. Jayakannan, *Biomacromolecules*,**2016**, *1*, 384-398.
48. L. Wang, G. Liu, X. Wang, J. Hu, G. Zhang and S. Liu, *Macromolecules*,**2015**, *48*, 7262-7272.
49. S. R. Mane, V. N. Rao and R. Shunmugan, *ACS Macro Lett.*, **2012**, *1*, 482-488.
50. J. Mattia and P. Painter, *Macromolecules*, **2007**, *40*, 1546-1554.
51. F-S. Yen, L-L. Lin, J-L. Hong, *Macromolecules*, **1999**, *32*, 3068-3079.
52. B. Kulkarni, B. Surnar and M. Jayakannan, *Biomacromolecules*,**2016**, *17*, 1004-1016.

Chapter 3

π-Conjugate Fluorophore-tagged and Enzyme-responsive L-Aspartic acid Polyester Nano-carrier and their Colour-tunable Intracellular FRET Probe in Cancer Cells

Abstract

The present investigation accounts one of the first example of enzyme-responsive and π-conjugate-tagged L-amino acid amphiphilic polymer and their fluorescence resonance energy transfer (FRET) probes for colour-tunable intracellular bio-imaging in cancer cells. Melt polymerizable oligo-phenylenevinylene (OPV) π-conjugated diol was tailor-made and subjected to thermo-selective melt transesterification reaction with multi-functional L-aspartic acid monomer to yield OPV-tagged amphiphilic luminescent polyesters. These amphiphilic polyesters self-assembled through strong aromatic π-π stacking and hydrophilic/hydrophobic non-covalent forces into < 200 nm size blue-luminescent nanoparticles in aqueous medium. The OPV-tagged polymer nanoparticles served as FRET donor and encapsulated water insoluble Nile Red (NR) fluorophore as a FRET acceptor. Detail photophysical studies revealed that both the OPV and NR were confined within Förster distance in the polymer nano-container and the nano-domains provided appropriate geometry for efficient excitation energy transfer from OPV to NR. Cytotoxicity studies in breast cancer (MCF 7), cervical cancer (HeLa) and normal (Wild-type MEF) cell lines revealed that both the nascent luminescent OPV nanoparticles and OPV-NR FRET probes were non-toxic to cells up to 100 μg/mL. Confocal microscope images confirmed the efficient transportation of polymer and FRET probes across the cell membranes and their preferable accumulation in the cytoplasm of the cells. Lysosomal tracker assisted live cell imaging provided direct evidence for the localization of the polymer nanoparticles at the lysosomal compartments in the cytoplasm. In vitro enzyme-responsive studies revealed that the aliphatic polyester backbone in the polymer nanoparticles was readily biodegradable by lysosomal enzymes like esterase, chymotrypsin, trypsin and also redox GSH species in the cytoplasm. Selective photoexcitation in confocal microscope exhibited bright OPV blue-luminescence and strong red-emission from NR followed by the excitation energy transfer and occurrence of FRET process at the intracellular environment in cancer cell lines. Both the polymer design and the biodegradable polymer FRET concept are completely new; thus, the present approach opens up new platform of research opportunities for natural L-amino acid based luminescent polymer probes for colour-tunable bio-imaging in cancer cells.

3.1 Introduction

Fluorescent-probe tagged amphiphilic polymers are emerging as dual-function nano-carriers to deliver anticancer drugs/genes to cancer tissues as well as luminescent biomarkers in cancer diagnosis.[1-7] Förster or fluorescence resonance energy transfer (FRET) is one of the most powerful non-invasive fluorescence probe[8] and it functions on the basis of selective photoexcitation energy transfer from donor to acceptor chromophores within the nano-confinement of ≤ 50 Å.[9] FRET technique is explored for real-time tumor-imaging,[10-11] drug release kinetics,[12-13] studying the self-assembly of amphiphilic block copolymers,[14] protein folding under physiological conditions,[15-16] quadruplex-to-duplex transitions in DNA,[17] molecular interactions at the mammalian cell surfaces,[18-20] two-photon imaging in cancers,[21-22] and sensing of bilirubin in human serum,[23] etc. Few applications are shown in figure 3.1.

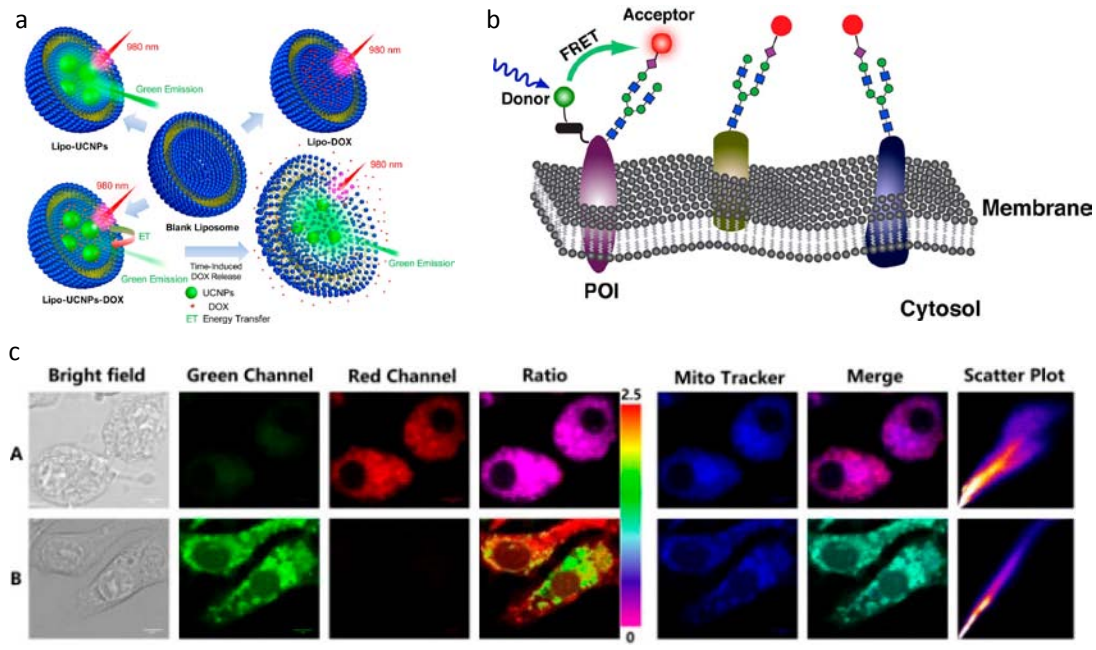

Figure 3.1: *Er^{3+} and Yb^{3+} doped nanoparticles for for DOX loading and potent theranostic materials (a) (Adapted from Huang et al, J. Phys. Chem. B,* **2016**, *120,* 4992−5001.*), FRET methodology for bio-imaging of cell surface glycans highly specific to pretien binding. (b) (Adapted from Lin et al, J. Am. Chem. Soc.* **2014**, *136,* 679−687*), Confocal fluorescence imaging for tracking of endogenous $OONO^-$ found preferentially in mitochondria using FRET based PNCy3Cy5 small molecules in stimulated RAW264.7 macrophages (c) (Adapted from Jia et al, J. Am. Chem. Soc.* **2016**, *138,* 10778−10781*).*

In the last 2-3 decades, significant advancements made in the area of conducting polymers for optoelectronic devices has opened new arena of opportunities for water soluble cationic π-conjugated polymers as luminescent bio-probes.[2, 24] Cationic and water soluble polyfluorenes are some of the most important π-conjugated polymers reported for FRET applications.[25-32] Polyacrylates based random and block copolymers having optical chromophores in the side chains were also reported for FRET applications.[12,14] Few examples are shown in figure 3.2. Unfortunately, the non-biodegradability of the rigid C-C backbone in the π-conjugated polymers and acrylates are still one of the major challenges to overcome for their wide applicability in biomedical research.

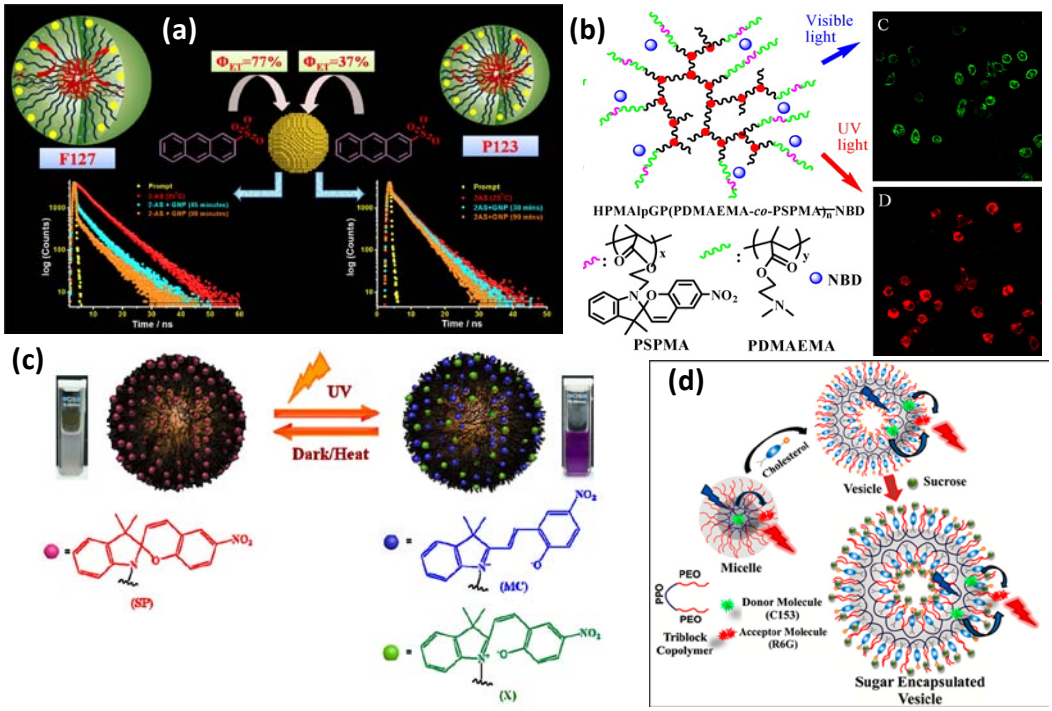

Figure 3.2: *Nano-metal surface energy transfer (NSET) from 2-anthracene sulfonate (2-AS) to gold nanoparticles in water soluble triblock copolymers.(Adapted from Rakshit et al, J. Phys. Chem. B* **2015**, *119*, 8457−8467*) (a), Photo and pH responsive hyperbranched acrylate based polymers for FRET bio-imaging and diagnostic applications (Adapted from Wang et al, Biomacromolecules* **2012**, *13*, 2585−2593*) (b), Fluorescent acrylate based Silica polymer hybrids for bio-imaging applications (Adapted from Achilleos et al, Langmuir* **2016**, *32*, 5981−5989*) (c), FRET (coumarin 153 donor and rhodamine 6G acceptor) based studies for monitoring micelles , vesicles and niosomes morphologies from pluronic triblock copolymer (F127)−cholesterol and their interaction with sugar (sucrose) molecules (Adapted from Roy et al, J. Phys. Chem. B* **2016**, *120*, 131−142*) (d).*

New synthetic approaches towards the development of luminescent π-conjugated chromophores in combination with biodegradable polymer backbone would provide new opportunities for biodegradable-cum-luminescent π-conjugated nano-scaffolds in a single system.[33-34] Further, this new design would also allow simultaneous tracing of the cellular uptake of the luminescent nano-carriers and their responsiveness to digestion at the intracellular regions in cancer cells. Unfortunately, up to our knowledge, no efforts have been taken until now to develop biodegradable luminescent polymers and their FRET probes which are very crucial for long-term application in cancer treatment.

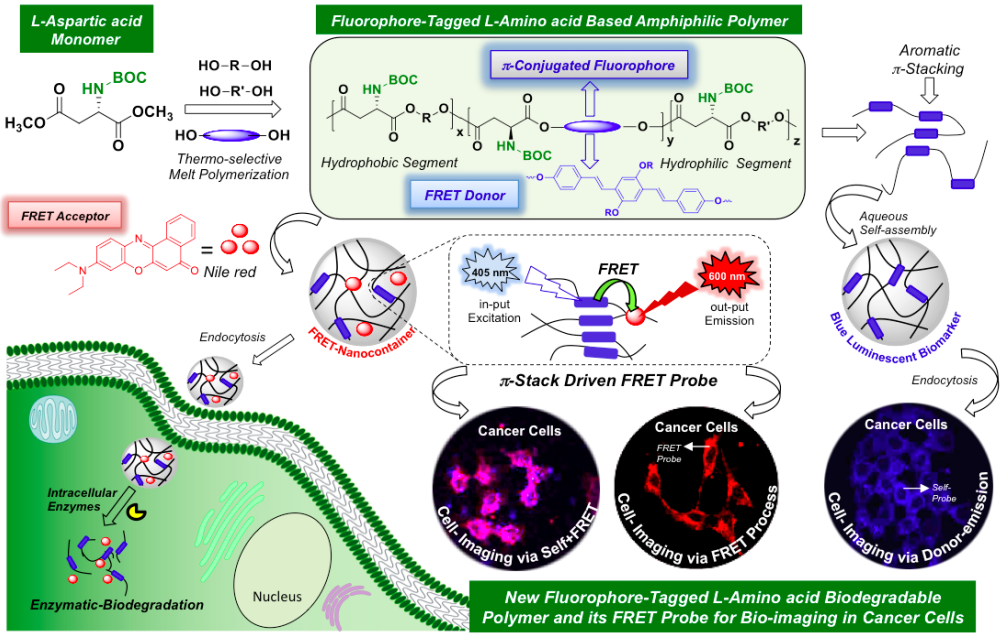

Figure 3.3: *Development of enzyme-responsive π-conjugated fluorophore-tagged L-aspartic acid polyester and its FRET probe for bio-imaging at the intracellular level.*

L-Amino acid based polymers are important biomaterials due to the large abundance of monomer resources in nature along with their excellent bio-availability and biodegradability under physiological conditions.[35] Polypeptides, [36] PEG-containing di-and tri-block polypeptide block copolymers, [37] poly(ester-amides), [38-41] poly(α-hydroxy acids), [42] polycarbonates, [43-47] and poly(disulfide)s[48-49] were developed from L-amino acid resources and they were employed for drug and gene delivery. From our laboratory, we reported solvent free melt polycondensation

approach for L-amino acid resources to synthesize wide range of linear poly(ester-urethane)s, [50-51] hyperbranched poly(ester-urethane)s, [52] disulfide containing polyesters[53] and functional aliphatic polyesters. [54] Enzyme and pH responsive L-aspartic amphiphilic polyester[55] and L-tyrosine poly(ester-urethane) [56] were also developed for delivery of multiple anticancer drugs. Unfortunately, most of these L-amino acid polymers were non-luminescent in nature; thus, their cellular uptake and enzymatic biodegradation at the intracellular compartments could not be studied by fluorescence techniques. To accomplish this goal, here we report a new polymer design by combining the π-conjugated fluorophore and enzyme-responsive L-amino acid based aliphatic polyesters. Our expertise in the area of melt polymerization synthetic methodologies for L-amino acid polymers and π-conjugated materials in bio-imaging[57-59] provided a unique opportunity to combine these two areas to construct a novel *enzyme-responsive* FRET probe concept. Aliphatic esters are one of the most sought after enzyme-responsive chemical stimuli in pro-drug industry (more than 49 %); thus, L-aspartic acid based aliphatic polyester was chosen as the enzyme-biodegradable backbone. [60] A new melt polymerisable π-conjugated oligo-phenylenevinylene (OPV) diol was tailor-made[33] and subjected to thermo-selective melt transesterification (developed in our lab) to accomplish the targeted polymer structures. This new enzyme-responsive and biodegradable FRET probe concept is shown in figure 3.3. The present investigation emphasises the design of π-conjugate-tagged L-amino acid based polymer luminescent probes in order to study the functioning of the FRET probe by detailed photophysical techniques, and also to demonstrate their intracellular bio-imaging capabilities in cancer cells. The new polymer luminescent probe has the following in-built features: (i) amphiphilicity in the L-aspartic polyester backbone and blue-luminescent characteristics accomplished by choosing appropriate OPV-diol along with hydrophilic/hydrophobic segments , (ii) the strong aromatic π-π-stacking interaction among the OPV chromophores produced π-aggregated species which acted as blue-luminescent self-probe as well as FRET donor, (iii) the encapsulation of water insoluble Nile Red (FRET acceptor) in the polymer nanoparticle cavity enabled the formation of OPV-NR FRET donor-acceptor pair, (iv) the FRET probe was found to be enzymatically-biodegradable, non-toxic and readily taken up by cancer cells, and (v) selective photoexcitation experiments in

confocal microscope facilitated the colour-tunable imaging with blue, red and magenta emission at the intracellular level in breast cancer (MCF 7), cervical cancer (HeLa) and normal embryonic fibroblast (WT-MEF) cell lines. Upon exposure to lysosomal-enzymes, the polymer nano-scaffold underwent biodegradation to excrete the polymer donor and NR acceptor molecules once the probing action was done at the cellular level. Detailed photophysical techniques such as absorption, emission and time-correlated fluorescence decay dynamic experiments were carried out to determine the Förster distance and to confirm the occurrence of FRET process between the OPV donor and NR acceptor. The FRET probe was employed as colour-tunable biomarker and the proof-of-concept was demonstrated *in vitro* at the intracellular compartments of cells. The present investigation opens up new platform of research activities for the development of biodegradable L-amino acid polymer FRET probes which is yet to be explored in the literature.

3.2 Experimental Section

Materials: L-Aspartic acid, 1,12-dodecandiol (DD) , hydroquinone, triethylphosphite, 4-hydroxybenzaldehyde, KOtBu (1.0 M in THF), triethylene glycol (TEG), ethylhexyl bromide, titanium tetrabutoxide ($Ti(OBu)_4$), 2-chloroethanol, Nile Red, potassium iodide, curcumin, horse liver esterase enzyme, MTT crystal (tetrazolium salt: 3-(4,5-dimethylthiazolyl)-2,5-diphenyltetrazolium bromide), fluoromount^{TM} aqueous mounting medium , 42,6-diamidino-2-phenylindole (DAPI), chymotrypsin, papain and glutathione (GSH) were purchased from sigma aldrich chemicals. Trypsin phosphate versene glucose (TPVG) solution 1X was purchased from Hi Media. Mammalian breast cancer MCF 7, cervical cancer (HeLa) and normal wild type-MEF cells were maintained in a phenol red containing Gibco DMEM with 10% (v/v) fetal bovine serum (FBS) and 1% (v/v) penicillin–streptomycin. 96-well and 6-well flat bottomed plastic plates were obtained from Costar and Lab TEK 8 well cover glass chamber were obtained from Nunc Lab Tek. Lysotracker® Green DND-26 was obtained from Cell Signalling Technologies (CST). Paraformaldehyde, HBr in glacial acetic acid, potassium carbonate, potassium sulphate, potassium hydroxide, sodium bicarbonate were purchased locally. HPLC THF and HPLC DMSO were obtained from Spectrochem Laboratories. Thionyl chloride, methanol,

THF, ethyl acetate, petroleum ether, DMF, DMSO and other solvents were purchased locally and purified before use. All the other reagents were purchased from Sigma Aldrich and used as such.

General Procedure: Primary characterization of synthesized polymers was done using ^{1}H-NMR and ^{13}C-NMR 400 and 100 MHz JEOL NMR Spectrophotometer respectively. $CDCl_3$ was used as a reference solvent and TMS was used as internal standard. Mass of the compounds synthesised were determined using Applied Bio system 4800 PLUS matrix-assisted laser desorption/ionization (MALDI)TOF/TOF analyzer and Gas Chromatography-Mass Spectrometry GC 2010 Shimadzu. Thermogravimetric analysis (TGA) was used to measure the thermal stability of the polymers using PerkinElmer thermal analyzer STA 6000 model under nitrogen environment at a heating rate of 10°C/min. Indium standards were used to calibrate the system before use. TA Q20 Differential Scanning Calorimetry (DSC) was used to obtain the DSC curves of polymers at a heating and cooling rate of 10°C/min. In order to remove thermal prehistory from samples the polymers were preheated to melt before recording their thermograms. The molecular weights of the polymer were obtained in THF using Gel permeation chromatographic (GPC) analysis with Viscotek VE 1122 pump, Viscotek VE 3580 RI detector and Viscotek VE 3210 UV/VIS detector with respect to polystyrene standards. Dynamic Light Scattering (DLS) from Malvern Instruments was used for estimating the size of polymer nanoparticles suspended in water. Microscopic images were obtained using Zeiss Ultra Plus scanning electron microscope for field emission scanning electron microscopy (FE-SEM) images, Veeco Nanoscope IV instrument in tapping mode for Atomic Force Microscopy (AFM) images and LSM710 confocal microscope for confocal images. Perkin Elmer Lambda 45 UV-vis spectrophotometer and SPEX Fluorolog HORIBA JOBIN VYON fluorescence spectrophotometer (with double gating 0.22 m Spex 1680 monochromator and excitation source as 450 W Xe lamp) were employed to obtain absorption spectra and emission spectra for dye and drug loaded polymer in aqueous media. Varioskan FLASH instrument was used for measuring absorbance in MTT experiments.

Synthesis of 1,4-Bis(2-ethylhexyloxy) benzene (1): Hydroquinone (15.0 g, 0.14 mol) and potassium hydroxide (30.6 g, 0.55 mol) were dissolved in dry DMSO (100 mL) and heated to 80 °C for 30 minutes. This was followed by dropwise addition of 2-ethylhexyl bromide (53.2 mL, 0.30 mol) and the reaction mixture was refluxed at 80 °C for 48 h under nitrogen atmosphere. The reaction mixture was cooled, DMSO was distilled off under vacuum, and the product was extracted in DCM using washing with 5% NaOH. The organic layer was dried over anhydrous Na_2SO_4 and solvent was evaporated to obtain brown solid mass. It was further purified using silica gel column using pet ether system. Yield = 30.0 g (66 %). ^{1}H NMR ($CDCl_3$, 400 MHz) δppm: 6.85 ppm (s, 4H, aromatic protons), 3.81 (m, 4H, -OC**H**$_2$), 1.72 (m, 2H, OCH_2C**H**), 1.51-1.36 (m, 16H, aliphatic protons), and 0.97-.92 (t, 12 H, C**H**$_3$). ^{13}C NMR ($CDCl_3$, 100 MHz) δ ppm: 153.51, 115.44, 71.28, 39.54, 30.61, 29.17, 23.93, 23.16, 14.19, 11.19. FT-IR (cm^{-1}): 2957, 2924, 2864, 1506, 1464, 1382, 1283, 1222, 1109, 1038. MALDI-TOF-MS: m/z calculated for $C_{22}H_{38}O_2$: 334.54 and found 357.30 [$M^+ + Na^+$] and 373.28 [$M^+ + K^+$].

Synthesis of 1,4-Bis(bromomethyl)-2,5-bis-(2-ethylhexyloxy) (2): Compound **1** (10.0 g, 0.03 mol) was dissolved in glacial acetic acid (30.0 mL), and paraformaldehyde (3.60 g, 0.12 mol) was added to this solution at 25 °C. The reaction mixture was stirred for 15 min followed by drop wise addition of HBr in glacial acetic acid (30.0 mL, 0.06 mol). The reaction mixture was heated to 80 °C and was refluxed for 6 h. The reaction mixture was cooled to 25 °C and carefully poured into large amount of water. A white precipitate was observed and this product was re-crystallized three times in hot isopropanol to yield pure product. Yield: 9.0 g (58 %). ^{1}H NMR ($CDCl_3$, 400 MHz) δ ppm: 6.86 ppm (s, 2H, aromatic protons), 4.54 (s, 4H, -C**H**$_2$Br), 3.89 (d, 4H, OC**H$_2$**), 1.79-1.74 (m, 2H, -OCH_2C**H**), 1.51-1.34 (m, 22H, aliphatic protons) and 0.98-.90 (m, 12 H, C**H**$_3$). ^{13}C NMR ($CdCl_3$, 100 MHz) δppm: 150.79, 127.45, 114.31, 71.01, 39.68, 30.72, 29.19, 28.84, 24.10, 23.14, 14.17, 11.32 . FT-IR (cm^{-1}): 2960, 2928, 2867, 1505, 1466, 1442, 1307, 1221, 1120, 1085, 1030 and 911.

Synthesis of Tetraethyl(2,5-bis(2-ethylhexyloxy)-1,4-phenylene)bis(methylene) diphosphonate (3): Compound **2** (4.0 g, 7.7 mmol) and triethylphosphite (2.90 mL, 17.0 mmol) were refluxed at 150 °C for 10 h. The excess of triethylphosphite was removed by vacuum distillation and the product was purified using silica gel using ethyl acetate and pet ether (20% v/v). Yield = 4.67 g (96 %).^{1}H NMR ($CDCl_3$, 400 MHz) δ ppm: 6.93 ppm (s, 2H, Ar-**H**), 4.05-3.96 (m, 8H, -POC**H**$_2$CH$_3$), 3.81-3.79 (m, 4H, OC**H$_2$**), 3.24-3.19 (d, 4H, C**H**$_2$P), 1.72-1.69 (m, 2H, -OCH$_2$C**H**), 1.46-1.31 (m, 16H, aliphatic protons), 1.23 (t, 12H, -CH$_2$C**H**$_3$) and 0.94-0.90 (m, 12 H, C**H**$_3$). ^{13}C NMR ($CDCl_3$, 100 MHz) δ ppm: 150.50, 119.38, 114.75, 71.24, 61.91, 39.74, 30.67, 29.18, 26.91, 23.98, 23.11, 16.42, 14.13, 11.22. FTIR (cm^{-1}): 2960, 2926, 2867, 1648, 1509, 1466, 1391, 1247, 1210, 1163, 1097, 1022, 955. MALDI-TOF-MS: m/z calculated for $C_{32}H_{60}O_8P_2$: 634.77 and found 657.47 [M^+ + Na^+] and 673.45 [M^+ + K^+].

Synthesis of 4-(2-Hydroxyethoxy) benzaldehyde (4): 4-Hydroxybenzaldehyde (5.0 g, 0.04 mol), potassium carbonate (14.14 g, 0.10 mol) was taken in dry DMF (60.0 mL) and heated at 80 °C for 10 min and further stirred for 1 h. 2-Bromoethanol (4.35 mL, 0.06mol), catalytic amount of KI were added and reaction was refluxed for 48 h. DMF was removed from the reaction mixture by vacuum distillation, and the product was extracted in DCM. The crude product was further purified in silica gel using pet ether and ethyl acetate system (4:1, v/v). Yield: 2.7 g (40 %). ^{1}H NMR ($CDCl_3$, 400 MHz) δ ppm: 9.89 (s, 1H, C**H**O), 7.84 (d, 2H, Ar-**H**), 7.03 (d, 2H, Ar-**H**), 4.16 (t, 2H, ArOC**H**$_2$), and 4.01 (t, 2H, C**H**$_2$OH). ^{13}C NMR ($CDCl_3$, 100 MHz) δppm: 190.99, 163.77, 132.14, 130.27, 114.90, 69.64, 61.23. FTIR (cm^{-1}): 3395, 2939, 2873, 1673, 1597, 1508, 1395, 1253, 1216, 1158, 1078. GC-MS m/z calculated for $C_9H_{10}O_3$= 166.17 and found 166.

Synthesis of Hydroxyl functionalized oilgo-phenylenevinylene (HO-OPV-OH): Compound **3** (4.0 g, 6.30 mmol) and compound **4** (2.2 g, 13.0 mmol) were taken in dry tetrahydrofuran (60.0 mL) and the contents were cooled to 4°C under nitrogen atmosphere. Potassium t-butoxide (37.0 mL in THF, 6.30 mmol) was added and the reaction was continued for 12 h with stirring at 25 °C. THF was evaporated

and the content was added to water, extracted using chloroform. It was dried over Na_2SO_4 , solvent was removed and the product was purified in silica gel column using pet ether and ethyl acetate system (50 % v/v). Yield = 2.1 g (50 %) ^{1}H NMR ($CDCl_3$, 400 MHz) δppm: 7.48-7.46 ppm (d, 4H, Ar-**H**), 7.35 (d, 2H, -C**H**=CH), 7.11 (d, 2H, -CH=C**H**) and (s, 2H, Ar-**H**), 6.94- 6.92 (d, 4H, Ar-**H**), 4.14- 4.12 (d, 2H, C**H$_2$**OH), 3.96 (d, 2H, Ar-C**H$_2$**), 3.94 (d, 4H, OC**H$_2$**), 1.84-1.79 (m, 2H, C**H**) , 1.58-1.34 (m, 16H, aliphatic protons), and 1.01-1.91 (m, 12 H, C**H$_3$**). ^{13}C NMR ($CDCl_3$, 100 MHz) δppm: 151.11, 131.45, 127.75, 126..79, 121.80, 114.84, 110.19, 71.86, 69.31, 61.60, 39.86, 31.02, 29.34, 24.34, 23.19, 14.21, 11.41. FTIR (cm^{-1}): 3430, 2924, 2860, 1686, 1451, 1290, 1168, 1075. MALDI-TOF-MS: m/z calculated for $C_{32}H_{60}O_8P_2$: 658.92 and found 658.55 [M^+].

Synthesis of Fluorescent Tagged L-Aspartic Polyester (P-OPV-x): Monomer **1** (0.50 g, 1.94 mmol), dodecanediol (0.20 g, 0.98 mmol) and triethylene glycol (0.13 g, 0.87 mmol) and hydroxyl functionalised OPV (64.0 mg, 0.097 mmol, 5 %) were weighed and taken in a melt condensation polymerisation test tube and melted at 100 °C and were purged with nitrogen gas. Ti $(OBu)_4$ (0.08 g, 2.3 mol %) was used as catalyst for melt condensation and was added to the melt which was further subjected to evacuation under vacuum of 0.01 mbar, and purged with nitrogen to remove traces of moisture from the melt content. This procedure was repeated thrice before raising the temperature of the melt reactor to 120 °C. The first step of polymerisation involved 4h purging with nitrogen followed by application of vacuum (0.02 mbar) for 2 h. The completion of polymerization was marked by formation of bright yellow viscous solid. The polymer was purified by dissolving in minimum amount of THF followed by precipitation in cold methanol. Yield: 0.73 g (92 %). ^{1}H-NMR (400 MHz , $CdCl_3$) δ ppm: 7.47 (d, 0.19H, Ar-**H**), 7.38-7.34 (d, 0.09H, C**H**=C**H**),7.11 (d, 0.14 H, -C**H**=C**H**), 7.06 (d, 0.05H, -C**H**=C**H)**, 6.90 (d, 0.20H, -Ar-**H**), 5.56 (m, 1H, -N**H**), 4.55 (s,1H, -C**H**), 4.32-4.25 (d, 0.94H, new TEG esters proton), 4.19 (s, 0.28H, new OPV ester protons), 4.15-4.04 (m, 2.48 H, -C**H$_2$**OH and new aliphatic ester), 3.95 (d, 0.23H, -OC**H$_2$**), 3.76-3.62 (m, 3H, -OC**H$_2$**C**H$_2$**), 3.06-2.78 (m, 2H, -C**H$_2$**), 1.65 (m, 5H, aliphatic protons), 1.45 (s, 9H, BOC protons), 1.27 (m, 11H, aliphatic protons), 0.97-0.92 (m, 0.72H, -C**H$_3$**).^{13}C-NMR (100 MHz, $CDCl_3$)

δ ppm: 174.57, 171.10, 80.08, 70.62, 65.96, 65.26, 50.10, 46.65, 36.89, 29.60, 28.38, 25.94.

Synthesis of Fluorescent Tagged L-Aspartic Polyester (P-OPV-12): Monomer **1** (0.25 g, 0.95 mmol) , dodecanediol (78.0 mg, 0.38 mmol) and triethylene glycol (83.0 mg, 0.55 mmol) and hydroxyl functionalised OPV (63.0 mg, 0.009 mmol) and catalyst titanium tetrabutoxide (0.07 g, 2.0 mol %) were weighed and taken in a melt condensation polymerisation test tube and melt polymerisation was followed similar to P-OPV-6 Yield: 0.38 g (93 %) %). ^{1}H-NMR (400 MHz , $CdCl_3$) δ ppm: 7.47-7.44 (d, 0.40H, Ar-**H**), 7.38-7.34 (d, 0.21H, C**H**=C**H**), 7.10 (d, 0.30 H, -C**H**=C**H**), 7.07 (d, 0.10H, -C**H**=C**H)**, 6.90 (d, 0.43H, -Ar-**H**), 5.51 (m, 1H, -N**H**), 4.58 (s,1H, -C**H**), 4.47 (s, 0.26 H –Ar-$OCH_2C\mathbf{H}_2$-COO), 4.31-4.25 (d, 1.04H, new TEG esters proton), 4.19 (s, 0.42H, new OPV ester protons), 4.15-4.06 (m, 2H, -$C\mathbf{H}_2$OH and new aliphatic ester), 3.95 (d, 0.42H, -$OC\mathbf{H}_2$), 3.76-3.62 (m, 3H, -$OC\mathbf{H}_2C\mathbf{H}_2$), 3.04-2.78 (m, 2H, -$C\mathbf{H}_2$), 1.65 (m, 4H, aliphatic protons), 1.45 (s, 9H, BOC protons), 1.27 (m, 9H, aliphatic protons), 1.01-0.90 (m, 1.32H, -$C\mathbf{H}_3$).^{13}C-NMR (100 MHz, $CDCl_3$) δ ppm: 178.40, 171.11, 127.72, 114.88, 80.10, 70.59, 68.95, 65.96, 52.06, 50.09, 39.85, 36.90, 31.01, 29.60, 28.38, 25.87, 24.32, 23.18, 14.20, 11.41.

Self Assemblies of Fluorescent P-OPV-x and P-0 copolymer: To study the self assembly of the fluorescent P-OPVs and P-0 copolymers in organic solvents , 0.1mg/mL polymer were dissolved in THF and drop casted on silica wafers, dried and subsequently spin coated with gold and observed using FESEM. The polymers with same concentrations were also dropcasted on mica sheets for their analysis using AFM technique. For aqueous self assembly, 5.0 mg of polymers were dissolved in 2.0 mL HPLC DMSO. To this was added Milli Q water (2.0 mL) dropwise. This solution was further dialysed against Milli Q water for 48 h by suspending the solution in a 3.5 kD semi-permeable membrane dialysis tube Spectrochem. The resultant dispersed solution of the polymers were filtered and lyophilized for further analyses.

Encapsulation of Dye: P-0 (5.0 mg) was dissolved in HPLC DMSO (2.0 mL) and Nile Red (0.1 mg dissolved in 2.0 mL HPLC DMSO) was added dropwise to it. Milli Q water (1.0 mL) was dropwise added with constant stirring. The stirring was

carried on for 12 h and the solution thus obtained was subjected to dialysis. The reservoir water was continuously replaced to ensure complete removal of DMSO. After 48 h the solution was filtered and used for further analyses. Identical procedure was followed for loading NR to other polymers. Dye loading content (DLC) and Dye loading efficiency (DLE) were calculated using the following mathematical formulations by measuring the absorbance of fluorophore in the resultant dialysed solutions [61] mentioned in chapter 2.

Photophysics and FRET experiments: The absorption and fluorescence studies were carried out keeping the optical density of OPV core as 0.1. OPV chromophore was excited at 397 nm and Nile Red chromophore was excited at 540 nm for obtaining emission spectra. For TCSPC life time studies nano-LED source with wavelength 371 nm and 550 nm for exciting OPV and Nile Red chromophores respectively were used, and their life time decay were obtained at emission maxima of 500 nm and 600 nm respectively. These decays were fitted by using DAS6 software. To determine molar extinction coefficient, various concentrations of OPV chromophore in THF where prepared ranging from 1.0 to 6.0 × 10^{-6} M and their absorbance were measured from UV spectrophotometer. The concentration of OPV chromophore was plotted against absorbance to determine the molar extinction coefficient as 78,000 M^{-1} cm^{-1}. The quantum yield of OPV chromophore was determined in water (dialyzed sample) and THF using quinine sulphate as reference (Φ = 0.546 for quinine sulphate) following our reported procedure. [62]

Cytotoxicity studies: MTT assay, which is based on the metabolic activity of tetrazolium bromide, 3-4, 5 dimethylthiazol-2,5-phenyltetrazolium bromide in living cells, was employed for analysing the biocompatibility of the newly synthesised polyesters in cervical cancer (HeLa) cell lines, breast cancer (MCF 7) cell lines and wild type mouse embryonic fibroblast (WT-MEF) cell lines. Cells were cultured for a period of 16 h, in 96-well plates bearing 1000 cells in each well in 100 µl of DMEM along with 10% FBS solution. The media was further aspirated and the resultant cells were exposed to various concentrations of P-0 and P-OPV-6 polymers in triplicates. For the relative measure of the viable cells a blank control of cells without any

polymer was also maintained in triplicates. The cells were allowed to grow in the presence of the polymer for 72 h, and there after the media in each well was replaced with 100 µl of freshly prepared stock solution of MTT (containing 5.0 mg/mL MTT in PBS diluted to 50 µg/mL in DMEM). The MTT treated cells were allowed to incubate for 4h at 37 °C. The DMEM was further replaced with 100 µl of DMSO, which dissolved the purple formazan crystals obtained due to treatment of living cells to MTT. The 96-well plate was shook well before measuring the absorbance of the formazan crystals at 570 nm using Varioskan FLASH instrument. The mean of all the triplicate values were calculated (omitting any values deviating significantly from other two values), and the corresponding value of the blank cells were treated as 100 % figure and the cell viability caused by the polymers were calculated relative to the blank reading. The P-0 loaded with Nile Red was analysed for their cytotoxicity to MCF 7 cells using the same procedure as above. The similar procedure was also followed for the fluorescent tagged P-OPV-6 copolymer both in nascent and NR loaded form.

Confocal Imaging: A 6-well cell culture plate was loaded with glass cover-slips and MCF 7 cells were cultured in them in the presence of DMEM with 10% FBS, at a density of 1×10^5 cells each. The cells were incubated for 16 h prior to the experiments and were further treated with P-0 loaded with Nile Red, and P-OPV loaded with Nile Red, keeping the concentration of the respective fluorophores as 2µg/mL. After incubating for 4 h, the fluorophore containing media was aspirated and the cells were further processed for fixing. In a typical cell fixing experiment, the cells were washed twice with PBS (2 × 1.0 mL). The cells were fixed on the coverslips by incubating them for 10 min in the presence of 4 % paraformaldehyde (1.0 mL) at room temperature. For the P-0 loaded nanoparticles treated cells, the cells were stained with DAPI while incubating for 2 min in dark. However for the P-OPV-6 loaded nanoparticles treated cells, the cells were stained with phalloidin by incubating them with phalloidin green for 20 min. The cells were rinsed once with PBS, and the coverslips were mounted on fresh glass slides using Fluoromount mounting medium. The coverslips were dried overnight in dark. The cells thereby fixed on the glass slides were then imaged using confocal microscope using the lasers 405 nm (as blue

channel), 561 nm laser (for red channel) and laser 488 nm (for green channel). The images thus obtained were processed in Image J software. For FRET experiments the cells were not stained with DAPI and phalloidin to avoid any interference with OPV and NR emission.

Lysosomal Tracking of polymer nanoparticles: In a typical experiment, 25000 cells were seeded in each well of an 8-well live cell chamber, and incubated at 37°C to grow for 16h. P-OPV+NR, P-0+NR and P-OPV were administered to the cells after replacing with fresh media. The concentration of chromophores was maintained same as that of confocal imaging experiments. Cells were incubated with the nanoparticles further for 4h, and the media was removed from the cells. The cells were rinsed with PBS once and 50.0 nM Lyso tracker® Green DND-26 was added to them and was immediately imaged under CSLM confocal microscope. Lyso tracker was excited using Laser source of 488nm and the images obtained were processed using Image J software.

FACS analysis: The quantification of the fluorophore taken up by cells was successfully carried out using flow cytometry cell analyzer. HeLa cells were seeded at a density of 1×10^5 in each well of a 6 well plate and were incubated and allowed to grow for 16 h under the presence of DMEM with 10% FBS at 37 °C. P-0 loaded with Nile Red and the corresponding free Nile Red (2.0 µg) were exposed to the cells, which were further incubated for 4 h. The media was aspirated from each well and the treated cells were washed with PBS (1.0 mL), and further, the cells were trypsinised by treating with trypsin for 1 min at 37 °C. Cells were centrifuged and pelleted down and re-suspended in 1.0 mL PBS. The suspension of cells was analysed using BD LSRFortessa SORP cell analyzer with 5 lasers and 18 colour detectors. The 561 nm laser was used to excite Nile Red and the bandpass filter was maintained at 610 ± 10 nm. A population of 10,000 cells were screened for emission histograms.

3.3 Results and Discussion

3.3.1 Synthesis of Fluorescent-Tagged OPV Polymers

Oligo-phenylenevinylene (HO-OPV-OH) was chosen as π-conjugated fluorophore diol and it was synthesized by multi-step organic reactions starting from hydroquinone as shown in scheme 3.1. Hydroquinone was converted into bis(2-ethylhexyloxy) benzene (**1**) using 2-ethyl-hexyl bromide and it was bromomethylated to yield compound (**2**). Compound **2** was reacted with $P(OEt)_3$ to yield bis-phosphonate ester (3). 2-Bromoethanol was coupled with 4-hydroxy benzaldehyde to yield compound **4**. The bis-phosphonate ester (**3**) was subjected to Witting-Horner reaction with **4** in the presence of base to yield the HO-OPV-OH following our earlier procedure. [33] L-Aspartic acid was converted into melt polymerizable multi-functional monomer (**1**), from chapter 2, as shown in scheme 1. [55] Two carboxylic acid functional groups were converted into methyl esters and the amine was protected by BOC group. The monomer (**1**) was polymerized with HO-OPV-OH, triethylene glycol (TEG) and dodecanediol (DD) to yield new classes of fluorescent-tagged amphiphilic polyesters (P-OPV-x) (see scheme-3.1).

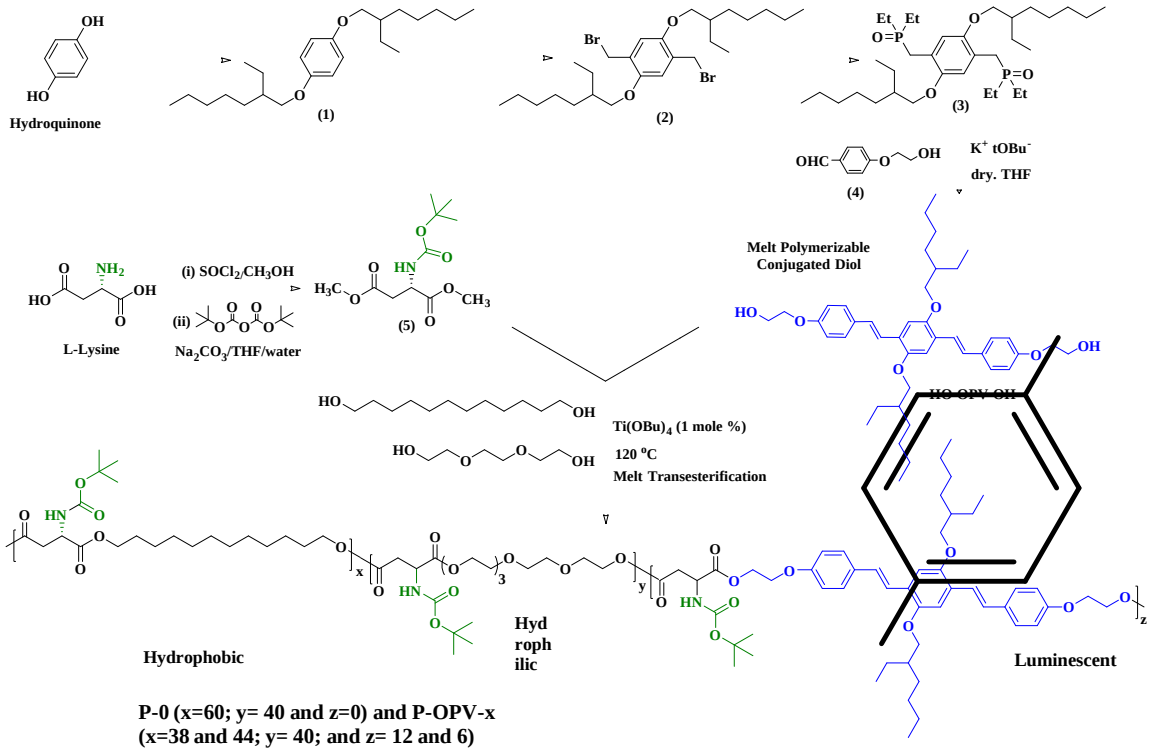

Scheme 3.1: *Synthesis of fluorescent OPV-tagged L-aspartic acid amphiphilic polyester. (5) is the same as (1) from chapter 2.*

(a)

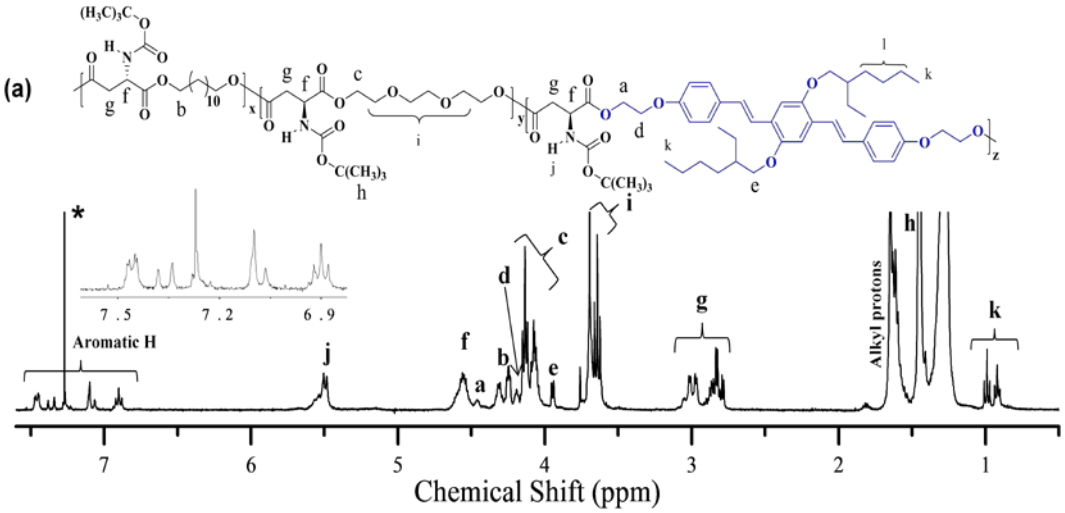

(b) Table containing the composition of polymers, molecular weights, and thermal properties

Polymer	DD unit[a] (^{1}H-NMR) [a]	TEG unit (^{1}H-NMR) [a]	OPV unit (^{1}H-NMR) [a]	M_n (g/mol) [b]	M_w (g/mol) [b]	M_w/M_n	T_g (°C) [c]	T_D (°C) [d]
P-0	60.0	40.0	0	7000	16000	2.6	-14.0	207
P-OPV-6	54.0	40.0	6.0	8100	18000	1.9	-10.0	190
P-OPV-12	44.5	43.5	12.0	4100	8200	2.0	-8.0	200

[a] Determined by 1H-NMR in $CDCl_3$. [b] Determined by GPC in THF at 25°C. [c] Determined by DSC at 10°/min in heating cycle. [d] Determined for 5 % weight loss by TGA at 10°/min under N_2

Figure 3.4: *(a) ^{1}H-NMR spectrum of P-OPV-6 in $CDCl_3$. (b) Table contains the composition of polymers, their molecular weights and thermal properties.*

The polymerization was carried out at 120 °C using $Ti(OBu)_4$ (~1 mole %) as catalyst under solvent free melt conditions. In this process, the di-ester underwent transesterification reaction to yield polyesters, and during this melt process the BOC urethane was found to be completely inert. [51,55] For all the polymerization reactions; the TEG content was always retained as 50 mole % in the feed in order to maintain the required hydrophilicity in the polymer backbone. The amounts of DD (40 and 45 %) and HO-OPV-OH (10 and 5 %) were varied in the feed so that the total diols content (TEG + DD + HO-OPV-OH) was always retained as 100 % in the feed (diols to monomer **1** ratio was maintained as 1:1). The chemical structures of the OPV-tagged fluorescent polymers were confirmed by ^{1}H NMR and the spectrum for

polymer is given in figure 3.4. The peaks in the spectrum were assigned to different types of protons in the chemical structure by alphabets. The spectrum showed newly formed ester peaks OPV–C**H**$_2$-OOC (proton-a) at 4.45 ppm, TEG-C**H**$_2$-OOC (proton-b) at 4.31 ppm, and DD-C**H**$_2$-OOC 4.15 ppm (proton-c), respectively. Further, the spectrum also showed peaks for the protons OPV–C**H**$_2$CH$_2$-OOC (proton-d), Ar-OC**H**$_2$-CH-EH (proton-e) and aromatic-**H** at 4.22 ppm, 3.95 ppm and 6.80- 7.50 ppm, respectively. All other protons were assigned with respect to their chemical structure. The comparison of the peak intensities of protons a, b and c gave the actual incorporation of OPV, TEG and DD amount in the amphiphilic polymer backbone (see table in figure 3.4). The intensities of BOC urethane protons at 1.44 ppm (proton-h) remained constant and it was not disturbed by the melt transesterification process. [54] This confirmed the selective transesterification of diesters towards diols in the formation of expected amphiphilic polyester structure. These amphiphilic polymers are referred as P-OPV-x, where x = 6 and 12 with respect to the actual incorporation of OPV amount in the polymer. The polymer without OPV chromophore is referred as P-0. The molecular weights of the polymers were determined by gel permeation chromotograpy and the details are given in the table in Figure 3.4 b. All the polymers showed mono-modal distribution and they exhibited M_n = 7.0- 8.0 × 10^3 g/mol and M_w= 16.0- 18.0 × 10^3 g/mol with polydispersity of ~ 1.9 to 2.6 (polydispersity of ~2.0 is typically expected for condensation polymerization). The sample P-OPV-12 was found to be partially soluble in THF for GPC analysis (see figure 3.5 for GPC chromatograms in THF). The polydispersity of the polymers are little higher than 2.0 which is typically acceptable for the melt polycondensation approach. [51] The degree of polymerization (X_n = M_n/M_o) or average number of repeating units were determined as 22- 25 which suggested the formation of moderate to high molecular weight polymers for lab-scale melt polymerization process. [50] The non-fluorescent polymer (without OPV chromophore) P-40 (from chapter 2) has been referred as P-0 in the present chapter. The dn/dc value for the polymer P-OPV-6 was determined by GPC chromatograms using various polymer concentrations (see figure 3.6). The dn/dc value was determined as 0.01 for P-OPV-6 which is similar to that of dn/dc value reported for aliphatic random copolymer poly(butyleneterephthalate)-poly(butylene adipate).[63] Thermogravimetric analysis showed that the polymers were stable up to

280 °C (see figure 3.7 a) and the differential scanning calorimetry exhibited only glass transition temperature in the range of -5 to 30 °C with respect to the amorphous nature of the polymers (see figure 3.7 b).

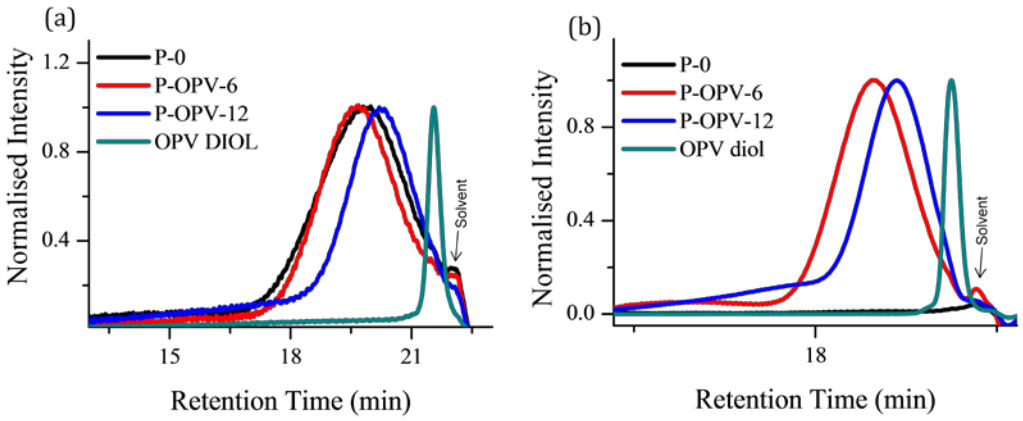

Figure 3.5: *GPC chromatograms of P-0, P-OPV-6 and P-OPV-12 copolymers and OPV Diol. (a) RI detector and (b) UV-Vis detector.*

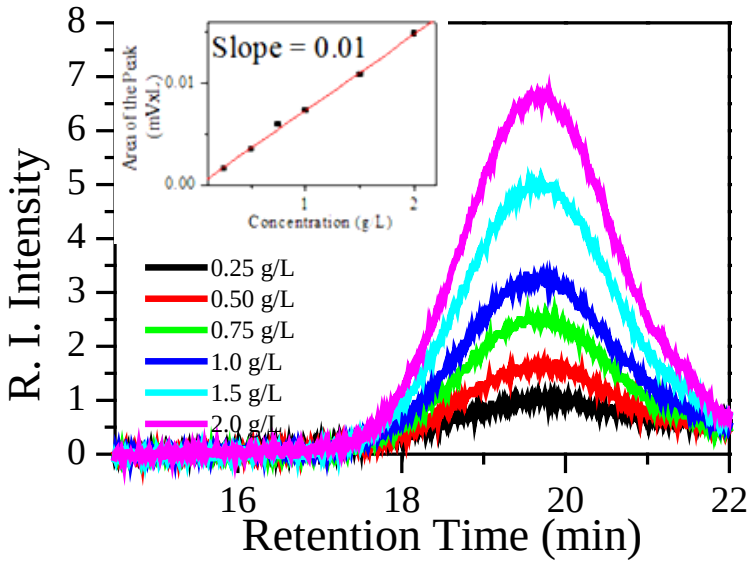

Figure 3.6: *GPC chromatograms of various concentrations of P-OPV-6 for determination of dn/dc value (R.I. Detector). Inset: The plot of area of the peaks vs concentration (slope = 0.01).*

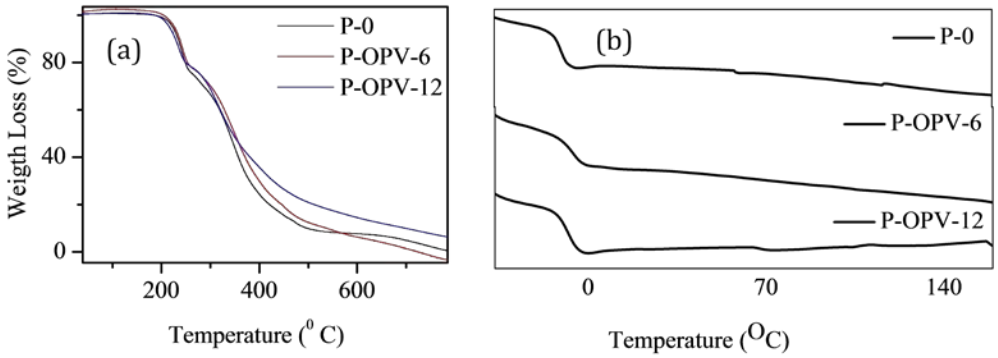

Figure 3.7: *TGA thermograms of P-0, P-OPV-6 and P-OPV-12 (a), DSC curves of P-0, P-OPV-6 and P-OPV-12 (b).*

3.3.2 *Aromatic π-stack Driven Polymer Self-assembly*

π-Conjugated chromophores are very well known to undergo strong aromatic π-stacking due to the overlap of π-cores depending on the solvents in which they are dissolved or dispersed. [57] Typically the polymer chains adopt expanded chain conformation and are largely isolated in dilute concentration in good solvents. In poor solvents or in the mixtures of good+poor solvents, the polymer chain-chain interactions become predominant which lead to the formation of micron-sized polymer aggregates. [59] In the present case, the L-aspartic acid polymer system was designed with π-conjugated OPV chromophore; thus, the polymer chains are expected to experience strong aromatic π-π stacking interactions. Since the polymer was designed with hydrophilic TEG-units, hydrophobic DD-units and aromatic OPV chromophores; they were expected to experience both amphiphilic and aromatic π-stacking non-covalent interaction together.

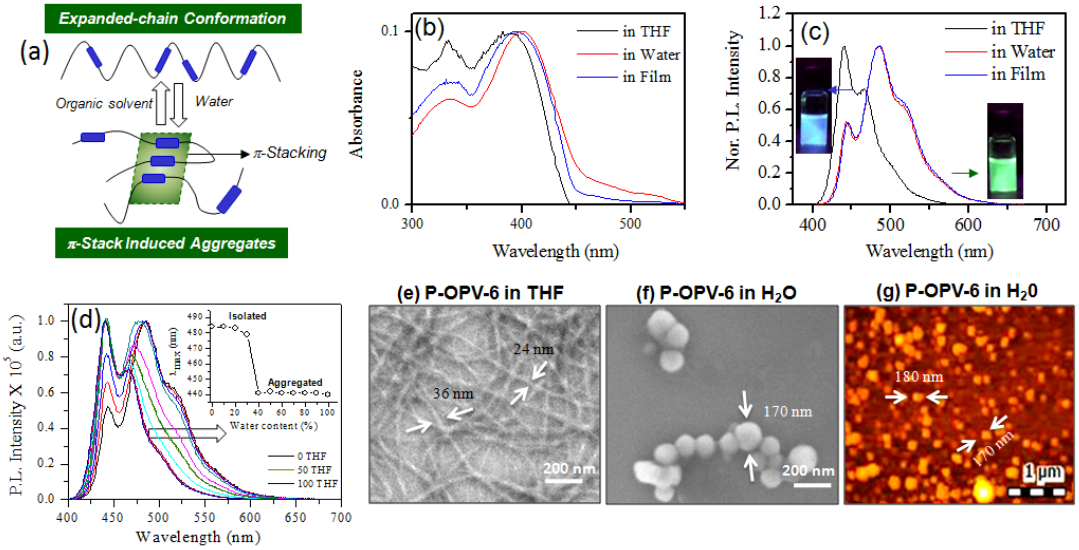

Figure 3.8: *(a) Schematic representation of aromatic π-π stacking in P-OPV-x polymers with respect to the good (THF) and poor (water) solvents. Absorbance (b) and emission (c) spectra of P-OPV-6 in THF, dialyzed aqueous solution and thin film (λ_{ex} = 397 nm and O.D. = 0.1). The photographs of the vials indicate the emission from polymer in THF and water. (d) Emission spectra of P-OPV-6 polymer in THF/water solvent combinations. The in-set figure showed the plot of emission maxima with respect to solvent compositions. FESEM images of P-OPV-6 in THF (e) and in water (f). AFM images of P-OPV-6 in water (g).*

To study these interactions, the polymer samples were subjected to photophysical studies in good solvent (tetrahydrofuran, THF), dialyzed aqueous solutions and in thin film. The absorbance spectra of P-OPV-6 in aqueous solution, thin film and in THF are showed in figure 3.8b (see figure 3.9 for P-OPV-12). The molar extinction coefficient of OPV was determined as 78,000 $M^{-1}cm^{-1}$ in THF (see figure 3.10).The dialysed polymer solution and thin film spectra showed 10 nm red-shift compared to polymers in THF. Additionally, a hump was observed with respect to aggregates of OPV chromophores at 475 nm. This trend suggested that the OPV chromophores were completely isolated and they were not aggregated in THF (good solvent). On the other hand, the inter-chain interactions became predominant and the OPV chromophores underwent strong aromatic π-stacking interactions in the aqueous medium. The extent of OPV aromatic π-stacking seem to have reached a maxima (10 nm red-shift) in the aqueous medium which is almost similar to that in thin film. Emission spectra of the OPV chromophores (see figure 3.8c) were found to be more sensitive to the aromatic π-stacking phenomena. OPV polymers showed the characteristic emission maxima at 440 nm with respect to isolated chromophores in THF.

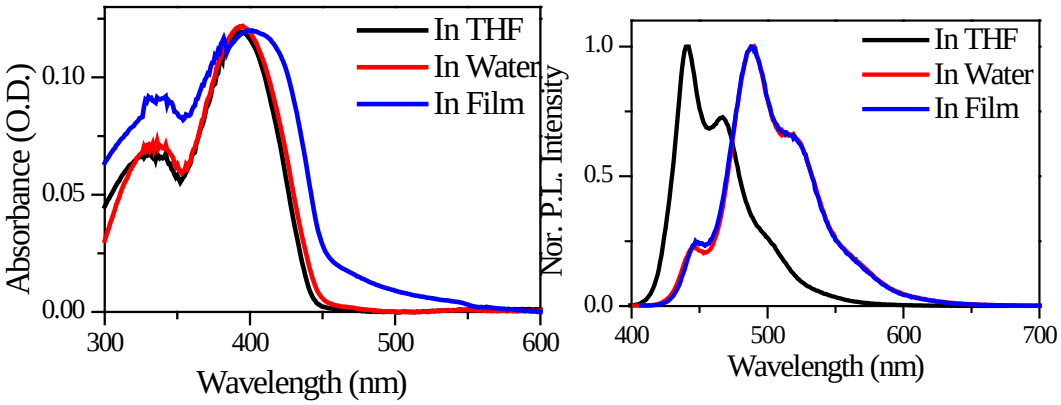

Figure 3.9: *Absorbance (a) and emission spectra (b) of P-OPV-12 in THF, dialysed and thin film state (λex = 394 nm and O.D. = 0.1) . The polymer was partially soluble in THF.*

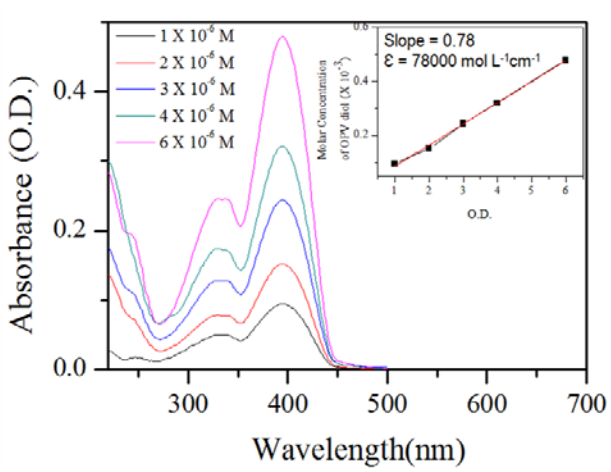

Figure 3.10: *Absorption spectra of various concentrations of OPV chromophore in THF for determination of molar extinction coefficient. Inset: The plot of molar concentration vs intensity of λ_{max} ($\mathcal{E}$ = 78000 M^{-1} cm^{-1}).*

The π-aggregation extent in water+THF composition system was quantified by a plot of λ_{max} *vs* the water THF content shown in figure 3.8 d (in-set showed a break point at 40% water in solvent mixture). It clearly suggested that the isolated OPV amphiphilic polymer chains underwent aromatic π-stacking upon increasing the water content in the solvent mixture. To visualize the polymer aggregates, the samples were subjected to field emission scanning electron microscope (FESEM) and atomic force microscope (AFM) analysis. The P-OPV-6 in THF showed (see Figure 3.8 e) thin helical nano-fibers having width 35 ± 8 nm. The length of these nano-fibres was measured to be ~ 2.0 μm which indicated their high aspect ratio ~ 40 to 60 with

respect to long-range supramolecular assemblies. The water dialyzed P-OPV-6 sample (see Figures 3.8 f and 3.8 g) showed exclusively the formation of spherical nanoparticles of < 200 nm in size. Both FESEM and AFM analysis have provided direct evidence for the morphological transformation from nano-fibrils to stable nanoparticles upon varying the solvent micro-environments from THF to water. Based on the photophysical studies, FESEM and AFM morphology, it may be concluded that the polymer chains adopt expanded chain conformation to produce helical nano-fiber morphology in good solvent like THF whereas they produced stable spherical nanoparticle in aqueous medium. In the present case, the aqueous nanoparticles were stabilized through both OPV aromatic π-stacking and hydrophilic interactions.

3.3.3 Encapsulation Capabilities and Cellular uptake

The encapsulation capabilities were studied for both luminescent amphiphilic polyesters with OPV chromophores (P-OPV-6) and non-luminescent polyester P-0 (polymer without OPV). NR was found to load in high amount quantity both in P-OPV-6 and P-0 nanoparticles. NR has good absorbance (molar extinction coefficient = 38,000 M^{-1} cm^{-1}) [64] and reasonably good quantum yield (= 0.018,); [65] hence, it is suitable as fluorophore for bioimaging applications. The dye loading content (DLC) was found to be 5.0 % and 4.0 % in P-OPV-6 and P-0 nanoparticles, respectively (DLEs were obtained as 50 % and 40 %, respectively). The NR loaded nanoparticles were referred to as P-OPV-6+NR and P-0+NR. DLS histograms of NR loaded P-0 showed the size of the nanoparticles as 140 ±2 nm (shown in figure 3.11a). The absorption and emission properties of NR fluorophore were retained even after loading. The DLS histograms of aqueous samples of P-OPV-6 and P-OPV-6+NR showed the existence of < 200 nm size nanoparticles (see Figures 3.11 b and 3.11 c).

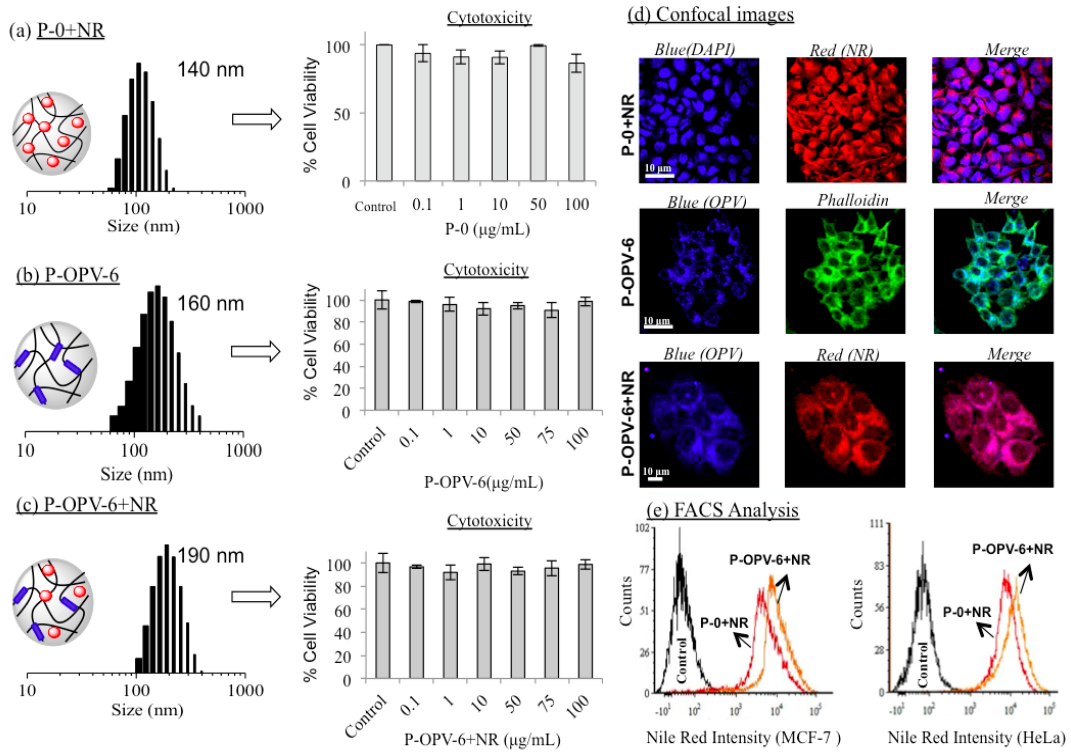

Figure 3.11: *DLS histograms and cytotoxicity in MCF 7 cell lines for P-0+NR nanoparticles (a), P-OPV-6 nanoparticles (b), and P-OPV-6+NR nanoparticles (c). Confocal microscope images of P-0+NR, P-OPV-6 and P-OPV-6+NR nanoparticles (d). FACS analysis histograms of P-OPV-6+NR in MCF 7 cell lines and HeLa cell lines (e) (10000 counts are used).Cells were incubated for 4h.*

Cytotoxicity of the nanoparticles P-OPV-6, P-0+NR and P-OPV-6+NR were studied in breast cancer (MCF 7), cervical cancer (HeLa) and normal (wild-type MEF) cell lines. The cytotoxicity of nanoparticles in MCF 7 cells are given in Figure 3.10, and data for HeLa and WT-MEF cell lines are given in figure 3.12. The polymer nanoparticles P-OPV-6, P-0+NR, P-OPV-6+NR were found to be non-toxic to cells up to 100 µg/mL. The biocompatibility exhibited by these polymer nanoparticles is one of the desirable traits for biomedical applications. To investigate the cellular uptake, P-0+NR, P-OPV-6 and P-OPV-6+NR nanoparticles were internalised in MCF 7 cells and subjected to CSLM microscope analysis. Confocal images were visualized at blue ($\lambda_{excitation}$ at 405 nm laser) and red ($\lambda_{excitation}$ at 561 nm laser) channels and their confocal images are shown in Figure 3.11 d. Top most row corresponding to P-0+NR

showed DAPI stained nucleus of cells and the emission from NR was largely observed in the cytoplasm in the cells.

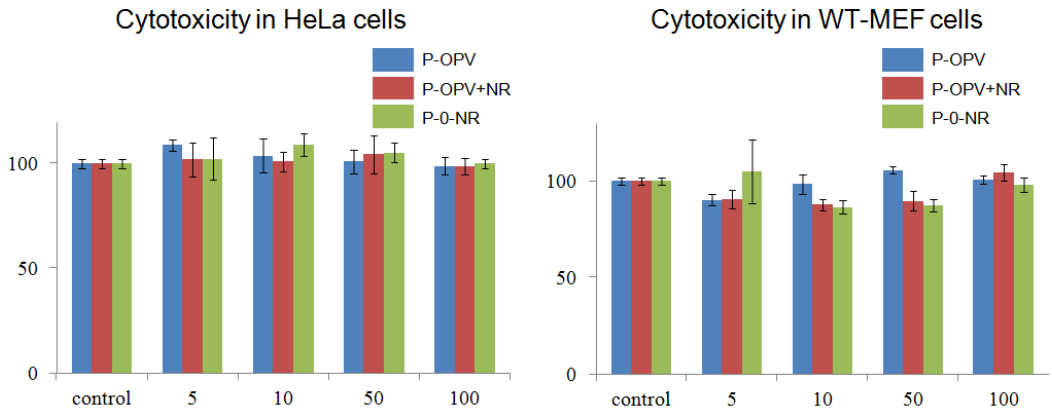

Figure 3.12: *Cytotoxicity of P-0-NR, P-OPV+NR, P-OPV nanoparticles upto 100μg/mL in HeLa and WT-MEF cell lines.*

The merged image of NR and DAPI showed no overlap of their red and blue emission at the nucleus indicating the accumulation of P-0+NR largely in the cytoplasm and not at the nucleus. The second row in the figure 4d shows the uptake of P-OPV-6 blue luminescent nanoparticles. The actin filament skeleton of the cells were stained with green emitting phalloidin (the nucleus is not stained; thus it appears dark) and the blue emission from OPV chromophores in the polymer was clearly observed. This was further supported by the merged image. The cellular uptake of P-OPV-6+NR showed dual emission with respect to OPV and NR in the blue and red channels, respectively (not stained with DAPI). The merged image showed distinct magenta colour from the cytoplasm arising by the combination of emission from OPV plus NR. These studies confirmed the ability of the polymer nanoparticle to carry fluorophores and internalise them in the cytoplasm in the cells. Further, fluorescence activated cell sorting (FACS) was used to substantiate the confocal microscopy results of internalisation of the biomarkers. To quantify the cellular uptake of the nanoparticles, flow cytometry experiments were carried out for P-0+NR and P-OPV-6+NR both in MCF 7 and HeLa cell lines (see figures 3.10 e). The intensities of NR delivered in HeLa cells and MCF 7 cells were relatively high and almost comparable. The high luminescent intensity for NR in FACS analysis is in very good agreement with the confocal images and it validated the ability of newly designed amphiphilic

polymer nanoparticles taken up by the cancer cells. Thus, the newly designed OPV conjugated L-aspartic polymer nanoparticles were stable in aqueous medium and retained the luminescent characteristics and readily transported across cell membranes into the cytoplasm of cancer cells.

3.3.4 FRET Probe Based on NR and OPV polymer

Fluorescence resonance energy transfer (FRET) from donor-acceptor fluorophores are excellent yet challenging probe for cellular imaging in cancer treatment. Having tested the OPV tagged L-aspartic polymer nano-scaffold for loading NR; here efforts were taken to construct the new FRET probe between OPV donor and NR acceptor for bio-imaging. The possibility of FRET occurrence was assessed by the FRET overlap integral between the emission spectrum of donor (OPV in the present case) and absorbance spectrum of acceptor (NR). The overlap of these spectra is shown in figure 3.13a and it was estimated to be more than 75 % for the occurrence of efficient FRET process. Figure 5b shows a schematic energy diagram of FRET between OPV donor and Nile Red acceptor. Upon selective photoexcitation (λ_{ex} = 397 nm); the OPV excitation energy can be utilized for two processes: (i) radiative self blue-emission of OPV chromophores at 450-525 nm, and (ii) transfer of excitation energy from OPV to NR through FRET process thereby red-emission can be observed from NR at 600 nm. In the second process, the blue-emission from the OPV chromophore was expected to decrease or vanish due to the excitation energy transfer to NR.

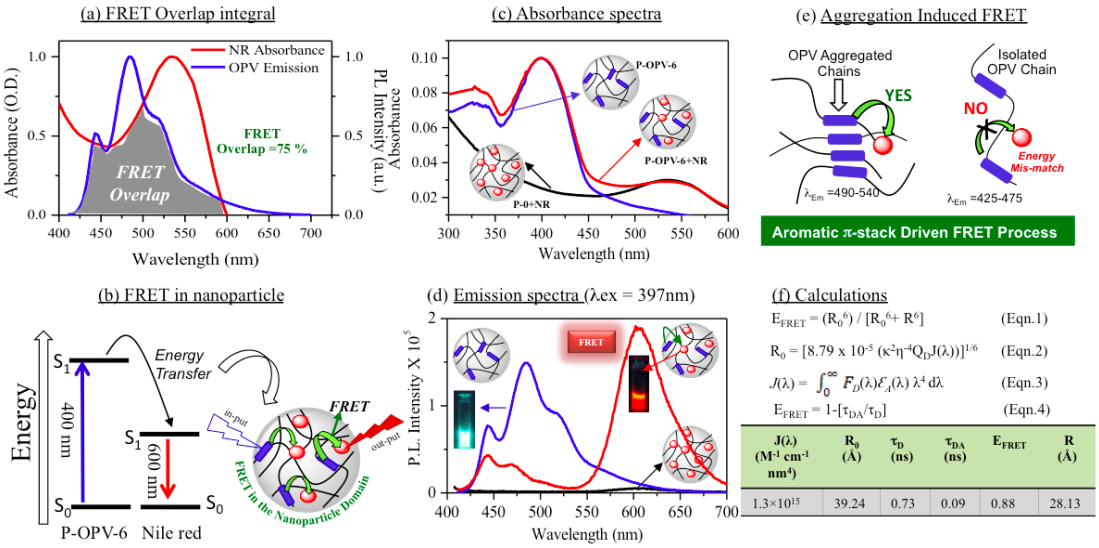

Figure 3.13: *(a) Overlap integral between the emission spectra of P-OPV-6 and absorbance spectra of NR. (b) Energy diagrams for the FRET process. (c) Absorbance spectra of P-0+NR, P-OPV-6 and P-OPV-6+NR in aqueous medium. (d) Emission spectra of P-0+NR, P-OPV-6 and P-OPV-6+NR [λ_{ex} = 397 nm in aqueous medium]. (e) Schematic representation of OPV aggregates on the occurrence of FRET process in polymer nanoparticle domain. (f) Equations used for calculation FRET in P-OPV-6+NR.*

The absorbance spectra of aqueous nanoparticles of P-OPV-6, P-OPV-6+ NR and P-0+NR are shown in figure 3.13c. The concentrations of OPV species in P-OPV-6 and P-OPV-6+NR were maintained as 0.1 O.D. and NR was maintained as O.D. = 0.03. The absorption maxima corresponding to OPV was observed at 397 nm and NR showed characteristic absorbance at 540 nm (see figure 3.13c). The three nanoparticles were excited at 397 nm (with respect to OPV absorbance) and their emission spectra were recorded and shown in figure 3.13d. At 397 nm excitation, the P-OPV-6 samples showed emission maxima at 480-500 nm with respect to the emission from OPV aggregated chromophores. At this excitation wavelength (397 nm), the P-0+NR nanoparticles (without OPV chromophore) did not show emission peak neither in the OPV nor in the NR regions. This confirmed that the NR chromophores were not excited at the OPV excitation wavelength. At 540 nm excitation (with respect to NR); the samples P-0+NR and P-OPV-6+NR showed emission exclusively for NR emission (see figure 3.14 (a)).

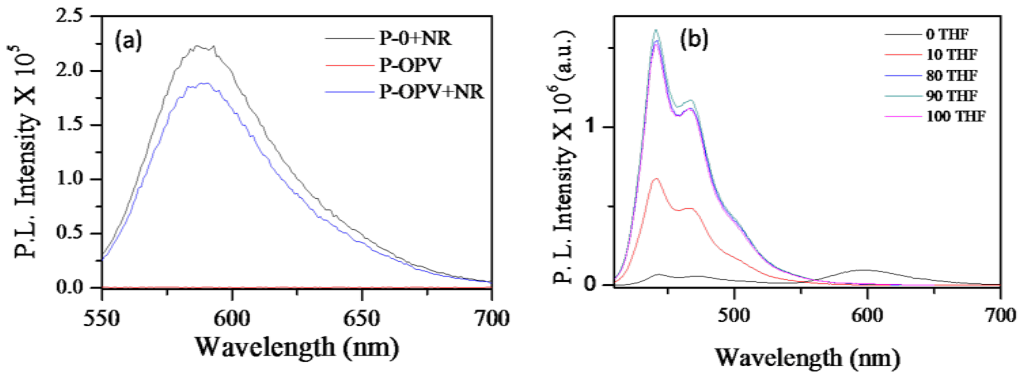

Figure 3.14: *Emission spectra of P-0+NR, P-OPV-6 and P-OPV-6+NR in water (λ_{ex} = 540 nm and O.D. = 0.03) (a), Emission spectra of P-OPV-6+NR in water upon addition of THF (λ_{ex} = 397 nm and O.D. = 0.1) (b).*

Interestingly at 397 nm excitation; the NR loaded OPV polymer nanoparticle (P-OPV-6+NR) exhibited high intense emission peak at 600 nm from NR chromophores (see Figure 3.13d). This observation was attributed to the excitation energy transfer from the OPV to NR chromophores in the nanoparticle domain. In this experiment, the OPV self-emission also drastically decreased due to the partial excitation energy transfer to NR fluorophore. This residual OPV self-emission appeared at 450 nm with respect to isolated OPV chromophores (compare figure 3.13d with figure 3.8c). It suggests that the OPV chromophores existed both as isolated and aggregated states in the polymer nanoparticle; however, only the aggregated OPV chromophores were involved in the excitation energy transfer to NR. The isolated OPV chromophores which did not participate in the FRET event showed self-emission at 450 nm. A model for this OPV aggregated chromophore directed FRET process is depicted in figure 3.13e. A control experiment was carried out to prove the aggregated OPV chromophore directed FRET hypothesis in the polyester nanoparticle domain. In this experiment, THF was added into the dialyzed P-OPV-6+ NR nanoparticle and the emission spectra were recorded using 397 nm excitation (see figure 3.14 (b)). The addition of THF immediately destabilized the aggregation of OPV chromophores rendering them isolated in the solution (as evident from the figure 3.8 d). As soon as THF was added, the FRET emission peak at 600 nm completely disappeared and the self-emission with respect to isolated OPV chromopheores appeared at 450 nm (see figure 3.14 b). This control experiment confirmed the hypothesis that FRET process exclusively occurred between aggregated OPV and NR as shown in Figure 3.8.

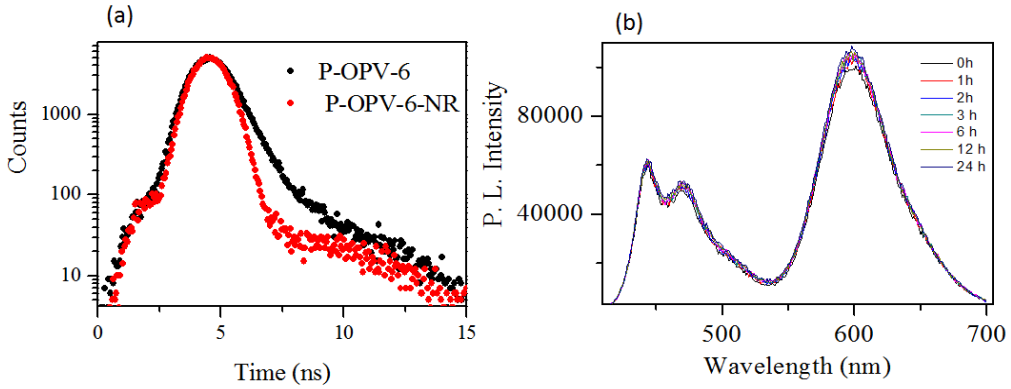

Figure 3.15: *TCSPC decay profiles of P-OPV-6 and P-OPV-6+NR (excitation soure = 390 nm LED and signals are collected at 450 nm. Concentration O.D. = 0.1 of OPV (a), Emission spectra P-OPV-6+NR in pH = 7.4 depicting the stability of the nanoparticle at physiological conditions . (λ_{ex} = 397 nm and O.D. = 0.1) (b).*

Förster distance between the donor-acceptor is an important criterion for occurrence of the efficient FRET process (see equations in Figure 3.13f). The FRET efficiency is represented by the equation: $E_{FRET} = (R_0^6) / [R_0^6 + R^6]$, where R and R_0 are the distance between donor and acceptor molecules and Förster distance at 50 % of FRET process.[6] E_{FRET} was obtained from the fluorescence life times of donor molecule alone (τ_D) and donor in the presence of acceptor (τ_{DA}) [6] using the equation: $E_{FRET} = 1-[\tau_{DA}/\tau_D]$. The values were determined by detailed calculations and the method is described in the supporting information (see figure 3.15 a). TCSPC fluorescence decay profiles of OPV chromophores in nascent polymer P-OPV-6 and in the presence of FRET acceptor NR (in sample P-OPV-6+NR) were recorded (see figure 3.15 a). As expected the OPV fluorescent intensities decay much faster in the presence of NR. [6] The decay rate constants were determined and employed in the E_{FRET} equation. Based on these calculations, the Förster distance and donor-acceptor distance were obtained as 39.24 Å and 28.13 Å, respectively (see table in Figure 3.13f), which are much lower than the < 50 Å cut-off. [6] The FRET efficiency E_{FRET} was estimated to be 88 % and these parameters are clearly evident for the efficient FRET process between the OPV chromophore and encapsulated NR fluorophore within the L- aspartic polymer nanoparticle domain (see Figure 3.13e). Based on the above detail photophysical studies and energy calculations, it can be concluded that the newly designed OPV tagged L-aspartic polymer nanoparticle provided appropriate nanoparticle geometry for efficient FRET probe based on OPV and NR donor-acceptor pair.

3.3.5 Enzymatic-biodegradation of FRET Probe

Aliphatic polyester linkages are susceptible for both hydrolytic degradation at the extracellular level and enzymatic-biodegradation by the lysosomal enzymes at the intracellular compartments. [66] Lysosomes are typically abundant with lipase, chymotrypsin, trypsin and esterase enzymes and they were employed for the biodegradation studies of poly(ester-amide)s, [39-40] polypeptides[67] and aliphatic polyesters[55, 68-69] by us and others. Recently Wang et al. reported that glutathione (GSH) was also capable of degrading poly(ester-amides) in the cytoplasm. [70] Based on this available literature, we have chosen four different enzymes: esterase, chymotrypsin, trypsin, papain[71] and GSH redox species to study the biodegrading ability of the L-aspartic polyester nanoparticles and their influence on their FRET process. Prior to this, the stability of the polymer nanoparticles were tested by incubating the P-OPV-6 (in the absence of enzymes) at 37 °C in PBS (pH = 7.4). The emission spectra were recorded at various time intervals and their spectra are shown in figure see figure 3.15 b. The intensity of emission peak at 440 nm was unaltered indicating the high stability of the FRET nanoparticles under physiological conditions. In the presence of the enzymes, the aliphatic polyester backbone underwent cleavage and disrupted the nanoparticle structure. This led to the separation between OPV and NR and thus causing loss or turn-off of the FRET process (see figure 3.16a). This influence of enzymes on the FRET probe functioning was studied by monitoring the response of nascent P-OPV-6 and P-OPV-6+NR loaded nanoparticles in the presence of various lysosomal enzymes. The effect of esterase enzyme on the self-blue emission of nascent P-OPV-6 nanoparticles and FRET red-emission from P-OPV-6+NR nanoparticles are shown in figures 3.16b and 3.16c, respectively.

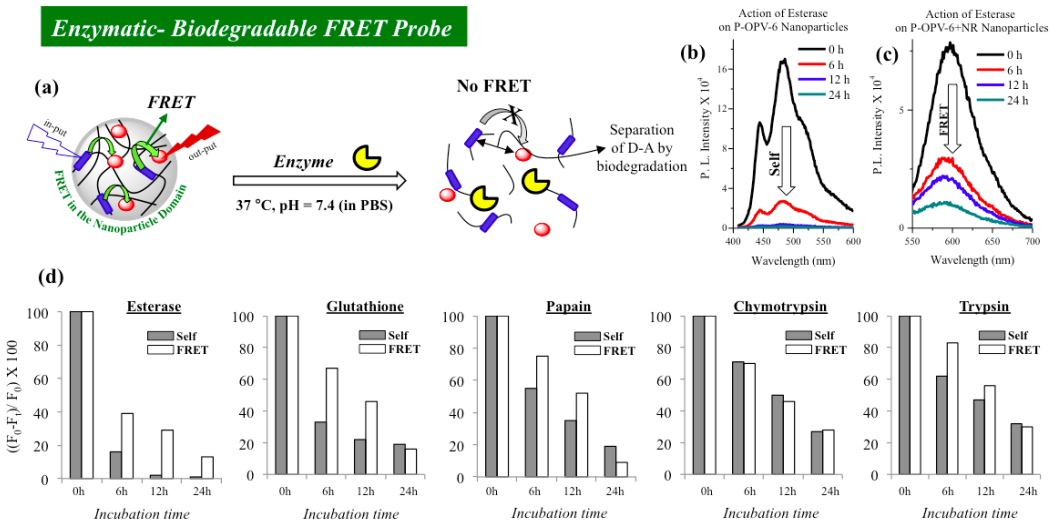

Figure 3.16: *(a) Schematic diagram of P-OPV-6+NR nanoparticle and the action of esterase enzyme on the biodegradation of the nanoparticle. (b)Emission spectra of P-OPV-6 nanoparticles in the presence of 10 U esterase enzyme at 37 °C (in PBS). (c) Emission spectra of P-OPV-6+NR nanoparticles in presence of 10U esterase enzyme at 37 °C (in PBS). (d) The plot of OPV self emission and FRET red-emission of P-OPV-6+NR in presence of enzymes in PBS (pH = 7.4) at 37 °C at various incubation times.*

The self-emission of OPV chromophore drastically reduces with increase in time with respect to the biodegradation of the polyester backbone by esterase enzyme. This process altered the hydrophilic and hydrophobic balance of the polymer and thereby causing the disruption of OPV self assemblies. A similar observation was made in the case other enzymes and GSH and these details are given in figure 3.17. The NR loaded P-OPV-6 nanoparticles (P-OPV-6+NR) exhibited drastic decrease in the NR emission and the FRET process was almost lost within 24 h of enzyme action (figure 3.16c). The change in the PL intensity was plotted using the expression: $[F_0-F_t]/F_0$ x100 where F_0 and F_t are emission intensity at initial and at time 't' with respect to the incubation time. These values were plotted against incubation time and shown in figure 3.16d. GSH and papain showed a reduction in emission intensity of both OPV self emission and FRET emission up to 20 % in 24 h. The reduction in self emission and FRET signal were up to 30 % in case of chymotrypsin and trypsin in 24 h (see figure 3.16d). Higher efficiency of reduction in the PL intensity was observed for esterase enzymes and within 12 h the polymer degraded completely. This observation revealed that all the enzymes employed in this experiment were capable of degrading the polymer chains; however the esterase enzyme was found to be more

active than others. These studies confirmed the enzymatic-biodegradation nature of the polymer chains at intracellular conditions. Further, the amphiphilic polyesters are stable at extracellular conditions and maintained their FRET characteristics.

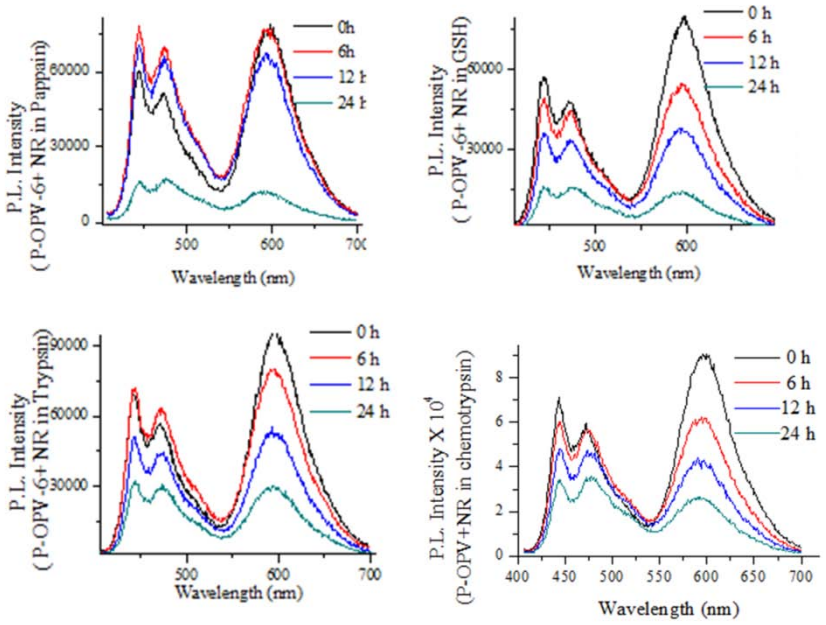

Figure 3.17: *Spectra of P-OPV-6 nanoparticles loaded with nile red in the presence of various hydrolytic enzymes at 37°C.*

Up on being taken up by cells, the probes would slowly biodegrade by enzymes and it would lead to loss of both OPV self-emission and FRET emission in 6-8 h time. Since, most of the intracellular bio-imaging applications are done for < 12 h, thus, the probe has sufficient stability for the imaging at the intracellular level. Once the imaging job is done, the probe would undergo slow biodegradation at the cellular level which is desirable for their excretion from the point of target.

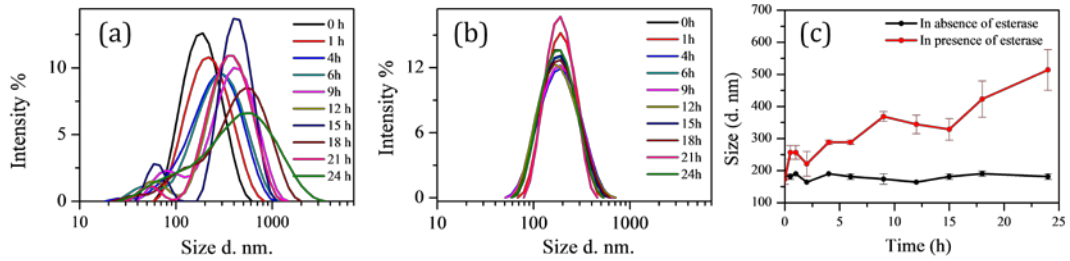

Figure 3.18: *(a) DLS histograms of P-OPV-6 in the presence of esterase enzyme in PBS (pH = 7.4) at 37 ℃. (b) DLS histograms of P-OPV-6 in PBS (pH = 7.4) at 37 ℃. (c) Plot of DLS size of the polymer nanoparticles in the presence and absence of esterase enzymes.*

The amphiphilicity of the polyester nanoparticles is disturbed by the biodegradation process and the degraded oligomers thus have relatively poor solubility or dispersion in water. As a result, the oligomers tend to precipitate from the aqueous medium which significantly increases the particle sizes from nano- to submicron range.[56,68] To study the biodegradation of P-OPV-6, DLS experiment was carried out in PBS (pH = 7.4) at 37 °C in the absence or in the presence of esterase enzyme. Upon biodegradation the nanoparticles do not possess tightly packed self-assembly; as a result, the particle size distribution transformed from mono to multi-modal as shown in figure 3.18a. In the absence of the enzyme, the sizes of the P-OPV-6 nanoparticles did not show any appreciable change (see Figure 3.18b). This experiment confirmed that the P-OPV-6 nanoparticles were stable at extracellular conditions and exclusively underwent biodegradation in the presence of enzymes. The polymer nanoparticle was found to be stable up to 6-8 h and it gradually degraded up to 24 h in the presence of esterase enzyme. After 24 h incubation, the biodegraded polymer sample was lyophilized and subjected to MALDI-TOF MS and GPC analysis (see figure 3.19 and 3.20).

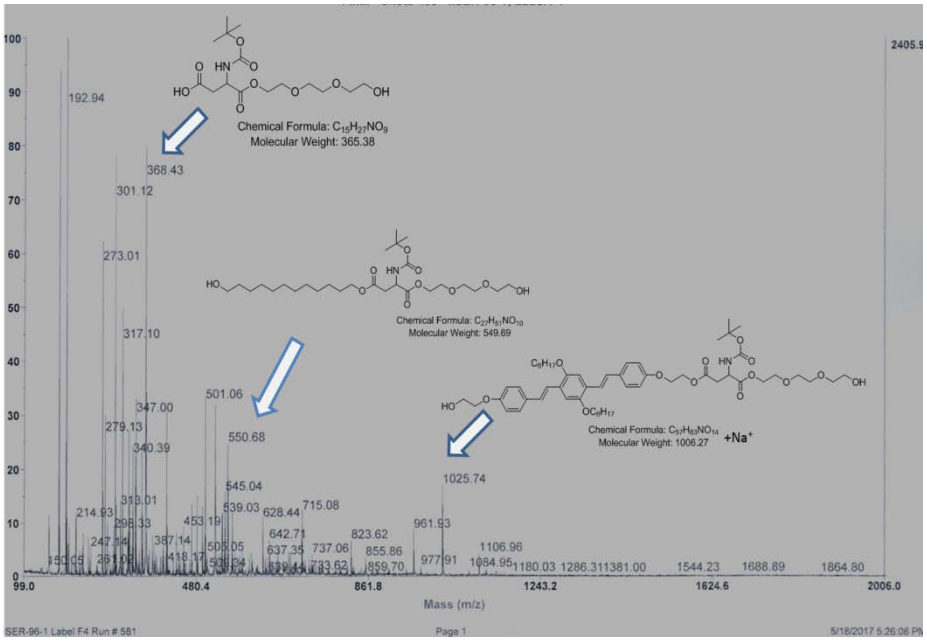

Figure 3.19: *MALDI-TOF Mass spectra of P-OPV-6 sample after 21 h of enzymatic degradation in PBS at 37 ℃. The peaks for the degraded low molecular weight chains are assigned.*

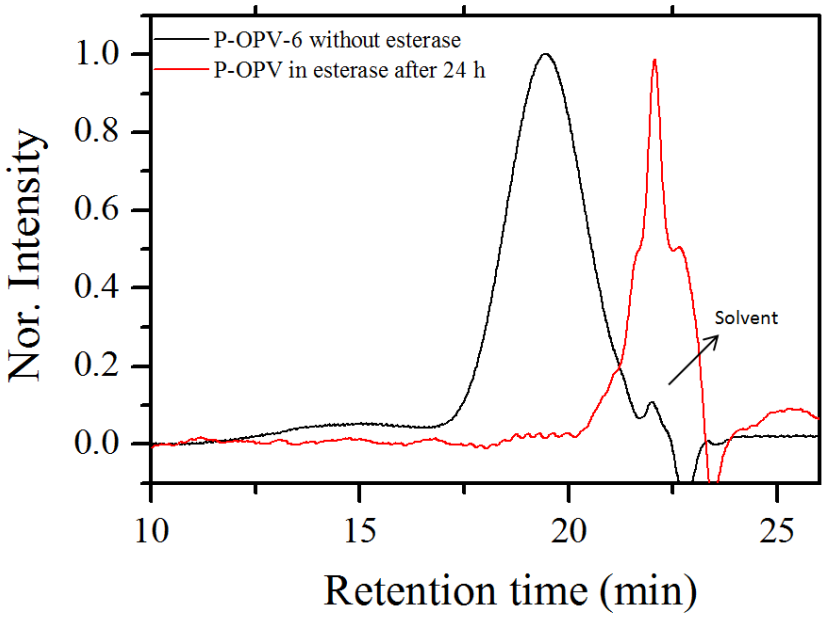

Figure 3.20: *GPC plots of P-OPV-6 before and after exposure to esterase enzyme action.*

The mass spectra showed peaks with respect to DD-Aspartic acid-TEG, Aspartic acid-TEG, and OPV-Aspartic acid-TEG degraded oligomeric units confirming the occurrence of the enzymatic-degradation of the aliphatic polyester backbone. The GPC chromatograms of degraded sample showed the disappearance of the high molecular weight chains and appearance of peaks with respect to oligomers that come along with solvent. Based on the above studies, it can be summarized that the newly designed OPV-tagged L-aspartic polyester FRET probe is highly biodegradable by wide range of lysosomal-enzymes, non-toxic, biocompatible and also suitable for bio-imaging applications.

3.3.6 FRET Probe for Bio-imaging in Cancer cells

FRET process was demonstrated at the intracellular level in breast cancer (MCF 7) and cervical cancer (HeLa) and also normal wild-type MEF cell line. Confocal microscopy with selective photoexcitation for OPV chromophore was employed to observe the FRET phenomenon in P-OPV-6+NR nanoparticles. P-OPV-6 and P-0+NR nanoparticles were chosen as donor and acceptor controls, respectively. The cells administrated with P-OPV-6 and P-0+NR nanoparticles were excited with 405 nm and 561 nm lasers, respectively and the images were captured both at blue (410 – 460 nm) and red channel (570- 635) depending upon the

requirement. At 405 nm excitation (OPV chromophores), the cells having P-OPV-6 nanoparticles showed bright blue-luminescence and no signal was observed in the red channel (Figure 3.21a). At 561 nm excitation (NR chromophore), the P-0+NR administered cells showed bright red-emission and no signal in the blue channel (see Figure 3.21b). This confirmed that both OPV and NR chromophores retained their individual emission characteristics without cross-talking with each other in CSLM experiments. Interestingly, at 405 nm excitation (OPV chrmophores), the P-OPV-6+NR nanoparticles exhibited blue-emission from OPV chromophore (in blue channel) and bright red-emission from NR (in red channel) followed by the occurrence of FRET between OPV donor and NR acceptor (see Figure 3.21c). The merged images showed magenta colour due to the combination of blue and red signals confirming the occurrences of FRET process at the intracellular level. At 561 nm excitation (with respect to NR excitation); the P-OPV-6+NR probe showed signals only in the red channel as a result of NR self-emission (no blue emission was found in blue channel).

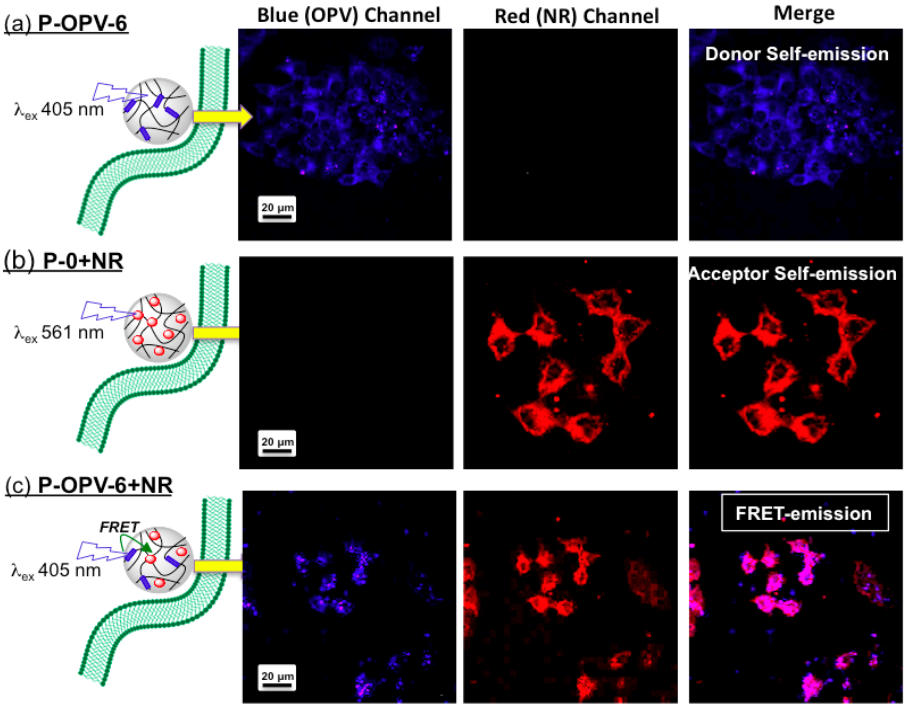

Figure 3.21: *Confocal microscope images in MCF 7 cells for P-OPV-6 (a), P-0+NR (b) and P-OPV-6+NR (c). The photoexcitation wavelengths for each panel are also given and the concentrations of the OPV chromophores in the polymer and NR are maintained as 0.1 O.D. and 0.03 O.D., respectively. The cells were incubated for 4h.*

In HeLa cell line the selective excitation of OPV chromophore at 405 nm showed bright emission from OPV (at blue channel) and red-emission from NR (in red channel) followed by FRET process (see figure 3.22a). The merged images of the two showed the overlap of blue and red regions to give magenta colour which confirmed the presence of donor and acceptor at the same site in the HeLa cells. The WT-MEF followed identical trends similar to MCF 7 and HeLa cell lines; however the intensities were relatively low (see Figure 3.22b). The energy transfer from OPV chromophores to NR were further elaborated in FACS analysis as shown in figure 3.11e. For the same concentration of NR in P-0+NR, both HeLa and MCF7 cells cell lines showed NR emission intensities of 7700 and 4800, respectively (see figure 3.11e). Under identical conditions the P-OPV-6+NR showed, two fold increase in the NR emission intensities of 15000 and 9200 for HeLa and MCF 7 cell lines, respectively (see figure 3.11e). The 2-fold increase in NR intensities in the presence of OPV donor was attributed to the occurrence of the FRET in the cells. The nascent blue luminescent P-OPV-6 nanoparticles, P-0+NR (non-luminescent polymer loaded with NR dye) and P-OPV-6+NR were incubated for 4 h in HeLa (cancer cell line) and WT-MEF (normal cell line). The CSLM images were recorded using 405 nm, 488 nm and 561 nm laser excitation sources for OPV, lysosomal tracker, and NR, respectively. The images were captured in the blue (410 – 460 nm), green (490 – 540 nm), and red (570 – 635 nm) channels, and they are shown in Figure 3.22 for HeLa cells.

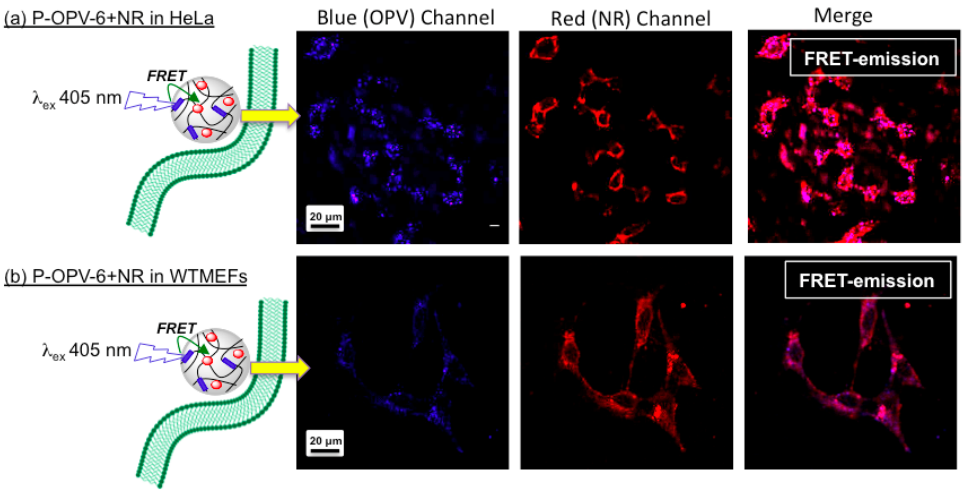

Figure 3.22: *CSLM images in P-OPV-6+NR in HeLa (a) and WT-MEF (b) cell lines.*

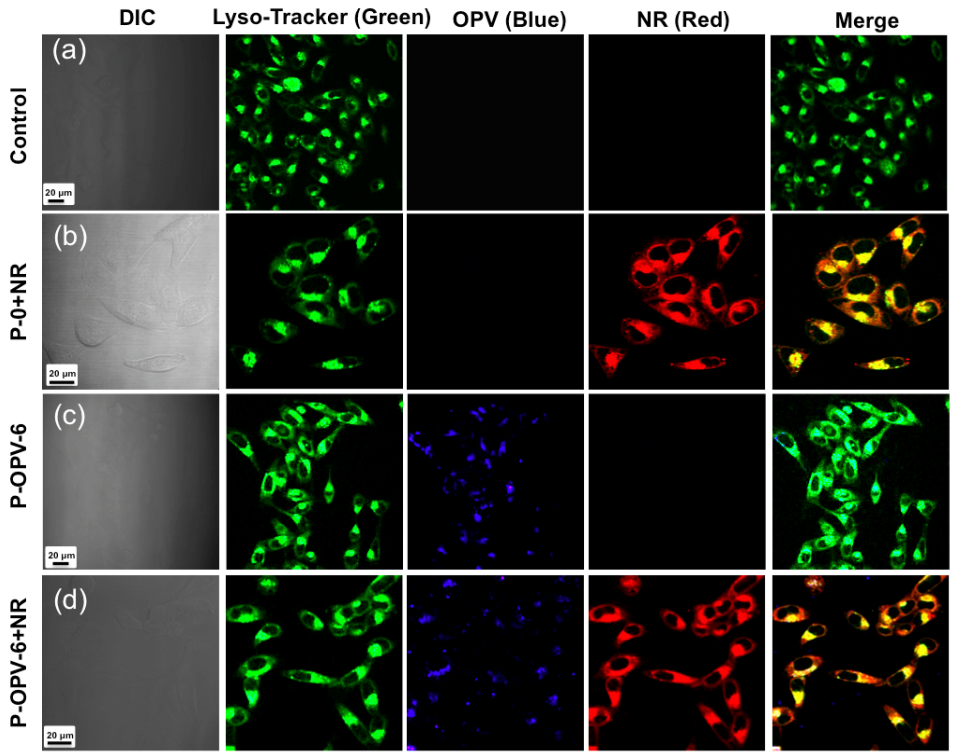

Figure 3.23: *Live cell confocal microscope images in HeLa cells for control (a), P-0+NR (b), P-OPV (c) and P-OPV-6+NR (d).*

The first row of panels in Figure 3.23a showed images of the cells incubated only with lysosomal tracker (without any nanoparticles). The lysosomes were clearly visible in the cytoplasm with bright green emission. The administration of lysosomal tracker stained the lysosomal compartments in the cells and the images appeared to be similar with literature report.[72] In Figure 3.23b, the NR loaded polymer nanoparticles P-0+NR exclusively showed bright red emission in the red channel. The merging of the P-0+NR nanoparticle image with the lysosomal tracker image confirmed that the P-0+NR nanoparticles were largely accumulated in the lysosomal compartments in the cytoplasm. The merged image was found to be yellow coloured followed by the combination of red and green emission together with NR in the lysosomal compartments inside the cells. In Figure 3.23c, the P-OPV-6 nanoparticles showed blue emission with respect to the OPV self-emission from the polymer . The closer observation of individual cells in the blue and green channel revealed the location of OPV polymer nanoparticles in the lysosomal compartments.

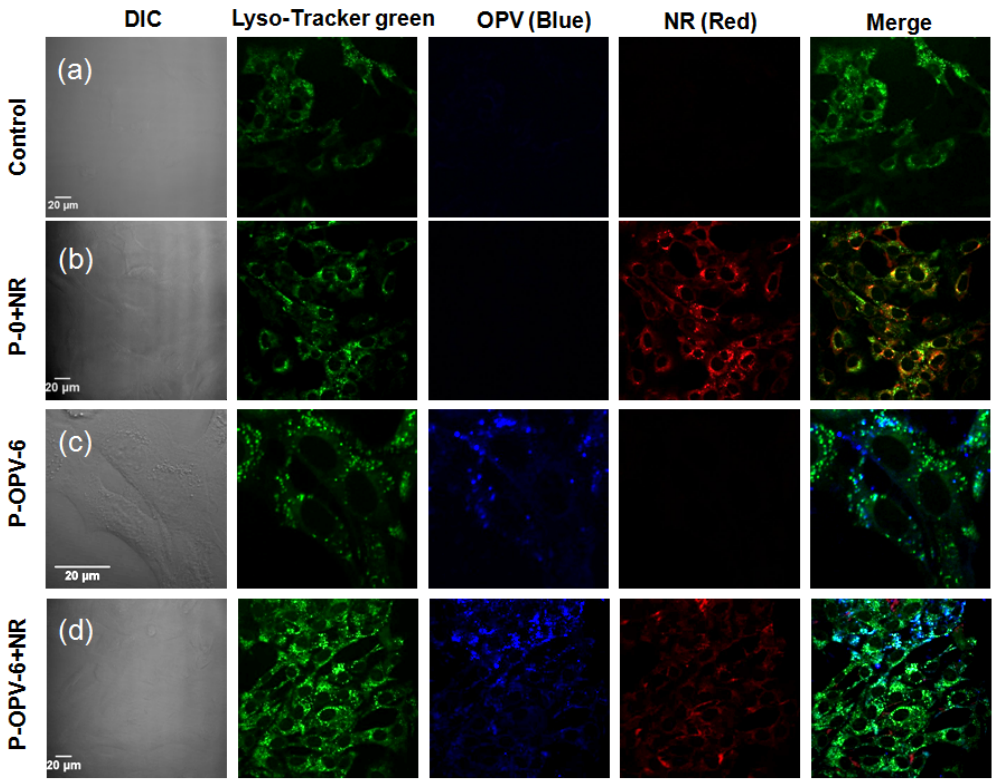

Figure 3.24: *Live cell confocal microscope images in WT-MEF cells for control (a), P-0+NR (b),P-OPV (c) and P-OPV-6+NR (d).*

In figure 3.23d, the P-OPV-6+NR nanoparticle images exhibited dual blue and red emission from OPV and NR chromphores. The merged image showed the co-localization of both OPV and NR chromophores in the lysosomal compartments. Live cell imaging experiments in WT-MEF cell lines also revealed a similar trend for the OPV polymer and their NR loaded nanoparticles (see figure 3.24). This live cell imaging CSLM studies provided direct evidence for the cellular uptake of the L-aspartic acid polymer FRET nanoparticles and their transportation in the cytoplasm by the lysosomes. Based on the live cell lysosomal tracker CSLM imaging (Figure 3.23) and enzyme-responsive biodegradation studies (Figure 3.16); it may be concluded that the custom designed L-aspartic polyester nanoparticles were readily taken up by the cells and transported-cum-digested in the lysosomal compartments in the cytoplasm of the cells. Though the concept was demonstrated here exclusively using OPV and NR FRET donor-acceptor pairs in L-aspartic acid polyester platform; the approach is not restricted to only these systems and in principle, it may be expanded to wide ranges of other L-amino acid resources.

3.4 Conclusion

To summarize new classes of π-conjugated luminescent L-amino acid based amphiphilic polyesters have been synthesized through solvent free melt condensation approach using L-aspartic acid monomers and custom designed OPV diol. Appropriate amphiphilicity was accomplished by carefully varying the compositions of OPV diol with hydrophilic triethylene glycol and hydrophobic 1,12-dodecane diol in one-pot melt condensation process. These polymers were shown to produce stable nanoparticles of < 200 nm in size under physiological conditions (pH = 7.4). They were found to be capable of loading hydrophobic water insoluble fluorophores like Nile Red. The polymer nano-aggregates were found to be highly sensitive to the environment and they exhibited one dimensional nano-fibrous morphology or spherical nanoparticles in organic or aqueous medium, respectively. Absorption, emission and time resolved fluorescent decay techniques were employed to study the occurrence of the FRET process between the OPV and NR chromphores in the nanoparticle domain. The OPV chromophores underwent strong aromatic □-□ stacking in the aqueous medium and these aggregated conjugated domains were found to provide more than 75 % FRET overlap between OPV and NR. Detailed photophysical studies and energy calculations revealed that the newly designed polymer nanoparticle assembly provided appropriate geometry for 88 % FRET efficiency having the Förster distance and distance between donor and acceptor as 39.24 Å and 28.13 Å, respectively. The nanoparticles were found to be biocompatible and non-toxic to cancer and normal cell lines. The aliphatic polyester backbone in the nanoparticle was found to be responsive to lysosome enzymes such as esterase, chymotrypsin, trypsin, and papain and GSH. These enzymes digested the polymer chains at the intracellular compartments, which make the FRET probe highly desirable for bio-imaging applications. Lyso-tracker assisted cellular uptake studies conformed that the nanoparticles co-localization in the lysosomal compartment in the cytoplasm. Confocal imaging with selective photo-excitation of FRET donor alone (OPV chromophore) produced bright blue-emission whereas bright-red emission was produced in the presence of FRET acceptor (NR chromophores) followed by the efficient FRET mechanism at the intracellular level. Merging of the blue and red emission produced magenta-emission owing to the greater colour-tunability of the

FRET probe for bio-imaging applications. Currently efforts are being taken to apply the FRET concept and the synthetic methodology in L-amino acid to expand the approach to other systems in cancer research.

3.5 **References:**

1) X. Duan; L. Liu; F. Feng; S. Wang *Acc. Chem. Res.* **2010**, *43*, 260-270.
2) F. Lv; T. Qiu; L. Liu; J. Ying; S. Wang *Small*, **2016**, *6*, 696-705.
3) C. Li; S. Liu *Chem. Commun.* **2012**, *48*, 3262-3278.
4) K. Li; B. Liu *Polym. Chem.* **2010**, *1*, 252-259.
5) P. Huang; D. Wang; Y. Su; W. Huang; Y. Zhou; D. Cui; X. Zhu; D. Yan *J. Am. Chem. Soc*, **2014**, *136*, 11748-11756.
6) R. Dong; B. Zhu; Y. Zhou; D. Yan; X. Zhu *Angew Chem. Int. Edn*. **2012**, *51*, 11633-11637.
7) Y. Huang; D. Wang; X. Zhu; D. Yan; R. Chen *Polym. Chem.* **2015**, *6*, 2794-2812.
8) G. O. Fruhwirth; L. P. Fernandes; G. Weitsman; G. Patel; M. Kelleher; K. Lawler; S. P. Poland; A. Brock; S. P. Poland; D. R. Matthews; G. Kéri; P. R. Barber; B. Vojnovic; S. M. Ameer-Beg; A. C. C. Coolen; F. Fraternali; T. Ng *Chem Phys Chem*, **2011**, *12*, 442-461.
9) H. Sahoo *J. Photochem. Photobiol. C: Photochem. Rev.* **2011**, *12*, 20-30.
10) X. Li; J. Mu; F. Liu; E. W. P. Tan; B. Khezri; R. D. Webster; E. K. L. Yeow; B. Xing *Bioconjugate Chem.* **2015**, *26*, 955-961.
11) J. Chen; W. Zhong; Y. Tang; Z. Wu; Y. Li; P. Yi; J. Jiang *Macromolecules* **2015**, *48*, 3500-3508.
12) X. Han; De-E. Liu; T. Wang; H. Lu; J. Ma; Q. Chen; H. Gao *ACS Appl. Mater. Interfaces*, **2015**, *7*, 23760-23766.
13) H. Chen; S. Kim; L. Li; S. Wang; K. Park; J-X. Cheng *Proc. Natl. Acad, Sci*. **2008**, *105*, 6596-6601.
14) P. Rajdev; D. Basak; S. Ghosh *Macromolecules*, **2015**, *48*, 3360-3367.
15) S. J. Miyake-Stoner; A. M. Miller; J. T. Hammill; J. C. Peeler; K. R. Hess; R. A. Mehl; S. H. Brewer *Biochemistry*, **2009**, *48*, 5953-5962.
16) H. Maity; G. Reddy *J. Am. Chem. Soc*, **2016**, *138*, 2609-2616.
17) F. He; Y. Tang; M. Yu; F. Feng; L. An; H. Sun; S. Wang; Y. Li; D. Zhu; G. C. Bazan *J. Am. Chem. Soc.* **2006**,*128*, 6764-6765.
18) W. Lin; Y. Du; Y. Zhu; X. Chen *J. Am. Chem. Soc.* **2014**, *136*, 679-687.
19) S. Rana; S. G. Elci; R. Mout; A. K. Singla; M. Yazdani; M. Bender; A. Bajaj; K. Saha; U. H. F. Bunz; F. R. Jirik; V. M. Rotello *J. Am. Chem. Soc.* **2016**, *138*, 4522-4529.
20) Q. Cui; X. Wang; Y. Yang; S. Li; L. Li; S. Wang *Chem. Mater.* **2016**, *28*, 4661-4669.
21) Y. Huang; F. Qiu; L. Shen; D. Chen; Y. Su; C. Yang; B. Li; D. Yan; X. Zhu *ACS Nano*, **2016**, *10*, 10489-10499.
22) F. He; X. Ren; X. Shen; Q-H. Xu *Macromolecules*, **2011**, *44*, 5373-5380.
23) T. Senthilkumar; S.K. Asha *Macromolecules*,***2015***, *48*, 3449-3461.
24) F. Qiu; Y. Huang; X. Zhu *Macromol. Chem. Phys*. **2016**, *217*, 266-283.

25) D. Ding; K. Li; W. Qin; R. Zhan; Y. Hu; J. Liu; B. Z. Tang; B. Liu *Adv. Healthcare Mater*, **2013**,*2*, 500-507.
26) A. H. Malik; S. Hussain; P. K. Iyar *Anal. Chem.*, **2016**, *88*, 7358-7364.
27) C. Zhu; Q. Yang; L. Liu; S. Wang *J. Mater. Chem*, **2011**, *21*, 7905-7912.
28) Y. Wang; S. Li; L. Feng; C. Nie; L. Liu; F. Lv; S. Wang *ACS Appl. Mater. Interfaces*. **2015**, *7*, 24110-24118.
29) S. Wang; B. S. Gaylord; G. C. Bazan *J. Am. Chem. Soc.* **2004**, *126*, 5446-5451.
30) Z. Kahveci; M J. Martínez-Tomé; R. Mallavia; C. R. Mateo *Biomacromolecules*, **2013**, *14*, 1990-1998.
31) Y. Huang; F. Qiu; D. Chen; L. Shen; S. Xu; D. Guo; Y. Su; D. Yan; X. Zhu *Small*, **2017**,*13*,1604062-1604073.
32) F. Qiu; D. Wang; R. Wang; X. Huan; G. Tong; Q. Zhu; D. Yan; X. Zhu *Biomacromolecules*, **2013**, *14*, 1678-1686.
33) B. Kulkarni; B. Surnar; M. Jayakannan *Biomacromolecules*, **2016**, *17*, 1004-1016.
34) T. Endres; M. Zheng; A. Kiliç; A. Turowska; M. Beck-Broichsitter; H. Renz; O. M. Merkel; T. Kissel *Mol. Pharmaceutics*, **2014**, *11*, 1273-1281.
35) T. J. Deming *Prog. Polym. Sci.* **2007**, *32*, 858-875.
36) T. J. Deming *Adv. Drug Delivery. Rev*. **2002**, *54*, 1145-1155.
37) K. Osada; K. Kataoka *Adv. Polym. Sci.* **2006**, *202*, 113-153.
38) H. Sun; F. Meng; A. A. Dias; M. Hendriks; J. Feijen; Z. Zhong *Biomacromolecules*, **2011**, *12*, 1937-1955.
39) H. Sun; R. Cheng; C. Deng; F. Meng; A. A. Dias; M. Hendriks; J. Feijen; Z. Zhong *Biomacromolecules*, **2015**, *16*, 597-605.
40) M. Deng; J. Wu; C. A. Reinhart-King; C. C. Chu *Biomacromolecules*, **2009**, *10*, 3037-3047.
41) A. C. Fonseca; M. H. Gil; P. N. Simões *Prog. Polym. Sci.* **2014**, *39*, 1291-1311.
42) Q. Yin; L. Yin; H. Wang; J. Cheng *Acc. Chem. Res.* **2005**, *48*, 1777-1787.
43) M. H. R. Magno; J. Kim; A. Srinivasan; S. McBride; D. Bolikal; A. Darr; J O. Hollinger; J. Kohn *J. Mater. Chem*. **2010**, *20*, 8885-8893.
44) L. Sheihet; K. Piotrowska; R. A. Dubin; J. Kohn; D. Devore *Biomacromolecules*, **2007**, *8*, 998-1003.
45) K. A. Aamer; K. L. Genson; J. Kohn; M. L. Becker *Biomacromolecules*, **2009**, *10*, 2418-2426.
46) E. Tziampazis; J. Kohn; P. V. Moghe *Biomaterials*, **2000**, *21*, 511-520.
47) N. Shpaisman; L. Sheihet; J. Bushman; J. Winters; J. Kohn *Biomacromolecules*, **2012**, *13*, 2279-2286.
48) J. Wu; L. Zhao; X. Xu; N. Bertrand; W. Choi; B. Yameen; J. Shi; V. Shah; M. Mulvale; J. L. MacLean; O. C. Farokhzad *Angew. Chem. Int. Ed*. **2015**, *54*, 9218-9223.

49) W. Lu; X. Wang; R. Cheng; C. Deng; F. Meng; Z. Zhong *Polym. Chem*. **2015**, *6*, 6001-6010.
50) S. Anantharaj; M. Jayakannan *Biomacromolecules*, **2012**, *13*, 2446-2455.
51) S. Anantharaj; M. Jayakannan *J. Polym. Sci., Polym Chem.* **2016**, *54*, 1065-1077.
52) R. Aluri; M. Jayakannan *Polym. Chem*. **2015**, *6*, 4641-4649.
53) S. Anantharaj; M. Jayakannan *J. Polym. Sci., Polym Chem.* **2016**, *54*, 2864-2875.
54) S. Anantharaj; M. Jayakannan *Biomacromolecules*, **2015**, *16*, 1009-1020.
55) S. Saxena; M. Jayakannan *J. Polym. Sci., Polym Chem.* **2016**, *54*, 3279-3293.
56) R. Aluri; M. Jayakannan *Biomacromolecules,* **2017**, *18*, 189-200.
57) N. Karnati; M. Jayakannan *Macromolecules,* **2016**, *49*, 4102-4114.
58) S. R. Amrutha; M. Jayakannan *Macromolecules,* **2007,** *40, 2380 – 2391*.
59) M. Goel; N. Karnati; Jayakannan M. *Macromolecules*, **2014**, *47*, 2592-2603.
60) J. Rautio; H. Kumpulainen; T. Heimbach; R. Oliyai; D. Oh; T. Järvinen; J. Savolainen *Nat. Rev.* **2008,** *7*, 255–270.
61) P. S. Pramod; R. Shah; C. Sonali; N. Balasubramanian; M. Jayakannan *Nanoscale*, **2014**, *6*, 11841- 11855.
62) P. Anilkumar; M. Jayakannan *J. Phys. Chem. C*. **2007,** *111***,** 3591-3600.
63) Rychter P. Rychter; M. Kawalec; M. Sobota; P. Kurcok; M. Kowalczuk *Biomacromolecules,* **2010**, *11*, 839-847.
64) I. A. Karpenko; A. S. Klymchenko; S. Gioria; R. Kreder; I. Shulov; P. Villa; Y. Mely; M. Hibert; D. Bonnet *Chem. Commun*. **2015**, *51*, 2960-2963.
65) A. Datta; D. Mandal; S. K. Pal; K. Bhattacharyya *J. Phys. Chem. B.* **1997**, *101*, 10221-10225.
66) A. Ghaffar; G. J. J. Draaisma; G. Mihov; A. A. Dias; P. J. Schoenmakers; S. Van der. Wal *Biomacromolecules,* **2011**, *12*, 3243-3251.
67) M. A. Woodruff; D. W. Hutmacher *Progress in Polymer Science* **2010**, *35*, 1217-1256.
68) M. Malhotra; B. Surnar; M. Jayakannan *Macromolecules,* **2016**, *49*, 8098-8112.
69) B. Surnar; M. Jayakannan *Biomacromolecules,* **2013**, *14*, 4377-4387.
70) J. Wang; X. Sun; W. Mao; W. Sun; J. Tang; M. Sui; Y. Shen; Z. Gu *Adv. Mater.* **2013**, *25*, 3670-3676.
71) Y. Ohya; S. Takamido; K. Nagahama; T. Ouchi; R. Katoono; N. Yui *Biomacromolecules,* **2009**, *10*, 2261-2267.
72) X. Jia; Q. Chen; Y. Yang; Y. Tang; R. Wang; Y. Xu; W. Zhu; X. Qian *J. Am. Chem. Soc.* **2016**, *138*, 10778-10781.

Chapter 4

AIE Tagged L- Amino acid Luminescent Biodegradable Polyesters as Multi-colour Tunable Intracellular FRET Nanoprobefor Bio-imaging in Cancer Cells

Abstract

Aggregation induced emission (AIE) chromophore tagged L-amino acid based biodegradable polyester have been designed and their fluorescent nano-scaffolds were explored as multi-colour tunable FRET nano-probe for bio-imaging in cancer cells. AIE capable hydroxyl functionalized tetraphenylethyelene (TPE) diol was tailor-made through multi-step reaction and it was subjected to melt transesterification with L-aspartic acid monomer to yield new blue-luminescent amphiphilic polyesters. The AIE active amphiphilic polyesters were further investigated by photophysical studies to their responsiveness to hydrophilic and hydrophobic environmental sensitivity. Dimethylsulfoxide + water solvent combination was chosen as to alter the aggregated geometry of self assembled polymers to understand the intrinsic details of polymer folding and unfolding due to environment change. These AIE polyesters were self assembled into compact spherical nanoparticles and they were found to be capable of encapsulating water insoluble red-fluorophore Nile red (NR) and green-fluorophore drug Curcumin (CUR). Two FRET probes TPE-NR and TPE-CUR were constructed in the TPE conjugated polymer nano-system as donor and CUR and NR as acceptors. Third FRET probe was build between CUR-NR using non-TPE amphiphilic polyester scaffolds. Detailed photophysics analysis allowed determining the Forester distance and FRET efficiency between the pairs. The biocompatibility of these nanoparticles were further demonstrated in the cancer cell lines such as breast cancer (MCF 7), and it was revealed that both the nascent TPE nanoparticles, TPE-CUR, TPE-NR and CUR-NR FRET probes were non-toxic to cells up to 100 μg/mL which made them ideal as bio-imaging agents. However at higher concentrations of CUR the nanoparticles showed good killing in the cells making them ideal for combating the cancer cells. Confocal and live cell imaging experiments threw light on the accumulation of these nanoparticles in the cytoplasm of the cells and demonstration of FRET within the cell lines showed the stability of the nanoparticles during the efficient uptake into the cells. The cleavage of these nanoparticles in the presence of lysosomal enzymes were demonstrated by using various enzymes and the FRET as probe was used to study the bio-degradation of these nanoparticles in 'in vitro' experiments. The detailed photophysical analyses and the bio-degradation studies made these nanoparticles highly complex yet well defined architectures for bio-imaging and cell killing experiments.

4.1 Introduction

Bio-resource based polymer materials have attained significant importance as an alternative for petroleum based polymers due to their large abundance in nature, excellent biodegradability and biocompatibility for diverse biomedical applications.[1,2] L-Amino acid based natural proteins, oligo-peptides and high molecular weight synthetic peptides and their self-assembled nano-scaffolds have made significant contributions in tissue engineering[3,4], bone-repair[5], delivery of anticancer drugs and genes[6,7]. Fluorescent techniques provide excellent opportunity to study the folding/unfolding and assembly/disassembly phenomena of these nano-assemblies under physiological conditions by steady state and time-resolved spectroscopes.[8] Fluorescence resonance energy transfer (FRET) is one of the powerful tool to study the intermolecular interactions between chemical entities and also the direct visualization of their internalization *in vitro* and *in vivo.* Forster distance of < 50 Å is critical between the energy donor-acceptor units to observe the FRET action which is accomplished either by direct chemical conjugation or confined them in self-assembled nano-domains [9]. Fluorescence resonance energy transfer (FRET) is also effectively utilized for studying several biochemical processes like receptor-mediated endocytosis of polymer nanocarriers, drug release kinetics, disassembly of nanocarriers at intracellular stimuli, etc. FRET process is also employed as bio-imaging tool for early diagnostics in cancer to improve the treatment efficacies.[10] Tryptophan and dansyl amide is one of the extensively explored FRET pair[11] to study the inter or intramolecular interactions in macromolecules like peptides and proteins and DNA etc. Few selective examples of FRET probes are shown in Figure 4.1. Figure 4.1 (i) shows the use of FRET pair Cy5 and Cy3 labelled at the TAR-DNA hairpin a trans-activation response region of hairpin isolated from human immunodeficiency virus-1 (HIV-1) and its structure was deduced and proposed to be have four bulges and a loop containing biotin in case of TAR-DNA and no bulges in the mutant of TAR-DNA hairpin using FRET studies between Cy5 and Cy3 dyes.[12] Using the same FRET diad with Cy3 as donor and Cy5 as acceptor, Danielis Rutkauskas studies and showed the simultaneous interactions of type II restriction endonucleases enzyme Ecl18kl with DNA sites to induce DNA loop

formation leading to formation of DNA-bound Ecl18kI dimer bridging tetramer causing disruption in DNA strand within 1 s (shown in figure 4.1 (ii))[13].

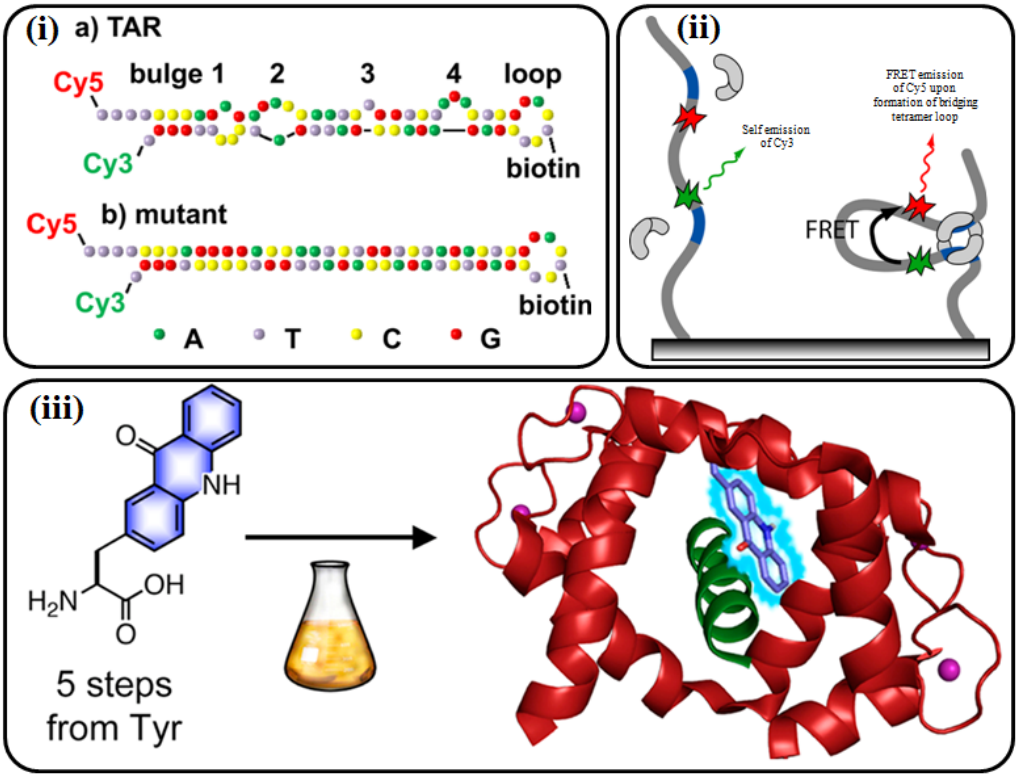

Figure 4.1: *The Cy5 and Cy3 labelled TAR-DNA and mutant hairpin showing loops with buldges (i), Tetramer of type II restriction endonucleases enzyme Ecl18kl with DNA forming loop for nuclease activity (ii), the protein structure of the biniding of helical peptide with donor linked CaM with methoxycoumarin FRET acceptor.(Figures taken from: Jixin Chen et al, J. Phys. Chem. B 2014, 118, 12130-12139., Danielis Rutauskas et al., J. Phys. Chem. B 2014, 118, 8575-8582, Lee C. Speight et al., J.Am. Chem. Soc. 2013, 135, 18806-18814).*

Catalytic activity of enzymes using Trp donor in caspase 3 enzyme and dansyl acceptor in caspase inhibitor have been demonstrated successfully in EColi.[14], the binding of helical peptides to calmodulin (CaM) causing protein conformational changes were studied using acridon-2-ylalanine as FRET donor and methoxycuumarin (Mcm) as FRET acceptor (shown in figure 4.1 (iii)[14]. Ring opening polymerization of N-carboxylanhydride (NCA) monomers of L-amino acid resources produced high molecular weight synthetic polypeptides. FRET probes were also employed for the study of the self-assembled nano-objects of these di and tri-block peptide copolymers[15]. Soumen Das et al[16] have studied NCA route based amphiphilic copolymer glycopolypeptide-b-poly(propyleneoxide) where hydrophobic PPO was used as initiator and these copolymers self assembled into spherical

polymerosomes of ~50 nm and these polymerosomes were loaded with hydrophilic dye calcein which acted as a donor and hydrophobic RBOE dye which acted as an acceptor of the FRET pair. Dual imaging of this FRET system was demonstrated at λ_{exc} 532 as well as 488 nm as shown in figure 4.2 a.[16] Diblock amphiphilic colpolymer of PEG-*block*-poly(*N*-hexylstearate L- aspartimide (PEG-b-PHSA) was synthesised with PEG as hydrophilic component and nine steric acid chains as hydropholic segment. The stability of spherical nanoparticles formed due to self assembly of these polymers was studied using FRET as a probe. Two dyes lipophilic fluorescent $DiOC_{18}$(3) {3,3'-Dioctadecyloxacarbocyanine perchlorate} was used as energy donor and lipophilic fluorescent $DiIC_{18}$(3) {1,1'-Dioctadecyl-3,3,3',3'-Tetramethylindocarbocyanine -5,5' Disulphonic acid} was used as FRET acceptor molecules and loaded physically in the nanoparticles. The stability of these nanoparticles were studied in serum albumin, alpha and beta globulins, or gamma globulins (which mimics proteins which form a major part of blood serum) as a function of change in FRET intensity and no change in the intensity showed the high stability of the polymeric nanoparticles.[17]

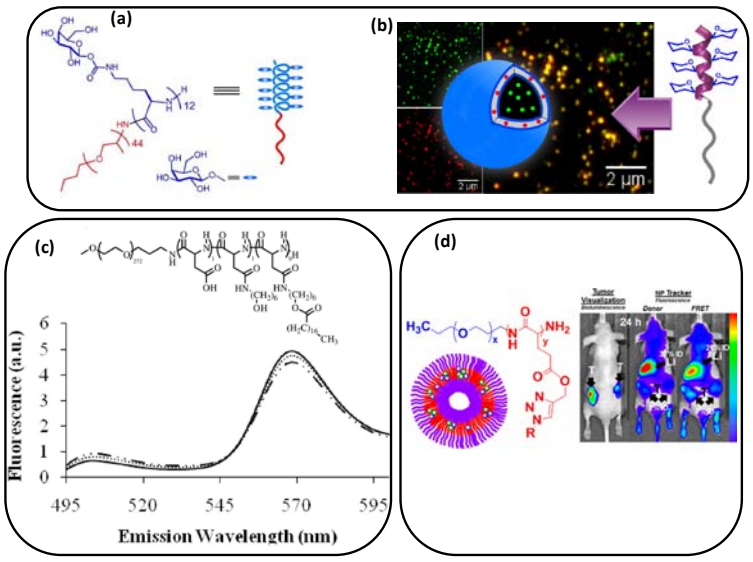

Figure 4.2: *Schematic structure of amphiphilic block glycopeptides and thier polymerosomes, NP loaded with calcein and RBOE and showing self emission and FRET emission (a,b) (figure a, b adapted from Das et al, Langmuir,* **2015**, *31,* 3402-3412.*), PEG-block-poly(N-hexylstearate L- aspartimide (PEG-b-PHSA) forms stable nanoparticles monitored using FRET emission (c)(Figure adapted from* Diezi et al *Mol. Pharm.* **2010**, *7,* 1355-1360)*, and the PEG-b-PPLG polymer structure and schematic of FRET pair loaded nanoparticles and FRET imaging in vivo experiments(d)(figure adapted from Quadir et al, Mol. Pharm.* **2014**, *11,* 2420-2430) .

Poly (γ-propargyl L-glutamate) (PPLG) was synthesised by N-carboxyanhydride (NCA) polymerisation of propargyl-L-glutamate and a block was made with hydrophilic PEG as an initiator and azide-alkyne chemistry was employed to attached flouro-phores Cy5.5 as donor and Cy7 as an acceptor. The excitation of Cy5.5 at 640 nm and FRET emission from Cy7 at 800 nm was observed. The effect of pH on the self assembly of the nanoparticles was studied as a function of FRET and with decrease in pH the relative FRET intensity was decreased and nanoparticles were found to be sensitive towards acidic conditions. The doxorubicin was loaded in the nanoparticles and was delivered successfully to the MDA-MB-468 cells and FRET was demonstrated in in-vivo in BALB/c tumour bearing rice to accumulation of the vesicles in the tumour sites [18]. Direct polycondesation approaches created the avenue for the development of several non-peptide polymer analogues such as poly(ester-amide)s[19], poly(ester-urethane-urea) [20], polycarbonates[21,22], polyurethanes[23], etc. From our group, we have reported solvent free dual ester-urethane melt polycondensation reaction for new classes of linear and hyperbranched poly (ester-urethane)s[23,24]. These L-amino acid based poly (ester-amide)s, polycarbonates and poly(ester-urethane)s were found to be enzyme, pH and GSH stimuli-responsive nanocarriers for drug and gene delivery. In general, L-amino acid polymers are non-luminescent in nature; thus, the full potential of these bio-polymers are un-tapped for thedevelopment of diagnostic medical probesbased on fluorescent bio-assay techniques.Only a few examples could be seen for bio-degradable polymer FRET probes in the literature. Wu et al. reported FRET probes based on coumarin dye and Nile red as donor and acceptor, respectively, in L-cysteine based poly(ester-amide) nanocarrier as redox-sensitive cancer theranostics platform (shown in figure 4.3)[9]. In chapter 3, FRET probes were reported by us using oligo-phenylenevinylene (OPV) π-conjugated chromophore as FRET donor and Nile red as FRET acceptor in polycaprolactone block copolymer and L-aspartic polymer backbones. Apart from these two examples, there is no attempt made in the literature for the construction of FRET probe based on the non-peptide L-amino acid polymers.

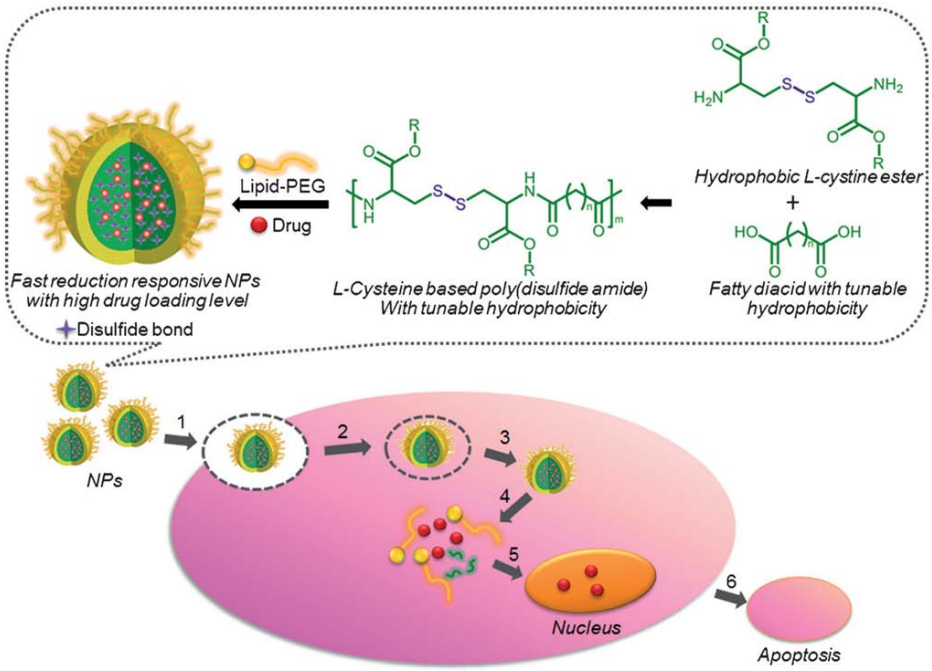

Figure 4.3: *Illustration of poly (disulphide amide) developed from L-cysteine amino acid for docetaxol-loaded redox stimuli responsive Cys-PDSA nanoparticles.(* Figure Adapted from Zhang et al, *Chem. Sci*. **2013**, *4*, 2143-2151*).*

Aggregation induced emission (AIE) is the new concept emerging for sensing and imagining applications in material and bio-medical field. AIE is originating from the aggregation induced luminescent chromophores in solid state or solvent-assisted aggregates. One of the first molecule which showed the AIE characteristics was hexaphenylsilole (HPS) which showed huge fluorescence emission in aggregated state due to restriction in the aryl rotors due to its propeller shape (see figure 4.4 b). [10] Three of the most used AIE probes are multi-phenyl substituted siloles, distryrylanthracene (DSA), and tetraphenylethylene (TPE) molecules (see figure 4.4). Ma et al showed TPE based N-isopropylacrylamide polymers which exhibited high luminescence emission in water and solid powder state form and were employed for long term bio-imaging (see figure 4.4 a) [25]. Quenching of conventional luminescent chromophore N,N-dicyclohexyl-1,7-dibromo-3,4,9,10-perylenetetracarboxylic diimide (DDPD) caused due to 'aggregation caused quenching' while change in environment from THF to water, and on the other hand, AIE in Hexaphenylsilole (HPS) under the same conditions showed high emission in water (see figure 4.4 b).[26] Chemical structures of 9,10-distyrylanthracene (DSA) are shown in figure 4.4 c and

the oligocarbazoles was reported by Xu et al showing restriction in movement in the chemicals bonds causing high green luminescence in water medium due to AIE[27]. For the past one decade, numerous experimental and theoretical evidences have been accumulated to propose the underlining principle behind this unique AIE phenomenon. It is proposed that restricted intermolecular rotation causes the arresting of rotational movement of C-C bonds in solid state and causing the emission of the excited state energy in form of radiative emission (instead of its loss in the non-radiative use in the rotation of the bonds)[10]. TPE belong to a class of molecules known as AIE molecules which are non-fluorescent in isolated state, however show high emission properties in aggregated states. This arises due to the restriction in the rotation amongst the molecules bonds which caused energy for excitation to release in a radiative pathway.

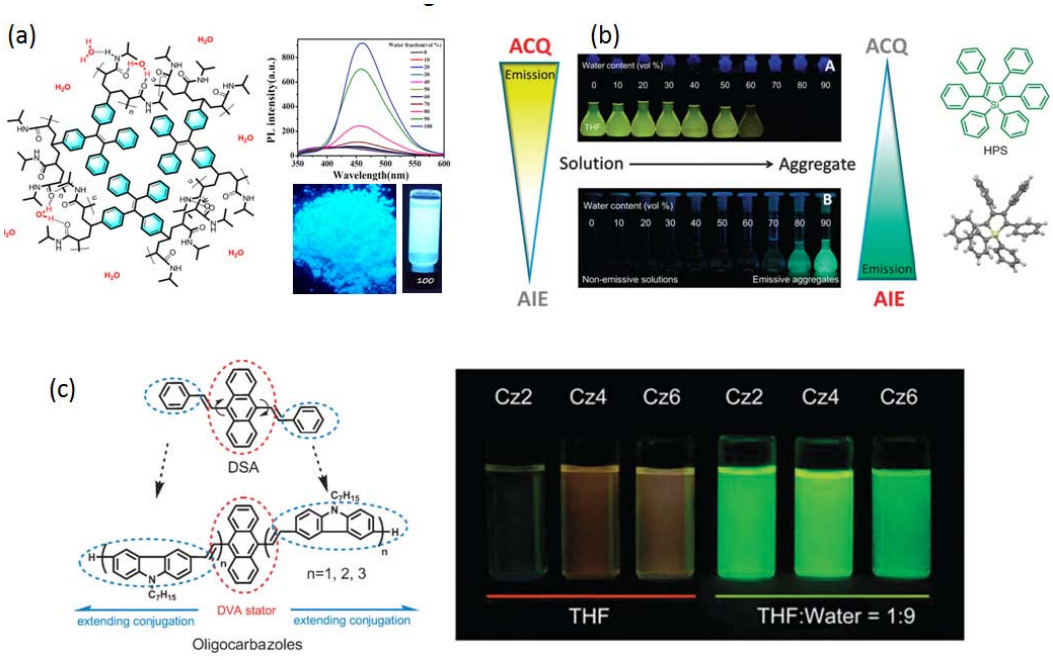

Figure 4.4: *Highly luminescent TPE based N-isopropylacrylamide polymers in solution and solid state showing high intense luminescence in water and solid state form (Images adapted from Ma et al, ACS Appl. Mater. Interfaces* **2016**, *8,* 8341−8348*) (a), Aggregation induced quenching in DDPD and AIE in (HPS) in THF water system (adapted from Hong et al,Chem. Soc. Rev.*, **2011**,*40,* 5361.*) (b) , restriction in movement in the chemicals bonds 9,10-distyrylanthracene (DSA) causinghigh green luminescence in water medium due to AIE (adapted from Xu et al, Chem. Commun.*, **2011**, *47,* 6602–6604*) (c).*

Polymers covalently tagged with molecules that possess AIE characteristics are often known as AIE active polymers. These polymers have gained interest due to interesting information they yield about the polymer structure and polymer folding unfolding processes. These provide opportunities to design and modify the molecular structures of the polymers and have been used for solid state films of high mechanical strength and luminescence. These polymers are find use in chemical or bio sensors and also in optoelectronic applications as organic light emitting diodes (OLEDs) and organic lasers etc. Wang et al reported a tyrosine functionalized tetraphenylethene, TPE-Tyr, which was crosslinked in the presence of horseradish peroxidase (HRP) and H_2O_2 and causing the TPE molecules to aggregate and show high fluorescence emission and these materials were employed for biosensor design for glucose detection. [28] (see figure 4.5 a). Xianghan et al, have reported the formation of red emitting TPE-functionalised trimethinecyanine (TPE-BICOOH) based liposomes vescicles used for bio-imaging applications shown in figure 4.5b. [29]

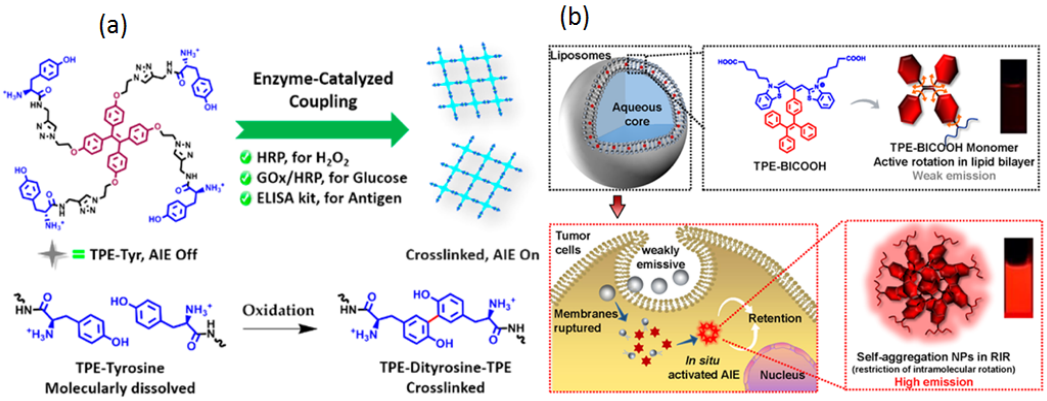

Figure 4.5: *AIE in TPE-Tyr molecular probes induced due to cross-linking caused in tyrosine molecules in presence of HRP and H_2O_2 (a) (figure adapted from Wang et al, Chem. Soc.* **2014**, *136*, 9890−9989*), Red TPE emissive liposomal materials (b) (adapted from Zhang et al, ACS Appl. Mater. Interfaces* **2018**, *10*, 25146−25153*).*

Unique tadpole shaped pH sensitive polymers were reported by et al Wang et al. These polymers have inbuilt Schiff base and the nanoparticles were loaded with anticancer drug and FRET energy transfer was demonstrated from TPE aggregated chromophore to DOX. These tadpole shaped polymers were used for cellular imaging as well as in anti cancer DOX delivery and inhibition in MCF 7 cells (see figure 4.6 a).[30] Han et al, used the FRET pair of TPE and DOX and used single photon

excitation to determine the release pattern of DOX at sub-cellular organelle based on pH-responsive multifunctional system (see figure 4.6 b). [31] Apart from anti cancer activities, TPE chromophores have been successfully demonstrated for their application in bacterial killing. Amphiphilic TPE-Bac was synthesised and employed as a bactericide and was made up of two long alkyl chains and two positively charged amines used for intercalating membrane of bacteria, leading to toxicity. Using photosensitizer reactive oxygen species (ROS) generation was also used for enhanced bacterial killing (see figure 4.6 c). [32] Metallo-organic AIE vesicles based on triarylamine carboxylate and Zn^{2+} have been reported for cell imaging applications. Anticancer drug 5-fluorouracil was loaded in these vescicles and dempostrated for cell killing, and these vescilces were also used for specific detection of Zn^{2+} ions as multipurpose nano-materials. [33]

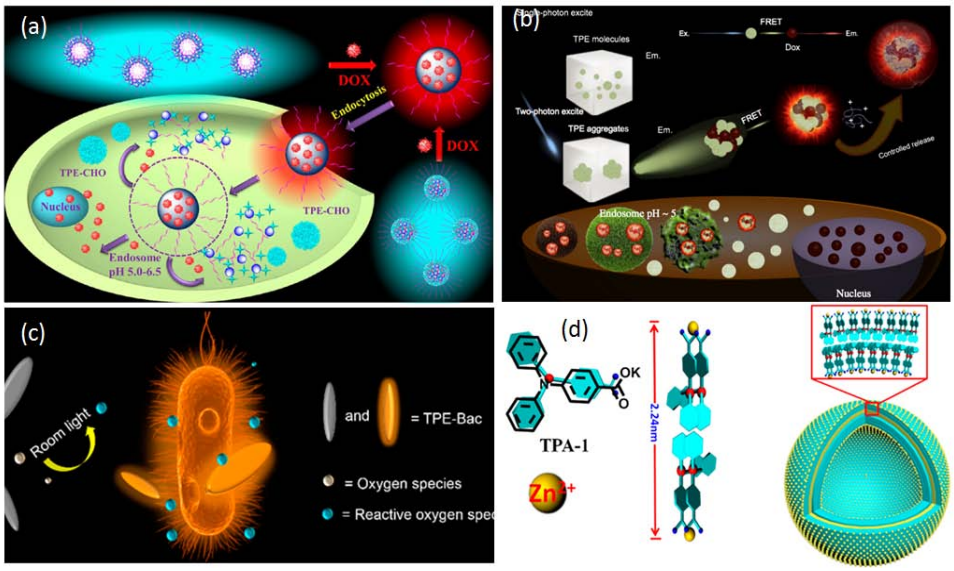

Figure 4.6: *Demonstration of aggregation induced FRET between aggregated species of TPE as donor and DOX as acceptor (a,b) (figures adapted from Wang et al, Biomacromolecules* **2016**, *17*, 2920−2929, *and Han et al, ACS Appl. Mater. Interfaces* **2015**, *7*, 23760−23766*), Use of amphiphilic TPE based cationic amines for bacterial cell killing (c) (Zhao et al, ACS Appl. Mater. Interfaces* **2015**, *7*, 7180−7188*), Formation of high definition AIE TPE based Vesicles for drug delivery and for zinc ion sensing (d) (Wei et al, ACS Appl. Nano Mater.* **2018**, *1*, 1819−1827*).*

The above discussion envisage that it would be appropriate to develop new biodegradable FRET platform based on anticancer drug as FRET fluorescent component and the FRET facilitating nano-object from bio-resources like L-amino acid polymers for bio-imaging in cancer cells to improve the treatment efficacies.

This concept would open up new avenue of research opportunities to design and develop biocompatible and biodegradable FRET probes for the long-term application of FRET concept in the biomedical applications.To accomplish this task, this chapter reports one of the first examples ofTPE-tagged L-aspartic acid based biodegradable polyester nano-platform and construction of FRET probes using curcumin drug and Nile red flrouorophore dye. This new L-amino acid polymer FRET probe concept is shown in Figure 1.

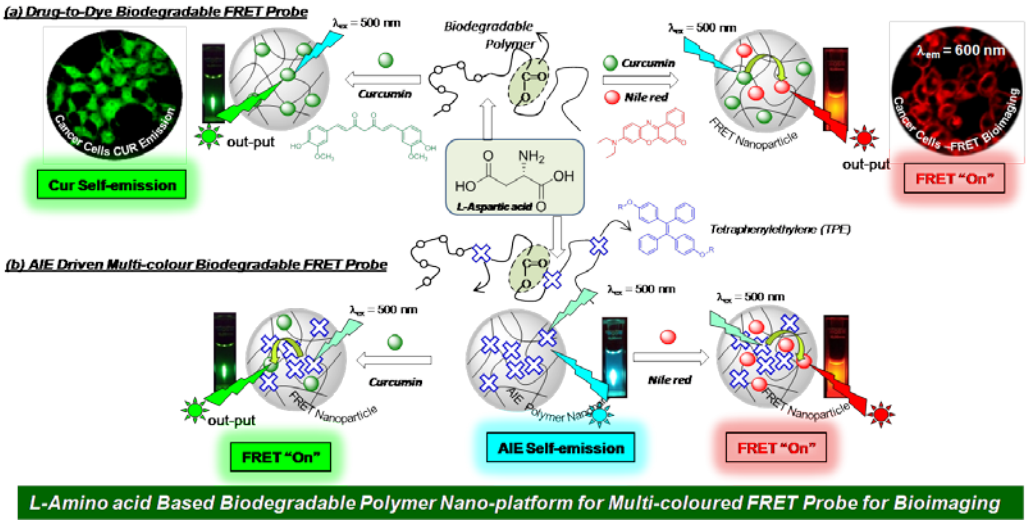

Figure 4.7: *Development of L-Aspartic acid polymer FRET probe build using Curcumin drug and Nile red fluorophore and their enzyme-stimuli responsive bio-imaging in cancer cells.*

The present investigation is emphasized to build new TPE-tagged biodegradable polymer and two AIE-assisted FRET probes were constructed between TPE→CUR and TPE→NR. An additional FRET probe was also made between CUR-NR in non-TPE polymer platform. In the present investigation curcumin exhibited dual action as donor and acceptor, respectively, towards TPE and Nile red to yield a cascade FRET probe TPE→CUR→NR. The performance of the FRET probes were demonstrated for bio-imaging in breast cancer MCF 7 cells. Self-assembly aspects of the amphiphilic polyester were studied in detail using fluorescence spectroscopy changes in TPE chromophore as well the perturbations in FRET between TPE-CUR, TPE-NR and TPE-CUR-NR FRET pairs. The amphiphilic luminescent polymer produced very stable nanoparticles of < 100 nm in aqueous medium which was capable of encapsulating water insoluble drugs such as curcumin and fluorophores

such as Nile red. In vitro cytotoxicity studies revealed that the curcumin loaded polymer nanoparticles exhibited more than 90 % cell killing in cervical and breast cancer cells. Photophysical studies confirmed the L-aspartic nanoparticle provided appropriate Forster distance < 25 A for the occurrence of FRET process TPE, CUR and NR in more than 85 % efficiency. Real-time in vitro FRET experiments proved that the polymer nanoparticles were stable in extracellular conditions and selectively underwent enzymatic-biodegradation in the presence of lysosomal enzymes to release the drug and fluorophores. Confocal microscope experiments with lyso-tracker staining enabled the identification of the co-localization of polymer nanoparticles in the lysosomes and supported the enzymatic-digestion process. Confocal microscope-assisted live cell FRET experiments showed evidence for the occurrence of the FRET process at the intracellular level. The distinct blue emission from TPE, green emission from the CUR and red emission form NR facilitated the monitoring of the live cell bio-imaging with selective photoexcitation of the FRET donors. The present investigation shed new insight into the building of TPE-curcumin-NR based FRET probes and bio-resource based L-amino acid based biodegradable polyester platform was cleverly explored to demonstrate the proof-of-concept in live cancer cell bio-imaging applications.

4.2 Experimental Section

Materials: L-Aspartic acid, triethylene glycol (TEG), 1,12-dodecanediol, titanium tetrabutoxide ($Ti(OBu)_4$) curcumin, nile red, horse liver esterase enzyme, tetrazolium salt: 3-(4,5-dimethylthiazolyl)-2,5-diphenyltetrazolium bromide) MTT, fluoromount aqueous mounting medium, DAPI (4', 6-diamidino-2-phenylindole, silicon wafers were purchased from Sigma Aldrich. Trypsin phosphate versene glucose (TPVG) solution was obtained from Hi-media.MCF 7 cells (mammalian breast cancer) were maintained in phenol red containing Gibco medium with 1% (v/v) penicillin-streptomycin, 10% (v/v) fetalbvine serum (FBS). 96-well plates and 6 well plates were obtained from costae and Lab Tek 8 well cover glass chamber were obtained from Nunc Lab Tek. Cell signalling technologies provided lyso tracker green DND- 26. Salts such as sodium sulfate, sodium bicarbonate were purchased locally. Solvents such as thinly chloride, methanol, DMSO, and other solvents were purchased locally and uses as it is. HPLC THF and HPLC DMSO were obtained from spectrochem laboratories.

General procedure: ^{1}H-NMR and ^{13}C-NMR recorded using 400 MHz and 100 MHz NMR spectrophotometer. Gel permeation chromatographic (GPC) plots were determined using Viscotek VE 1122 pump, Viscotek VE 3580 RI detector, and UV/vis detector w.r.t polystyrene standards. Dynamic light scattering DLS was employed to determine size of nanoparticles and Malvern instrument was used for it. Zeiss Ultra Plus scanning electron microscope was employed to generate the field emission scanning electrons microscope (FESEM) images of the nano fibres and nanoparticles. The Atomic force microscopy (AFM) images were generated by VeecoNanoscope IV instrument in tapping mode. The fixed cell and live cells images were obtained from LSM710 confocal microscope. PerkinElmer Lambda 45 UV-vis spectrophotometer and SPEX Fluorolog HORIBA JOBIN VYON fluorescence spectrophotometer having with excitation source 450 W Xe lamp and double gating 0.22 m Spex 1680 monochromator.

Synthesis of (E)-4,4'-(1,2-diphenylethene-1,2-diyl)diphenol (compound 1) : 4-Hydroxy benzophenone (10.0 g, 0.05 moles) was dissolved in dry THF (100.0 mL) in a 250 mL two neck RB under nitrogen environment. To this was added Zinc dust

(10.0 g, 0.15 moles) and placed in ice cold conditions. Titanium tetrachloride (8.34 mL, 0.08 moles) was added dropwise at 0°C and the reaction mixture was stirred for 0.5 h. The reaction mixture was brought to 25°C and was further refluxed for 12 h. After reaction completion, THF was evaporated and the product was extracted in ethyl acetate. The product was purified using silica column (50% v/v, ethyl acetate/pet ether), and it was obtained as white crystalline powder. Yield = 6.5 g g(71%).^{1}H-NMR in $CDCl_3$ (400 MHz): δppm : 7.13- 7.04 (m, 10H, Ar-H), 6.92-6.86 (dd, 4H, Ar-H), 6.61-6.54 (dd, 4H, Ar-H), 4.70 (bs, 2H, O**H**). MALDI-TOF m/z Calcd for $C_{26}H_{20}O_2$: 364.15, found M^+ 364.05. The structure was synthesized following the reference *ACS Appl. Mater. Interfaces* **2016**, *8*, 13724-13734.

Synthesis of (E)-2,2'-(((((1,2-diphenylethene-1,2-diyl)bis(4,1-phenylene))bis(oxy))bis(ethane-2,1-diyl))bis(oxy))bis(ethan-1-ol) [Referred in chapter as TPE Diol): Compound **1** (1.0 g, 0.03 moles) was taken in a 250 mL two neck RB and dissolved in dry DMF (50.0 mL) and to this was added potassium carbonate (2.85 g, 0.23 moles) and refluxed at 80°C for 0.5 h. The reaction mixture was cooled to 25°C and to this was added chloro-ethoxyethanol (0.86 mL, 6.9 mmoles) under nitrogen environment. Followed by this KI (0.46 g, 2.7 mmoles) was added to the reaction mixture and the reaction mixture was refluxed for 24 h. After reaction completion DMF was removed by vacuum distillation and the product was purified using silica column. The product was isolated at 1% v/v DCM methanol system and was obtained as light yellow flaky solid (yield=0.9 g).^{1}H-NMR in $CDCl_3$ (400 MHz) : δppm : 7.13- 7.04 (m, 10H, Ar-H), 6.92-6.86 (dd, 4H, Ar-H), 6.61-6.54 (dd, 4H, Ar-H), 4.70 (bs, 2H, O**H**). ^{13}C-NMR in $CDCl_3$ (100 MHz):157.06, 144.25, 139.73, 136.78, 132.63, 131.45, 127.78, 126.32, 113.72, 72.68, 69.73, 67.21, 61.82. MALDI-TOF m/z Calcd for $C_{34}H_{36}O_6$: 540.25, found M^+ 540.14.

Synthesis of TPE-tagged Luminescent Polyester(P-TPE): L-Aspartic aicd monomer (reported in chapter 2, 0.6 g, 2.3 mmol), TPE diol(0.06 g, 0.12 mmol), dodecanediol (0.21 g, 1.03 mmol), and triethylene glycol (0.17 g, 1.15 mmol) were taken in a melt condensation test tube and were melted at 100°C under nitrogen atmosphere.

Catalytic amount of $Ti(OBu)_4$(1 mol %) and benzoquinone (1 pinch) was added into the polymer tube and the tube was degassed using 0.01 mbar of vacuum and purged with nitrogen for 5 minutes each three times. The polymerisation was carried out at 120°C for four hours followed by application of vacuum for 2h at same temperature. The obtained polymer was purified by precipitation in methanol. Yield: 0.75 g (85 %)^{1}H-NMR (400 MHz , $CdCl_3$) δ ppm: 7.07 (m, 0.30 H, Ar-**H**), 7.01 (m, 0.19H,Ar-**H**) , 6.92 (m, 0.21 H, -m-Ar-**H**), 6.64 (m, 0.21 H, -o-Ar-**H**)), 5.50 (bs, 1H, -N**H**), 4.57 (s,1H, -C**H**), 4.32-4.24 (d, 1.48 H, new TEG esters), 4.13-4.08 (d, 2.24 H, new aliphatic ester), 3.76- 3.62 (m, 5.03H, oligoethylene protons -OC$\mathbf{H}_2$C$\mathbf{H}_2$), 3.01- 2.85 (m, 2H, -C$\mathbf{H}_2$), 1.66 (m, 5H, aliphatic protons), 1.45 (s, 9H, BOC protons), 1.27 (m, 9H, aliphatic protons). ^{13}C-NMR (100 MHz, $CDCl_3$) δ ppm:174.57, 171.10, 80.08, 70.62, 65.96, 65.26, 50.10, 46.65, 36.89, 29.60, 28.38, 25.94.

Self Assembly of AIE Luminescent Polymer P-TPE: The self assembly of amphiphilic AIE active P-TPE was obtained by dissolving 5.0 mg of polymer (13.5×10^{-6} M) in HPLC DMSO (2.0 mL) followed by dropwise addition of milli Q water (2.0 mL) and stirred for 12 h before transferring the content into a semi-permeable dialysis tube with molecular weight cut-off of 1.0 kD. This was dialysed for 48 h against large volumes of milli Q water with frequent replacement of water. The resultant solution was filtered using what-man paper and were used as it is for photophysics experiments and lyophilized and stored for biology experiments. The dialysed solutions were subjected to DLS studies and the gold spin coated samples of dried samples of dialysed polymer on silica wafer were subjected to FESEM studies. The dropcatedsamples on the mica sheet were subjected to AFM studies to visualise the structure of polymer adapted upon self assembly.

Encapsulation of Hydrophobic Nile red and Anti Cancer drug CUR and their Dual Loading: Dialysis method mentioned in the previous section was employed for loading highly luminescent hydrophobic dye NR and water insoluble drug Curcumin. The feed for NR and CUR were maintained as 100.0μgand 500.0μg respectively for both individual loading and dual loading. The dialysed solutions thus obtained were filtered and frozen and lyophilised and stored at 4°C and used for further analyses. The luminescent polymers P-TPE were loaded with NR, CUR and combination of NR

and CUR following the same procedure as mentioned. The frozen samples were used for most of the analyses unless mentioned otherwise. Molar exctinctioncoeffecients were used as 38000 mol L^{-1} and 55800 mol L^{-1} for NR and CUR respectively. Loading capability of P-0 nanoparticles were calculated using mathematical formulas 1 and 2 provided in chapter 2 under the experimental section.

Characteristic AIE photophysics of P-TPE polymer: The TPE conjugation in the backbone transformed the non fluorescent polymeric chains into AIE characteristic highly luminescent polymer. To study the acquired AIE properties P-TPE polymer was subjected to photophysicalstudies under different solvent environments using water and DMSO which were chosen to create aqueous and organic environment for the polymer. Water and DMSO compositions were varied from 10 to 100 %and the absorbance and fluorescence spectra of the resultant dispersed polymer solutions were recorded. The O.D. of TPE chromophore was maintained at 0.1 and fluorescence spectra were generated at λ_{exc} of 330 nm.

FRET pair between TPE+CUR, TPE+NR, CUR+NR: P-0 nanoparticles loaded with CUR and NR, and dual loaded with CUR and NR were prepared by dialysis method and have been named as PCUR, PNR, PCRU+NR and were used for absorbance and fluorescence studies. The CUR and NR were excited at λ_{max} 420 nm and 540 nm respectively in the individual and dual loaded samples to generate the fluorescence spectra. Similarly the P-TPE nanoparticles were excitedλ_{max} 330 nm and the CUR loaded and NR loaded nanoparticles were excited at λ_{max} 420 nm and 540 nm respectively. The O.D. in each samples were maintained with respect to TPE core as 0.1 O.D. and respective CUR and NR were maintained as the same ratio as that of dual loaded P-TPE/ P-0 polymer.

Environment dependent Colour TunableAIE Assisted FRET: The role of environment on the polymer structure decides the stability of the polymer as potentialnano-carrier. The effect of environment on the FRET could provide direct evidence to the structure of polymer nano-scaffold. The nanoparticlesat 2.7×10^{-7} M concentration with potential FRET pairswere subjected to various concentrations of DMSO and water ranging from 100% water to 10% water to see the effect of increasing DMSO concentration on FRET distance as a consequence of disassembly of the nano-particle. To study the effect of change in environment in the polymer structure three different FRET pairs were used: 1) P-0 non luminescent copolymer dual loaded with CUR and NR in hydrophobic cavity with CUR as donor and NR as acceptor, 2) the luminescent aggregated P-TPE copolymerloaded with CUR with TPE as donor and CUR as acceptor, 3) the luminescent aggregated P-TPE copolymer loaded with NR where TPE act as donor and NR as acceptor. The TPE, CUR and NR chromophores were excited at 330, 420 and 540 nm respectively.

Colour TunableAIE Assisted triple chromophorecomposite FRET: The triple component FRET studies were carried by developing CUR and NR dual loaded nanoparticles ofP-TPE using the dialysis method explained before. The absorbance of the triple component FRET pair was recorded and the O.D. of TPE chromophore was maintained at 0.1 O.D. The nascent P-TPE, P_{CUR} , P_{NR} , P-TPE_{CUR} P-TPE_{NR}nanoparticles where used at TPE concentration at 0.1 O.D. and the corresponding CUR and NR concentrations obtained in the dual loaded samples were used for all the nanoparticles. The triple component fluorescent nanoparticles P-TPE_{CUR+NR} were also maintained at same concentrations.The triple component nanoparticles were excited at λ_{330} to excite the TPE chromopohore and at λ_{420} to excite the CUR chromophore and at λ_{540} to execute the NR chromophore to understand in details the FRET changes during the range of the DMSO and water composition changes.

Cytotoxicity experiments for bio-imaging abilities: In order to use the nanoparticles as bio-imaging it was essential to monitor their toxicity to the cells thereby confirming their compatibility to the living cells. For this an MTT assay was used as a probe to monitor the ability of tetrazolium bromide 4,5 -dimethylthiazol-2,5-phenyltetrazolium bromide (MTT) which oxidises in the presence of living cells. MCF 7 cell lines and HeLa cell lines were chosen for this purpose. Here the experimental protocol for MCF 7 cells has been explained, and in HeLa cell same procedure was followed. 1000 cells in each were seeded in a 96 well plate and grown for 16 h. Various concentrations of P-TPE, P_{CUR}, P_{NR}, P-TPE_{CUR}, P-TPE_{NR}, and P-TPE_{CUR+NR} were used for independent experiments and were subjected to the cells. The cells were incubated for 72h in the presence of nanoparticles. The experiment was carried out in triplicates and the viable cells were grown with respect to a blank control of cells without any polymer. There after 100 μL of fresh stock solution of MTT (containing 5 mg/mL MTT in PBS diluted to 50 μg/mL in DMEM) was added to each plate prior to which the existing media was aspirated and cells were incubated for 4h at 37 °C.The DMEM was removed and 100 μL of DMSO was added to each plate, which dissolved the purple formazan crystals. The absorbance of the formazan crystals was measured at 570 nm after shaking the plates for 5 min using Varioskan FLASH instrument. The average of all the triplicate values was determined. The readings from the blank set of cells were treated as 100% and relative to it a plot of cell viability vs the concentration of the polymers were plotted. A similar experiment was carried out for CUR loaded nanoparticles at higher concentrations of CUR (ranging from 1.0 -25.0 μg) to study the potential of the FRET bio-imagers as potential cell killing agents.

Confocal assisted Bio-imaging: A 6 well plate with sterile cover slips were used to image MCF 7 cell lines and HeLa cells. The procedure has been explained for MCF 7 cells, and same protocol was followed for the HeLa cells. The plates were washed with PBS and media before seeding 10^5 cells in each well. The cells were cultured for 16h under CO_2 at 37°C and exposed to them to the P-0 and P-TPE loaded nanoparticles. The cells were exposed to P_{CUR}, P_{NR}, P_{CUR+NR}, *P-*TPE_{CUR}, *P-*TPE_{NR}, *P-*TPE_{CUR+NR} nanoparticles keeping the concentration of TPE as 10.0 μg/mL and corresponding amount of CUR and NR were maintained according to the DLCs

obtained for triple component FRET nanoparticles, and were incubated for 4h. The fixing of the cells were carried out using general protocol of washing the coverslips with cells grown on them twice with 1.0 mL PBS. Cells were further fixed using 4% PFA (1.0 mL) for 10 minutes at room temperature. Cells were stained using DAPI for 2 min in dark (For P_{NR}, P_{CUR}, P_{CUR+NR} samples only) followed by another washing with 1.0 mL PBS. (P-TPE nanoparticles loaded samples were treated with phalloidin for 20 min prior to fixing). The cover slips with processed cells were further mounted on sterile glass slides using 70% glycerol as mounting media. The coverslips were dried overnight in the dark. The cells were further imaged using Confocal microscope and CUR, and TPE were excited using 405 nm laser as source, NR was excited using 561 nm laser, and , phalloidin and DAPI were excited 488 and 405 nm lasers respectively. The DAPI and TPE were imaged in blue channels, CUR and phalloidin were imaged in green channel, and NR was imaged in red channel respectively. The FRET experiments were carried out by incubating the cells at different time intervals with the nanoparticles and the fluorophores were excited at the same wavelengths.

Lysosomal Tracking of Polymer Nanoparticle: A 4 well live cell chamber was employed to carry out live cell imaging experiments. The concentration of fluorophores was maintained at 2.0 μg/mL for each experiment. 25000 cells were seeded in each well of the chamber and incubated at 37°C for 16 h. P-TPE, *P-TPE*$_{NR}$ *and* P_{NR}nanoparticles were administered to the cells and allowed to expose for 9h prior to experiment (CUR samples were not chosen to avoid cross talk between lysotraker green and CUR signals). The plate stained using 50.0 Lyso trackers Green DND-26 and the well were immediately imaged using CSLM confocal microscope. Lyso tracker was excited using 488 nm laser source and imaged in green channel. All other fluorophores were excited using same laser as that for fixed cell imaging. The images were processed using Image J software.

FACS Analysis: Flow cytometry cell analyzer was employed to liberate the actual quantity of fluorophore taken up by the cells. Density of cells were taken as 10^5 in each well of a six-well plate and grown for 16 h and further subjected to same concentration for P_{CUR}, P_{NR} *and* P_{CUR+NR}nanoparticles as used for confocal imaging experiments. The cells were incubated for 4h with the nanoparticles, and the media was aspirated from each well and the cells were further washed with PBS and trypsinised and pelleted and redispersed in PBS and subjected to FACS analysis using BDLSRFortessa SORP cell analyzer with 5 lasers and 18 colour detectors. A population of 10000 cells were screened for emission histograms.

4.3 Results and Discussion

4.3.1 Synthesis of melt Polymerisable TPE Diol

The melt polymerisable TPE diol was designed as shown in scheme 4.1. Self coupling of 4-hydroxy benzophenone using McMurry coupling in presence of Zinc dust and titanium tetrachloride yielded tetraphenylethylene di-phenol compound (**1**). It was further coupled with chloroethoxyethanol in basic conditions to yield TPE diol (**2**).The proton NMR of TPE-diol is shown in figure 4.8a. and different protons of the molecule have been assigned to different peaks on the spectra with alphabets. The aromatic protons from the phenyl rings appeared together in the down field region above 6.5 ppm and the aliphatic protons appeared between 3.5 to 4.2 ppm.

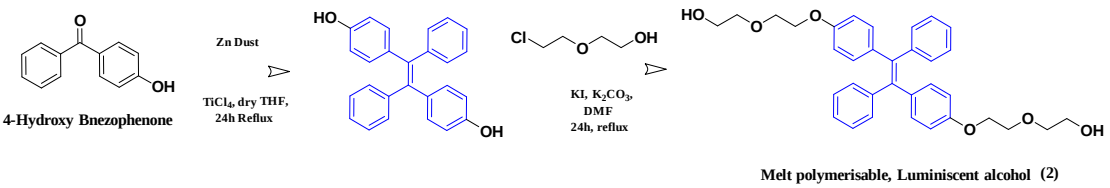

Scheme 4.1: *Synthesis of TPE-diol*

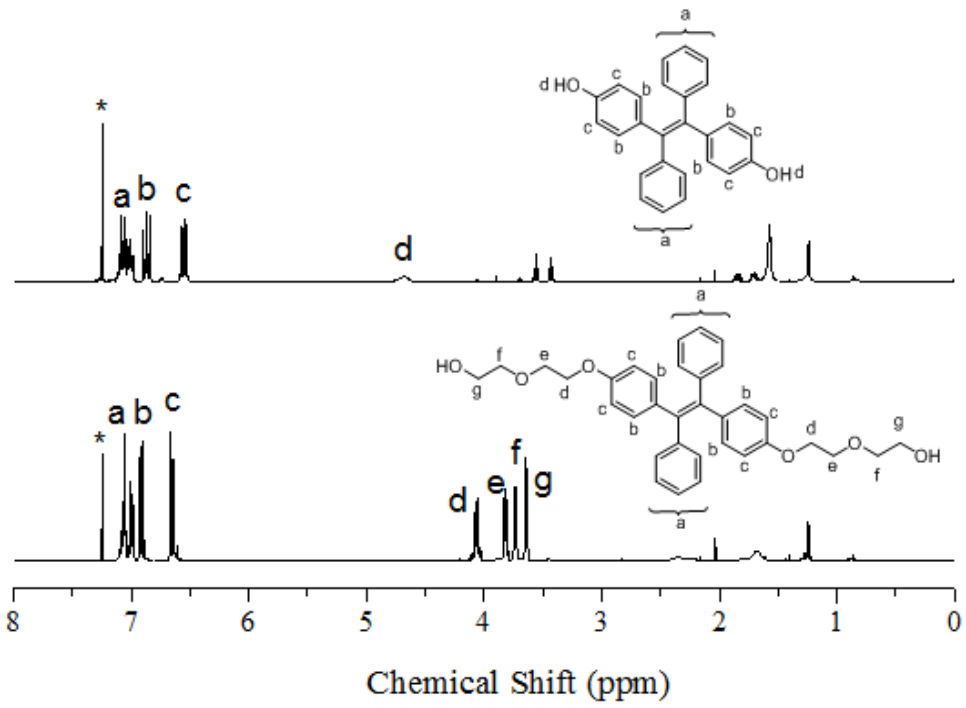

Figure 4.8: *^{1}H (a) and ^{13}C-NMR (b) of TPE-diol in $CDCl_3$*

4.3.2. Synthesis of TPE-tagged amphiphilic polyesters

The BOC protected L-aspartic diester monomer 1 (from chapter 2) was subjected to melt trans-esterification with TPE-diol, 1,12-dodecanediol (DD) and triethylene glycol (TEG)at 120 °C in the presence of $Ti(OBu)_4$ catalyst. The resultant amphiphilic fluorescent polymer has three components in the backbone: (i) TPE unit as AIE fluorophore, (ii) DD-containing segments as hydrophobic unit, and TEG-segments as hydrophilic unit. The structure of the polymer is shown in scheme 4.2 and each segment is shown by brackets. The hydrophilic content was retained as 40 %, and the TPE and DD amounts were varied as 5 % (or 10 %) and 57 % (or 50 %), respectively, in the backbone.

Scheme 4.9: *Synthesis of TPE-tagged L-aspartic acid based amphiphilic polyester through melt condensation polymerisation.*

The incorporation of the TPE in the polymer backbone was analyzed by ^{1}H-NMR and a representative spectrum of the polymer is shown in figure 4.10. The protons corresponding to the polymer have been marked in the polymer structure and on the NMR spectra. The aromatic peaks in the TPE chromophore were found to be intact at 7.08, 7.02, 6.93, and 6.67 ppm embedded in the backbone of the polymer chain. The-NH and the chiral -CH protons appeared at 5.5 and 4.57 ppm. The 4 new

TEG esters appeared at 4.33 and 4.26 ppm and that of DD new esters appeared at 4.15 and 4.07 ppm. The oligoethylene protons from the TEG counterpart of the polymer appeared at 3.77 – 3.64 ppm which masked the disappearance protons from the NMR. The aspartic acid –C**H**$_2$-CH protons appeared at 3.03- 2.84 ppm. The aliphatic protons appeared at 1.66 and 1.29 ppm and the BOC protons were retained at 1.45 ppm, confirming the formation of the amphiphilic luminescent polyesters. The ^{13}C NMR data (shown in the appendix) also confirmed the formation of polyester with each carbon peak intact. The feed of TEG diol was maintained as 50%, of DD diol was maintained at 45% and TPE diol was maintained at 5% with respect to the aspartic di ester monomer. The composition of the TPE-segments, DD-hydrophobic segment and TEG-hydrophilic segments were determined by comparing the integration of peaks at 4.32 ppm, 4.25 ppm and 4.12 ppm respectively. The % incorporation of TPE diol, TEG diol and DD diol were found to be 5.3, 37.6 and 57.0 % respectively.

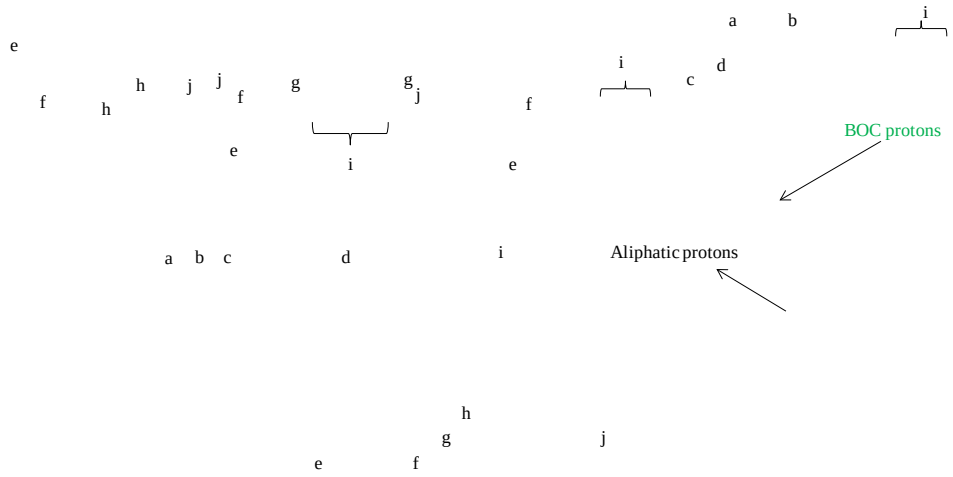

Figure 4.1: *^{1}H-NMR of TPE-tagged amphiphilic polyester P-TPE in $CDCl_3$.*

The molecular weights were determined by the GPC analysis (Figure 4.9a) The molecular weights of the polymers were found to be M_n = 4300 g/mol and M_w = 10,000 g/mol with polymer dispersity of M_w/M_n = 2.3. TGA showed (Figure 4.9b) that the polymers were found to be thermally stable up to 200°C, decomposed in two steps, first hump corresponding to loss of BOC unit followed by complete decomposition of polymer. . The polymers without TPE-content is further referred as P-0 and the TPE-containing polymer were referred as P-TPE-5 (having 5 %TPE units in the backbone).

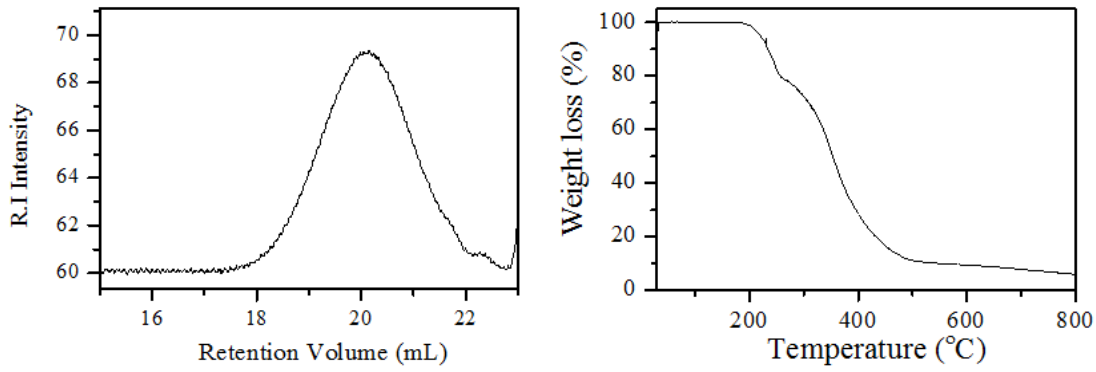

Figure 4.1: *GPC and TGA profile of P-TPE-5 polymer.*

4.3.3. Self Assembly of AIE Luminescent Polymer P-TPE

Polymer chains exhibit expanded conformations when they are dissolved in good solvents whereas in bad solvents they collapse into coil like structures thereby causing the polymers to form micron to nano-sized aggregates. In the present investigation, the conjugation of tetraphenylethene units in the polymer backbone provide unique opportunity to investigate the solution state dynamics of the L-amino acid polymers via aggregated induced emission characteristics. To study the self assembly of the polymers DMSO and water are chosen as good and bad solvents combinations. The polymer chains completely solvated in DMSO and adopt expanded chain at very dilute solutions (low concentration at optical density O.D. = 0.1). The collapsing of polymer chains in water brings the TPE chromophores in closer vicinity to produce AIE phenomena. As a result, the TPE chromophores showed are unique "turn-ON" fluorescence phenomena in aggregated state (in water) and became turn-

Off non-fluorescent state in DMSO. This AIE phenomenon exhibited by the TPE chromophore embedded in the backbone of the polymer chain gives direct evidence about the state of the polymer in DMSO and water like systems. By varying the composition of DMSO+water composition, one could readily tune the fluorescent On-Off characteristics of the polymer backbone. Interestingly, the TPE exhibits strong turn-On in the aqueous phase which is an added advantage for biological imaging applications. Figure 4.10a, shows the absorbance spectra of P-TPE (concentration= 2.0 μg/ mL, optical density of TPE = 0.1) in various compositions of water and DMSO.

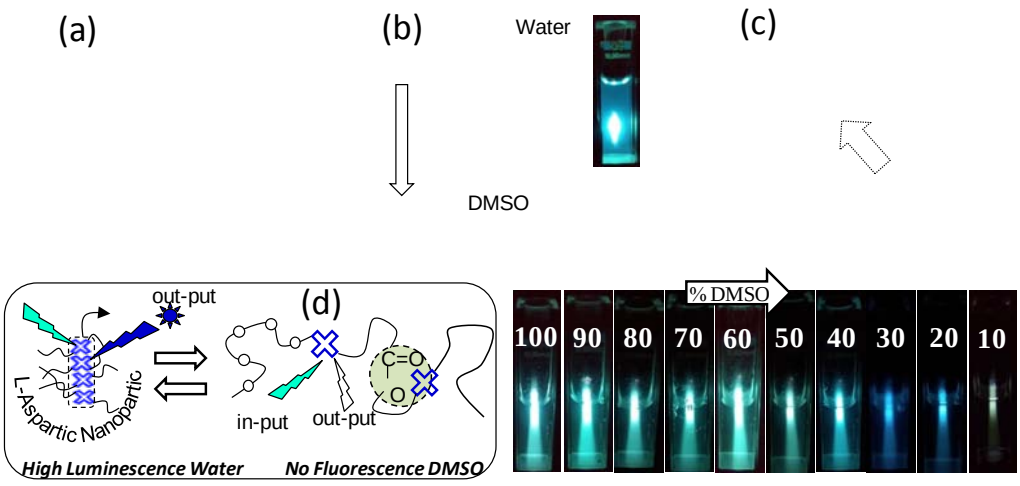

Figure 4.1: *The absorbance spectra of P-TPE in water-DMSO combination (ranging from 100% water to 10% water) (a), the fluorescence spectra of P-TPE in various water-DMSO combination excited at λ_{exc} 330 nm (b), the plot of λ_{em} max at 470 nm in fluorescence spectra of P-TPE vs the % of water in water DMSO combinations.(c), the schematic of expanded conformation of P-TPE amphiphilic polymer with ester backbones in good solvent DMSO, and spherical nanoparticles in water (d) along with the photographs of vials at various DMSO water concentrations excited atλ_{exc} 330 nm with slit width 2 nm.*

The spectra showed that the TPE chromophore absoption and the spectral features of TPE chromophore were retained almost identical in water and DMSO and at all compositions. The absorbance maxima corresponding to TPE chromophore was found at 310 nm. The fluorescence spectra for the P-TPE were generated by recording the fluorescence emission of P-TPE at various water DMSO compositions at excitation wavelength of 330 nm to generate spectra up to 650 nm for future studies.

The fluorescence emission of TPE showed difference in the spectral features when polymer transits from water to DMSO. The fluorescence emission shown in figure 4.10b showed emission for polymer in water with λ_{em} maxima at 470 nmwith intensity at 7×10^5which reflected on maximum aggregation state of TPE core that was direct evidence towards the aggregated state of the amphiphilic polyester in water. With increase in DMSO, on the other hand the polymer was expected to transit into expanded conformation thereby disassembling the stable nanoparticles and as a consequence rendering the TPE core isolated. The increase in DMSO content in the DMSO+water mixture caused a gradual decrease in intensity of TPE emission and eventually a 150 fold decrease in intensity was observed. This observation was due to the de-staking of the TPE chromophores and caused a drastic reduction in the aggregated induced fluorescence intensity of TPE. The transition of polymer from isolated to aggregated polymer structure was further plotted in the form of intensity of luminescence at λ_{em} 470 nm vs composition of water in DMSO+water mixture and it has been shown in figure4.10c. The plot shows a drop of PL intensity at 100% water to 10 % water composition. It should be noted that the break point at 40% water at which an immediate drop in the intensity was observed (shown in figure 4.10c) This is a direct evidence towards the transition of polymer from spherical nanoparticles in water to expanded conformation in good solvent as DMSO.The schematic of this transition from the coil like polymer state in water to trhe expenaded conformation in good solvent such as DMSO has been shown in figure 4.10 d, where in the TPE chromophores are forced to pack into the hydrophobic cavity of the nanoparticles of the coil like miscelle of teh polymer formed due to collapsing in water. During this phase upon exciting the aggregated TPE chromophores the emission energy is generated cause its characteristic emission. However in DMSO the polymer chains expand and the TPE chromophore move away from each other and without the aggregation these isolated chromophores are no longer emissive in nature. The naoaprticles were subjected to various environmental conditions that is from Water to DMSO enviromnment and the nanoparticles were excited at monochromatic wavelength in the fluorescence spectrophotometer at 330 nm and the emission of individual systems were capture and shown in figure 4.12 d. In water the maximum aggregation caused by the collapsing of the nanoparticles was observed as bright blue

light emission and the emission wore oof with increase in DMSO content hence proving the above mechanism.

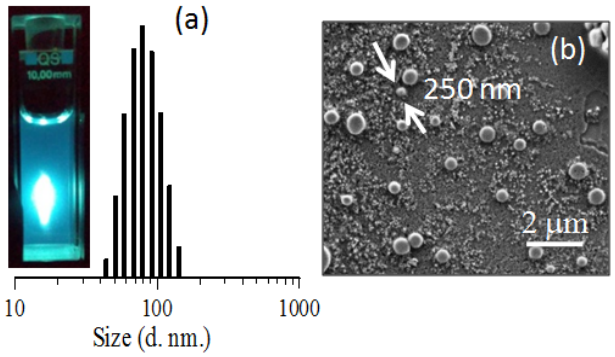

Figure 4.13: *The DLS histogram of P-TPE dispersed in water, schematic representation of P-TPE-5 nanoparticles and photograph of vial containing P-TPE nanoparticles excited at* λ_{ex} *330 nm (a), FESEM (b).*

P-TPE polymer were self-assembled in water by dialysing the polymer solution in DMSO+water (2:3 v/v mixture, 5.0 mg/mL) using semi-permeable membrane of molecular weight cut off 3000 Da. The dialysis was continued in distilled water followed by periodically replenished with fresh water for 48 h. At the end of the dialysis, the DMSO was completely removed the aquous polymer solution was found to be stable for more than a month. Figure 4.13a shows the DLS histogram of the dialyzed polymer solution and the histrogram was found to be mono-model distribution with respect to the formation of 120 nm nano-aggregates in the aqueous solution. Under the UV irradiation, the dialyzed solution exhibited bright cyan colored with respect to the AIE from the TPE core in the polymer nano-aggregates. The FESEM images of P-TPE aqueous aggregates showed the formation of spherical nanoparticles. From the above studies, it can be concluded that the custom designed TPE-tagged L-aspartic acid based amphiphilic polyester is capable of self-assembled into stable and blue-luminescent nanoparticle for diverse applications including bio-imaging in cancer therapy.

3.4. Encapsulation of Nile red and Curcumin Drug

The TPE-tagged L-aspartic acid amphiphilic polyester nano-assemblies was further explored fortheir capabilities of loading of water insoluble molecules. The loading of various dyes and drugs were tested for the polymer non-luminescent polymerP-0 (without TPE-tagging) and the blue luminescent P-TPE. CUR is excellent anticancer cum anti-inflammatory drug; however, the poor water solubility has been major obstacle for its delivery in biological systems. Polymer nano-carriers were reported to be excellent choice to encapsulate curcumin and deliver it to cancer cells and achieve antimicrobial activity. The loading of curcumin in the amphiphilic polymer nanoparticle was carried out using dialysis method as described earlier in DMSO+water mixture using semi-permeable membrane. The drug loading content (DLC) and drug loading efficiency (DLE) were determined as 7.6 % and 55 % using absorbance spectroscopy. Among the commercial fluorophore molecules, fluorescein (A widely used fluorescent molecular probe for bio-imaging) and Nile red (NR) were found to exhibit good DLC of 4.2 % and 7.6 % with DLE of 30% and 45 %, respectively. Various other fluorophores such as rose Bengal, rhodamine B and other drugs like doxorubicin showed relative less loading DLC (< 2.0 %); hence, they were not included for the present studies. The drug and fluorophore encapsulated polymer nanoparticles were subjectedto DLS, FESEM and AFM analysis and the data is shown in figure 4.12. In figure 4.12a, the curcumin drug encapsulated polymer nanoparticle (referred as P_{CUR}) showed the existence of 150 ±nm in the DLS histograms and its FESEM and AFM images confirmed their spherical shape with sizes in agreement with the DLS. In figure 4.14 (b), the NR loaded nanoparticles (referred as P_{NR}) showed nanoparticles of size 200±50 nm in DLS which matched very well with the FESEM and AFM images. These images show spherical nanoparticles of size less than 200 nm. To investigate the dual encapsulation capability of drug+fluorophore in the L-aspartic polymer nanoparticle, the combination of CUR and NR was chosen since their individual nanoparticles showed distinct greenish yellow and red emission (see vials in figure 4.14 (a,b)). The CUR and NR dual loaded polymer nanopartcicles (referred as P_{CUR+NR}) exhibited DLC of 4.8 % and 7.8 % (DLE = 40 % and 58 %) for CUR and NR, respectively. The size of the P_{CUR+NR} was found to be 130 nm (Figure 4.14c). The above encapsulation studies

revealed that the amphiphilic L-aspartic polyester is efficient nano-carrier for water insoluble natural drug such as curcumin, water insoluble fluorophores like Nile red, and also the dual loading led to enhanced uptake of the NR and CUR in a single nano-particle.Having successfully loading the CUR and NR in high quantities in the P-0 nanoparticles the encapsulation capabilities of P-TPE amphiphilic copolymers were evaluated for CUR and NR. Dialysis method was used for loading CUR and NR individually and in combination in the P-TPE copolymer and the results have been summarised in table 4.2.The DLC and DLE values in table 4.2indicate that the introduction of TPE chromophore in the backbone of P-0 did not affect the loading capabilities of the P-0 amphiphilic polyester and the loading of the hydrophobic dyes and drugs was enhanced in the P-TPE polymer.

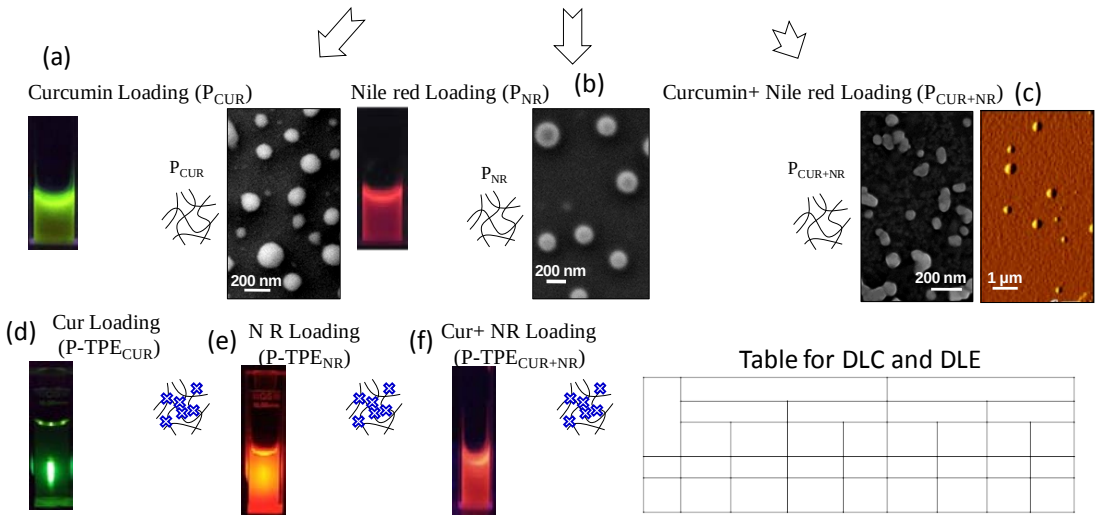

Figure 4.14: *The fluorescence emission photograph vial, the DLS histogram, schematic of dye/drug loaded nanoparticles, FESEM image, AFM image of P-0 loaded with CUR as P_{CUR} (a), P-0 loaded with NR as P_{NR} (b), P-0 dual loaded with CUR and NR as PCUR+NR (c),And P-TPE loaded with CUR as P-TPE_{CUR} (d), P-TPE loaded with NR as P-TPE_{NR} (e), P-TPE dual loaded with CUR and NR as P-TPE_{CUR+NR} (f).*

Polymer	Individual Loading				Dual Loading			
	Curcumin		Nile Red		Curcumin		Nile Red	
	DLC (%)	DLE (%)	DLC(%)	DLE (%)	DLC (%)	DLE (%)	DLC (%)	DLE (%)
P-0	**4.83**	**48.32**	**1.11**	**55.6**	**5.62**	**56.2**	**1.92**	**95.82**
P-TPE	**7.9**	**93**	**0.9**	**46**	**6.8**	**85**	**2.07**	**50**

Table 4.1: *Showing the DLC and DLE for DOX, CUR, TPT, NR loaded nanoparticles via dialysis method.*

4.3.5. Photophysical Properties and FRET probes

Förster Resonance Energy Transfer (FRET) is one of the most sensitive and non-invasive technique that has been used in cellular imaging in cancer therapy.In the present investigation multi-colour tuneable and four different types of FRET probes were constructed based on the amphiphilic polyester nanoparticle platform as followed: (i) blue-to-red FRET probe based on CUR encapsulated PTPE system in which the TPE chromophores in the polymer backbone as donor and the encapsulated CUR as acceptor (named as $F_{TPE\text{-}CUR}$), blue-to-red FRET probe based on NR encapsulated PTPE system in which the TPE chromophores in the polymer backbone as donor and the encapsulated NR as acceptor (named as $F_{TPE\text{-}NR}$), green-to-red FRET probe based on CUR plus NR encapsulated in the non-luminescent polymer system inwhich the CUR and NR chromophoresbehaved as donor and acceptor, respectively, (named as $F_{CUR\text{-}NR}$), and (iv) a triple cascade blue-to-green-to-red FRET based on CUR plus NR encapsulated PTPE system in which the TPE act as donor to CUR acceptor and CUR subsequently act as donor to NR acceptor (named as $F_{TPE\text{-}CUR\text{-}NR}$).

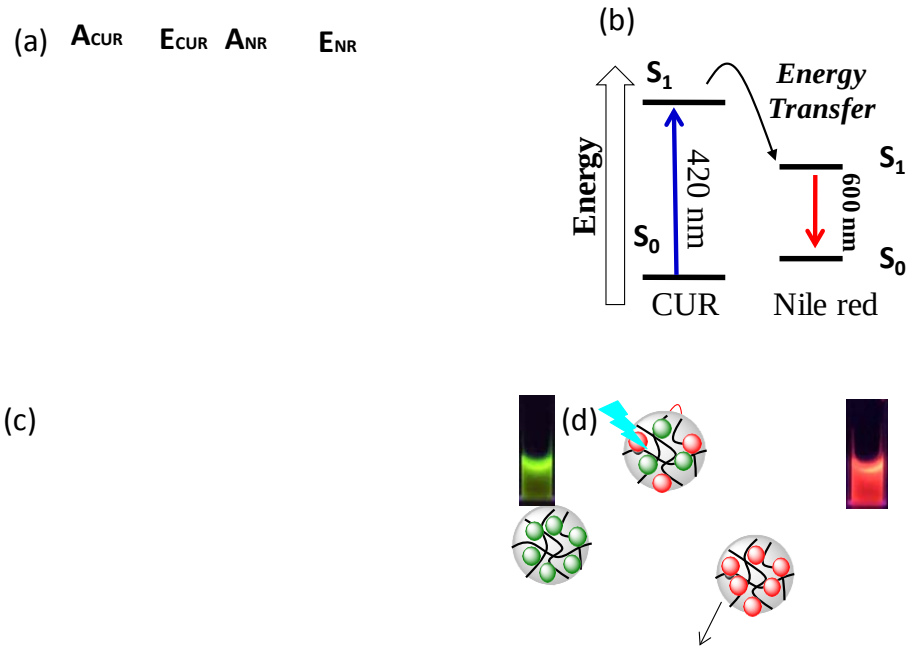

Figure 4.15: *The absorbance and emission of P_{CUR} and P_{NR} plot showing overlap of emission of P_{CUR} and absorbance of P_{NR} (a), the energy level diagram showing excitation of CUR chromophore at 420 nm from S_0 to S_1 and transfer of energy from S_1 of CUR to S_1 of NR and emission of NR at 600 nm (b), the absorbance spectra (c) and the fluorescence spectra (d) of P_{CUR}, P_{NR} and P_{CUR+NR}. The inset of absorbance and fluorescence spectra shows the emission of nanoparticles in cuvettes and the schematics of the loaded nanoparticles.*

The CUR and NR dual loaded in non-luminescent polymer nanoparticle ($F_{CUR\text{-}NR}$) and its individual loaded nanoparticles were subjected to absorbance and fluorescence studies and the spectra have been shown in figure 4.15.The probability of occurrence of FRET between CUR and NR was studied by comparing the absorbance and emission spectra of donor and acceptor nanoparticles respectively as shown in figure 4.15 a. The absorption of CUR in range of 400-600 nm and the emission upon excitation at λ_{exc} 420 nm generates emission spectra spanning from 450 nm to 600 nm. The absorption of NR chromophore on the other hand was observed between 500 nm – 600 nm showing a major overlap between the two spectra, indicating a high probability of FRET occurrence between the two. The phenomenon of FRET occurring between CUR donor and NR acceptor has been shown schematically in figure 4.15b. The CUR molecules at ground state are excited at λ_{max} and upon relaxation this excited state energy is transferred to the neighbouring

acceptor molecule NR via FRET and NR shows its characteristic emission at λ_{ems} = 600nm. The emission energy of excited CUR molecules is utilised for exciting the NR molecules because a reduction in the emission intensity of CUR self emission is observed simultaneously. This energy transfer has been shown schematically in figure 4.15b where in the donor CUR and acceptor NR are contained compactly inside a single self assembled nanoparticles providing optimum alignment and packing of donor and acceptor molecules for FRET to happen. The occurrence of FRET was further substantiated by studying free CUR and NR molecules dispersed in water. P_{CUR} shows absorption between 400 nm-500nm and P_{NR} shows absorption between 500nm -600 nm (Figure 4.15c). The dual loaded F_{CUR+NR} shows dual absorption characteristics of both CUR and NR giving rise to two peaks ranging from 400 – 500 nm and 500 – 600 nm of co-loaded CUR and NR in same nano-confinement. Figure 4.13d demonstrates the occurrence of FRET phenomenon where in the P_{CUR} nanoparticles are excited at λ_{exc} 420 nm (λ_{max} of CUR was 420 nm), and emission from NR is observed at λ_{em} 600 nm. The individually loaded P_{NR} were also excited at same wavelength and only a residual emission from the nanoparticles was observed. This shows that in the dual loaded nanoparticles upon exciting at 420 nm shows intense emission peaks of NR originating from energy transfer from excited CUR to NR species confirming FRET.

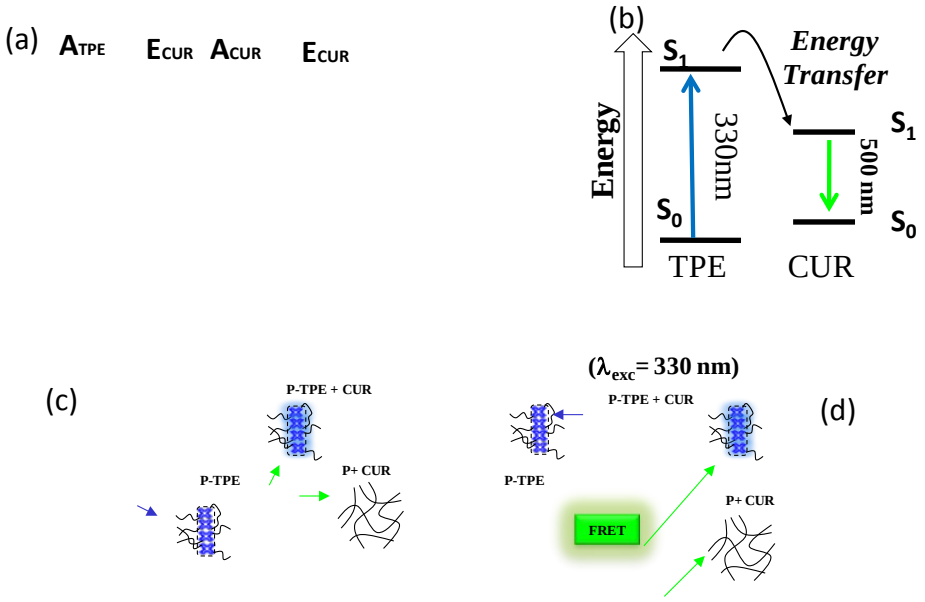

Figure 4.16: *The absorbance and emission of P-TPE and P_{CUR}plot showing overlap of and absorbance of TPE and CUR respectively(a), the energy level diagram showing FRET between TPE and CUR molecules (b) and the absorbance spectra of P_{CUR}, P_{NR} and* $F_{TPE\text{-}CUR}$*(c), and the fluorescence spectra of P_{CUR}, P_{NR} and* $F_{TPE\text{-}CUR}$*(d).*

The occurrence of FRET between the luminescent P-TPE nanoparticles with encapsulated CUR hydrophobic drug was investigated in Figure 4.14.These nanoparticles were subjected to absorbance and fluorescence studies like P_{CUR+NR} nanoparticles discussed in previous section. These spectra have been shown in figure 4.16 a and it was observed that TPE chromophore absorbed light in range of 300-400 nm with λ_{abs} maxima at 320 nm and the excitation of these nanoparticles gave emission band in range of 400- 600 nm which λ_{em} maxima at 470 nm. The absorbance spectra of P_{CUR} showed λ_{abs} maxima at 440 nm and upon excitation at 440 nm, the emission of CUR was obtained with λ_{em} maxima at 500 nm. The figure 4.16a shows 70% overlap between the emission of TPE and absorbance of CUR and this formed one of the essential criteria for FRET to occur between TPE as donor and CUR as acceptor. The energy level diagrams of TPE and CUR as donor acceptor pairs have been shown in figure 4.16b where in the energy difference between S_0 state of TPE to S_1 state is 330 nm and upon excitation the TPE in their excited state transfer the energy to S_1 state of CUR molecule thereby exciting the ground state CUR molecules to their S_1 state and upon relaxation the FRET energy transfer yields emission of

acceptor molecule instead of donor molecule. To further see the energy transfer P-TPE, P_{CUR} and $F_{TPE\text{-}CUR}$ nanoparticles were subjected to photo physicalanalysis. The O.D of dual chromophore containing $F_{TPE\text{-}CUR}$nanoparticles were maintained keeping TPE absorbance at 0.1 O.D. and correspondingly the CUR O.D. was measured as 0.25 O.D and for the subsequent analysis these O.Ds were maintained as it is (see figure 4.16c). P-TPE and $F_{TPE\text{-}CUR}$nanoparticles were excited at 330 nm to see the fate of energy emitted by TPE chromophores. P_{CUR} nanoparticles were also excited at 330 nm to rule out the possible emission of CUR chromophore at TPE excitation. The figure 4.16d shows the fluorescence spectraof the three nanoparticles and it was observed that the TPE chromophore showed emission at 470 nm maxima and P_{CUR} showed only residual emission at the same excitation wavelength. The dual chromophorecontaining$F_{TPE\text{-}CUR}$nanoparticles on the other hand showed reduction in emission intensity of TPE chromophore and a emission spectra was observed at λ_{em} maxima at 500 nm corresponding to CUR chromophore and this was the direct evidence of FRET between TPE and CUR fluorophores.

The FRET phenomenon was studied for $F_{TPE\text{-}NR}$ in Figure 4.17. These nanoparticles were further subjected to absorbance and fluorescence studies. These spectra have been shown in figure 4.17a and similar absorbance and emission spectra were formed for the P-TPE polymers with λ_{em} maximaat 470 nm. This emission showed a convincing overlap with the absorbance of NR chromophores with lay in region of around 70 % overlap. he absorbance spectra of P_{NR} as shown before had λ_{abs} maxima at 540 nm and the emission generated from TPE chromophore was sufficient for exciting the ground state species of the NR which showed emission in region of 500- 700 nm with $_{em}$ maxima at 600 nm.The energy level diagrams of TPE and NR FRET pair have been shown in figure 4.17b.The energy gap between S_0 and S_1 state was 330 nm and the energy gap between the S_0 and S_1 of NR has been shown in the diagram and the energy transfer from the S_1 excited state of TPE causes excitation on NR acceptor molecule with emission at 600 nm.

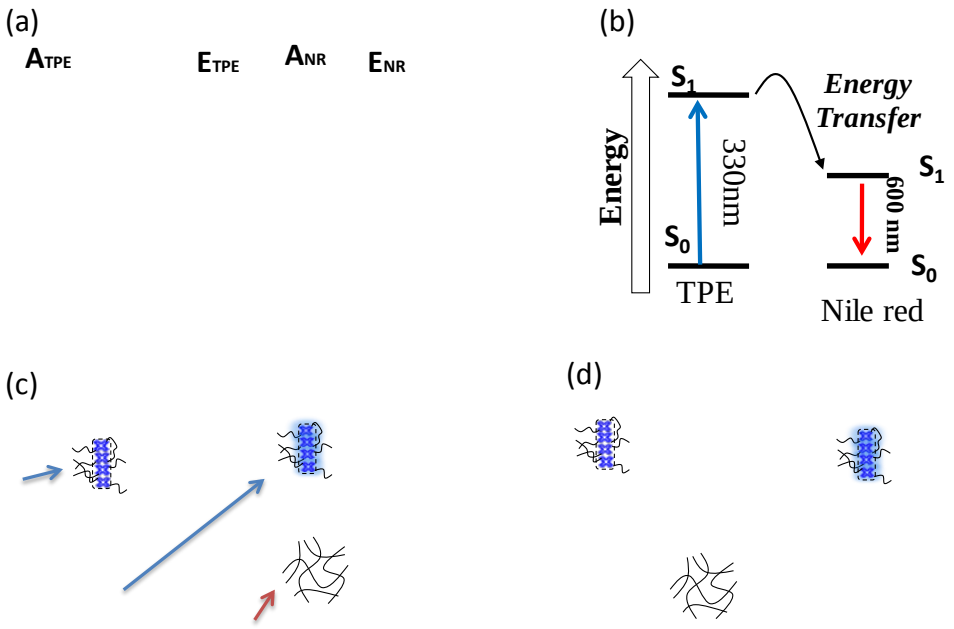

Figure 4.17: *The absorbance and emission of P-TPE and P_{NR}plot showing overlap of and absorbance of TPE and NR respectively(a), the energy level diagram showing FRET between TPE and NR molecules (b) and the absorbance spectra of P-TPE, P_{NR} and P-TPE_{NR}(c), and the fluorescence spectra of P-TPE, P_{NR} and P-TPE_{NR} (d)*

The subsequent energy transfer from P-TPE to NR chromophore was validated by exposing the P-TPE, P_{NR} and $F_{TPE\text{-}CUR}$nanoparticles to absorbance and fluorescence studies the spectra are shown in figure 4.17 (c,d). The dual chromophore composite P-TPE_{NR} nanoparticles showed characteristic absorption of both TPE and NR matching with the individual chromophores showing the intact nature of the chromophores inside the nanoparticles. The concentrations of the donor TPE and acceptor NR were maintained constant in individual nanoparticles P-TPE and P_{NR} as that of dual component $F_{TPE\text{-}CUR}$nanoparticles. The FRET studies were carried out by exciting the three nanoparticles at excitation wavelength of donor TPE molecule at 330 nm. P-TPE showed huge emission at 470 nm and the PNR showed residual emission at this excitation, however the dual chromophore composite $F_{TPE\text{-}CUR}$showed reduction in donor emission and FRET emission from NR residues at λ_{em} maxima at 600 nm which confirmed FRET between the two species.

4.3.7. Solvent Influence on AIE-assisted FRET Phenomena

The FRET stability of F_{TPE-NR} nanoparticles were studied as a reflection of transformation of aggregates in water and DMSO solvents. As mentioned earlier the solvents such as water aid the formation of stable nanoparticles which are ideal for loading hydrophobic dye NR. However in organic solvents such as DMSO these polymers undergo disassembly where in the loaded cargo move out of the hydrophobic core into the solution. The FRET formed between the polymer chains and the loaded acceptor molecule can be altered as the distance between the two increases upon disassembly of the polymer. The change in the FRET forms a direct correlation with the change in the nano-aggregates of the amphiphilic polymer.

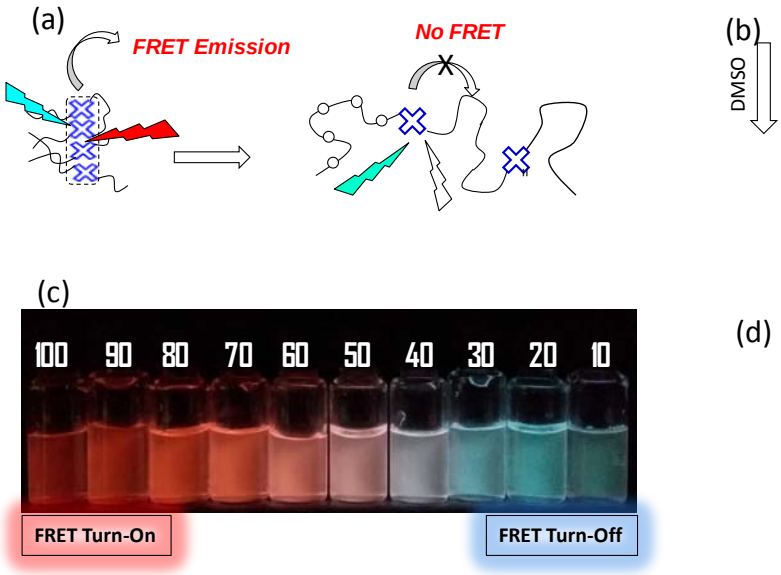

Figure 4.18: *The schematic presentation NR loaded P-TPE nanopartcile in water showing FRET emission from NR and disappearance of FRET emission and appearance of self emission of TPE upon disassembly of nanoparticles in organic solvent DMSO breaking the polymer assembly (a). P.L. Intensity of P-TPE$_{NR}$ nanoparticles which change in DMSO water environment (b), colour transition of P-TPE$_{NR}$ nanoparticles from red to blue with change in water content ranging from 100 to 10 (c), plot of fluorescence intensity at λnm at 470 and 600 nm against water composition (d).*

This change in the FRET emission of TPE and NR pair has been shown in figure 4.18. Figure 4.18a represents a schematic frame of tightly packed P-TPE nanoparticles loaded with NRstabilised in water. The compactness of these nanoparticles is shown by the FRET emission from the NR residues upon excitation of donor TPE molecules. In DMSO this self assembly is disrupted and NR moves out

of the vicinity of the donor TPE component and FRET disappears. This causes the self emission of TPE as no more FRET occurs. This trend in emission was monitored using fluorescence spectroscopy wherein the F_{TPE-NR} nanoparticles were subjected to various DMSO water compositions and were excited at λ_{exc}=330 nm. The representative fluorescence spectra have been shown in figure 4.18 b. At 100 % water content the emission of TPE was found to be 1×10^5 at λ_{ems} at 470 nm and NR showed emission at λ_{ems} as 600 nm of intensity 5×10^5. However upon decreasing the content of water to 10a% the emission of TPE chromophore increased to $1.4 \times10^5$and that of NR decreased to 4.4×10^5. A systematic increase in the intensity of TPE chromophore was observed with further increasing the DMSO content concomitant with decrease in emission intensity of NR. This was the direct evidence towards the gradual disassembly transition experienced by the nanoparticles wherein the NR acceptor molecules gradually moved away from the donor molecule causing disruption in FRET. At maximum disassembled state at 40 % water and 60% DMSO composition the emission from NR acceptor completely vanished and maximum emission from TPE donor molecules was observed. At this point the dissembled state essentially maintained NR away from vicinity of donor molecule which showed minimal FRET. However beyond 40% water, the DMSO content became too high that the polymer entered completely expanded conformation state where in it also disturbed the aggregation between the TPE molecules and further the emission of TPE aggregated species also decreased gradually with DMSO content. This observation can be correlated with figure 4.18 where in the disassembly of the polymer showed a break point at which the self assembly completely broke into expanded form. The transition from FRET emission of NR to self emission of TPE donor molecule drew a parallel connection with the morphology transformation from the nanoparticles in water to expanded conformation in DMSO and therefore it formed a sensitive tool to visualize the transformation in the polymer architectures. This transition was visualised in the nanoparticles when these were irradiated under UV light and one can see the colour transformation from red to blue as the polymer transits from compact coil like structure to expanded structure in organic solvents. The emission intensities of TPE donor chromophore and acceptor NR chromophores were further plotted against the water composition in the system and it was observed that the emission intensity of

TPE and NR followed opposite trend with NR showing highest emission at 100% water content and this emission gradually decreased to minimal emission with increase in DMSO content. The TPE on the other hand initially showed increment the emission as the FRET energy was available for self emission upto 40% water content which further decreased upon increasing the DMSO content as the TPE aggregated molecules transited to isolated species.

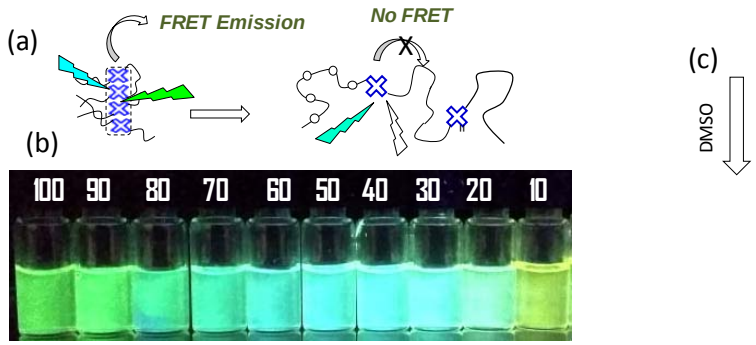

Figure 4.19: *The schematic presentation P-TPECUR nanoparticles exhibiting FRET emission from CUR residue upon exciting TPE chromophores in water anddisassembly of nanoparticles in DMSO and self emission in absence of FRET. (a). colour transition from green to blue to no emission of P-TPE$_{CUR}$ nanoparticles with change in water composition from 100 to 10 (b), P.L. Intensity of P-TPE$_{CUR}$ nanoparticles which change in DMSO water environment (c).*

The solvent influence on the FRET features $F_{TPE\text{-}CUR}$ has been shown schematically in figure 4.19. Upon subjecting these nanoparticles to DMSO they experience disassembly and cause FRET disappearance and self emission of TPE chromophore is observed. The sensitivity of FRET emission towards the dynamic purlieu with respect to to solvent was studied similar to that of $P_{TPE\text{-}NR}$ nanoparticles explained previously. It was observed that at 100 % water a complete energy transfer occurred from TPE donor molecules to the CUR acceptor molecules and and emission from CUR was observed at λ_{ems} maxima of 500 nm corresponding to CUR. No emission was observed from TPE indicating a closer packing between TPE and CUR compared to TPE and NR (see figure 4.19a). This was crucial information gained from FRET between TPE and CUR, because as the DMSO content was increased in the system there wasn't much change observed in emission of CUR up till 70 water 30 DMSO compositions. However at 60 water and 40 DMSO compositions the

emission at λ_{ems} maxima of 500 nm completely disappeared and a new blue shifted emission peak was observed with λ_{ems} maxima of 480 nm which corresponded to TPE emission (see figureλ_{ems} maxima at 470 nm). The 10 nm red shift however could possibly due to molecular interactions between TPE and CUR even after FRET was turned off. However unlike TPE-NR FRET pair a cross over point in the P-TPE_{NR} nanoparticles was not observed in this case and complete energy transfer was observed from TPE to CUR and complete retaining of the emission energy was observed by TPE donor molecule.The absence of the crossover between emission of TPE and CUR across water DMSO change showed the presence different environments within the hydrophobic core of nanoparticles where both NR and CUR were packed within the nano-assemblies. 20 and 10 % water content showed loss of TPE emission due to complete disassembly of the polymer scaffold into expanded conformation rendering the TPE molecules in isolated form. The L-aspartic acid amphiphiliccopolymers proved to be highly interesting architectures for holding unique colortunable FRET pairs and were observed to form two highly efficient FRET phenomena.

4.3.8. Enzyme-responsive FRET probe

The amphiphilic polyesters were found to cleave under the presence of various hydrolytic enzymes such as esterase, glutathione, papain, trypsin and chymotrypsin under physiological conditions from our previous studies (ref). Out of these esterase was found to be most efficient in cleaving the polymer backbone and releasing the loaded cargoes. Therefore, the F_{CUR+NR} nanoparticles with in-built ester backbone was subject to similar conditions and exposed to esterase enzyme at pH 7.4 in PBS. FRET between CUR and NR was chosen as an ideal probe to understand the biodegradable nature of the nanoparticles. As these nanoparticles are capable of confining donor CUR and acceptor NR in precise distance and orientations to create the efficient FRET phenomenon, hence any change in the FRET emission of transfer to acceptor or donor molecule would directly reflect on the stability of the nanoparticles under the above mentioned lysosomal conditions. The affect of esterase enzyme on the esters backbone of amphiphilic nascent polyester could be visualised as dis-assembly of the stable nano-micelles due to chopping off the polymer chains to smaller chains. This

would as a result change the distance and orientation of donor and acceptor molecules within the nanoparticles confinement thereby altering the signals arising due to energy transfer which would be disturbed. In a in vitro experiment the dual loaded P_{CUR+NR} nanoparticles were incubated in PBS with pH = 7.4 at 37°C for 24 h to mimic physiological conditions, and their emission spectra were generated at various time intervals and have been plotted in figure 4.20 the emission from the NR molecules were found to be intact with the passage of time which reflected on the high stability of the F_{CUR+NR} nanoparticles in the physiological conditions as shown in figure 4.20. On the other hand interestingly , when the P_{CUR+NR} nanoparticles were incubated in presence of esterase enzyme at similar conditions, a gradual decrease in emission of NR (originating from FRET) was observed and it reduced to 1000 folds in 2 h

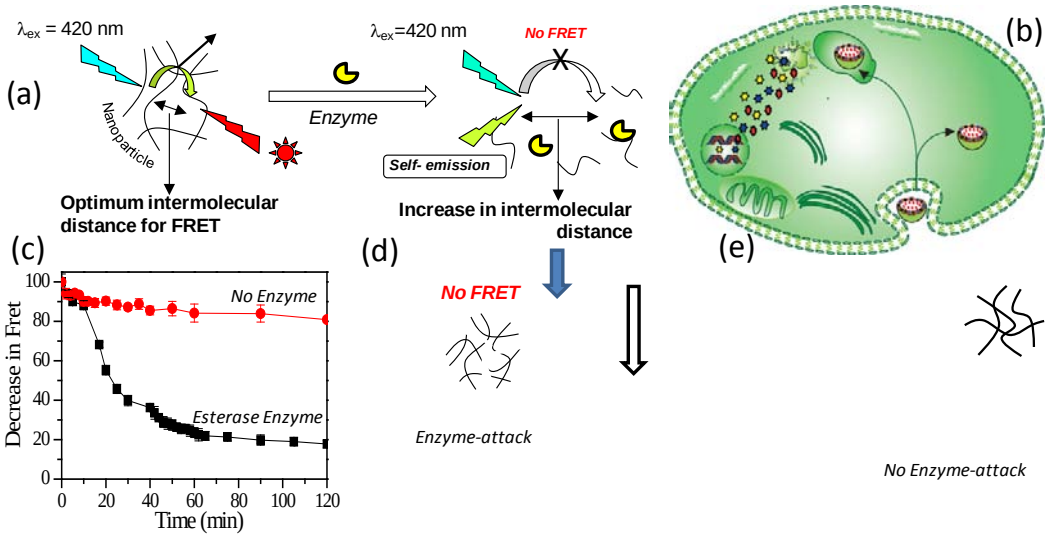

confirming the disruption of P_{CUR+NR} nanoparticles and affecting the FRET intensity.

Figure 4.20: *Schematic representation of cleavage mechanism of esterase enzyme on* P_{CUR+NR} nanoparticles (a), *cell diagram of energy level diagram of donor absorbance and acceptor emission(b), energy overlap between CUR emission spectra and NR absorbance (c), absorption spectra of* P_{CUR} *(black line),* P_{NR} *(red line) and* F_{CUR+NR} *(blue line (d)), emission spectra of* P_{CUR} *(green line),* P_{NR} *(red dotted line) and* F_{CUR+NR} *(red solid line) upon excitation at* λ_{exc} *420 nm (e).*

The schematic representation of the nanoparticles being disrupted by the esterase enzyme has been shown in figureinset. The changes in the FRET emission from donor to acceptor in absence and presence of the esterase enzyme with time have been plotted and shown in figure 4.20.The FRET emission was found to reduce upto

80 % in 2h maintaining the FRET emission, however the same nanoparticles under the presence of esterase enzyme lost their FRET emission upto 20% within 2h. These studies concluded that the P-0 amphiphilic nanoparticles were highly stable in physiological conditions and are capable of retaining their loaded cargoes intact with time. However the same nanoparticles can readily respond to the presence of esterase enzyme rich environment of lysosomes of cells thereby releasing the loaded cargoes. Therefore P-0 nanoparticles were found to biodegrade in presence of a naturally occurring enzyme and it demonstrated excellent capability to load and deliver loaded cargoes at intracellular regions, and could be employed for bio-applications such as cellular imaging.

4.3.10. Cellular uptake and Confocal Imaging

The custom designed P-TPE polymer was initially tested for cellular uptake in cancer cell lines.Hela and MCF 7 cancer cell lines were chosen and incubated with nascent P-TPE nanoparticles and fixed and excited and imaged with 405 nm laser and in cyan channel respectively. Bright cyan emission was observed from the cytoplasm of the cells irrespective of the kind. The merged image shown in figure 4.21 (e,f) showed the overlap of the TPE signal from the cells and these findings proved the capabilities of these amphiphilic nanoparticles as bright luminescent bio-agents for cellular imaging applications.

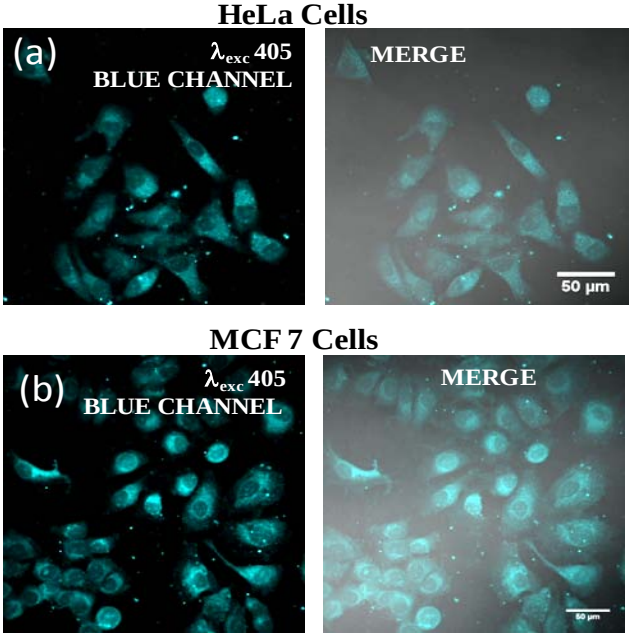

Figure 4.21: *Confocal images of P-TPE in blue channel upon excitation with 405 nm laser in HeLa cells (e) and in MCF 7 cells (f).*

4.3.11. FRET Probe nanoparticles in Bio-imaging

The P_{CUR+NR}, P_{CUR}, P_{NR} nanoparticles were chosen to study their potentials as bio-imaging agents. To avoid crosstalk with TPE chromophores the CUR was carefully excited at 488 nm and NR was excited at 541 nm laser and imaged in green and red channels respectively. The figure 4.22 shows the confocal images of the three nanaoprticles in MCF 7 cells. P_{NR} nanoparticles imaged at 488 nm showed no emission (see second panel in figure 4.22 (a)) and bright emission covering the cytoplasm of the cells was observed. The green channel and red channel panels were merged and shown in fourth panel in each column.

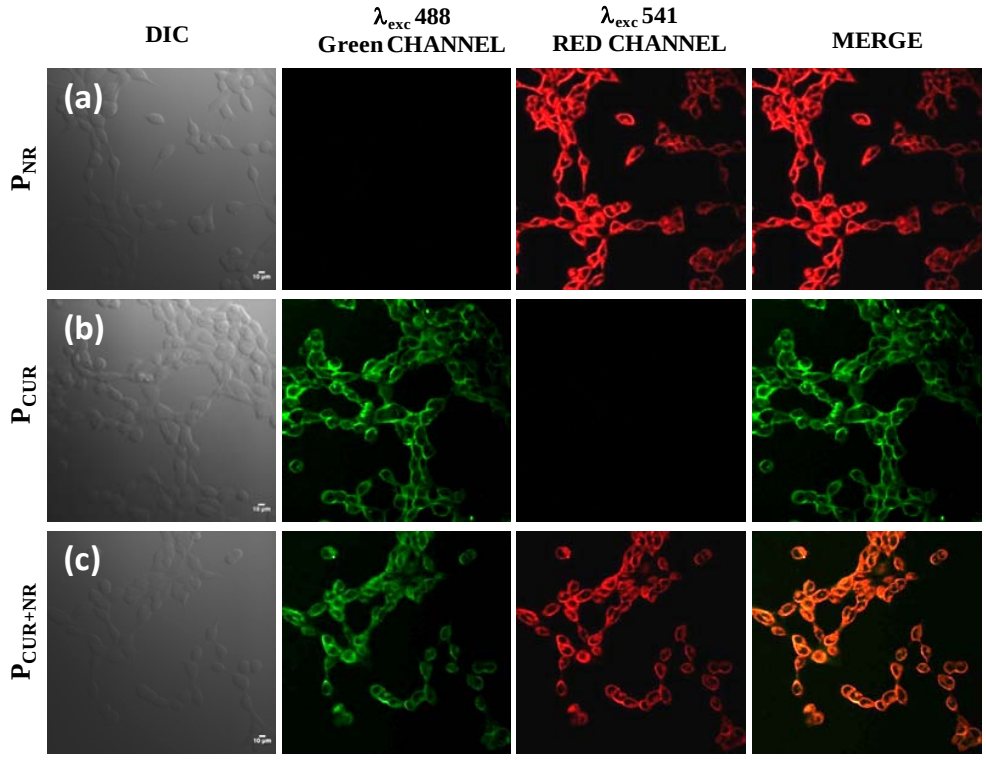

Figure 4.22: *Confocal image of P_{NR} nanoparticles imaged at laser 541 nm (a), P_{CUR} nanoparticles imaged at 488 nm (b), P_{CUR+NR} nanoparticles imaged at 488 nm and 541 nm (c) in MCF 7 cells. (Scale Bar in DIC imaged = 10 μm).*

The fixed MCF 7 cells incubated with P_{CUR} nanoparticles were further imaged at both 488 nm and 541 nm. Bright green emission from the cytoplasm of the cells was observed and the red channel showed no signal from the cells. The dual loaded

nanoparticles upon divulging to the cells showed signals in both the green and the red channel due to individual emission of the CUR and NR species present at the cytoplasm of the cells. The merged image (see figure 4.22 (c) fourth panel) on the other hand elucidated the co-presence of the CUR and NR species in the cytoplasm of the cell and it encouraged to carry out the FRET experiments to seek the potential and demonstrate the stability of the amphiphilic nanoparticles at intracellular levels to

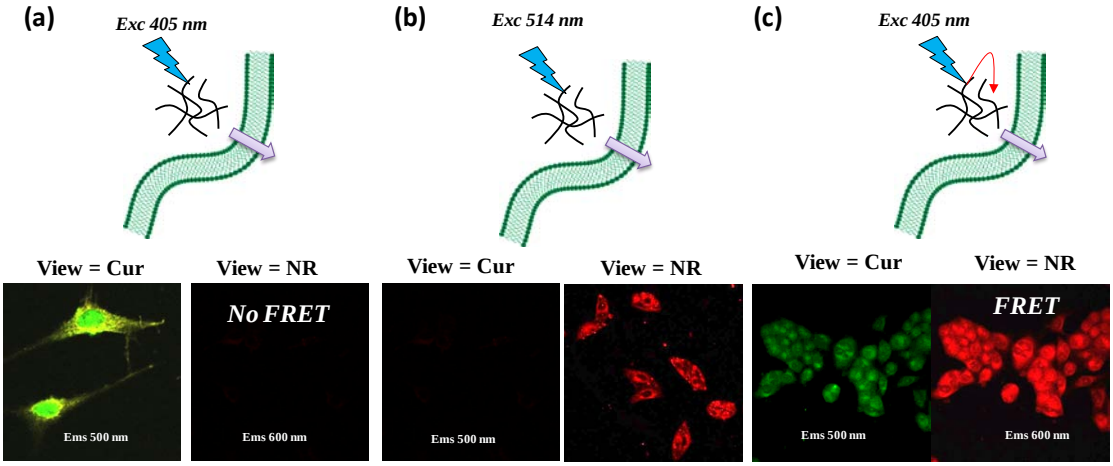

transport the physically loaded FRET pair across the cell membranes into the intracellular regions.

Figure 4.23: *Confocal image of P_{CUR} nanoparticles imaged at laser 405 nm (a), P_{NR}nanoparticles imaged at 541 nm (b), P_{CUR+NR} nanoparticles imaged at405 nm (c) in MCF 7 cells.*

Further the MCF 7 cells were incubated with excited at 488 nm and imaged at both green and red channels and bright green emission due to CUR residues were observed from within the cytoplasm regions with no red signals in the red channel (see figure 4.23 (a)). The P_{CUR} loaded cells were labelled with phalloidin and was imaged in yellow channel to determine the presence of CUR in the cytoplasm of the cells. No emission in the red channel was observed due to absence of NR species in the nanoparticles. The P_{NR} incorporated cells were excited using both the lasers 488 and 541 nm and emission only from the red channel was observed as shown in figure 4.23 (b). This experiment enabled the absence of cross talk between the two fluorophores which made it possible to study FRET at cellular levels. The P_{CUR+NR} interestingly showed emission in both the green and the red channel which

demonstrated FRET at intracellular level. Comparing the red channel to figure 4.23 (a), it was inferred that emission in the red channel form the cytoplasm was indeed due FRET from the CUR donor to the NR acceptor moieties. The merged imaged shown in the fourth panel showed the coexistence of the donor CUR and acceptor NR within the cellular regions, which further corroborated the findings. The merged images along with the FRET emission from the NR species distinctly evinced the ability of the L-aspartic acid based amphiphilic copolymers to adequately transport the loaded hydrophobic cargoes into the cellular regions of the cancer cells which demonstrated their abilities as bio-imaging and cargo-carriers in the intracellular regions. The role of esterase enzyme on the ester rich backbone of the amphiphilic polyester were further studied using time dependent FRET as real time imaging in MCF 7 cells. The alterations in FRET intensity from NR was studies as a function of esterase enzymes cleaving the ester backbone of the amphiphilic polyester. The MCF 7 cells were incubated with PCUR+NR nanoparticles keeping concentration of CUR as 2.0 μg and the resultant cells were excited using 488 nm lasers. The self emission of CUR was imaged at blue channel, and FRET emission from NR was imaged in the red channel at various time intervals upto 9 h. The figure 4.24 (b) shows the self and

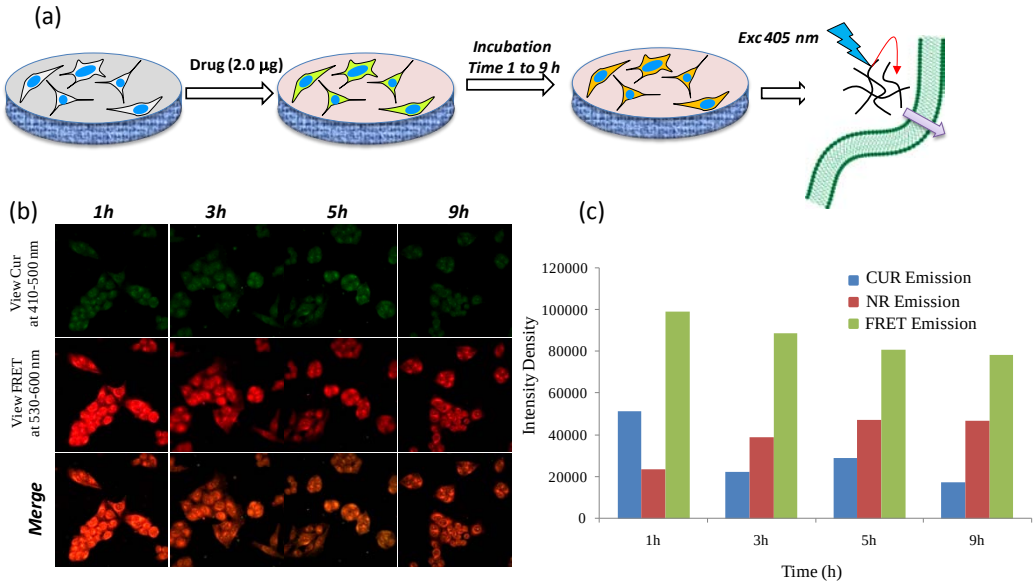

FRET emission of the nanoparticles from the MCF 7 cells at time intervals 1, 3, 5, and at 9 h.

Figure 4.24: *The schematic representation of cell grown in petridish for cellular uptake of nanoparticles (a), the Confocal imaging of the P-CUR+NR nanoparticles at various time*

intervals (b), the plot of intensity of confocal emission of CUR, NR and FRET emission with time (c).

The schematic representation in figure 4.24 (a) shows the MCF 7 cells incubated with drug/dye at concentration of 2.0 μg and incubation of cells upto 9 h and subsequent uptake of nanoparticles into the cells via endocytosis. The figure 4.24 (c) shows the low self emission of CUR species high FRET emission from the NR species. The self emission and FRET emission were monitored at higher time intervals and were quantified by plot shown in figure 4.24(c). The self emission of CUR donor species reduced with time from 50000 upto 20000 from 1 h to 9 h showing the release of CUR from the cavity of micelles of the nanoparticles due to disruption in the ester backbone of the polymer. The FRET emission was affected as well due to release of the donor. The real time FRET experiment revealed the affect of esterase cleavage on the backbone of amphiphilic polyesters disrupting the stable nanoparticles and causing the FRET pair to move apart from the hydrophobic cavities. Over a period of time the decrease in self emission and FRET emission from the nanoparticles shows the affect of lysosomal enzymes on the nanoparticles. Similarly, the FRET studies were extended to P-TPE loaded NR nanoparticles in MCF 7 cells were show in the figure 4.25.

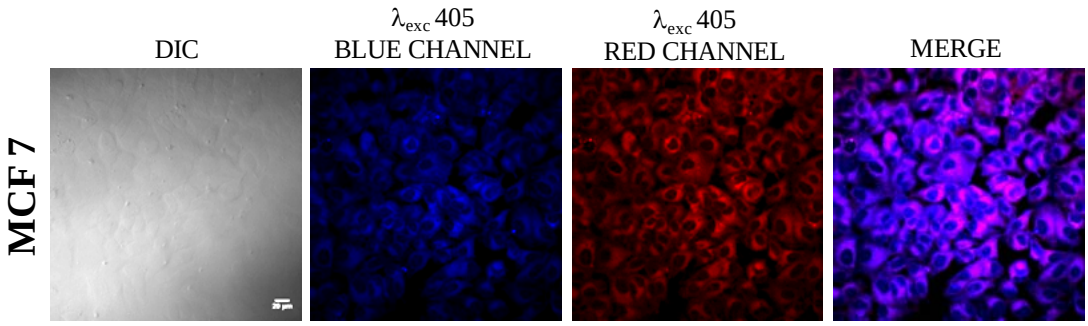

Figure 4.25: *TPE and NR imaged in blue and red channel in MCF 7 cells.*

4.3.12. Triple component Blue-Green-Red cascade FRET

The schematic of dual loaded P-TPE nanoparticles stabilising CUR and NR fluorophores have been shown in figure 4.26 (a). The nanoparticles shows the aggregated species of TPE generating emission energy upon excitation at 330 nm and

this emission energy was transferred to nearby CUR species which in turn emitted energy for exciting another nearby hydrophobic NR molecule. This resulted in red emission from the dual loaded P-TPE_{CUR+NR} nanoparticles. The FRET between these triple components however was found to disrupt under the influence of DMSO causing polymer chain expansion as shown in figure 4.26. The figure 4.26 (b) further shows the possible energy transfer from the S_1 of TPE exciting the CUR ground state species which in turn excited the ground state NR species. This FRET energy emission could be tune by changing the water DMSO composition for the system and the photographs of the vials showing a whole range of emission colours have been shown in figure 4.26 (c). The nanoparticles dispersed in 100 % water showed red emission and the colour intensity reduced as the DMSO content in system increased to pale red up to 60% water and at 50 % water a complete disappearance of red colour was observed concomitant with appearance of white emission. It was believed the residual emission of NR, CUR and self emission of TPE merged to give the white emission. On further increasing the DMSO content the NR residues moved completely away from the donors (TPE and CUR) and further blue emission also disappeared with increasing DMSO content. THE multi FRET “turn on” and “turn off” probe were further studied by exciting the P-TPE_{CUR+NR} nanoparticles at three wavelengths λ_{exc} 330 nm, 440 nm, and 540 nm to understand the fate of individual chromophores and the FRET change with respect to solvent environment (water composition varying from 100 to 10 %).

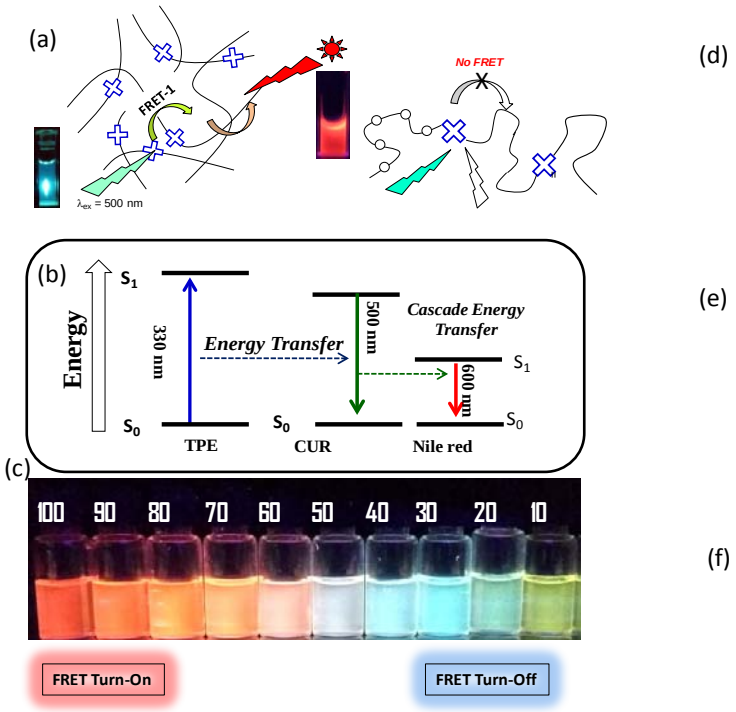

Figure 4.26: *The schematic presentation P-TPE$_{CUR+NR}$ dual loaded nanoparticles exhibiting FRET between TPE and CUR as first FRET pair and TPE and NR as second FRET pair, and disappearance of FRET emission in DMSO from expanded polymers(a), energy level diagram for energy transfer from one donor to two acceptors (CUR and NR) (b), colour transition covering range from red to blue via emission from P-TPE$_{CUR+NR}$ nanoparticles with change in solvent environment.(c), P.L. Intensity of P-TPE$_{CUR+NR}$ nanoparticles w.r.t to solvent environment upon excitation at λ_{exc} 330 nm (d), at λ_{exc} 440 nm (e) and at λ_{exc} 540 nm (f) .*

Figure 4.26 (d) shows emission spectra of P-TPE$_{CUR+NR}$ nanoparticles at TPE excitation λ_{exc} 330 nm. The nanoparticles experience three kinds of interaction changes when the system was gradually changed from water to DMSO environment. Firstly, the FRET energy transfer from TPE to CUR and further to NR species gets affected, secondly a shift in emission of NR species was observed due to change in environment from water to DMSO, and thirdly the emission of TPE changes due to its transition from aggregated to isolated species. The P-TPE$_{CUR+NR}$ nanoparticles upon excitation at λ_{exc} 330 nm showed complete energy transfer from TPE residues as shown in figure 4.26 (compared to complete energy transfer from TPE to CUR species) and only residual emission from CUR was observed at 490 nm with high

emission from NR residue confirming the process of FRET intact in presence of dual acceptors. Upon increasing the DMSO content upto 20% an increase in emission of both NR and CUR species were observed and these attained maximum intensity. Beyond this point the emission of NR reduced gradually as it moved away from the TPE donor molecule and CUR emission increased as the FRET intensity was reducing between the CUR and NR species. The decrease in the NR emission was observed upto 40% water composition and CUR reached its maximum increase upto 1.7×10^5. Beyond this composition a red shift of 40 nm was observed in emission of NR species which represented the change in environment from water to DMSO. This change was reflected on the emission intensity of CUR with consequent decrease in its emission and with gradual increase in emission of NR. These observations indicated that as NR moved away from the donor species CUR its emission reduced and FRET efficiency reduced which in turn increased the emission of CUR as acceptor from TPE. However the emission of CUR beyond 30% water reduced as the scaffold was no longer intact. In the whole composition range no emission was observed from TPE as the at high DMSO content the TPE was no longer in aggregated state. The demonstration of P-TPE_{CUR-NR} dual loaded, dual FRET characteristic nanoparticles developed from L-aspartic acid based amphiphilic polyesters threw light on the highly complex yet stable configuration attained by the self assembled micelles from the polyesters which could be used for multi colour imaging and studying processes at molecular level in bio-systems making these novel class of polymers an attractive class of bio-materials.

4.4 Conclusion

To conclude, a new class of AIE inherent L-aspartic acid based amphiphilic polyesters have been synthesized by melt condensation polymerisation using melt stable L-aspartic acid monomers and custom tailored TPE diol under solvent free conditions. Highly stable nanoparticles were generated in aqueous environments by using optimised composition of hydrophilic (TEG) and hydrophobic (DD) diols into the polymer system. These nanoparticles were stable under physiological conditions and formed nanoparticles of size < 100 nm upon loading highly hydrophobic nile red dye and water insoluble Curcumin drug. The system was found to form nano-architectures where in TPE in the backbone of polymer chain were found to aggregate

to create highly luminescent nanoparticles restricted to solvents such as water. The sensitivity of the polymer structures towards changing environment was further studied using the water and DMSO compositions exhibiting expanded conformation in organic and highly aggregated coil like structure in aqueous solvents. The nanoparticles were for the first time used to demonstrate three FRET pairs within the nano-domains of the nanoparticles namely: TPE-CUR, TPE-NR and CUR-NR using extensive absorption, emission and TCSPS studies. FRET overlap higher than 70% in each case was observed and the FRET phenomenon was further extended to triple chromophore component system i.e., CUR and NR dual loaded P-TPE polymer and an efficient transfer of energy was observed from TPE to NR via CUR from emission spectra. The FRET efficiency and energy transfer was further altered using various combinations of water and DMSO and fine tuning (over wide range visible light spectra) of the nanoparticles were achieved making these nanoparticles ideal for imaging purposes. These loaded nanoparticles were non-toxic and biocompatible to cells and higher concentration of CUR loaded nanoparticles showed efficient killing in cancer cells such as HeLa and MCF 7 cells.

References

1. J. K. Oha; D. I. Leea; J. M. Park *Prog. Polym. Sci.* **2009**, *34*, 1261–1282.
2. R. Tong; J. Cheng *Bioconjugate Chem.* **2010**, *21*, 111-121.
3. R. N. Shah; N. A. Shah; M. M. D. R. Lim; C. Hsieh; G. Nuber; S. I.,Stupp *PNAS* **2010**, *107*, 3293-3298.
4. P. Zhang; A. G. Cheetham; Y-a. Lin; H. Cui *ACS Nano* **2013**, *7*, 5965-5977.
5. I. Pountos; M. Panteli; A. Lampropoulos; E. Jones; G. M. Calori; P. V. Giannoudis *BMC Med.* **2016**, *14*, 103-118.
6. H. Xu; Q. Yao; C. Cai; J. Gou; Y. Zhang; H. Zhong; X. Tang *J. Control. Release* **2015**, *199*, 84-97.
7. L. Yin; Z. Song;, K. H. Kim; N. Zheng; H. Tang; H. Lu; N. Gabrielson; J. Cheng *Biomaterials*, **2013**,*34*, 2340-2349.
8. A. Wagh; S. Y. Qian; B. Law *Bioconjugate Chem.* **2012**, *23*, 981−992.
9. X. Zhang; J. Yu; Y. Rong; F. Ye; D. T. Chiu; K. Uvdil *Chem. Sci.* **2013**, *4*, 2143-2151.
10. J. P. Celli; B. Q. Spring; I. Rizvi; C. L. Evans; K. S. Samkoe; S. Verma, B. W. Pogue; T. Hasan *Chem. Rev.* **2010**, *110*, 2795-2838.
11. K. Matsuoak; H. Arai; H. Oka; T. Koyama; K. Hatano *ACS Macro Lett.* **2012**, *1*, 266-269.
12. J. Chen; N. K. Poddar, L. J. Tauzin; D. Cooper, A. B. Kolomesky; C. Landes *J.Phys. Chem. B* **2014**, *118*, 12130-12139.
13. D. Rutkauskas; M. Petkelyte; P. Naujalis; G. Sasnauskas; G. Tamulaitis; M. Zaremba; V. Siksnys *J.Phys. Chem. B* **2014**, *118*, 8575-8582.
14. L. C. Speight; A. K. Muthusamy; J. M. Goldberg; J. B. Warner; R. F. Wissner; T. S. Willi; B. F. Woodman; R. A. Mehl; E. J. Petersson *J. Am. Chem. Soc.* **2013**, *135*, 18806-18814.
15. E. C. Izgu; A. Bjorkbom; N. P. Kamat; V. S. Lelyveld; W. Zhang; T. Z. Jia; J. W. Szostak *J. Am. Chem. Soc.* **2016**, *138*, 16669-16676.
16. S. Das; D. K. Sharma, S. Chakravarty; A. Chowdhury; S. S. Gupta *Langmuir* **2015**, *31*, 3402-3412.
17. T. A. Diezi; Y. Bae; G. S. Kwon *Mol. Pharm.* **2010**, *7*, 1355-1360.
18. M. A. Quadir; S. W. Morton; Z. J. Deng; K. E. Shopsowitz; R. P. Murphy; T. H. Epps,III; P. T. Hammond *Mol. Pharmaceutics* **2014**, *11*, 2420-2430.
19. B. M. Upton; A. M. Kasko *ACS Sustainable Chem. Eng.* **2018**, *6*, 3659-3668.
20. A. M-Fernández; G. A. Abraham; J. L. Valentín; J. S. Román *Polymer*, **2006**, *47*, 785-798.
21. H. R. Kricheldorf; S. Bohme; G. Schwarz; C-L. Shultz *Macromoleucles*, **2004**, *37*, 1742-1748.

22. S. Limgier; Y. Spiesschaert; B. Dhanis; S. De Wildeman; F. E. Du Prez *Macromoleucles*, **2017**, *50*, 5346-5352.
23. S. Ananthraj; M. Jayakannan *Biomacromoleucles*, **2012**, *13*, 2446-2455.
24. R. Aluri; M. Jayakannan *Biomacromoleucles*, **2017**, *18*, 189-200.
25. H. Ma; C. Qi; C. Cheng; Z. Yang; H. Cao; Z. Yang; J. Tong; X. Yao; Z. Lei *ACS Appl. Mater. Interfaces* **2016**, *8*, 8341-8348.
26. Y. Hong; J. W. Y. Lam; B. Z. Tang *Chem. Soc. Rev.* **2011**, *40*, 5361-5388.
27. B. Xu; J. He; Y. Dong; F. Chen; W. Yu; W. Tian *Chem Commun.* **2011**, *47*, 6602-6604.
28. X. Wang; J. Hu; G. Zhang; S. Liu; *J. Am Chem. Soc.* **2014**, *136*, 9890-9893.
29. X. Zhang; B. Wang; Y. Xia; S. Zhao; Z. Tian; P. Ning; Z. Wang *ACS Appl. Mater. Interfaces* **2018**, *10*, 25146-25153.
30. X. Wang; Y. Yang; Y. Zhuang; P. Gao; F. Yang; H. Shen; H. Guo; D. Wu *Biomacromoleucles*, **2016**, *17*, 2920-2929.
31. X. Han; De-E Liu; T. Wang; H. Lu; J. Ma; Q. Chen; H. Gao *Appl. Mater. Interfaces* **2015**, *7*, 23760-23766.
32. E. Zhao; Y. Chen; H. Wang; S. Chen; J. W. Y. Lam; C. W. T. Leung; Y. Hong; B. Z. Tang *Appl. Mater. Interfaces* **2015**, *7*, 7180-7188.
33. Y. Wei; L. Wang; J. Huang; J. Zhao; Y. Yan *ASC Appl. Nano Mater* **2018**, *1*, 1819-1827.

Chapter 5

L-Amino acid Based Hydroxyl and Carboxylic dual functional AIE Based Polyesters from Melt Condensation Solvent free route for Cisplatin and Doxorubicin delivery to Cancer Cells.

Abstract

Esterase enzyme responsive hydroxyl and carboxylid c dual functional polyesters were synthesised from natural amino acid residues. L-aspartic acid was converted into di-ester functionalmonomer containing acetal protecting amine groups. The methyl esters of the aspartic acid monomer underwent melt-transesterification with dodecane diols, an aliphatic hydrophobic di-functional alcohol to produce high molecular weight polyesters under the presence of melt-transesterification catalyst Titanium tetrabutoxide at 150℃. The hydroxyl functionalised polyesters were synthesised by acid assisted deprotection of the acetal gropus in each repeating units of the polymer. The free hydroxyl groupd were further converted into carboxylic functional group based polymers by using ring opening of succinic anhydride and were well characterised using proton and carbon NMRs. The GPC analyses further showed monmodal distribution of the polesters and the thermal properties of the polyester using TGA analyses showed that these polymers were stable upto 300℃. The DSC analysis of these polesters revelaed that they were amorpohus in nature. The hydrophilic hydroxyl and carboxylic gropus along witht he ahydrophobic aliphatic backbone made these polymer amphiphilic in nature and enabled these to self assemble into spherical nanoaprticles in water. Successful and high amount of DOX loading was achieved and the cellualr uptake and killing were demonstrtaed in MCF 7 cells. The carboxylic polymers were further covalently stiched to a seconf anticancner drug cisplatin there killign were demonstarted in the cancner cells. These polyesters were further transformed into AIE active polymers by introducing custom designed tetraphenylethene units in the backbone during melt condensation process making these polymers nanoscaffolds luminescent in nature. The DOX loaded AIE active polymers wereused to demonstarte FRET at the cellualr level where agrregated TPE acted as donor andDOX acted as acceptor. The new class of hydroxyl and carboxylic polyesters were found to be ideal candidates for bio-imaging as well cell killing agents makinf them ideal for theranostic applications.

5.1 Introduction

Designing of multi-purpose polymer nano-carriers are emerging as challenging event since their demand for biomedical applications have been increased many folds in the last two decades.[1] Polymer nano-carriers are required to have inherent basic characteristics for them to be eligible to become functional biomaterials.[2] Few of these structural criteria may be listed as biocompatibility, biodegradability, susceptible to intra or extra-cellular stimuli-responsiveness and importantly bear functional handles to for targeting ligands, drugs or fluorophores for targeted drug or gene delivery[3,4]. Despite a large number of polymer nano-carriers are reported to be exhibiting very good biocompatibility with respect to their inert macromolecular architectures; the biodegradation of their backbone seems to be tightly controlled by enzymes or intracellular species under physiological conditions.[5] Among the chemical linkages, aliphatic polyesters, polycarbonates, polyamides, polyurethanes (or carbamates) and poly(ester-amide)s, poly(ester-urethane)s have proven to exhibit excellent biodegradation by the liposomal enzymes at the intracellular compartments. Based on the pro-drug literature, it may be categorically pointed out that more than 49 % of the clinical pro-drug market is associated with aliphatic ester chemical linkages that are readily biodegradable to become active drug at the site of action (shown in figure 5.1)[6]

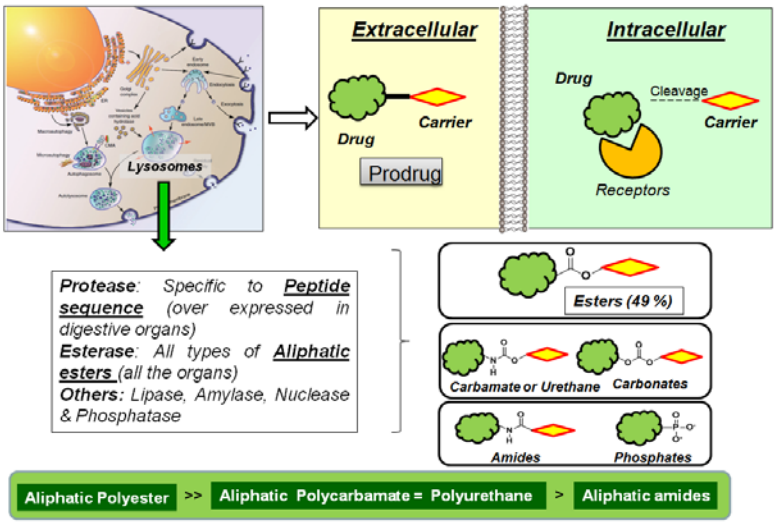

Figure 5.1: *The schematic of human intracellular region rich showing the components of the cells, with lysosomal compartments rich in degradation enzymes, based on which most pro-drugs are designed.*

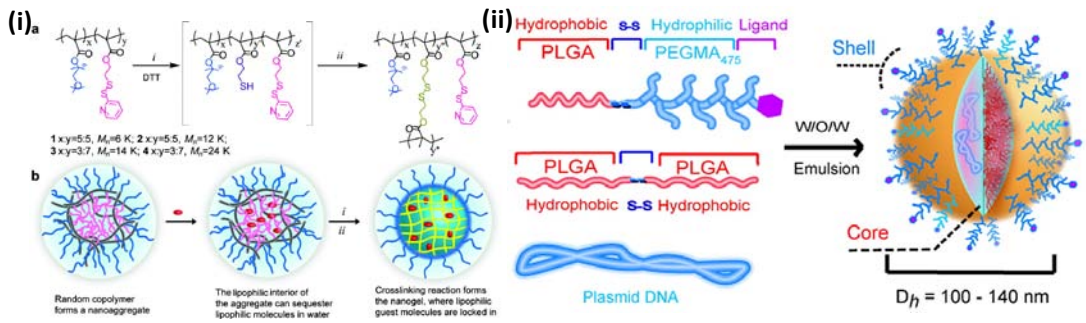

Figure 5.2: *GSH and pH Stimuli Responsive Nanoscaffolds (Adapted from references Ryu et al, JACS* **2010**, *132*, 17227-17235 *and Saeed et al, Bioconjugate Chem,* **2011**,*22,* 156-158*)*

Both pH and redox degradable polymers were also proven to be promising for disassembly of nano-carriers; however, additional chemical linkages in their backbone are often required to enable their biodegradation and clearance from the system under physiological conditions. This lead to the development of dual responsive polymer nano-carriers has both pH and enzyme or redox and enzyme responsiveness build to together to accomplish both disassembly and biodegradation simultaneously under intracellular environment. (see figure 5.2).[7,8] Biodegradable aliphatic polyesters can be made either by polycondensation route or ring opening polymerization (ROP) of cyclic monomers.[9] Polycondensation of di-acids (or di-acid chlorides) with diols in solution polymerization or melt transesterification of di-carboxylic esters with diols under solvent free conditions are established to yield high molecular weight aliphatic polyesters[10]. Poly(adiphate), poly(sebasate) and poly(cyclohexyldimethyldicarboxylate) are some of the very good examples for polycondensation approach. ROP process is largely applicable to make poly (L-lactides), poly(L-glycolides)s, polycaprolactones, or poly(α-hydroxyl acids) from unnatural L-amino acid resources[11,12] (see figure 5.3). Aliphatic polyesters produced by both polycondensation and ROP approaches are explored for their applications in biomedical applications and their extensively reviewed by [13].

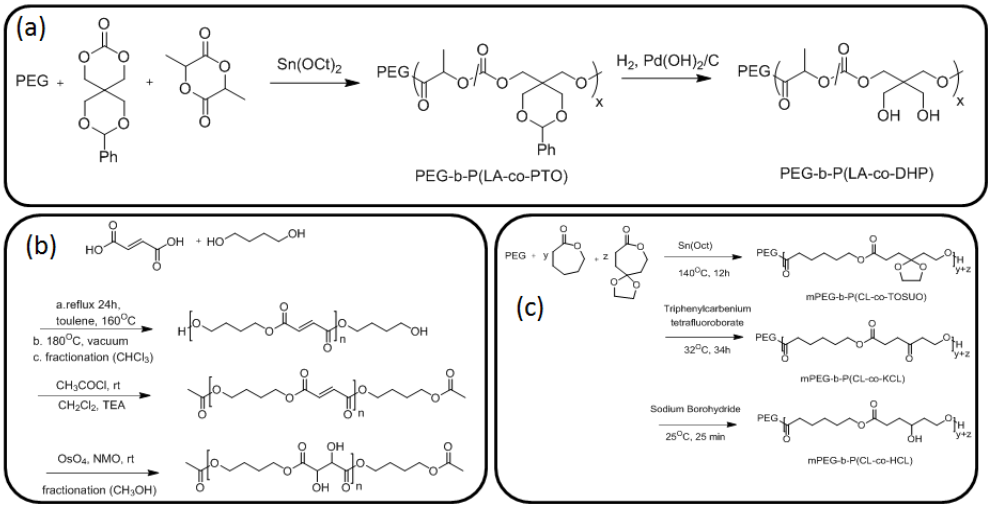

Figure 5.3: *Synthesis of Hydroxyl functionalised polyesters.*

These aliphatic polyesters merely satisfy the basic requirements of biocompatibility and biodegradability; however, they are not suitable for multi-functional nano-carriers. The introduction of additional functional groups is important requirements to make them suitable multipurpose nano-carriers. It is very important to mention that the introduction of functional groups in the aliphatic polyester backbone is required to be carefully chosen since it should not interference with the polymerization reactions. One of the elegant ways to accomplish the above synthetic challenge is by masking the required functional group by suitable substitution which should be inert under the polymerization protocol. The masked group could be removed and the aliphatic polyester can be made functionalised at the post-polymerization stage. This approach is routinely employed in polymer synthesis and it is schematically shown in Figure 5.4

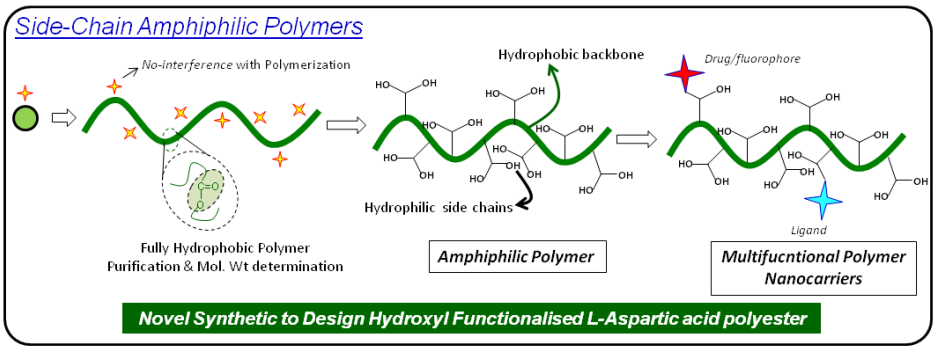

Figure 5.4: *Schematic representation of biodegradable hydroxyl functionalised polyesters from amino acid.*

Functional poly(L-lactide)s and polycaprolactone(PCL)s were successfully made by this approach by masking the functional groups which are inert towards the ring opening process. This approach particular achieved for diverse functional groups like azide, hydroxyl, ketone, amine, carboxylix acid, etc in the PCL system [14]. It is important to mention that from our laboratory Baburao et al. has reported successful development of carboxylic acid functionalized di- and tri-block PCL copolymers and employed then as pH responsive vesicles for oral drug delivery of inflammatory drugs as well as enzyme-responsive nano-carriers for intravenous administration of anticancer drugs. This approach was also extended to make Pt-drug tagged nano-carriers for combination therapy of dual drugs to breast cancer cells (see figure 5.5).

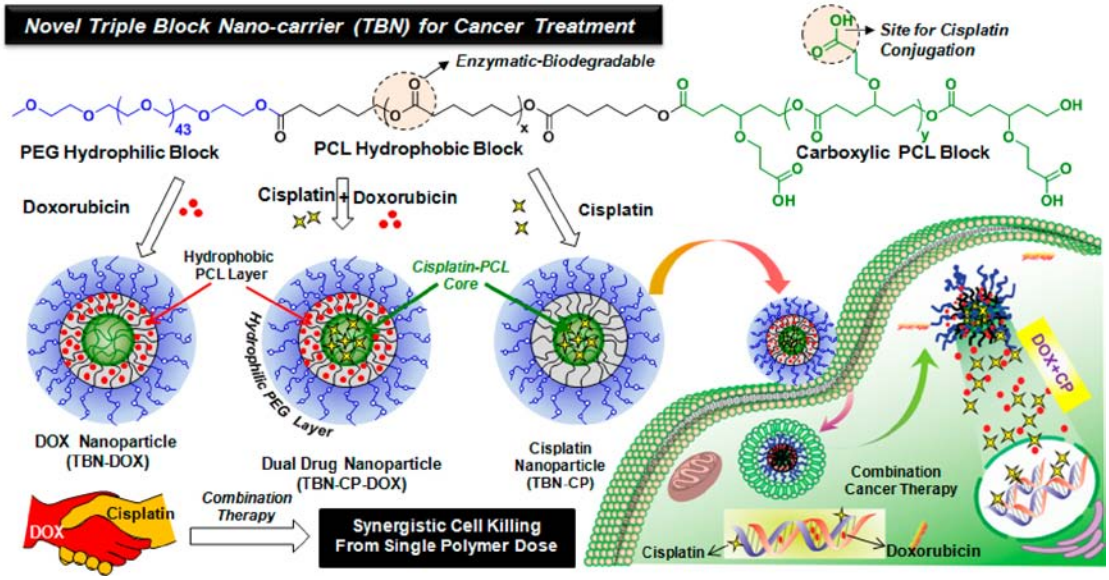

Figure 5.5: *pH responsive vesicles for drug delivery based on polycaprolactones (adapted from Bapurao et al. Biomacromolecules,* ***2016****, 17,* 4075- 4085*).*

Enzyme catalysed biosynthetic approaches is another important methodology widely established for functional polyesters. In this process unmasked hydroxyl functionalized carboxylic acids or mixtures of dicarboxylic acids and multi-functional alcohols (having both 1° and 2°) were subjected to polymerization using modified or natural enzymes to produce moderate to high molecular weight polymers. Poly(hydroxybuterate) (PHB)s are one of the merging commercial biodegradable polymers produced by enzymatic fermentation approach in Industrial level[15].

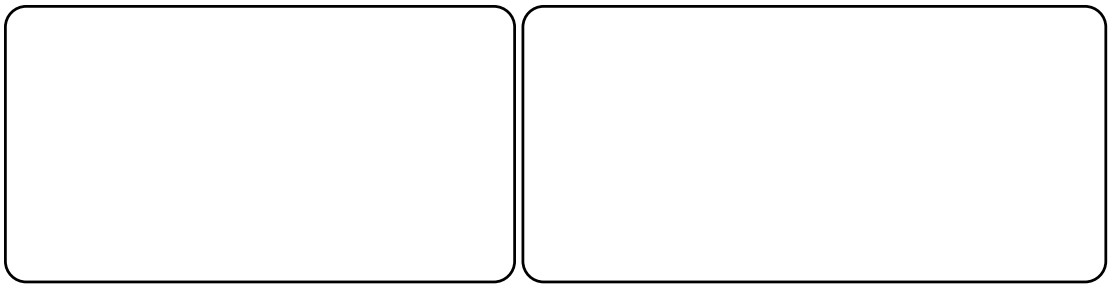

Figure 5.6: *Enzyme catalysed synthesis of hydroxyl functionalised polyesters. (Chemical reactions adapted from Hao et al, Biomacromolecules,* **2005***, 6,* 3474-3480*., Japu et al Biomacromolecules* **2015***, 16,* 868−879*.)*

Designing functional polyesters based on melt polymerization is particularly changeling task since large number of masking units is not stable under high temperature melt conditions and their partial dissociation (even less than 1 %) would lead to the formation insoluble cross-linked gels. Recently hydroxyl functional polyurethanes, polyamides and polyacetals were reported by cleverly masking the bis-hydroxyl units by thermally stable acetal chemical linkages and de-protecting them after the polymerization to yield their corresponding hydroxyl functionalized polymers. Biscyclicacetalized D-glucose derivate was polymerized with dimethyl sebacete and commercial diols to yield random hydroxyl functionalized random copolyesters.[17] These functionalized polyesters produced via poly-condensation route are largely studied for their mechanical and thermal properties to understand their structure-property relationships; however, no effort has been to tested their application in biomedical field. This partially associated with their inability to behave as nano-carriers due to their lack of appropriate geometry for self-assemble them into stable nano-assemblies in aqueous medium (see figure 5.7) [18]. Hence, there are new research opportunities to design and develop multi-purpose functional aliphatic polyester nano-assemblies for biomedical applications, particularly in the area of drug delivery in cancer treatment.

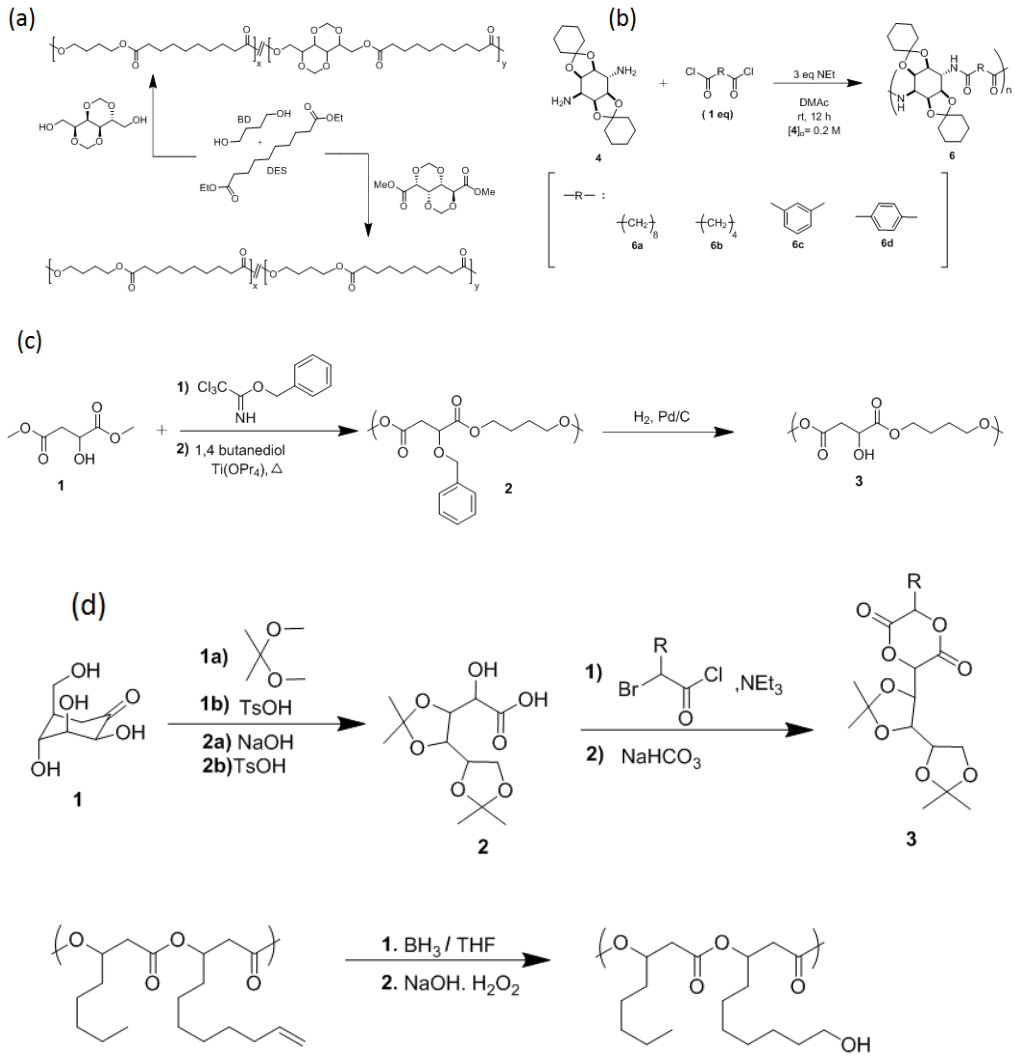

Figure 5.7: *Various synthetic ways to synthesis hydroxyl polyesters. (Chemical reactions adapted from Begines et al, J. of Polym. Sci. Part A: Polym. Chem,* **2012**, *50,* 4638-4646. *Taniguchi et al, Polym Int* **2006**, *55,* 1385-1397*).*

L-Amino acids are important biological monomers and their wide availability makes them excellent choice for the development of functional polymers. Efforts have been put from our group to development polycondensation approach to polyesters, poly(ester-urethane)s and amphiphilic structures were optimised using PEG-chain as hydrophilic derivatives. These polymers were proven to enzyme-responsive biodegradable polymer nano-carriers for drug delivery and bio-imaging applications that are described in the earlier chapters. The present approach reports one of the first examples for hydroxyl functionalized L-amino acid based polymer nano-carriers in the polymer literature. This concept was accomplished in L-aspartic acid system by cleverly developing new melt polymerizable acetal protected di-carboxylic ester monomer and subject it to melt trans-esterification with commercial diol to make

acetal-polyester. Fully hydrophobic acetal polyester was converted into hydroxyl functionalized amphiphilic polyester upon post polymerization de-protection. Multipurpose capabilities of the hydroxyl polyester were demonstrated by various structural modification and their drug delivering capabilities are established in detail. This new concept is schematically shown in Figure 5.8.

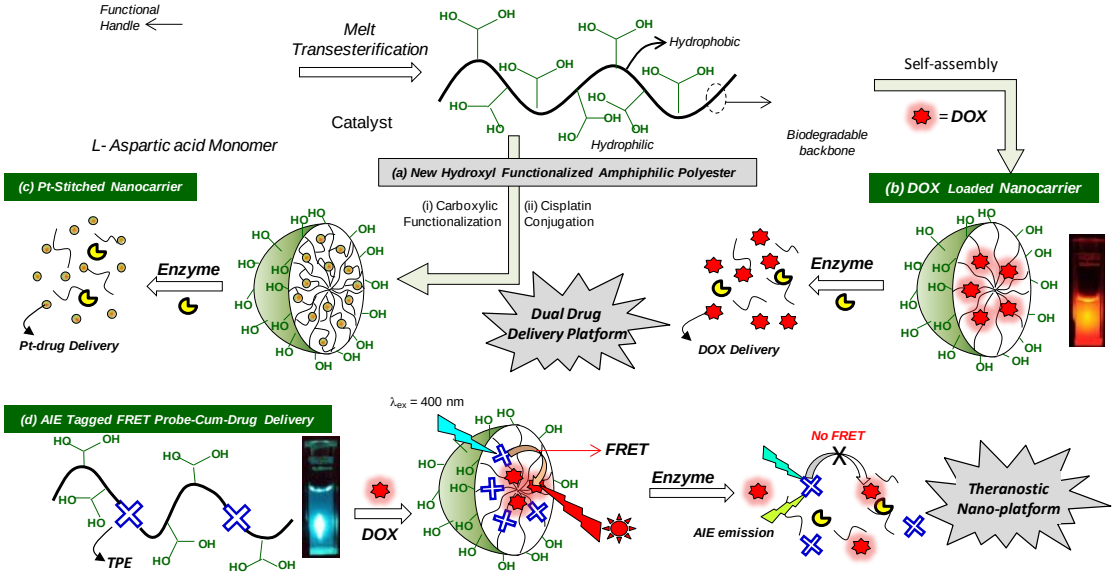

Figure 5.8: *Design and Development of hydroxyl functionalized L-amino acid nano-assemblies and their application as theronostic system for delivery of DOX and Pt-drug, and bio-imaging through FRET process in cancer cells.*

The present investigation is emphasised to design and develop the hydroxyl functionalized polyester nano-carrier platform, for the first time, in L-amino acid system, and demonstrate their application in cancer cells. The structure of the polyester was appropriately engineered to accomplish amphiphilicity in which the rigid backbone structure and hydroxyl functional units provide hydrophobicity and hydrophilicity, respectively. This facilitated the polymers to produce stable nanoparticle of < 100 nm in size in aqueous medium. Triple-action capabilities of the hydroxyl polyester was demonstrated as follows (shown in Figure 5.8): (i) the self-assembled polymer nanoparticles exhibited very good encapsulation for doxorubicin (DOX) and the DOX was delivered by the biodegradation of aliphatic polyester backbone by lysosomal enzymes exclusively at the intracellular level, (ii) aggregation induce emission probe molecule TPE was incorporated in the polymer backbone to

make AIE-assisted fluorescent hydroxyl polyester and its DOX encapsulated nanoparticle was employed as theranostic FRET probe in bio-imaging and drug delivery simultaneously in single polymer system (iii) the hydroxyl groups were ring opened with succinic anhydride to produce carboxylic functionalized polyester which was employed for the conjugation of cisplatin drug to deliver the Pt-drug to cancer cells.

5.2 Experimental Section

Materials: L-Aspartic acid, 2,2- bishydroxymethyl propionic acid, dimethosy propane,1,2-dodecanediol, p-toulene sulphonic acid, titanium tetrabutoxide ($Ti(OBu)_4$), horse liver esterase enzyme, doxorubicin HCl, tetrazolium salt: 3-(4,5-dimethylthiazolyl)-2,5-diphenyltetrazolium bromide) MTT, fluoromount aqueous mounting medium, DAPI (4', 6-diamidino-2-phenylindole, silicon wafers hydrobenzotriazole and N'- ethylcarboiimide hydrochloride were purchased from Sigma Aldrich. Trypsin phosphate versene glucose (TPVG) solution was obtained from Hi-media.MCF 7 cells (mammalian breast cancer) were maintained in phenol red containing Gibco medium with 1% (v/v) penicillin-streptomycin, 10% (v/v) fetal bovine serum (FBS). Solvents such as thinly chloride, methanol, DMSO, and other solvents were purchased locally and uses as it is. HPLC THF and HPLC DMSO were obtained from spectrochem laboratories.

General procedure: ^{1}H-NMR and ^{13}C-NMR were recorded using 400 Mhz and 100 MHz NMR spectrophotometer with TMS as internal standard. Thermal stability of the polymers was measured by thermal gravimetric analysis (TGA) using PerkinElmer thermal analyzer STA 600 model, under nitrogen environment. Gel permeation chromatographic (GPC) plots were determined using Viscotek VE 1122 pump, Viscotek VE 3580 RI detector, and UV/vis detector w.r.t polystyrene standards. Dynamic light scattering DLS was employed to determine size of nanoparticles and Malvern instrument was used for it. Zeiss Ultra Plus scanning electron microscope was employed to generate the field emission scanning electrons microscope (FESEM) images of the nano fibres and nanoparticles. PerkinElmer Lambda 45 UV-vis spectrophotometer and SPEX Fluorolog HORIBA JOBIN VYON fluorescence spectrophotometer (with excitation source 450 W Xe lamp and double

gating 0.22 m Spex 1680 monochromator) were used for obtaining absorption and fluorescence spectra for dye and drug loaded polymers.

Synthesis of 2,2,5-trimethyl-1,3-dioxane-5-carboxylic acid : 2,2- bishydroxymethyl propionic acid (10.0 g, 0.075 mol), was taken in a two neck round bottom flask in dry acetone (100.0 mL). This was followed by addition of pTSA (0.71 g, 0.004 mol) and further stirring made the solution clear. pTSA was dried using azeotropic distillation with toluene prior to use. Dimethoxy propane (18.60 mL, 0.112 mol) was added to this solution drop wise and the reaction mixture was stirred for 4h at 25°C. After the reaction completion, 2 drops of tri-ethyl amine was added to the solution to neutralise the excess pTSA and acetone was further removed from the reaction mixture by rota-evaporation. The resultant residue was dissolved in water and the product was extracted in ethyl acetate. Pure crystalline white powder was obtained as the product. (Yield = 26.0 g, 77 %). ^{1}H-NMR in $CDCl_3$ (400 MHz) δppm : 4.23- 4.20 (2H, d, -C**H$_2$**), 3.72- 3.69 (2H, d, -C**H$_2$**), 1.47- 1.44 (6H,d, -C(C**H**$_3$)), 1.23 (3H, s, -C(C**H**$_3$)). (Procedure adopted from *ACS Appl. Mater. Interfaces*, **2016**, *8* (22), 13724–13734).

Synthesis of dimethyl (2,2,5- trimethyl-1,3-dioxane-5-carbonyl) aspartate (2): Amine salt of L-aspartic acid reported in chapter 2 (10.0 g, 0.05 mol) was dissolved in dry DCM (150.0 mL) using DIPEA (26.5 mL, 0.15 mol) at 25°C with constant stirring. To this solution was added hydrobenzotriazole (6.86g, 0.0502 mol), and N'-ethylcarboiimide hydrochloride (8.6 g, 0.0558 mol) followed by addition of compound (2) (7.06 g, 0.040 mol) and the reaction was stirred at 25°C for 24 h. The DCM was rota evaporated from the reaction mixture and crude product was extracted in ethyl acetate. The resultant product was purified using silica column at in pet ether/ethyl acetate system at 30% EA solution and yellowish white coloured liquid was obtained as the pure product with yield =16.0 g, 75 %. ^{1}H-NMR in $CDCl_3$ (400 MHz) δppm : 7.97 (bs, 1H, -NH), 4.83 (s, 1H, -CH), 3.88- 3.76 (dd, 2H, -CH_2), 3.70-3.76 (s, 5H, -CH_2 + -OCH_3), 3.59 (s, 3H, -OCH_3), 2.95- 2.78 (dd, 2H, -NH-CH_2), 1.37 (s, 6H, -$C(CH_3)_2$, 0.91 (s. 3H, -C-CH_3). ^{13}C-NMR in $CDCl_3$ (100 MHz): 174.71, 171.19, 98.53. 66.85, 52.63, 51.91, 48.63, 40.16, 36.28, 28.33, 18.35, 17.61.

Synthesis of acetal functionalised polyester (P-Ac): Monomer 2 (0.62 g, 1.89 mmol) was taken with dodecanediol (0.38 g, 1.89 mmol) were taken in a melt polymerisation tube and the mixture was melted at 100°C with constant N_2 purging. 1.0 mol% $Ti(OBu)_4$ was added to the melt and the tube was degassed at 0.01 mbar vacuum followed by purging with N_2 for five minutes each. The degassing and nitrogen purging was repeated 3 times and temperature of the melt was raised to 150°C. The N_2 at 150°C was continued for 4h and this was followed by application of vacuum of 10^2 mbar for 2h. The obtained viscous polymer was further purified by precipitation in methanol. Yield: 0.83 g (98.0 %). ^{1}H-NMR (400 MHz , $CdCl_3$) δ ppm: 8.04 (s, 1H, -N**H**), 4.91 (m, 1H, -C**H**), 4.17 (t, 2H, -COOC**H$_2$**), 4.09 (t, 2H, -NHCOOC**H$_2$**), 3.96 (d, 1H, -C**H$_2$**), 3.88 (d,1H, -**CH$_2$**), 3.77 (d, 2H, -C**H**$_2$), 3.06-2.87 (m, 2H,-CH-C**H**$_2$), 1.64 (m, 4H, -COOCH$_2$C**H**$_2$), 1.48 (s, 6H, -C(C**H**$_3$)$_2$), 1.26 (bs, 16 H, -aliphatic protons), 1.02 (s, 3H, -C**H**$_3$).^{13}C-NMR (100 MHz, $CDCl_3$) δ ppm: 174.08, 171.74, 97.77, 66.92, 65.84, 64.57, 48.33, 39.96, 36.36, 29.38, 28.39, 24.77, 18.07, 17.74.

Synthesis of hydroxyl functionalised polyester (P-OH): Polyester PA (0.46 mg, 1.01 mmol) was taken in a round bottom flask and dissolved in dry DCM (4.0 mL), to this was added trifluoroacetic acid (0.78 mL, 0.1 mmol), and water (0.78 mL) under ice cold conditions, and the reaction mixture was brought to 25°C and stirred for 2h. The DCM and water were removed from the reaction mixture using rota-vaporator, and TFA was removed by distillation with toluene, at high vacuum conditions. The polymer was obtained as turbid white viscous solid. (Yeild) ^{1}H-NMR (400 MHz , $CDCl_3$) δ ppm: 8.04 (s, 1H, -N**H**), 4.91 (m, 1H, -C**H**), 4.17 (t, 2H, -COOC**H$_2$**), 4.09 (t, 2H, -NHCOOC**H$_2$**), 3.96 (d, 1H, -C**H$_2$**), 3.88 (d,1H, -**CH$_2$**), 3.77 (d, 2H, -C**H**$_2$), 3.06-2.87 (m, 2H,-CH-C**H**$_2$), 1.64 (m, 4H, -COOCH$_2$C**H**$_2$), 1.48 (s, 6H, -C(C**H**$_3$)$_2$), 1.26 (bs, 16 H, -aliphatic protons), 1.02 (s, 3H, -C**H**$_3$).

Synthesis of hydroxyl functionalised AIE polyester (P-OH-TPE): The L-amino acid based AIE polyester was synthesised in similar way as that PA polyester explained in section 5.2.5. The details for the polymerisation is given: Monomer 2 (0.62 g, 1.89 mmol) was taken with dodecanediol (0.38 g, 1.89 mmol) were taken in a melt polymerisation tube and the mixture was melted at 100°C with constant N_2 purging. 1.0 mol% $Ti(OBu)_4$ was added to the melt and the tube was degassed at 0.01 mbar

vacuum followed by purging with N_2 for five minutes each. The degassing and nitrogen purging was repeated 3 times and temperature of the melt was raised to 150°C. The N_2 at 150°C was continued for 4h and this was followed by application of vacuum of 10^2 mbar for 2h. The obtained viscous polymer was further purified by precipitation in methanol. Yield: 0.83 g (98.0 %). ^{1}H-NMR (400 MHz , $CdCl_3$) δ ppm: 8.04 (s, 1H, -N**H**), 4.91 (m, 1H, -C**H**), 4.17 (t, 2H, -COOC**H$_2$**), 4.09 (t, 2H, -NHCOOC**H$_2$**), 3.96 (d, 1H, -C**H$_2$**), 3.88 (d,1H, -**CH$_2$**), 3.77 (d, 2H, -C**H**$_2$), 3.06-2.87 (m, 2H,-CH-C**H**$_2$), 1.64 (m, 4H, -COOCH$_2$C**H**$_2$), 1.48 (s, 6H, -C(C**H**$_3$)$_2$), 1.26 (bs, 16 H, -aliphatic protons), 1.02 (s, 3H, -C**H**$_3$).^{13}C-NMR (100 MHz, $CDCl_3$) δ ppm: 174.08, 171.74, 97.77, 66.92, 65.84, 64.57, 48.33, 39.96, 36.36, 29.38, 28.39, 24.77, 18.07, 17.74.

Self Assembly, Loading Studies, and Biodegradation Studies: The self assembly of amphiphilic polyesters were carried out using the dialysis method explained in chapter 2, 3 and 4. Polyesters PA and PH_{TPE} dissolved in DMSO were dialysed against water to prepare their spherical nanoparticles. For loading of doxorubicin for every 5.0 mg of polymer 0.5 mg Doxorubicin was used. Prior to use doxorubicin HCl was neutralised using tri-ethyl amine. To remove unloaded drug molecules were removed using semi-permeable dialysis membranes of cut off 1.0 kD. The resultant dialysed solutions were filtered, lyophilised and stored at 4°C. For biological experiments the lyophilised nanoparticles were re-dispersed in media prior to use. For photo-physical experiments and DLS measurements, the dialysed filtered solutions were used as it is. DLC (Drug Loading Content) and DLE (Drug Loading Efficiencies) were measured using the equations (1) and (2) mentioned in previous chapters. The biodegradation studies were carried out by taking the P-TPE_{DOX} nanoparticles with 70.0 μg loaded DOX in a dialysis tube of 1kD cut off and placed in a beaker containing PBS buffer. The solution was incubated at 37°C and the absorbance of the solution outside the dialysis membrane was measure at fixed times interval. This in-vitro set up was close to the environment of the blood and normal tissues. To mimic the lysosomal conditions, the same set up was used, with addition of 10 U of horse liver esterase enzyme. The absorbance of the solution in reservoir was measure and the relative amount of Doxorubicin with respect to the total initial

DOX concentration was plotted against time as the release profile of the nanoparticles.

Cellular Uptake studies of DOX : Breast Cancer cell lines were seeded in 6 well plates placed with sterile glass cover slips in each well and grown for 16 h in DMEM having 10 % FBS at 37 °C. The cells were further incubated with free DOX, nanoparticles containing DOX keeping the concentration of DOX at 2.0 μg. The uptake studies were carried out for 4h, and the drug containing media was aspirated from the cells and cells were fixed using para-formaldehyde and mounted on glass plates. Before cell fixing, the cells were washed twice with 1mL PBS to remove the DOX and nanoparticles loaded with DOX that were not taken up by the cells. The actin filaments of the cells were stained with with phalloidin conjugated to Alexa 594 (Invitrogen) and the procedure was carried out dark light. The excess phalloidin dye was washed with PBS solution twice (1 mL). The cells upon mounting on the glass slides were dried before imaging on the LSM710 Confocal Microscope. Similar procedure was opted for the TPE conjugated polymers and their corresponding DOX loaded nanoparticles too. The TPE chromophores were excited using 405 nm, and DOX was excited using 568 nm laser, and the phalloidin was excited with laser 488 nm and imaged in blue, red, and green channel respectively. The hydroxyl functionalised polyester P_{TPE}-OH (0.15 g, 0.36 mmol) was dissolved in 5.0 mL dry DCM in a 10.0 mL RB flask, and to this was added Et_3N (300.0 μL, 2.20 mmol) under ice cold conditions and stirred for 5 min, followed by addition of succinic anhydride (54.2 mg, 0.54 mmol). Brought the reaction mixture to 25°C and stirred at room temperature for 24 h. Following the reaction, the DCM was dried and the polymer was dialysed against a large amount of distilled water for 48 h. Dried the polymer NMR provided in annexure.

Synthesis of $[Pt(NH_3)_2(OH_2)_2]^{2+}$ and Cisplatin stitching to carboxylic polyesters

Cisplatin (50.0 mg, 99.6 mmol) and silver nitrate (56.0 mg) were dispersed in water (20.0 mL) and was stirred constantly at 25°C for 24 h under dark conditions. Formation of milky white precipitate of silver chloride was indicative of formation of aquated cisplatin complex. The precipitate was removed by centrifuging the aqueous solution for 15 min and via filtration through 0.22 μm filter. The aqueous solution

thus obtained was lyophilized and stored at 4°C for further use.The stitching of cisplatin aqua complex was carried out dissolving P-$_{CAR}$ polymer (40.0 mg) in 20 mL distilled water (saturated with sodium carbonate) followed by dialysis for 24 h. The solution was filtered and to this was added cisplatin aqua complex (4.0 mg) stirred at 25 °C for 48 h under dark conditions. After the lumps of the cisplatin aqua-complex completely dissolved into the solution, the solution was filtered and dialysed against water for 48 h. The obtained cis-platin stitched polymer was then filtered and lyophilised for further studies. O-phenylenediamine assay used to determine the cisplatin content has been described. Dialysed polymer solution (40.0 μL) was added to OPD solution (0.5 mL) in DMF solvent of concentration 1.2 mg/mL, and was heated at 100°C for 2h. The absorbance of the solution was measured and the intensity of the λmax at 706 nm was obtained (corresponding to OPD-Pt complex). The molar exctintion coefficient of the OPD-Pt complex is 24,310 L.mol^{-1}.cm^{-1} and this was used in lamberts beer law to calculate the amount of Pt present in the polymer.

Characteristic AIE photophysics of P-TPE polymer: The TPE conjugation in the backbone transformed the non fluorescent polymeric chains into AIE characteristic highly luminescent polymer. To study the acquired AIE properties P-TPE polymer was subjected to photophysicalstudies under different solvent environments using water and DMSO which were chosen to create aqueous and organic environment for the polymer. Water and DMSO compositions were varied from 10 to 100 %and the absorbance and fluorescence spectra of the resultant dispersed polymer solutions were recorded. The O.D. of TPE chromophore was maintained at 0.1 and fluorescence spectra were generated at λ_{exc} of 330 nm. Solvent dependent studies were carried by using DMSO and water solvents on the polymer folding dynamics. P$_{TPE}$-OH polymer (1.0 mg/ mL) dispersed in water was excited at 330 nm and its emission spectra was recorded. The solvent composition of the polymer was varied from water to DMSO by increasing the DMSO amount in the system till 90% DMSO and the emission spectra of the nanoparticles in these systems were recorded at the same excitation wavelength.

FRET emission studies: Dialysed solution P_{TPE}-OH nanoparticles loaded with doxorubicin (DOX) named as P_{TPE}-OH+DOX in the paper were subjected to absorbance and fluorescence studies. The TPE chromophores were excited at 330 nm and DOX species were excited at 490 nm and for FRET studies the nanoparticles were excited at 330 nm and their emission spectra were generated. The TPE absorbance was maintained as 0.1 O.D. and corresponding DOX amount was maintained respectively based on the loading content.

5.3 Results and Discussion

5.3.1 Synthesis of Acid sensitive functionalised L-aspartic acid monomer

An acid cleavable, yet melt stable acetal group was synthesised by coupling 2,2-bishydroxymethyl propionic acid and dimethoxy propane to form the acetal containing acid in the presence PTSA using acetone as a solvent. The nucleophilic addition of the alcohol of the acid to the dimethyl acetal lead to the formation of cyclic acetal in the presence of acetone (ketone).

Scheme 5.1: *Synthesis of multifunctionalised L-aspartic acid based di-ester containing amide blocked amine.*

The acetalisation was catalyzed in acidic conditions using PTSA with elimination of acetone molecule which further aided the formation of the product. The formation of acetal group was confirmed by the formation of new C-C bond as shown in scheme 5.1. The reaction between the starting materials leads to the formation of new C-C bond. The compound (1) was well characterised by ^{1}H and ^{13}C NMR and the proton NMR has been shown in figure 5.9 with assigned protons with alphabets. The four diastereotopic protons adjacent to chiral carbon centre of the compound appeared as two doublets at 4.19 and 3.7 ppm respectively. These protons were essential to monitor, as the post polymerisation would affect these protons most. The six ptorons on the acetal group appeared at 1.24 ppm and these were anticipated to vanish upon acidic hydrolysis of the acetal group. Further this compound was coupled to the diester of L-aspartic acid to form a stable amide bond containing new melt polymerisable monomer (2). The highlights of this monomer were the exceptional stability at high temperatures more than 120°C, to increase the melt polymerisation temperature at 150°C, which could help in enhancing the kinetics of the reaction and thus could aid in building up of higher molecular weight polyesters. The amide unit in the monomer would impart high thermal stability and would enhance hydrogen bonding to the polymer making them highly compact and compact structures. The formation of the monomer (2) was well characterised by the proton and carbon NMRs and was used for further polymerisation. The characteristic –NH peak was observed at 8.03 ppm (see figure 5.9) and the chiral –CH proton from the aspartic acid appeared at 4.83 ppm. As mentioned earlier any substutuion adjacent to the chiral carbon the acetal component would affect the diasteretropic protons the most, and the cloase doublet at 4.19 and 3.7 further split into two double doublets at 3.94-3.90 and 3.86-3.82 corresponding to two different protons c and d as shown in figure 5.9. The other two protons appeared as two doublets and appeared as 3.75 and 3.72 ppm as shown in figure 5.9. The ester peaks from the aspartic counterpart appeared at 3.73 (merging with the protons of acetal counterpart) and 3.64 as a singlet. The 6 H and 3 H from the methyl groups appeared at 1.44 and 0.97 ppm as singlets.

Figure 5.9: *^{1}H-NMR of molecule (1) and amide protected acetal functionalized multifunctional L-aspartic acid monomer.*

5.3.2 Synthesis of Hydroxyl Functionalised Polyesters

The L-aspartic acid (natural resource) containing two carboxylic units and an amine groups were synthetically modified into functional monomers for melt polycondensation. The carboxylic acid groups were converted into methyl esters and the amine was converted into amide containing acid labile acetal group. From the earlier work in this thesis, it has been shown that di-esters would undergo trans-esterification process in the presence of diols at 120° C. The BOC anhydride group in all the previous chapters used for protecting the amine group restricted the use of higher temperature as it would cleave beyond 120° C. However, the acetal amide was very stable upto 200° C and the TGA profile of the monomer has been shown in figure 5.12. The acetal amide substituted monomer was subjected to melt polymerization with di-alcohol in presence of $Ti(OBu)_4$ at 150° C. The acetal unit was found to be stable under these melt conditions and produced new esters linkages and this gave rise of development of a new class of amide branched polyesters.

Scheme 5.2: *Synthesis of L-aspartic acid based functional polyesters.*

In the melt condensation process, the multifunctional monomer underwent transesterification with diols to produce linear polyesters and the acetal amide groups was not disturbed in each repeating units (see scheme 5.2). The melt condensation was carried out at 150° C, keeping the mole ratios of the monomer 2 and aliphatic diol (dodecanediol) as 1:1in presence of 1 mole % $Ti(OBu)_4$, as melt catalyst for 4h under continuous flow of nitrogen purge. The polymer was formed as viscous mass followed by application of vacuum (0.01 bar) for 2h. The obtained polymer were dissolved in minimum amount of THF and precipitated in cold methanol to produce pure polymer. The polymer was referred to as P-A (acetal based polymer). NMR spectroscopy was used to determine the melt polymerization. The methyl ester peaks appeared in the proton NMR of the monomer at 3.73 and 3.64 pm at 'e' and 'f'. These esters would react with alcohol to produce new ester peaks which appeared at 4.11 and 4.09 ppm at'd'' and 'e'' as shown in figure 5.10. The acetal amide group – $CCH_2OC(C\mathbf{H}_3)_2$ was not disturbed by the melt-condensation polymerization reaction and it was found to be intact and completely inert and appeared at 1.44 ppm. The comparison of intensities the –$C\mathbf{H}_2$ protons at 'h' with the acetal protons at 'j' and 'i' and the new esters peaks at 'd'' and 'e'' peaks in the polymer 1H-NMR confirmed the formation of the polyester. The comparison of ratios of intensity of new ester peaks and disappearance of the methyl esters of the monomer were used to calculate the number of repeating units in the polymer. The carbon NMR further substantiated the formation of the polymer form the L-aspartic acid monomer and has been shown in

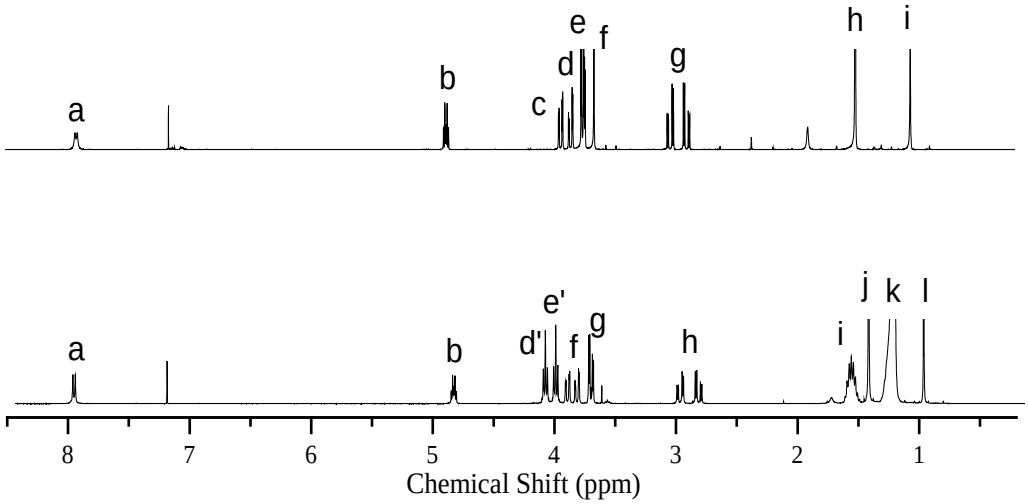

Figure 5.10: *^{1}H-NMR of L-Aspartic acid monomer and polymer.*

The ^{13}C-NMR further gave insight to the formation of high molecular weight polyesters as shown in figure 5.11. The peaks of major importance were the methyl ester peaks which appear at 52.63 and 51.91 in the monomer (see figure 5.11) participate in the melt tranesterification. When analysed the carbon NMR of teh polymer showed presence of new esters peaks at 65.84 and 64. 57 which was indicative of the formation of the polymer. It was interesting to note that the peaks of the methyl esters of the monomer had completely disappeared from the polymer NMR and this indicated that all the methyl esters had undergone trans-esterification, which was crucial for the formation of the high molecular weight polymer.

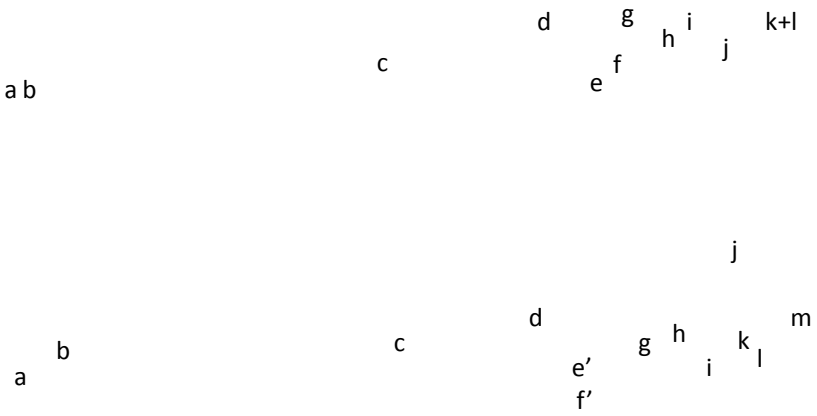

Figure 5.11: *^{13}C-NMR of L-Aspartic acid monomer and polymer.*

5.3.3 Characterisation of Polymers

The molecular weights were determined by the GPC analysis (Figure 5.12 b) . The polymers without TPE-content is further referred as P-0 and the TPE-containing polymers are referred as P-TPE5 (having 5 % of TPE units in the backbone). The TGA profiles shown in figure 5.12 shed light on high thermal stability of the L-aspartic acid based acetal monomer upto a high temperature of 200°C which encouraged using these under high temperature melt conditions. The stability of acetal group at more than 120°C enabled to increase the temperature of melt reactor to upto 150°C which improved the kinetics of the reaction and helped in increasing the molecular weight of the polyesters. It should be noted that this high temperature stability gave this monomer over the BOC protected L-aspartic acid unit as BOC unit is unstable above temperatures more than 120°C. The synthesis of polyesters at 150 °C helped to push the, molecular weight by providing external thermal energy to enhance the kinetics of the reaction. As the monomers were successfully transformed

into polymers the TGA curves of polymer showed enhanced stability of the polymers over the monomer. The stability of the P-A polymer was found up to 300°C which was 100 degrees higher than the monomer confirming the formation of thermally stable polyesters. The de-protected hydroxyl functionalised polyester showed similar trend of thermal stability and was found to be highly thermally stable as well. The GPC chromatogram of P-Ac polyester predicted the molecular weight M_n = 12000, M_w = 35000 with PDI = 2.3. The molecular weight obtained from the GPC chromatogram was slightly underestimated yet comparable to the M_n obtained from NMR of 15000. The hydroxyl and acetal functionalised polyesters were found to be amorphous in nature (figure 5.12 c)

(a) (b) (c)

Figure 5.12: *The TGA profiles (a), the GPC chromatograms (b), and DSC curves(c) of P-Ac, Monomer, and P-OH.*

5.3.4 Doxorubicin loaded spherical nanoparticles

The doxorubicin loading capabilities of the polyester P-H were studied to understand the self assembly behaviour of the L-aspartic acid based amphiphilic polyester. the doxorubicin HCl was neutralised by stirring with tri-ethylamine and was used to encapsulated in the amphiphilic polyester. The loading of Rhodamine B was tried in the scaffold and it was observed that RhB was stable in the nanoaprticle formed for 4 days and faintly it was loaded. The hydrophilic DOX HCl a also loaded in the nanostructure indicating towards the vecicular structure. However, low loading and less stability showed that the structures were not well developed. However a high loading of 70 μg/mg of Doxorubicin was found to load in the nano-scaffold with high stability which reflected towards the highly stabilised micellar structure of the nano-scaffold. To further under understand the nature of this nano-scaffold, the dialysed solution of the DOX loaded scaffolds were subjected to DLS studies and it was found

that the nanoparticles formed a mono-modal histogram with size 180 nm. The DOX loaded nanoparticles were further subjected to AFM imaging and it was found that the nanoparticles were indeed spherical in nature and the size of the nanoparticles was found to be in the range of 100- 200 nm. See figure 5.13. The efficacy of any drug loaded scaffold lies in its release triggered by extracellular or intracellular stimuli. The ester rich polyester backbone was exposed to horse liver esterase enzyme and the release of Doxorubicin was monitored. The dialysed solution of dox laoded polyester was confined in a dialysis tube of 1kD cutoff in easterase rich environment. The presence of enzyme would ensure to chop off the ester backbone and cause the release of doxorubicin drug into the reservoir. The measure of doxorubicin release was measured by measuring the absorbance of the solution outside the membrane at various times intervals and it was observed. A control experiment was carried out keeping the dialysed solution in solution of pH 7.4 which mimicked the physiological blood conditions

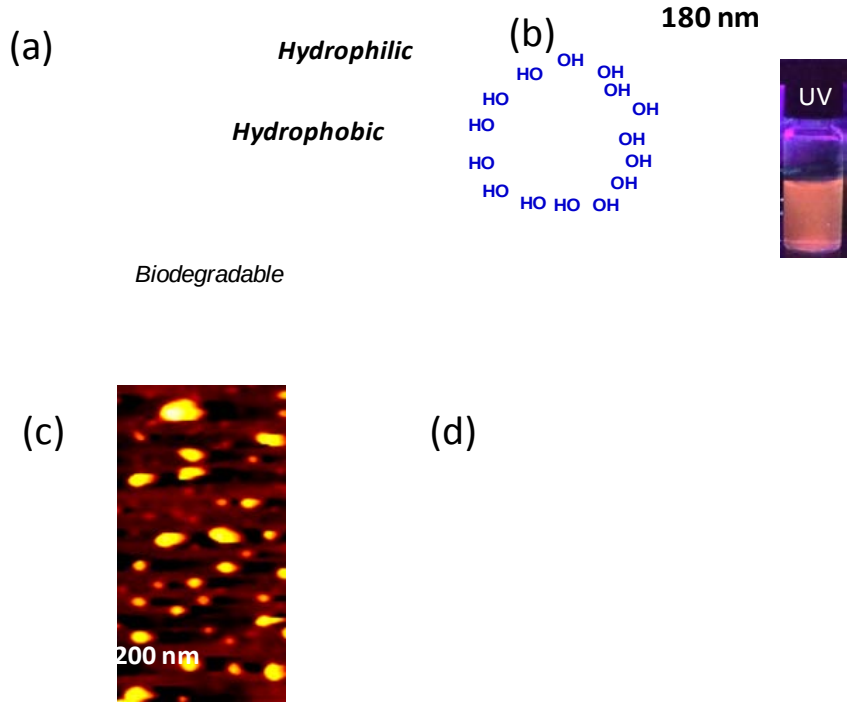

Figure 5.13: *Schematic of self assembled nanoparticle of Hydroxyl functionalised Polyester loaded with DOX (a), DLS and photograph of DOX laoded nanoparticles under UV lamo (b), AFM of P-H nanoparticle loaded with DOX (c), esterase sensitive release of DOX from the nanoparticles (d).*

The intensity of absorbance at λ_{abs} wavelength of doxorubicin revealed the amount of doxorubicin released from the cavity of nanoparticles of the polymers. Monitored up to 35 h at pH 7.4 at 37°C it was found that the doxorubicin leached out only 10% from the nano-cavity of the micelle and 90 % of the loaded cargo was stable in the scaffold, which reflects on the efficacy of the nano-scaffold in the blood physiological conditions. The nano-scaffold stability in presence of esterase enzyme was determined by the cleavage of the ester backbone, which de-stabilize the loading capabilities of the small polymer chains (resulted from the cleavage of the long chain polyesters) and released the loaded cargo. Doxorubicin was found to release up to 50% within 35 h which was three times higher than in absence of esterase. The complete release of the doxorubicin needed more optimisation. The biodegradability of the polyester was hence demonstrated suing the esterase enzyme and it was speculated that lysosomal esterase could act as trigger the release of the loaded cargo in the intracellular regions once the nanoparticles are taken up by the cells.

The ability of the nanoparticles as drug delivery agent was studied by the demonstration of cellular uptake of doxorubicin in MCF 7 cells. These cells treated with doxorubicin were further subjected analyzed by confocal microscopy. MCF 7 cells were treated with 2.0 μg concentration free DOX as well as polymer loaded with same amount of doxorubicin for 4h. The doxorubicin was excited using the laser 561 nm in confocal microscope and imaged in the red channel. A control was also maintained keeping the cells without the nanoparticles and imaged under red channel to ensure the absence of any background noise from the cells. Alexa dye conjugated with phalloidin was used to selectively stain cytoskeleton actin filaments network of the cells. This was excited at 488 nm and imaged in green channel. The phalloidin imaging gave insight to the morphology of the cell under consideration (figure 5.14 top row). The treatment of doxorubicin caused no significant change to the morphology of the cells making them available to give information on the cellular uptake of the doxorubicin. Image J software was used to produce the images of the cells for the uptake of the doxorubicin. The killing of cells occurs via DNA intercalation mechanism of doxorubicin in the nucleus of the cell, therefore determination of location of doxorubicin within the cell was crucial to analyse. Therefore the nucleus of the cells was stained with DAPI to render them blue in color

under excitation of 405 nm laser and these were imaged under blue channel. Looking at the images of the cells in figure 5.14 the green and blue channel showed the location of the nucleus with respect to the actin filaments stained by phalloidin. In the second column the DAPI staining gives the position of the nucleus in the cells. The third column in the figure shows red emission, and in the control no signal appeared from the cells confirming no red background signal from the cells. The third column in each figure was representative of the phalloidin stained which showed the intact morphologies of the cells.

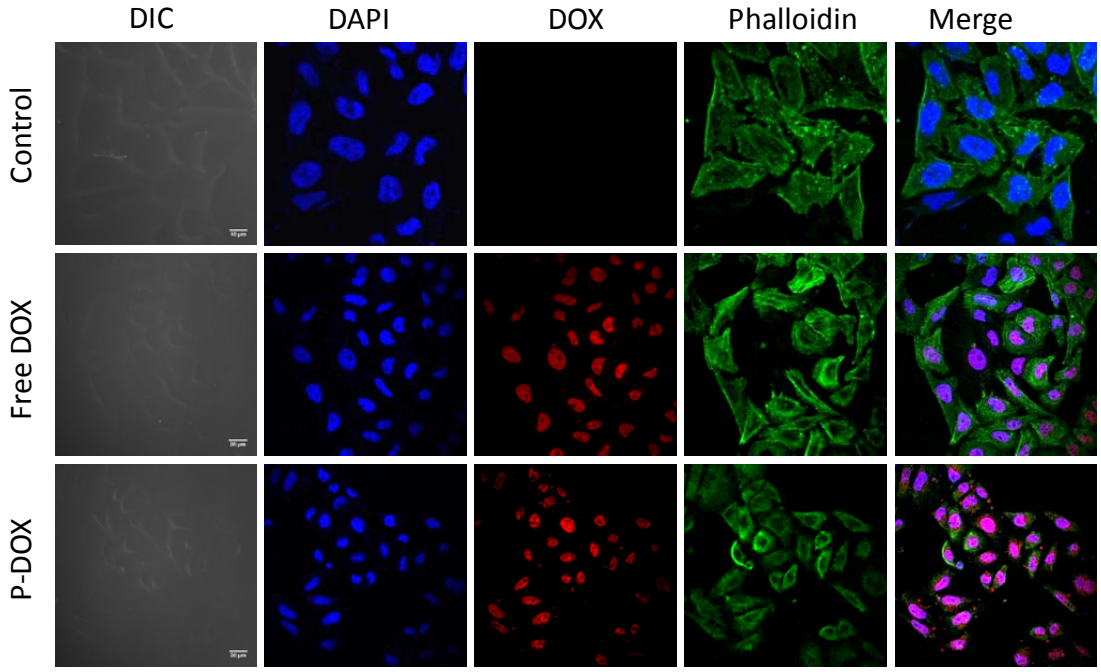

Figure 5.14: *The cellular imaging of control cells (top most row), free DOX (second row) and Polymer loaded with DOX (third row) in MCF 7 cell lines.*

The merged image shown in figure 5.14 showed clear demarcation of the nucleus and doxorubicin uptake in the cells. The free doxorubicin and DOX loaded nanoparticles were exposed to the MCF 7 cells keeping the concentration of the doxorubicin molecule same, to understand the efficacy of the nano-particle in drug delivery. Free DOX diffused in the cells and was found accumulate in the nucleus and was shown by the magenta colour as the overlap of the DAPI and the DOX. The nanoparticles however were taken up by the endocytosis and the DOX was delivered to the cytoplasm of the cells and it made way to the nucleus of the cells as show ion figure 5.14 third panels where red emission was visible throughout the cells. It was

interesting to note that the emission intensity of DOX from the nucleus was higher than the free DOX and it was qualitative evidence towards higher uptake of the DOX in the cells.

5.3.5 Synthesis of Carboxylic functionalised Polyesters and Pt-Prodrug

The carboxylic functionalised polyesters were synthesised to enhance the functionality of the hydroxyl polymer by using succinic anhydride, the anhydride of butanedioc acid. The nucleophilic hydroxyl in the presence of the base causes the hydrolytic cleavage of the succinic anhydride ring by attacking at one of the carbonyl group of the ring, resulting in addition of the nucleophile (polymer chain in this case) and formation of succinic acid. The presence of two hydroxyl groups on each repeating unit of the polymer enhanced the possibility of rendering two carboxylic groups on each repeating unit of the polymer in close vicinity, and ideal position for binding of cis-platin aqua complex discussed later in section.

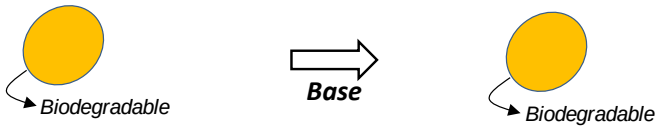

Figure 5.15: *Synthesis of Novel Carboxylic functionalised L-aspartic acid Based polyesters*

The post polymerisation was carried out by using 0.5 equivalents of succinic anhydride with aim to synthesis 50% carboxylic units on the entire polymer chain to retain the amphiphilic character of the polymer. (The stiching of the hydrophobic cisplatin would compromise the hydro-philicity of the hydroxyl polymer). The successful incorporation of carboxylic groups in the L-aspartic acid based was followed by covalent stitching of the cisplatin aqua complex to synthesis of the Cisplatin conjugated polyesters. Dialysis method was used to remove the unattached cisplatin molecules and OPD assay was carried out to determining the amount of binding to the polyesters.

(a)

(b)

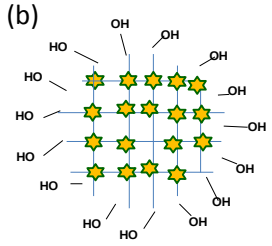

(c)

(d)

Figure 5.16: *Cisplatic aqua complex and stiching to P-OH-SA (a), The self assembly of carboxylic functionalised polyesters stitched with cisplatin (b),DLS of Pt Pro drug (c) and their loading determination using OPD.*

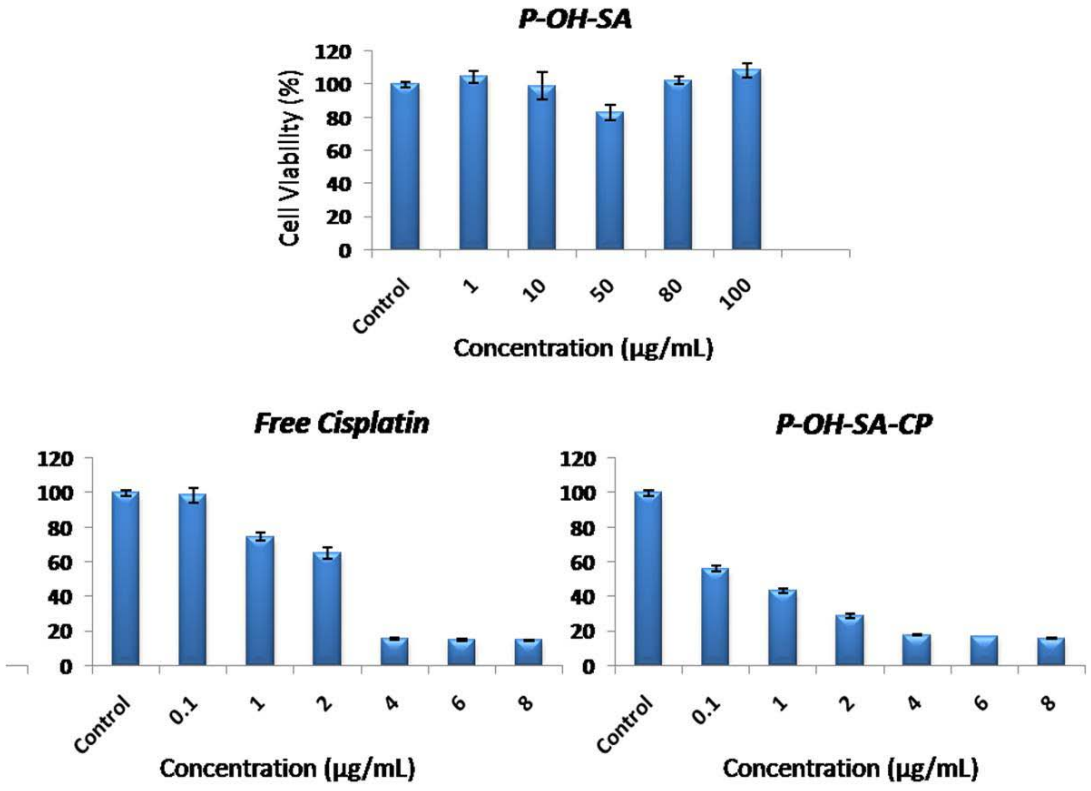

Figure 5.17: *MTT assay for Pt based Pro- drug of P-SA*

Cytotoxicity of the polymer was investigated in breast cancer cell lines (MCF 7), by incubating different concentrations of nascent polymer with cells for 72h. The MMT assay revealed that 100% cells were viable in presence of polymer upto 100 µg/mL, i.e. the polymer is highly biocompatible even at high concentrations. The cell killing efficacy of free cisplatin and polymer-stitched with cisplatin were also determined using the MTT Assay. As can be seen from figure 5.17, both the free CP and P-OH-SA-CP stitched polymer were able to achieve > 80 % cytotoxicity in MCF 7 cells at a concentration of 8 µg/mL which makes these polymers as efficient platinum drug carrier. `

5.3.6. Synthesis of TPE tagged Hydroxyl-polyester

The unique luminescent properties inherited by aggregation induced emission was rendered to the hydroxyl functionalised amphiphilic polyester by covalently attaching to tetra-phenylethene units in the backbone of the polyester by using melt stable TPE diol (2) used in chapter 4. In the melt polycondensation set up, monomer (2) (see scheme 5.1) was taken with 0.97 moles of dodecanediol and 0.03 moles of TPE diol. TPE diol (3.0%) was used as feed and comparing the peaks from the proton NMR it was found to incorporate 3.23 % which showed the robust nature of melt poly-condensation. (Scheme 5.3) The percentage incorporation of the acetal monomer and that TPE diol were determined using the proton NMR. The peaks at 4.17 and 4.06 corresponded to two new ester peaks from the acetal methoxy ends and 4.32 and 4.24 belonged to new esters from the TPE diol. The eventual deprotection of the TPE conjugated polyester yielded the formation of hydroxyl functionalised P-OH-TPE as shown in scheme 5.3.The ^{1}H-NMR for the P-Ac-TPE and P-OH-TPE has been shown in fugre 5.18. The aromatic peaks appered in the region from 7.5 -6.5 ppm and the other protons have been marked with alphabets on the spectra (see figure 5.18). The important peak worth noticing was the 6 methyl protons that appeared at 1.48 ppm in the spectra which disappeared upon deprotection with the TFA acid. This marked the formation of the hydroxyl polymer and furthers the amphiphilic polyester P-OH_TPE was used for future studies.

Scheme 5.18: *Synthesis of AIE active hydroxyl functinalised polyesters*

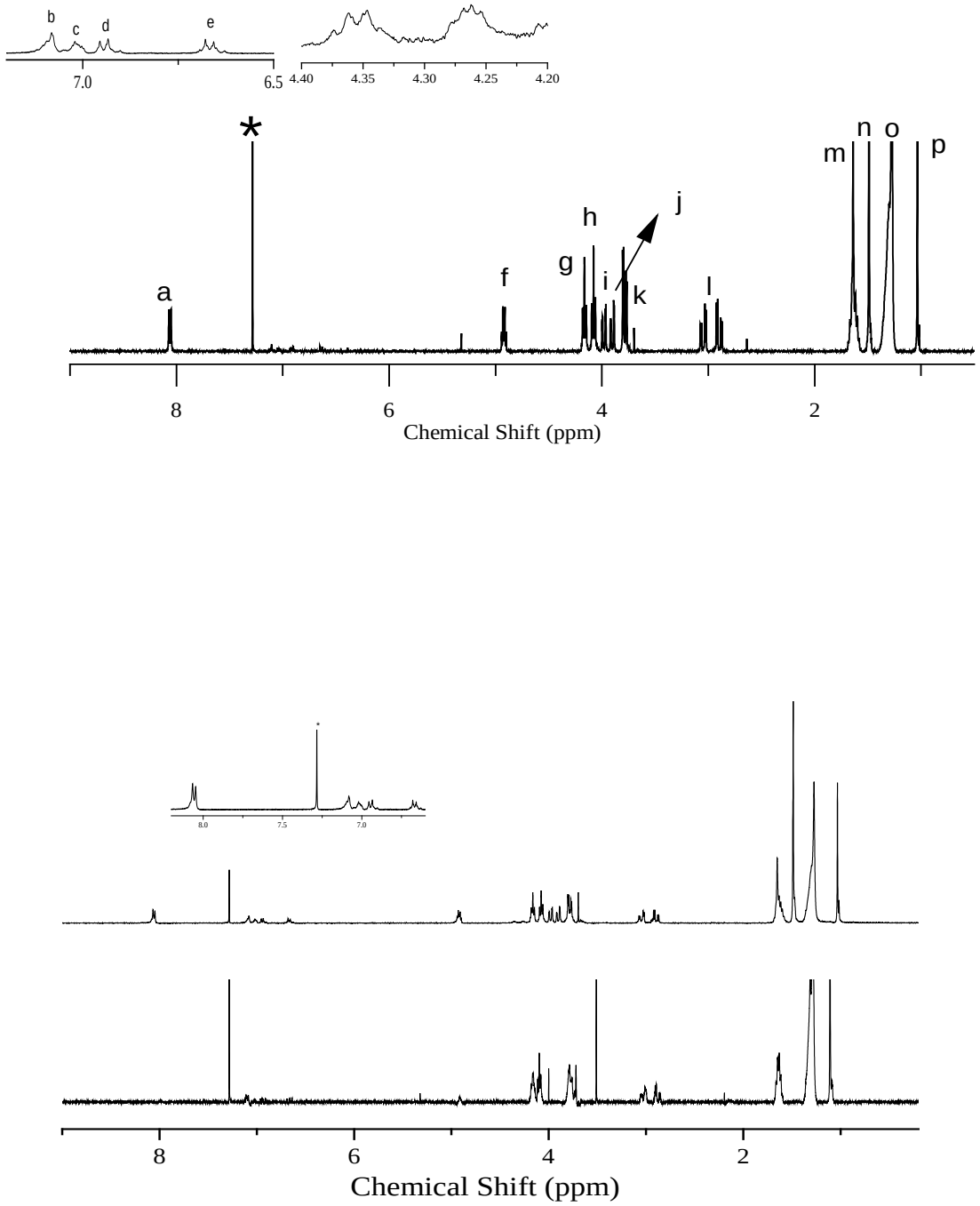

Figure 5.18: *^{1}H-NMR of TPE conjugated Acetal and Hyroxyl functionalised Polyester.*

Mn = 14000
Mw = 35000
PDI = 2.4

Figure 5.19: *GPC chromatogram for P-Ac-TPE in THF*

5.3.7. AIE-assisted TPE-DOX Theronastic FRET probe

DMSO was chosen as a good solvent to understand the expanded morphology of the polymer and water was chosen as a bad solvent to study the collapsed state of the polymer. The polymer forms nano-particle in aqueous environment following dialysis method explained in the experimental section. The DLS of the nanoparticles have been shown in figure 5.20 the size of the particle was found to be ~ 200 nm which was further corroborated using AFM imaging which showed spherical nanoparticles. The incorporation of TPE diol in the main chain backbone of the polymer offered the insight to the folding and unfolding of the polymer based on the emission properties of the TPE which shows emission upon excitation only upon aggregation. In aqueous solutions the polymer chain confine into coil like nanoparticles causing aggregation in the TPE molecules therefore, it is evident that polymer chains in aqeuos solutions give maximum aggregation emission. However in DMSO the polymer chain expand causing the TPE molecules to move far apart from each other and this affects the TPE e mission by diminishing it. Therefore the TPE conjugated polyesters where dialysed and subjected to chain in environment from DMSO to water environment, and the changes in the emissive properties of the polymer were observed from the emission spectra generated from these solutions.

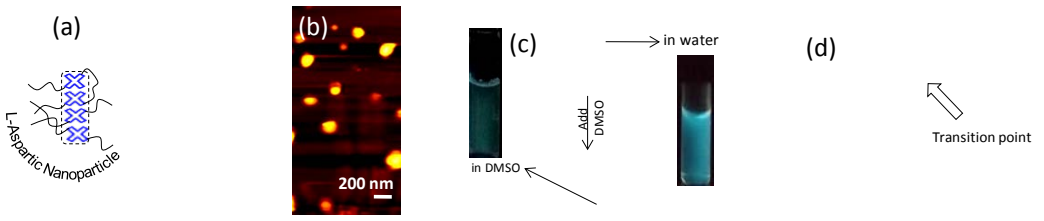

Figure 5.20: *The schematic of TPE conjugated polyester nanoparticle in water and its DLS (a), the AFM image of the TPE conjugated nanoparticles (b), the emission of P-$_{TPE}$ in various water-DMSO combination (c), the plot of λ_{em} max at 470 nm in fluorescence spectra of P-TPE vs the % of water in water DMSO combinations.(d).*

As predicted before the emission of the nanoparticles in water was maximum and fluorescence was "turned on". The fluorescence could be fined tune by varying the DMSO water composition as shown in figure 5.20 (b) and it could be "turned off" in DMSO. The tuning and stability of TPE self emission made it ideal for biological imaging applications. The absorbance signature of the TPE chromophore was same in all the compositions of the DMSO water ruling out the possibility of the emission due to solubility. The polyester solution were excited at λ_{abs} max of TPE chromophore i.e., at 330 nm. The fluorescence emission varied in intensity at λ_{ems} 470 nm which was due to TPE chromophores in the aggregated states with maximum intensity at 4×10^5 (see figure 5.20). Therefore the micellar nanoparticles were ideal to provide the hydrophobic core that brought the TPE chromophore in close vicinity as much to cause the aggregation. The plot of the intensity vs solvent composition showed a transition point at 50 % water DMSO composition from which the intensity of the aggregated species reduced drastically showing the impact of the disassembly of the polymer scaffold in DMSO solvent and reflecting at the transition point of the polymer from compact nanoparticles to the expanded fibrous structure.

5.3.8 Encapsulation of Doxorubicin Drug

As the acetal polymer had formed an ideal hydrophobic core for encapsulation of high loading of DOX in its core, therefore efforts were made to load the P-TPE acetal polymer with doxorubicin hydrophobic anticancer drug. DOX was loaded into the nanoparticles using dialysis method and high loading content was observed for the DOX loading. As the schematic in the figure shows fluorescence output 'turn off' state of the polyester in the DMSO solvent, the TPE molecules gain their emission once in the aggregated state that is in the nanoparticles from as shown in figure 5.21 b. The self emission of the fine tuned TPE self assembled polymer successfully formed essential for the transfer to DOX molecule confined within the nano-cavity. The aggregated TPE species acted as a donor species and formed FRET pair with the DOX as acceptor species and the schematic of the FRET between the aggregated TPE and DOX molecule.

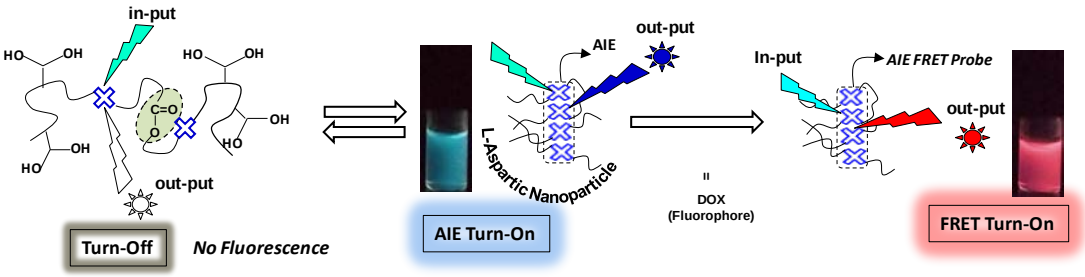

Figure 5.21: *Self assembled nanoparticles of TPE hydroxyl polymer and ODX loaded nanoparticles.*

5.3.9 TPE + DOX FRET probe

The incorporated TPE species forced into aggregated form gave huge aggregation induced emission and it was further used for the FRET to the DOX acceptor molecules. This kind of self assembly related behaviour was crucial for the nanoparticles to act as dual functional nano material as it provided both the therapeutic as well imaging characteristics. The DOX loading rendered the nanoparticles with therapeutic activities and made these essentially anticancer agents. The TPE emission on the other hand acted as indicator of the nanoparticles in its

stable self assembled form. The FRET between aggregated TPE species and the acceptor DOX molecules gave the polymers three important characteristics namely:

1) Self emitting TPE molecules that could help track the polymers in live cells to understand the uptake and entry of the nanoparticles in the cells.
2) The efficient loading of DOX molecule in the nanoparticles made these essentially nano-materials for cancer cell killing.
3) The FRET between the TPE and DOX species made possible the tracking of the nanoparticles as well as the point of release if the DOX into the cells based on difference in the FRET emission based on the intracellular stimuli acting on the nanoparticles.

These characteristic properties of the nanoparticles made the L-aspartic acid based hydroxyl functionalised polyesters into intelligent nanomaterials that could be used for theranostic applications.

The FRET pair encapsulated nanoparticles containing donor TPE aggregated species as well as the acceptor DOX drug molecules made these nanoparticles ideal to understand the effect of the esterase enzyme on the ester backbone of the polymer. The schematic in figure 5.22 shows the FRET emission from the DOX drug molecules from the TPE emission.

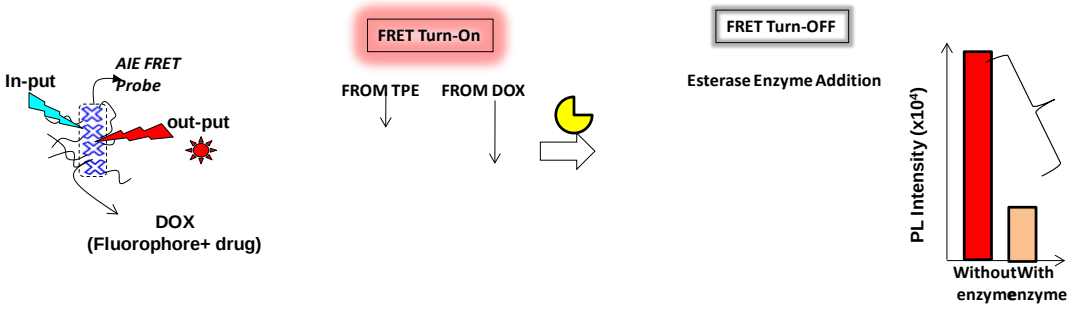

Figure 5.22: *FRET based DOX loaded nanoparticles.*

The schematic shows formation of self assembles stable spherical nano-particle confining the aggregated TPE chromophore and the DOX drug molecules in close proximity of each other, which causes efficient energy transfer from the TPE chromophores to the DOX species. The fluorescence emission of the DOX loaded P-TPE acetal nanoparticles has been show in figure 5.22 b and it was observed that upon excitation of DOX loaded nanoparticles at λ_{exc} 330 nm the emission foe TPE aggregated chromophores was observed at λ_{exc} maxima of 450 nm with intensity of 5×10^4, as well as the signature peak of the DOX species were also observed at 550nm and 600 nm (a signature emission of the doxorubicin, shown in figure 5.22 b). FRET containing nanoparticles were subjected to esterase enzyme and the fluorescence emission was monitored after 4 h and it was observed that the emission from DOX vanished and and the TPE emission was found to increase as it no longer participated in FRET and the emission reached to 7×10^4 which indicative of the regaining of the FRET energy. This observation was made on the basis of effect of the esterase enzyme on the backbone of the polymer constituting the nanoparticles. As anticipated the polymer nanoparticles are taken up by the endocytosis and the lysosomal esterase would act as stimuli to cleave the ester rich backbone of the polymer causing release of the doxorubicin molecules which could act on the cellular DNA to kill or inhibit growth of cancer cells.

The P_{TPE} acetal nanoparticles laoded with DOX were incubated with MCF 7 cells and the cells were fixed and studied for the uptake of the nanoparticles. It was ensured however that the un-encapsulated nanoparticles in the media were washed thoroughly before fixing the cells. The TPE chromphores were excited using 405 nm in confocal microscope, and the DOX species were excited with 488 nm laser and imaged in blue and red channels respectively. For FRET experiments DOX was not excited but its emission was observed at red channel upon exciting the TPE chromophores. The red emission observed from the DOX species was direct evidence towards the FRET occurrence within the cellular domains.

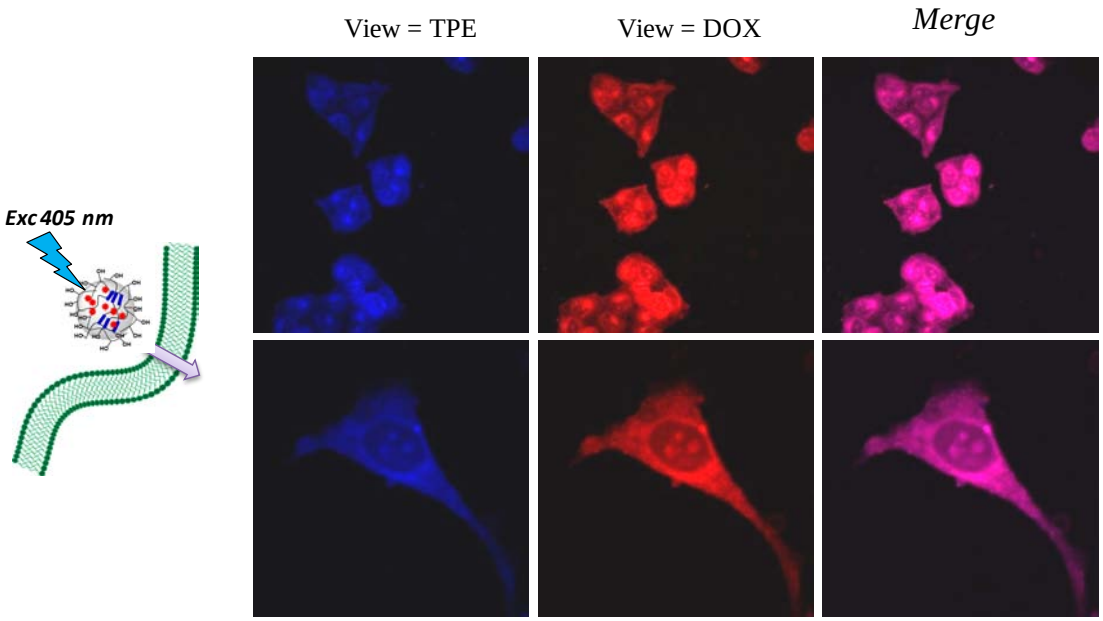

Figure 5.23: *Demonstration of FRET in MCF 7 cells*

The merged image shown in figure 5.23 extreme right panel shows the the co-accumulation of TPE and DOX residues throughout the cells maintaining the fact that the L-aspartic acid based hydroxyl polyesters were ideal for delivery of DOX throughout the cell making them ideal carrier for DOX drug species.

5.4. Conclusion

A promising class of L-amino acid based completely biodegradable, enzyme responsive hydroxyl and carboxylic dual functional polyesters were synthesised. L-aspartic acid was converted into di-ester functionalmonomer containing acetal protecting amine groups. The methyl esters of the aspartic acid monomer underwent melt-transesterification with dodecane diols, an aliphatic hydrophobic di-functional alcohol to produce high molecular weight polyesters under the presence of melt-transesterification catalyst Titanium tetrabutoxide at 150°C. The hydroxyl functionalised polyesters were synthesised by acid assisted deprotection of the acetal gropus in each repeating units of the polymer. The free hydroxyl groupd were furter converted into carboxylic functional groups by using ring opening of succinic anhydride. The hydroxyl and carboxylic functionalised polymers were well characterised using proton and carbon NMRs which showed complete disappearance of the ester groups of the monomer essential for building up of high molecular weight polymers.. The GPC analyses further showed monmodal distribution of the polesters and the thermal properties of the polyester using TGA analyses showed that these polymers were stable upto 300°C. The DSC analysis of these polesters revelaed that they were amorpohus in nature. The hydrophilic hydroxyl and carboxylic gropus along witht he ahydrophobic aliphatic backbone made these polymer amphiphilic in nature and enabled these to self assemble into spherical nanoaprticles in water. Successful and high amount of DOX loading was achieved and the cellualr uptake and killing were demonstrtaed in MCF 7 cells. The carboxylic polymers were further covalently stiched to a second anticancner drug cisplatin there killign were demonstarted in the cancner cells. These polyesters were further transformed into AIE active polymers by introducing custom designed tetraphenylethene units in the backbone during melt condensation process making these polymers nanoscaffolds luminescent in nature. The DOX loaded AIE active polymers wereused to demonstarte FRET at the cellualr level where agrregated TPE acted as donor andDOX acted as acceptor. The new class of hydroxyl and carboxylic polyesters were found to be ideal candidates for bio-imaging as well cell killing agents makinf them ideal for theranostic applications.

References

1. N. Larsona; H. Ghandeharia *Chem Mater*. **2012**, *24* 840–853.
2. Sutton D, Nasongkla N, Blanco E, Gao J. *Pharm Res.* **2007**, *24*, 1029-46.
3. Gauthier MA, Gibson MI, Klok HA. *Angew Chem Int Ed Engl.* **2009**, *48*, 48-58.
4. J. Zhao; H. Wang; J. Liu; L. Deng; J. Liu; A. Dong; J. Zhang *Biomacromolecules* **2013**, *14*, 3973-3984.
5. C. Hahn; H. Keul; M. M**ö**ller *Polym Int* **2012**, *61*, 1048-1060.
6. J. Rautio, H. Kumpulainen, T. Heimbach, R. Oliyai, D. Oh, T. Järvinen and J. Savolainen, *Nat. Reviews*,**2008**, *7*, 255-270.
7. Ja-Hyoung Ryu, Reuben T. Chacko, Siriporn Jiwpanich, Sean Bickerton, R. Prakash Babu, and S. Thayumanavan* *J. Am. Chem. Soc.*, **2010**, *132* (48), pp 17227–17235
8. A. O. Saeed; J. P. Magnusson; E. Moradi; M. Soliman; W. Wang; S. S. K. J. Thurecht; S. M. Howdle; C. Alexander *Bioconjugate Chem.*, **2011**, *22* , 156–168
9. R. Tong; Ind. Eng. *Chem. Res*. **2017**, *56*, 4207-4219.
10. X. Hu; Shi. Liu; X. Chen; G. Mo; Z. Xie; X. Jing *Biomacromolecules*, **2008**, *9*, 553-560.
11. Q. Hao; J. Yang; Q. Li; Y. Li; L. Jia; Q. Fang; A. Cao *Biomacromolecules*, **2005**, *6*, 3474-3480.
12. C. Japu,; A. Martínez de Ilarduya; A. Alla; Y. Jiang; K. Loos; S. Muñoz-Guerra *Biomacromolecules* **2015**, *16*, 868−879
13. J. Wu; P. Eduard; L. Jasinska-Walc; A. Rozanski; B. A. J. Noordover; D. S. van Es; Cor E. Koning *Macromolecules* **2013**, *46*, 384−394
14. L. Chang; L. Deng; W. Wang; Z. Lv; F. Hu; A. Dong; J. Zhang *Biomacromolecules* **2012**, *13*, 3301−3310.
15. B. J. Kline, E. J. Beckman, A. J. Russell *JACS* **1998**, *120*, 9475-9480.
16. C. K. Williams *Chem. Soc. Rev*., **2007**, *36*, 1573-1580.
17. B. Begines; F. Zamora; E. Benito; Ma de G. García-Martín, J. A. Galbis *Journal of polymer science part a polymer chemistry* **2012**, *50*, 4638-4646.
18. I. Taniguchi; W. A. Kuhlman; A. M. Mayes; L. G. Griffith *Polym Int* **2006**, *55*, 1385-1397.

6. Overall Conclusion

It may be concluded that this thesis work aims at developing multifaceted polymeric nano-structures, which can be used for more potent drug delivery applications, especially for cancer treatment. For the same effect, L-Amino based di- and tri-block copolymers were used to synthesize amphiphilic and biodegradable polyester molecules which were also fluorescent. Owing to their fluorescent nature these polymeric nano-assemblies could also be employed for bio-imaging in future.

Among L-amino acid, L-aspartic acid was explored as a multi-functional monomer for melt condensation approach. In presence of hydrophobic and hydrophilic diols, it yielded amphiphilic copolymers which were sensitive to pH. The polymer could undergo transformation under two triggering factors: i) low pH or high acidic environment, where the BOC urethane groups undergo cleavage to yield cationic NH_3^+cations, and ii) presence of esterase enzyme, which acts by cleaving the ester backbone of the polymer. The L-aspartic acid polymer was also loaded with curcumin (CUR), doxorubicin (DOX), and topotecan (TPT) drug molecules, and obtained drug polymer conjugate showed high internalisation of the drugs into the nucleus and cytoplasm in breast (MCF 7) and cervical (HeLa) cancer cell lines.

For more effective visualization, along with several other benefits, L-amino acid based polymer was developed, which also demonstrated FRET because of π-conjugation. L-aspartic acid monomers with hydrophilic triethylene glycols and hydrophobic dodecanediol yielded highly luminescent multi-function polymers when trans-esterified with oligo-phenylenevinylene (OPV). When aforementioned polymer was encapsulated with the Nile Red (NR) dye, resulting polymer complex showed extremely efficient excited energy transfer from OPV to NR. OPV-NR FRET probes and OPV-only tagged probes showed cytotoxicity in normal cell lines (Wild-type MEF, WT-MEF), and cancer cells {breast cancer (MCF 7), cervical cancer (HeLa) cells}. Using the FRET, cellular uptake study was conducted, which revealed that these probes could easily transport through cell membranes and accumulate in the cytoplasm. Live cell imaging suggested endocytotic pathway as the mode of entry of

these nanoparticles. The polymers were bio-degradable, owing to various enzymes found in lysosomes.

When tetraphenylethyelene (TPE) diol was incorporated in tagged L-aspartic acid based biodegradable polyester, a new blue-luminescent amphiphilic polyester was obtained, which showed an aggregation induced emission (AIE). This new polymer self assembled into compact spherical nanoparticles, and could encapsulate both hydrophobic NR and green-fluorophore drug Curcumin (CUR). Two new FRET systems with TPE-NR and TPE-CUR pair were constructed along with a third probe with CUR-NR FRET pair in a non-TPE polyester. All four systems, i.e. nascent TPE nanoparticles, TPE-CUR,TPE-NR, and CUR-NR FRET, were found to be non-toxic to cells. The FRET as probe was used to study the cell uptake, and subsequent bio-degradation of these nanoparticles in *in vitro* experiments.

L-aspartic acid polyester was converted to enzyme-responsive hydroxyl and carboxylic acid dual functional polyesters by melt esterification ofmethyl esters of the aspartic acid monomer with dodecane diol. The hydroxyl group obtained from acid assisted deprotection converted to carboxylic functional group by using ring opening of succinic anhydride. The resultant amphiphilic polymer was found to self-assemble into spherical nanoparticles in water. The obtained polymer showed high loading capacity for DOX, and covalent stitching with cisplatin, resulting in exhibition of anti-cancer activity of MCF 7 cells. The polymer was further made luminescent by incorporating TPE in the backbone. The AIE polymer thus formed showed FRET with TPE acting as donor andDOX acting as acceptor.

7. Future direction

The hydroxyl based polymers synthesised in the chapter 5 have opened up avenue for a variety of chemical conjugation of drugs, ligand for targeting receptors, fluorophores. A plethora of conjugations can broaden the scope of functionalization in the polymeric scaffolds. In another attempt the BOC protected L-aspartic acid based polyesters have been de-protected completely to develop high charged cationic polyesters that were functionalised post polymerisation by fluorophore dansyl units and as a proof of concept were used for cell imaging applications. These cationinc polymers in future are anticipated to act as potential antibacterial agents and conjugating these with fluorophore can be used to study and compare interaction and uptake of neutral vs cationinc polymers in the human cells. The cationinc polymers also may find applications in binding DNA and could be used for gene delivery agents.

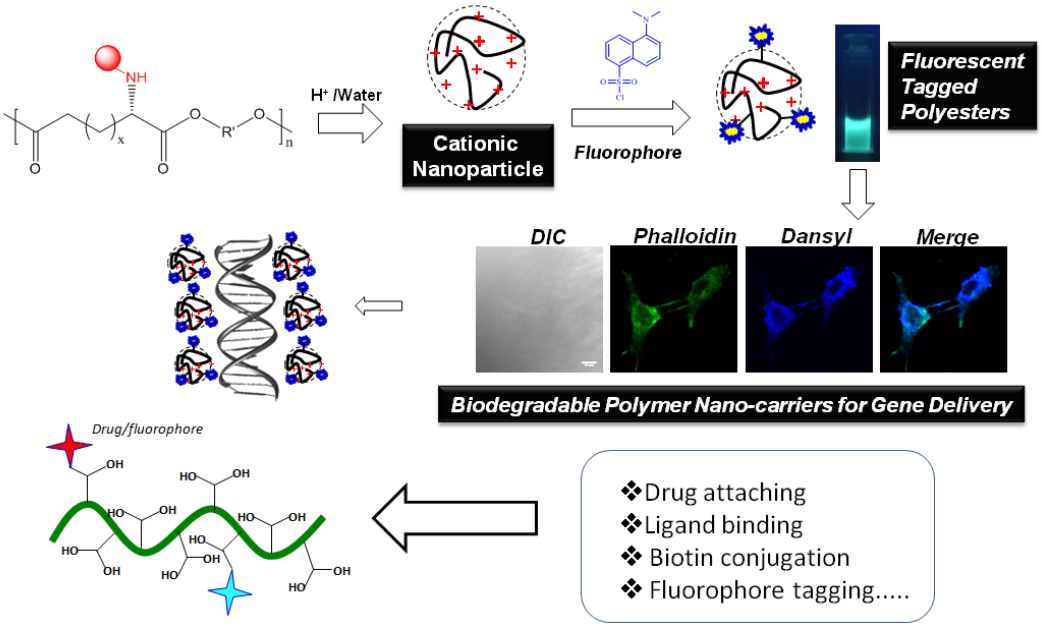

8. List of Publications

1. Sonashree, S.; Jayakannan, M. Enzyme and pH Dual Responsive L-Amino acid Based Biodegradable Polymer Nano-carrier for Multi-drug Delivery to Cancer Cells, ***J. Polymer Sci., Part A: Polym. Chem,*** **2016**, *54*, 3279-3293 (appeared as cover page).
2. Sonashree, S.; Jayakannan, M. π-Conjugate Fluorophore-tagged and Enzyme-responsive L-Amino acid Polymer Nano-carrier and their Colour-tunable Intracellular FRET Probe in Cancer Cells, ***Biomacromolecules,*** **2017**, *18*, 2594-2609.
3. Aluri, R.; Sonashree, S.; Joshi, D.; Jayakannan, M. Multi-stimuli-responsive Amphiphilic Poly(ester-urethane) Nano-assemblies Based on L-Tyrosine for Intracellular Drug delivery to Cancer Cells. ***Biomacromolecules***, **2018**, *19*, 2166-2181(*not included in the thesis*)
4. Sonashree, S.; Jayakannan, M. TPE-Tagged Polymer Nano-assemblies for Aggregation Induced Emission (AIE) Assisted FRET Probe. *Sonashree Saxena & Manickam Jayakannan , Manuscript Submitted.*
5. Sonashree, S.; Jayakannan, M. Development of Hydroxyl Functionalised L-Aspartic Acid Polyester and its AIE Probe for Cancer Treatment. *Sonashree Saxena & Manickam Jayakannan, Manuscript under preparation.*

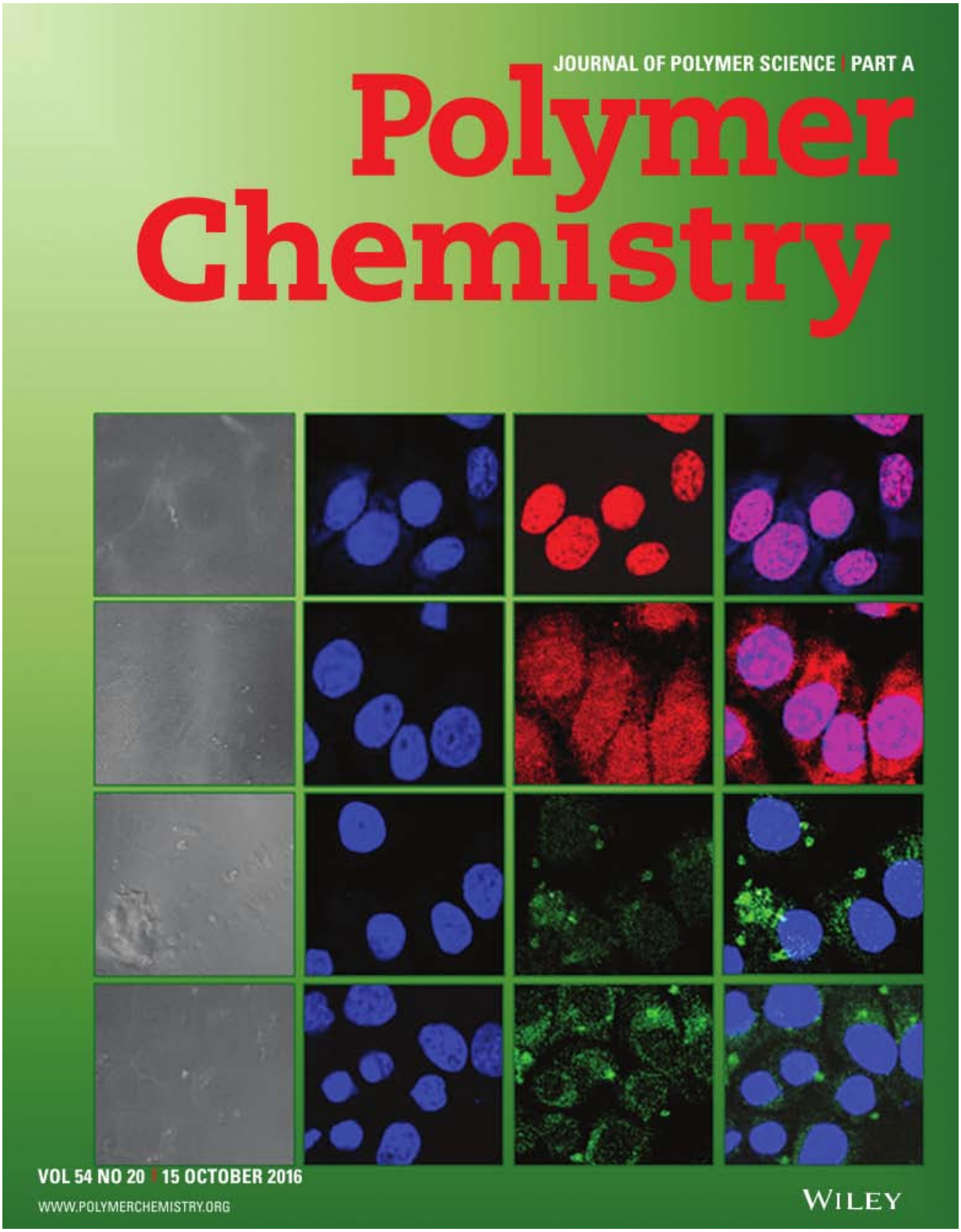

Saxena, S.; Jayakannan, M. Enzyme and pH Dual Responsive L-Amino acid Based Biodegradable Polymer Nano-carrier for Multi-drug Delivery to Cancer Cells, *J. Polymer Sci., Part A: Polym. Chem*, 2016, *54*, 3279-3293 (appeared as cover page).

JOURNAL OF POLYMER SCIENCE Polymer Chemistry WWW.POLYMERCHEMISTRY.ORG ARTICLE

Enzyme and pH Dual Responsive L-Amino Acid Based Biodegradable Polymer Nanocarrier for Multidrug Delivery to Cancer Cells

Sonashree Saxena, Manickam Jayakannan

Department of Chemistry, Indian Institute of Science Education and Research (IISER) Pune, Dr. Homi Bhabha Road, Pune 411008, Maharashtra, India

Correspondence to: M. Jayakannan (E-mail: jayakannan@iiserpune.ac.in)

Received 17 May 2016; accepted 15 June 2016; published online 19 July 2016

DOI: 10.1002/pola.28216

ABSTRACT: We report a new pH and enzyme dual responsive biodegradable polymer nanocarrier to deliver multiple anticancer drugs at the intracellular compartment in cancer cells. Natural L-aspartic acid was converted into multifunctional monomer and polymerized to yield new classes of biodegradable aliphatic polyester in-build with pH responsiveness. The transformation of side chain BOC urethanes into cationic NH_3^+ in the acidic endosomal environment disassembled the polymers nanoparticles (pH *trigger-1*). The biodegradation of aliphatic polyester backbone by esterase enzyme ruptured the nanoassemblies and released the drugs in the cytoplasm (*trigger-2*). The polymer scaffolds were capable of delivering multiple drugs such as doxorubicin, topotecan, and curcumin (CUR). The cytotoxicity of the nascent and drug-loaded nanoparticles were tested in cervical (HeLa) and breast (MCF-7) cancer cell lines. The nascent polymer nanoscaffolds were found to be nontoxic to cells whereas their drug-loaded nanoparticles exhibited excellent killing. Confocal microscopic images revealed that the drug-loaded polymer nanoparticles were taken up by the cells and the dual degradation process delivered the drugs to nucleus and established the proof-of-concept. The present investigation opens up new platform for L-amino acid based polyester scaffolds, for the first time, in the intracellular drug delivery in cancer treatment. © 2016 Wiley Periodicals, Inc. J. Polym. Sci., Part A: Polym. Chem. **2016**, *54*, 3279–3293

KEYWORDS: polyesters; drug delivery systems; self-assembly; pH responsiveness; enzyme responsiveness

INTRODUCTION Polymer nanoassemblies responsive to intracellular stimuli are emerging as important class of nanocarriers for delivering anticancer drugs and genes in cancer therapy.[1,2] Polymer nanocarriers are typically taken up by the cells through endocytosis process and they are internalised by acidic early and late endosomes ($6.0 \geq pH = 5.0$) at cellular level (Fig. 1).[3] Subsequent disassembly or degradation of polymer assemblies at the lysosomal compartments by enzymes delivered the drugs/genes in the cytoplasm for apoptosis or cell death.[4] Therefore, the development of intracellular multistimuli polymers provide excellent opportunity to enhance the drug delivering capabilities of polymer nanoassemblies.[5] In the last few years, polymer scaffolds having intracellular responsiveness to enzyme,[6–11] pH,[12–19]or combination of these triggers together[20–23] were reported for drug delivery. In most of these examples, pH and enzyme were employed to disassemble the polymer scaffold; unfortunately, the fate of digestion (or biodegradation) of the remaining long polymer chains were not clearly understood. This is partially associated with the nonbiodegradation of majority of the synthetic polymer carriers and also the selection of their monomer constituents from un-natural resources. Hence, it would be more appropriate to design biodegradable polymer nanocarriers based on biological monomer resources for cancer treatment and biomedical applications. Among the natural resources, L-amino acids are particularly interesting since their sequence and structure control the three dimensional assemblies of proteins and their enzymatic action in biological system.[24,25] L-Amino acid based synthetic amphiphilic oligopeptides[26] and diblock polypeptides[27–30] were tailor-made and their supramolecular nanoscaffolds were employed for tissue engineering,[31,32] drug and gene delivery,[33,34] etc. Unfortunately, these synthetic peptides were known to encounter difficulty for biodegradation at the intracellular level.[35] Digestive enzymes such as α-chymotrypsin and trypsin (available in intestine) were found to be highly specific in action to cleave peptide sequences in proteins. For example, α-chymotrypsin-enzyme selectively cleaves C-terminal of phenyl alanine, tyrosine and tryptophan peptide linkages[36–38] whereas trypsin-enzyme cleaves the C-terminal of arginine and lysine in peptides.[7] Hence, it is very difficult to predict or programme the enzymatic biodegradation of synthetic polypeptides in drug

Additional Supporting Information may be found in the online version of this article.

Article

Cite This: Biomacromolecules 2018, 19, 2166−2181

pubs.acs.org/Biomac

Multistimuli-Responsive Amphiphilic Poly(ester-urethane) Nanoassemblies Based on L-Tyrosine for Intracellular Drug Delivery to Cancer Cells

Rajendra Aluri, Sonashree Saxena, Dheeraj Chandra Joshi, and Manickam Jayakannan*

Department of Chemistry, Indian Institute of Science Education and Research (IISER) Pune Dr. Homi Bhabha Road, Pune 411008, Maharashtra, India

Supporting Information

ABSTRACT: Multistimuli-responsive L-tyrosine-based amphiphilic poly(ester-urethane) nanocarriers were designed and developed for the first time to administer anticancer drugs in cancer tissue environments via thermoresponsiveness and lysosomal enzymatic biodegradation from a single polymer platform. For this purpose, multifunctional L-tyrosine monomer was tailor-made with a PEGylated side chain at the phenolic position along with urethane and carboxylic ester functionalities. Under melt dual ester-urethane polycondensation, the tyrosine monomer reacted with diols to produce high molecular weight amphiphilic poly(ester-urethane)s. The polymers produced 100 ± 10 nm spherical nanoparticles in aqueous medium, and they exhibited thermoresponsiveness followed by phase transition from clear solution into a turbid solution in heating/cooling cycles. Variable temperature transmittance, dynamic light scattering, and ^{1}H NMR studies revealed that the polymer chains underwent reversible phase transition from coil-to-expanded chain conformation for exhibiting the thermoresponsive behavior. The lower critical solution temperature of the nanocarriers was found to correspond to cancer tissue temperature (at 42−44 °C), which was explored as an extracellular trigger (stimuli-1) for drug delivery through the disassembly process. The ester bond in the poly(ester-urethane) backbones readily underwent enzymatic biodegradation in the lysosomal compartments that served as intracellular stimuli (stimuli-2) to deliver drugs. Doxorubicin (DOX) and camptothecin (CPT) drug-loaded polymer nanocarriers were tested for cellular uptake and cytotoxicity studies in the normal WT-MEF cell line and cervical (HeLa) and breast (MCF7) cancer cell lines. In vitro drug release studies revealed that the polymer nanoparticles were stable under physiological conditions (37 °C, pH 7.4) and they exclusively underwent disassembly at cancer tissue temperature (at 42 °C) and biodegradation by lysosomal-esterase enzyme to deliver 90% of DOX and CPT. Drug-loaded polymer nanoparticles exhibited better cytotoxic effects than their corresponding free drugs. Live cell confocal microscopy imaging experiments with lysosomal tracker confirmed the endocytosis of the polymer nanoparticles and their biodegradation in the lysosomal compartments in cancer cells. The increment in the drug content in the cells incubated at 42 °C compared to 37 °C supported the enhanced drug uptake by the cancer cells under thermoresponsive stimuli. The present work creates a new platform for the L-amino acid multiple-responsive polymer nanocarrier platform for drug delivery, and the proof-of-concept was successfully demonstrated for L-tyrosine polymers in cervical and breast cancer cells.

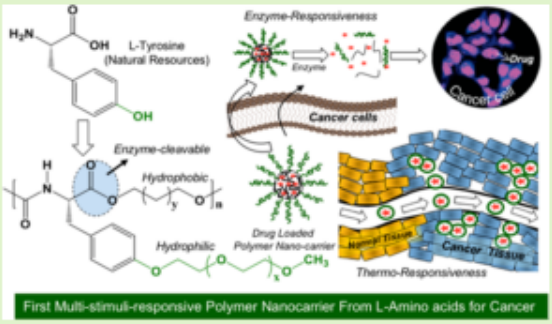

INTRODUCTION

Polymers from L-amino acid resources are important classes of synthetic nanoscaffolds for gene, anticancer drug delivery to cancer cells,[1−3] tissue engineering,[4,5] and so forth. Ring-opening polymerization of NCA monomers from L-amino acids produced well-defined di- and triblock synthetic polypeptides,[6,7] and the self-assembled fibrillar networks, micelles, and vesicles from these polypeptides were explored for diverse applications in the material science and biomedical fields.[8−10] The synthetic polypeptides are found to be excellent biocompatible materials;[11] however, the inherent limitation of the biodegradation of high molecular weight polypeptide chains by intracellular enzymes appears to be one of the major concerns for their long-term applications.[12] In the last decade, significant efforts have been taken to develop nonpeptide polymer analogues from L-amino acid resources based on polycondensation approaches as an alternative strategy for synthesizing biodegradable polymeric nanomaterials.[13] Poly(ester-amide)s,[14−18] poly(ester-urea),[19] poly(disulfide-urethane)s,[20] poly(ester-urea-urethane),[21] and polycarbon-

Special Issue: Biomacromolecules Asian Special Issue

Received: February 25, 2018
Revised: April 13, 2018
Published: April 17, 2018

Aluri, R.; Sonashree, S.; Joshi, D.; Jayakannan, M. Multi-stimuli-responsive Amphiphilic Poly(ester-urethane) Nano-assemblies Based on L-Tyrosine for Intracellular Drug delivery to Cancer Cells. *Biomacromolecules*, 2018, *19*, 2166-2181 (Appeared as cover)

Article

pubs.acs.org/Biomac

π-Conjugate Fluorophore-Tagged and Enzyme-Responsive L-Amino Acid Polymer Nanocarrier and Their Color-Tunable Intracellular FRET Probe in Cancer Cells

Sonashree Saxena and Manickam Jayakannan*

Department of Chemistry, Indian Institute of Science Education and Research (IISER) Pune, Dr. Homi Bhabha Road, Pune 411008, Maharashtra, India

Supporting Information

ABSTRACT: The present investigation accounts one of the first example of enzyme-responsive and π-conjugate-tagged L-amino acid amphiphilic polymer and their fluorescence resonance energy transfer (FRET) probes for color-tunable intracellular bioimaging in cancer cells. Melt polymerizable oligo-phenylenevinylene (OPV) π-conjugated diol was tailor-made and subjected to thermo-selective melt transesterification reaction with multifunctional L-aspartic acid monomer to yield OPV-tagged amphiphilic luminescent polyesters. These amphiphilic polyesters self-assembled through strong aromatic π−π stacking and hydrophilic/hydrophobic noncovalent forces into <200 nm size blue-luminescent nanoparticles in aqueous medium. The OPV-tagged polymer nanoparticles served as FRET donor and encapsulated water insoluble Nile Red (NR) fluorophore as a FRET acceptor. Detail photophysical studies revealed that both the OPV and NR were confined within Förster distance in the polymer nanocontainer and the nanodomains provided appropriate geometry for efficient excitation energy transfer from OPV to NR. Cytotoxicity studies in breast cancer (MCF 7), cervical cancer (HeLa) and normal (Wild-type MEF) cell lines revealed that both the nascent luminescent OPV nanoparticles and OPV-NR FRET probes were nontoxic to cells up to 100 μg/mL. Confocal microscope images confirmed the efficient transportation of polymer and FRET probes across the cell membranes and their preferable accumulation in the cytoplasm of the cells. Lysosomal tracker assisted live cell imaging provided direct evidence for the localization of the polymer nanoparticles at the lysosomal compartments in the cytoplasm. In vitro enzyme-responsive studies revealed that the aliphatic polyester backbone in the polymer nanoparticles was readily biodegradable by lysosomal enzymes like esterase, chymotrypsin, trypsin, and also redox GSH species in the cytoplasm. Selective photoexcitation in confocal microscope exhibited bright OPV blue-luminescence and strong red-emission from NR followed by the excitation energy transfer and occurrence of FRET process at the intracellular environment in cancer cell lines. Both the polymer design and the biodegradable polymer FRET concept are completely new; thus, the present approach opens up new platform of research opportunities for natural L-amino acid based luminescent polymer probes for color-tunable bioimaging in cancer cells.

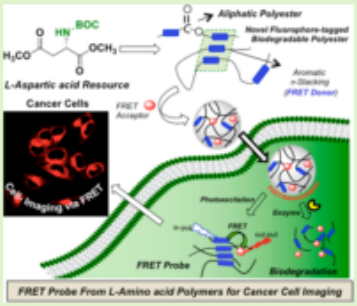

FRET Probe From L-Amino acid Polymers for Cancer Cell Imaging

INTRODUCTION

Fluorescent-probe tagged amphiphilic polymers are emerging as dual-function nanocarriers to deliver anticancer drugs/genes to cancer tissues as well as luminescent biomarkers in cancer diagnosis.[1−7] Förster or fluorescence resonance energy transfer (FRET) is one of the most powerful noninvasive fluorescence probe,[8] and it functions on the basis of selective photo-excitation energy transfer from donor to acceptor chromophores within the nanoconfinement of ≤50 Å.[9] FRET technique is explored for real-time tumor-imaging,[10,11] drug release kinetics,[12,13] studying the self-assembly of amphiphilic block copolymers,[14] protein folding under physiological conditions,[15,16] quadruplex-to-duplex transitions in DNA,[17] molecular interactions at the mammalian cell surfaces,[18−20] two-photon imaging in cancers,[21,22] sensing of bilirubin in human serum,[23] and so on. In the last 2−3 decades, significant advancements made in the area of conducting polymers for optoelectronic devices has opened new arena of opportunities for water-soluble cationic π-conjugated polymers as luminescent bioprobes.[2,24] Cationic and water-soluble polyfluorenes are some of the most important π-conjugated polymers reported for FRET applications.[25−32] Polyacrylate-based random and block copolymers having optical chromophores in the side chains were also reported for FRET applications.[12,14] Unfortunately, the nonbiodegradability of the rigid C−C backbone in the π-conjugated polymers and acrylates are still one of the major challenges to overcome for their wide applicability in biomedical research. New synthetic approaches toward the development of luminescent π-conjugated chromophores in combination with biodegradable polymer backbone would provide new opportunities for biodegradable-cum-luminescent π-conjugated nanoscaffolds in a single system.[33,34]

Received: May 19, 2017
Revised: July 11, 2017
Published: July 12, 2017

DOI: 10.1021/acs.biomac.7b00710
Biomacromolecules 2017, 18, 2594−2609

9. Appendix

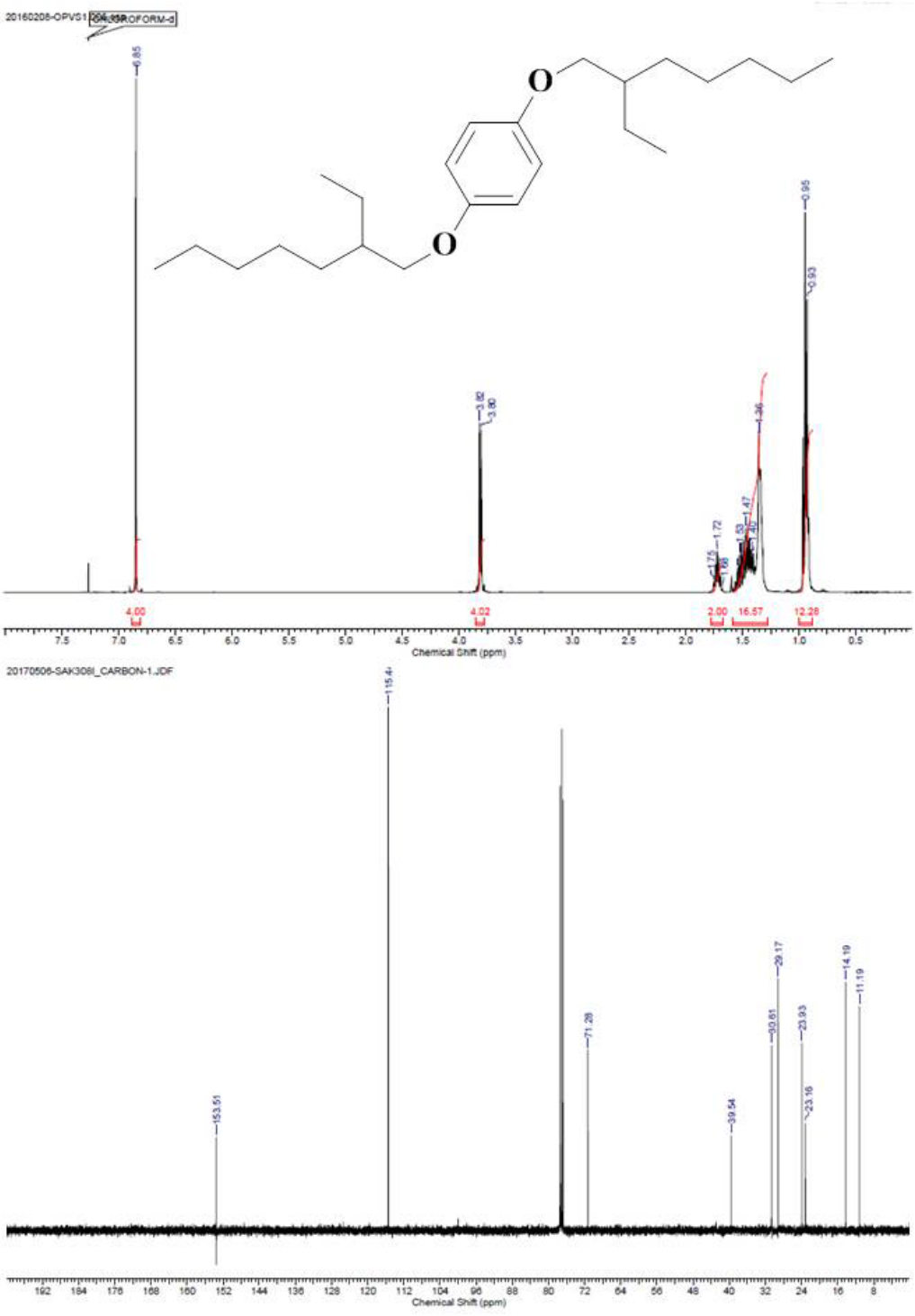

^{1}H-NMR and ^{13}C-NMR of *1,4-Bis(2-ethylhexyloxy) benzene*

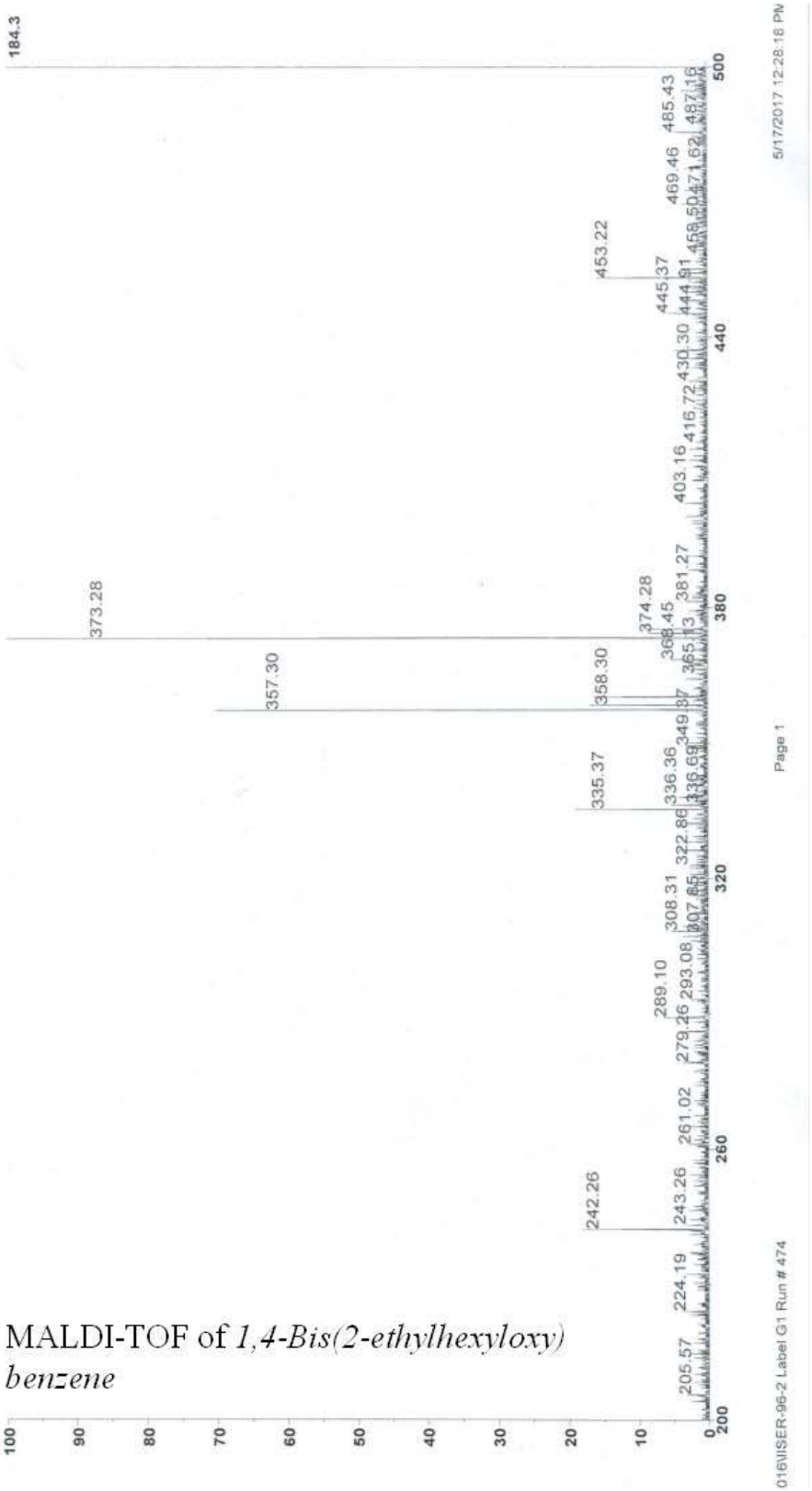

MALDI-TOF of *1,4-Bis(2-ethylhexyloxy) benzene*

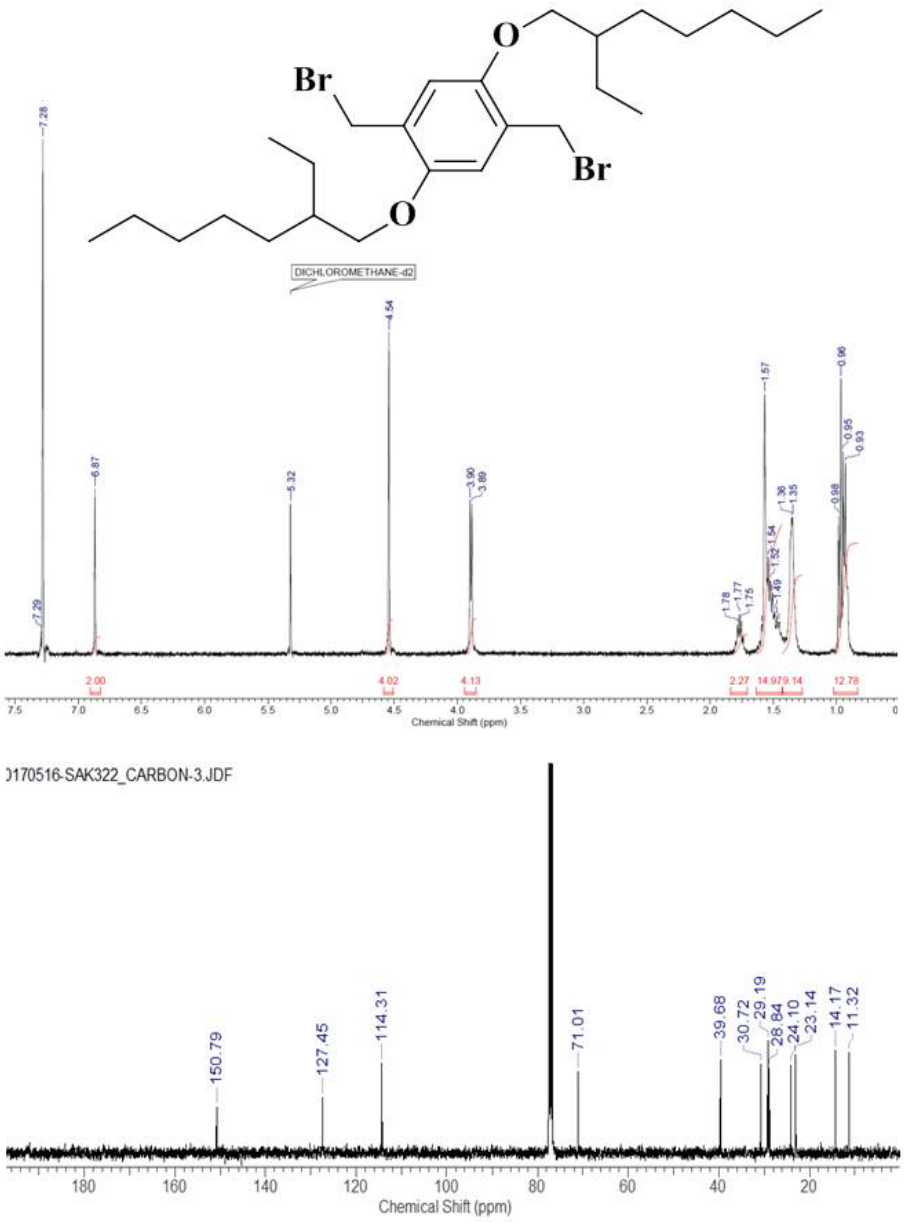

^{1}H-NMR and ^{13}C-NMR of *1,4-Bis(bromomethyl)-2,5-bis-(2-ethylhexyloxy)*

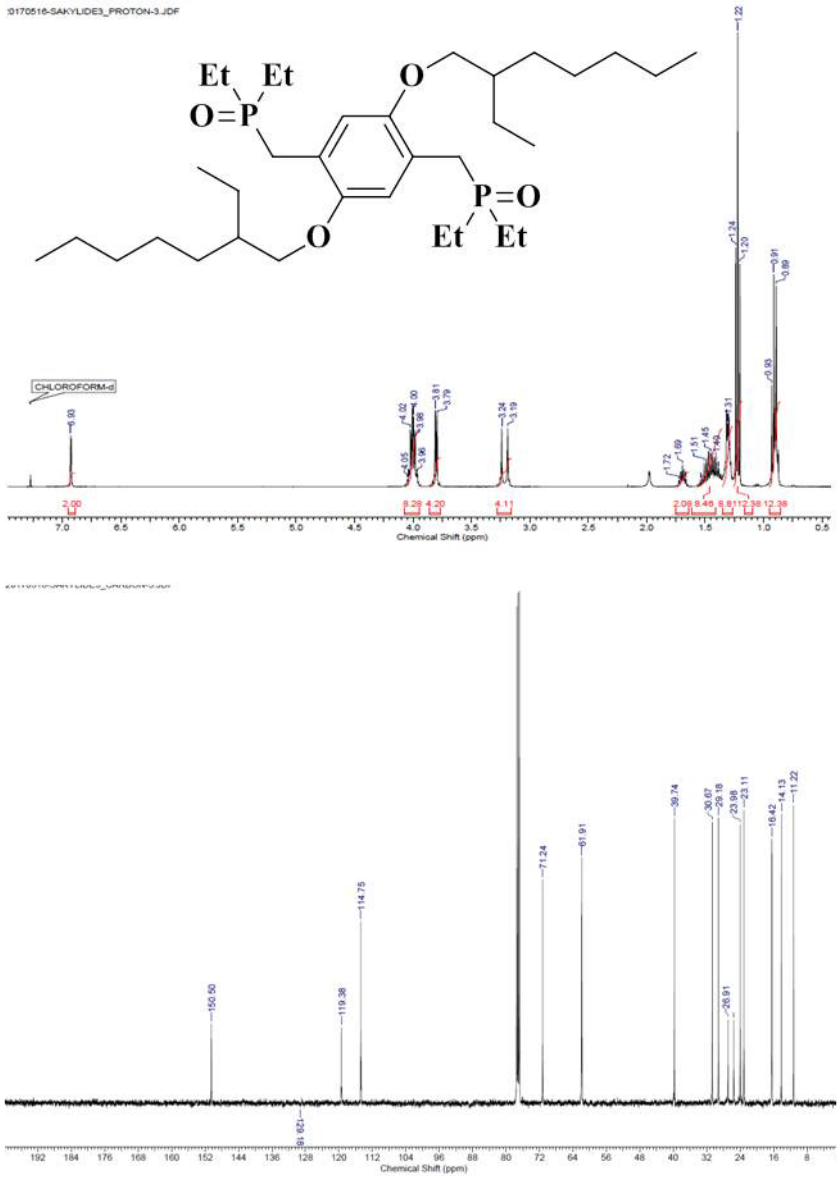

Tetraethyl(2,5-bis(2-ethylhexyloxy)-1,4-phenylene) bis(methylene) diphosphonate

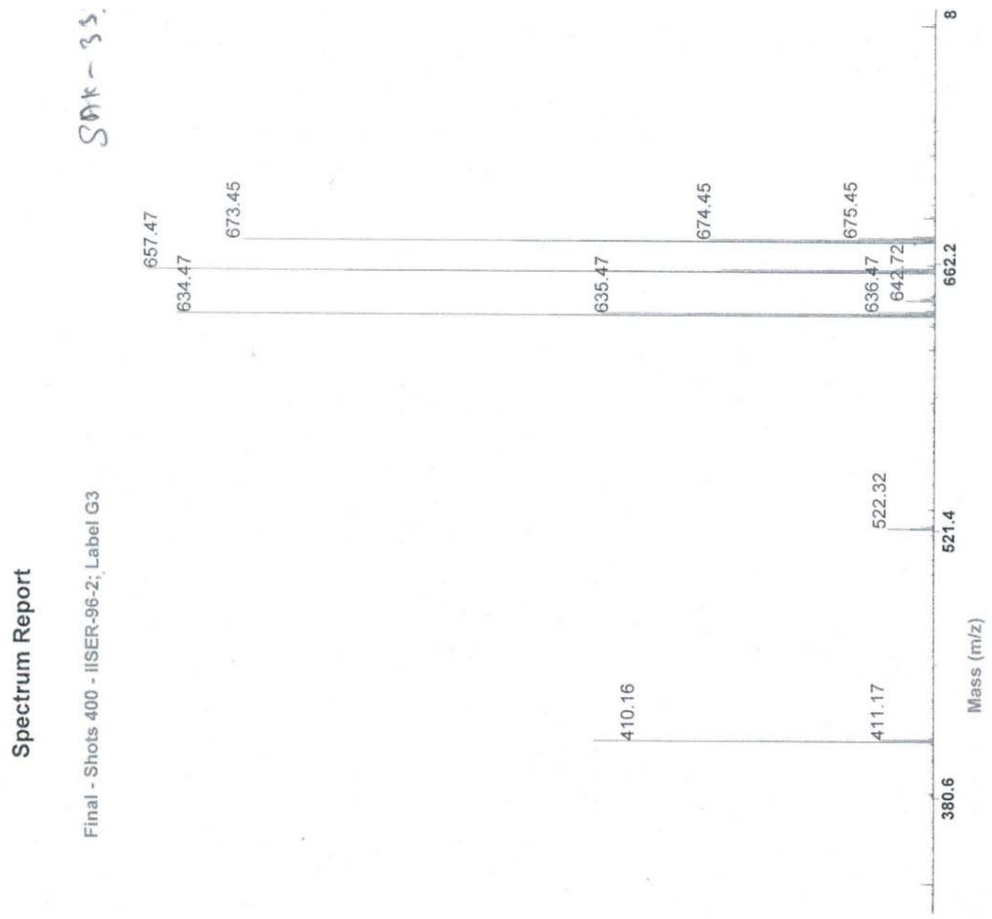

MALDI-TOF of *Tetraethyl(2,5-bis(2-ethylhexyloxy)-1,4-phenylene) bis(methylene) diphosphonate*

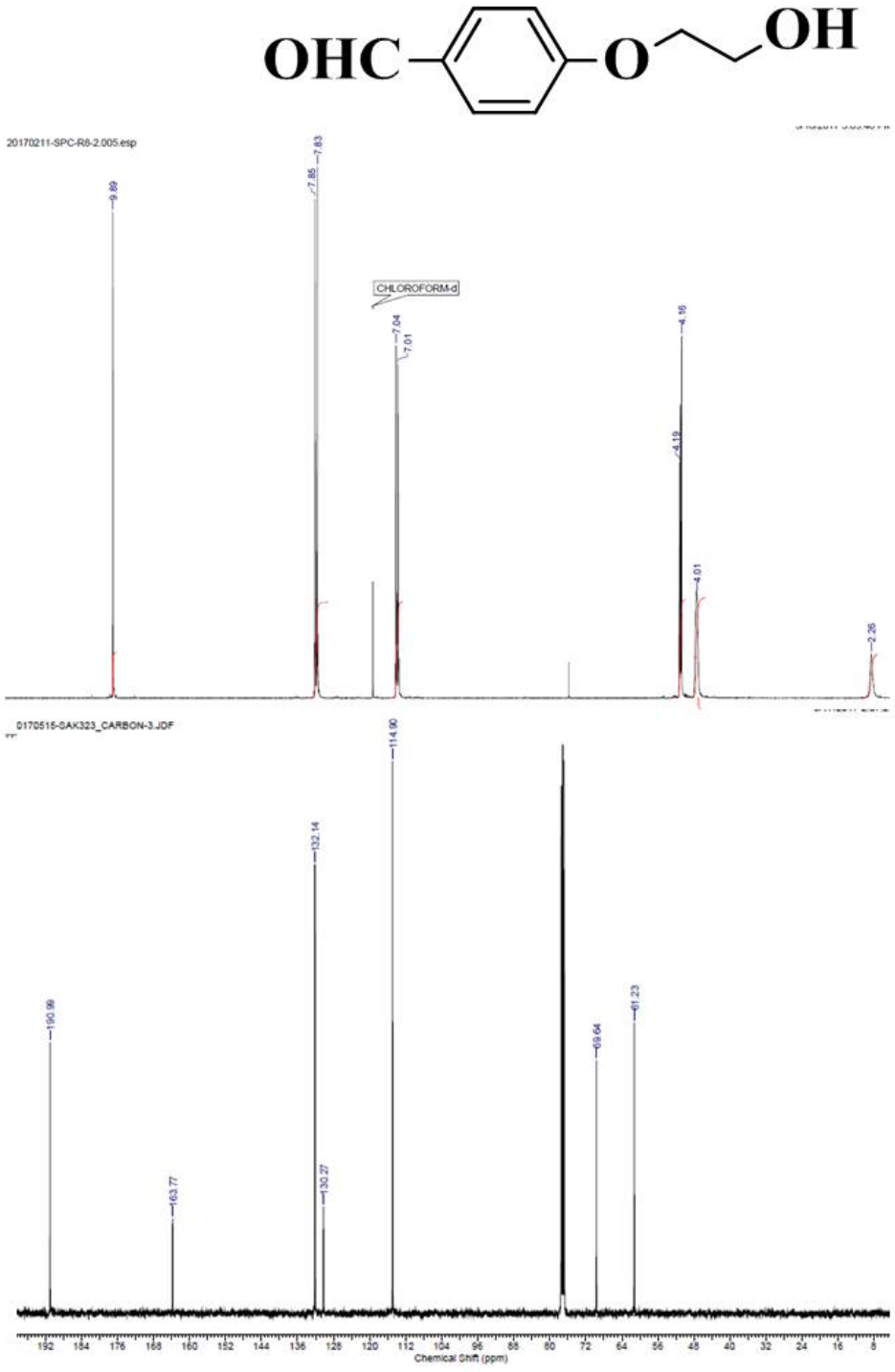

^{1}H-NMR and ^{13}C-NMR of *4-(2-Hydroxyethoxy) benzaldehyde*

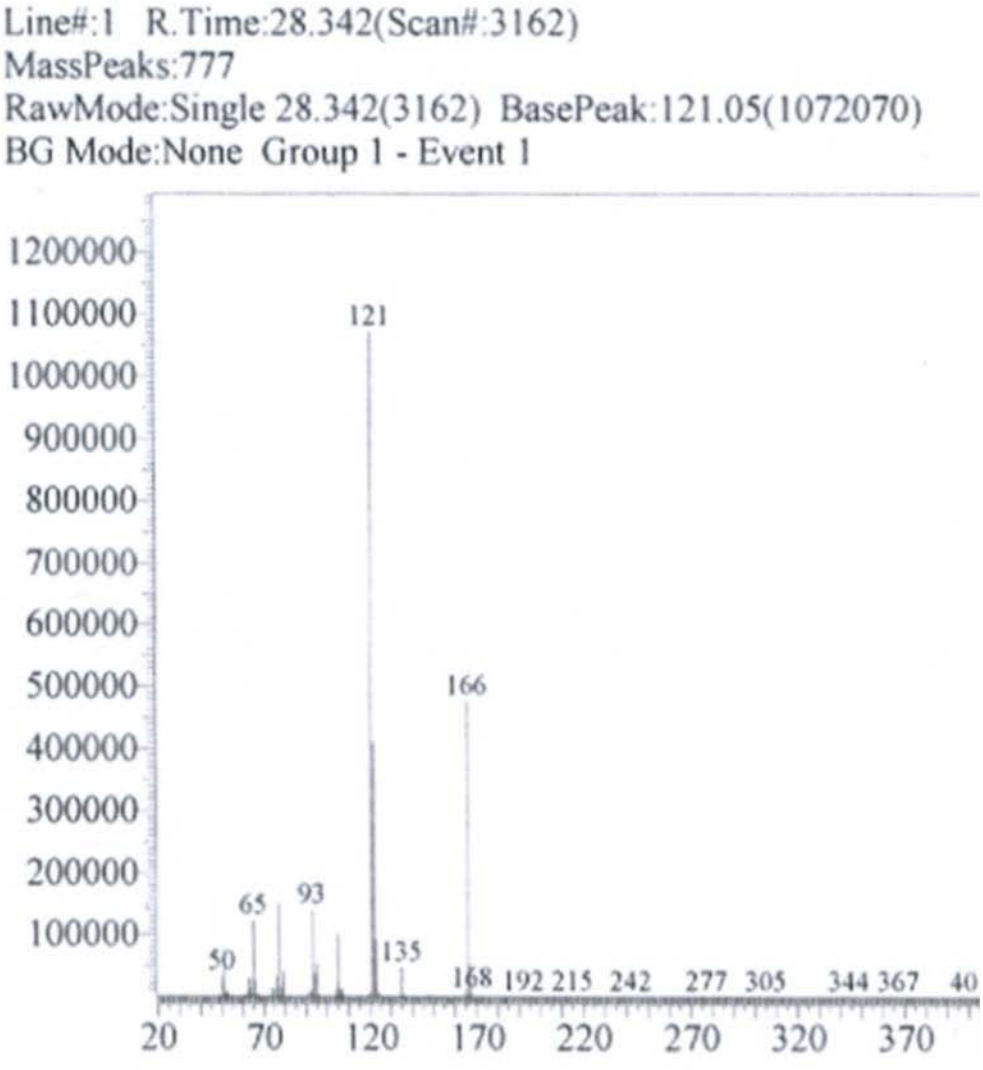

GCMS Spectra of *4-(2-Hydroxyethoxy) benzaldehyde*

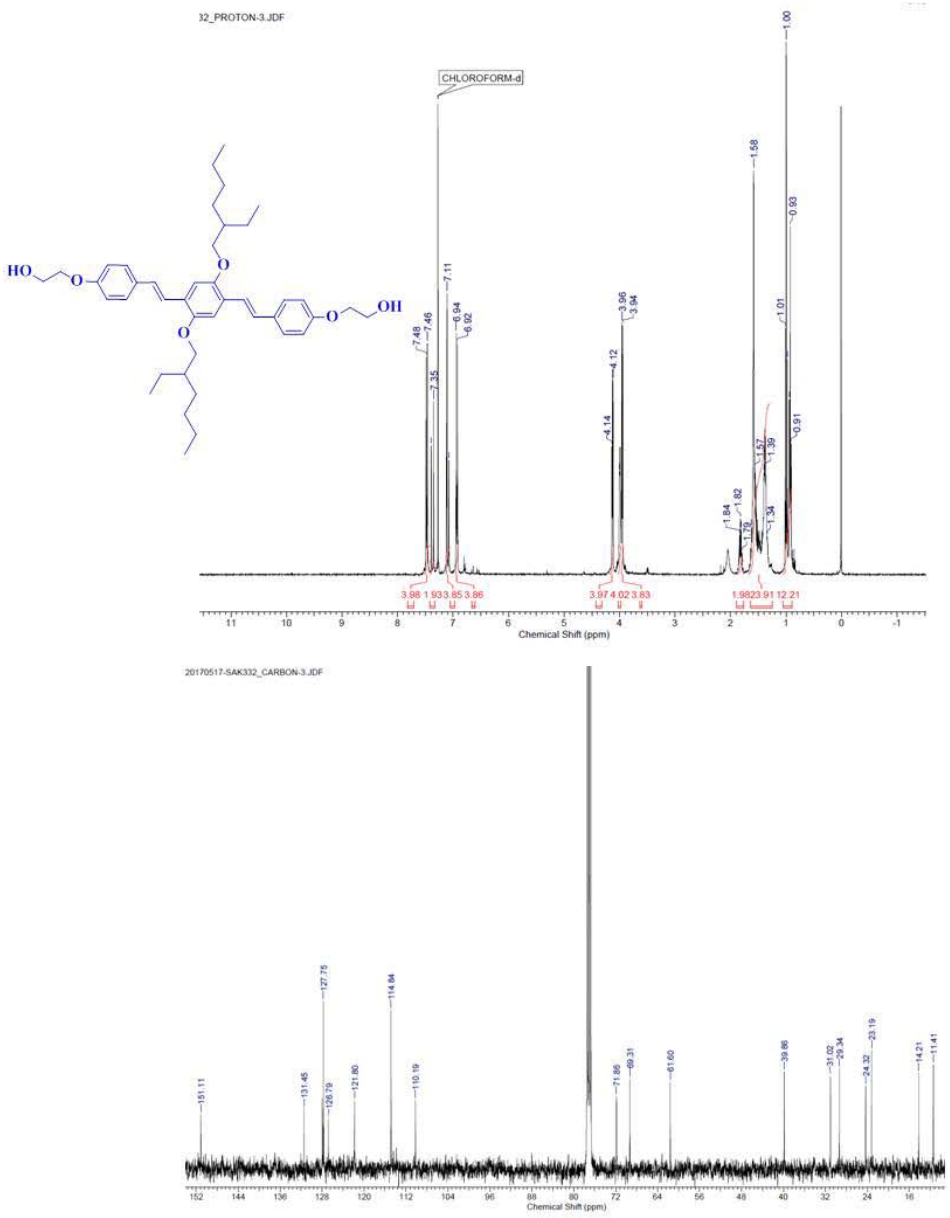

^{1}H-NMR and ^{13}C-NMR of *Hydroxyl Functionalized Oligophenylenevinylene*

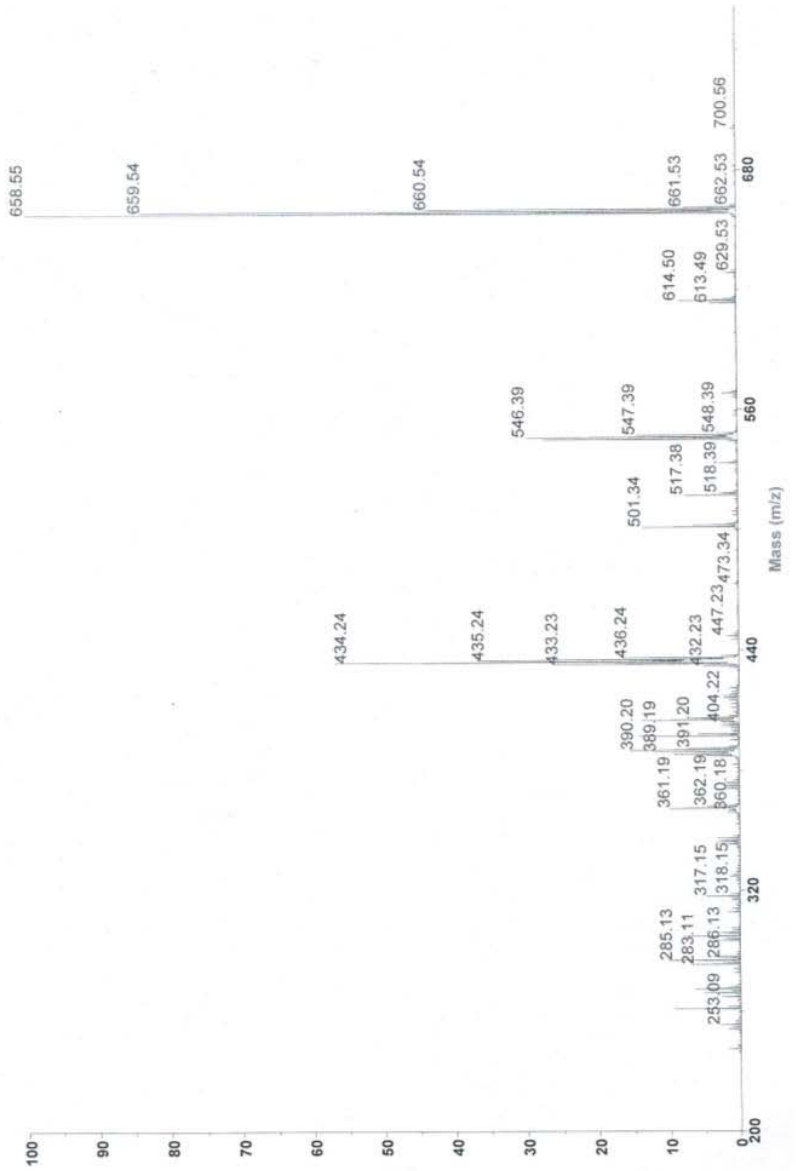

MALDI-TOF spectra of *Hydroxyl Functionalized Oligophenylenevinylene*

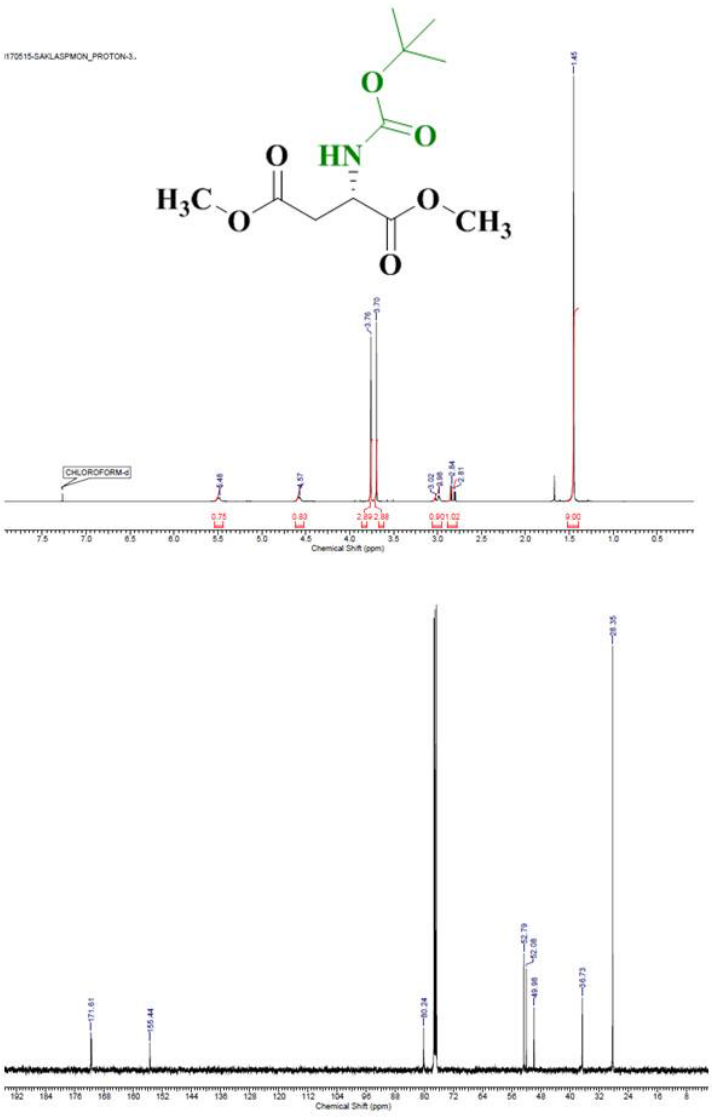

^{1}H-NMR and ^{13}C-NMR of *Dimethyl 2-((tert-butoxycarbonyl)amino)succinate*

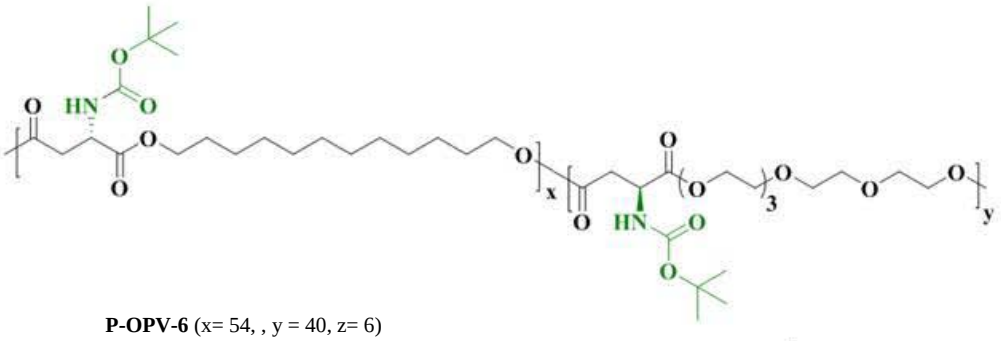

P-OPV-6 (x= 54, , y = 40, z= 6)

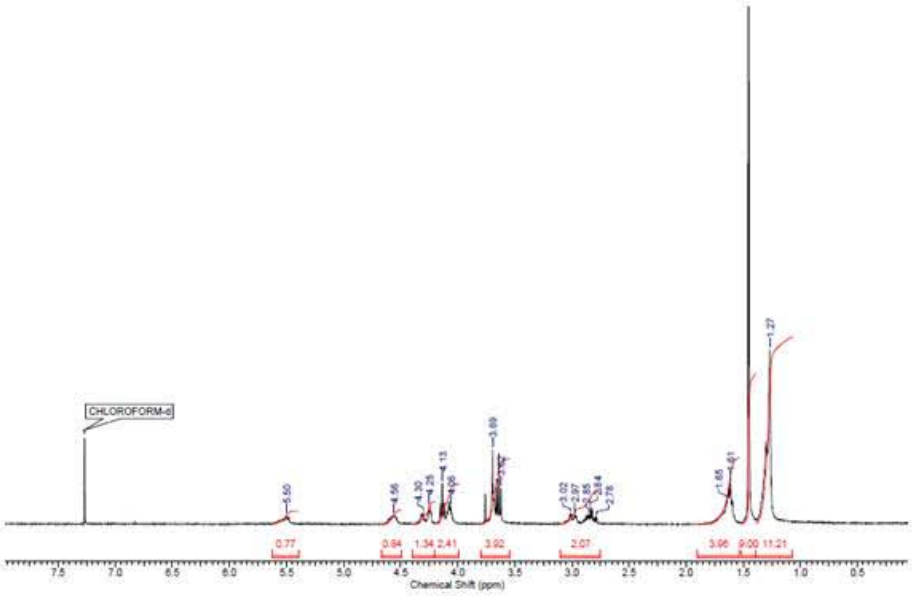

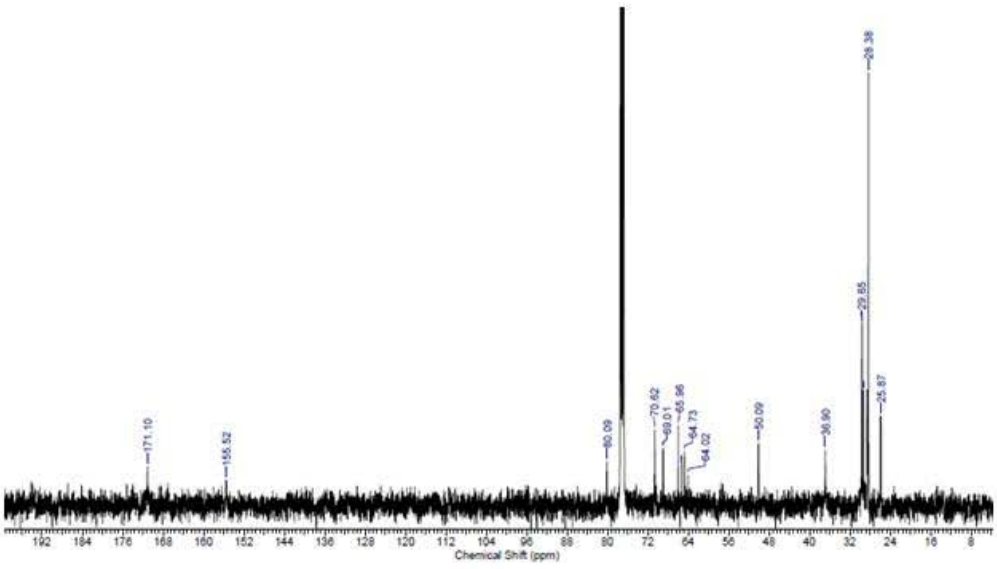

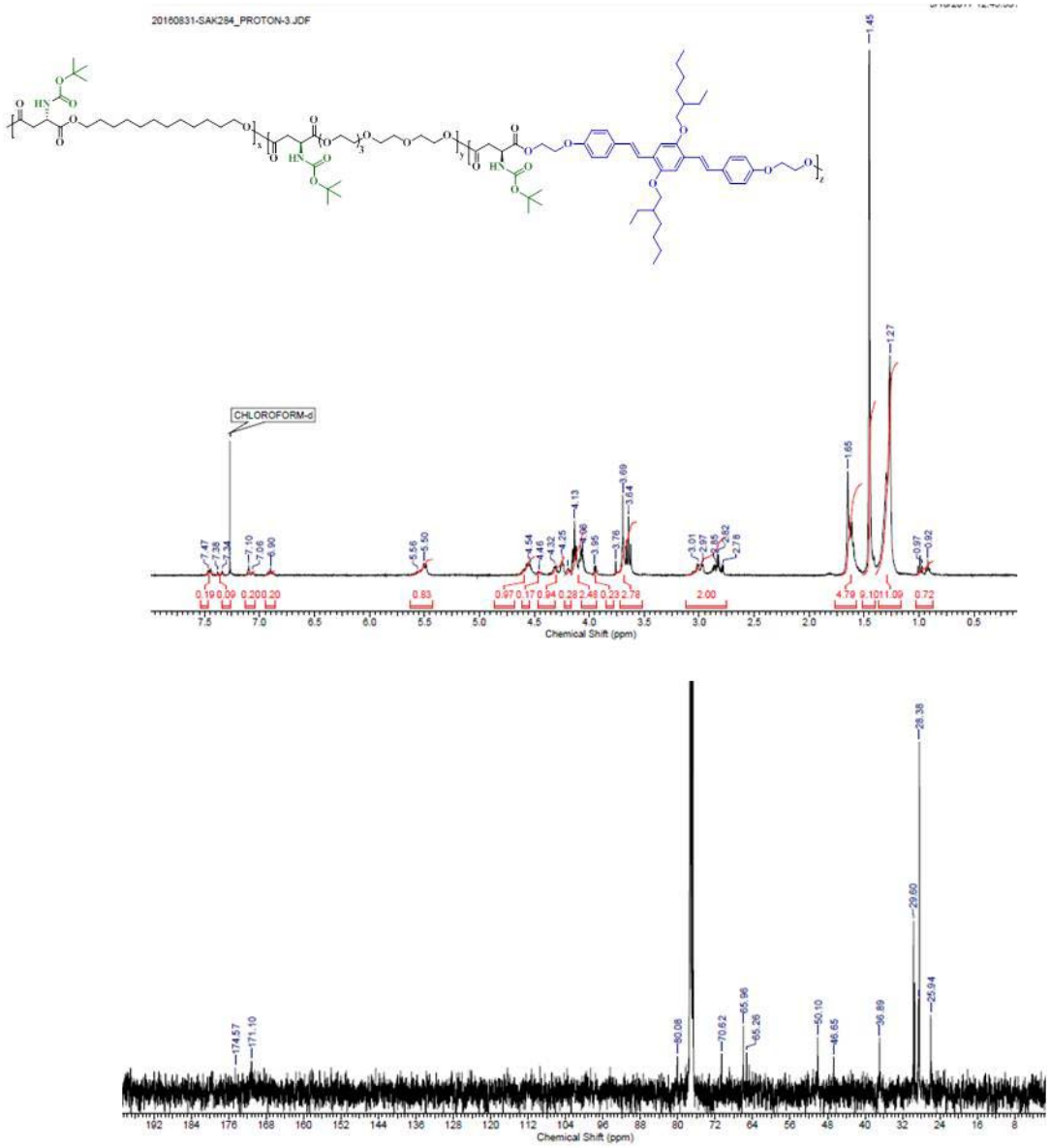
20160831-SAK284_PROTON-3.JDF
CHLOROFORM-d
Chemical Shift (ppm)
Chemical Shift (ppm)

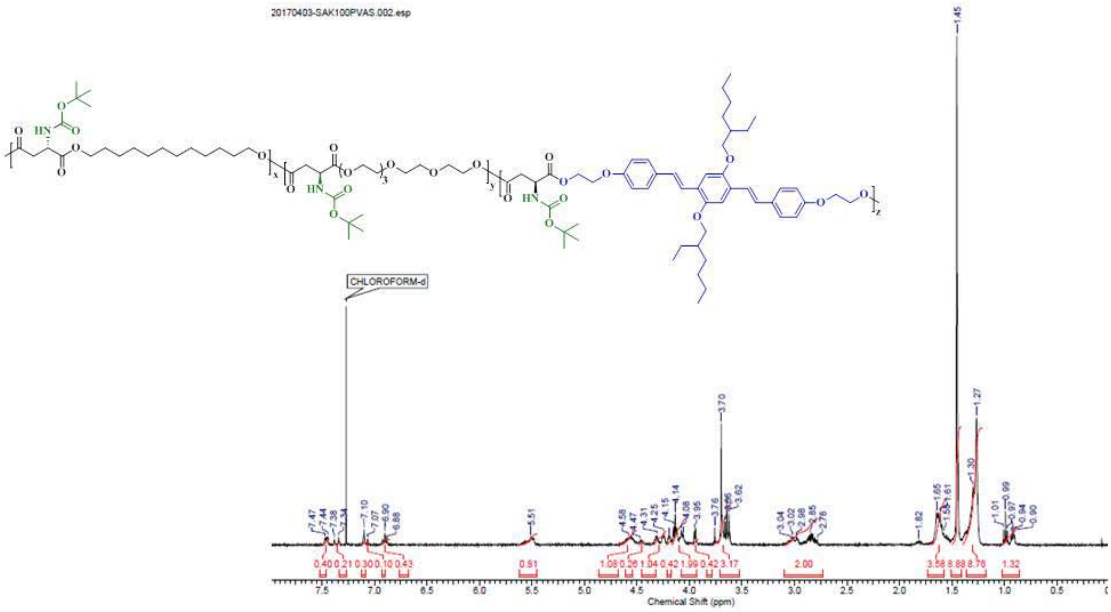

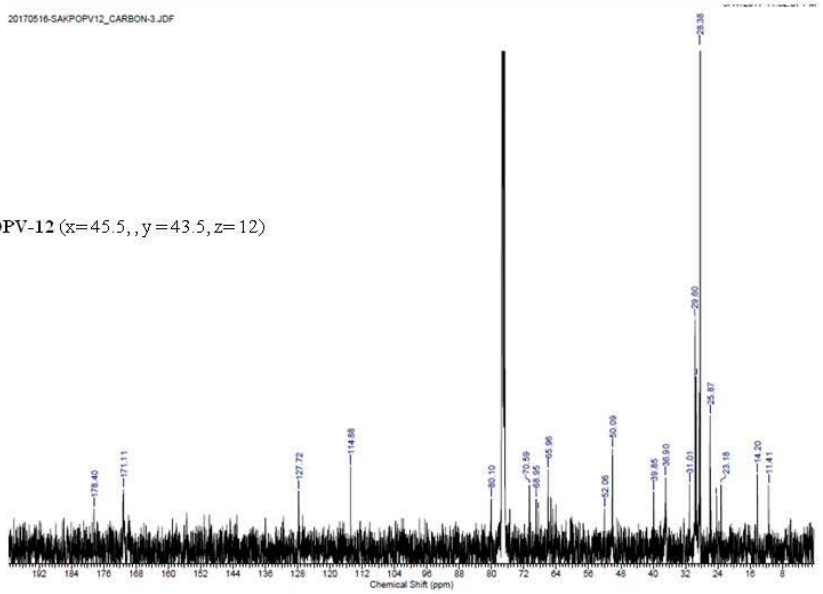

P-OPV-12 (x=45.5, , y=43.5, z=12)

NMRs of the Molecules synthesised in Chapter 4

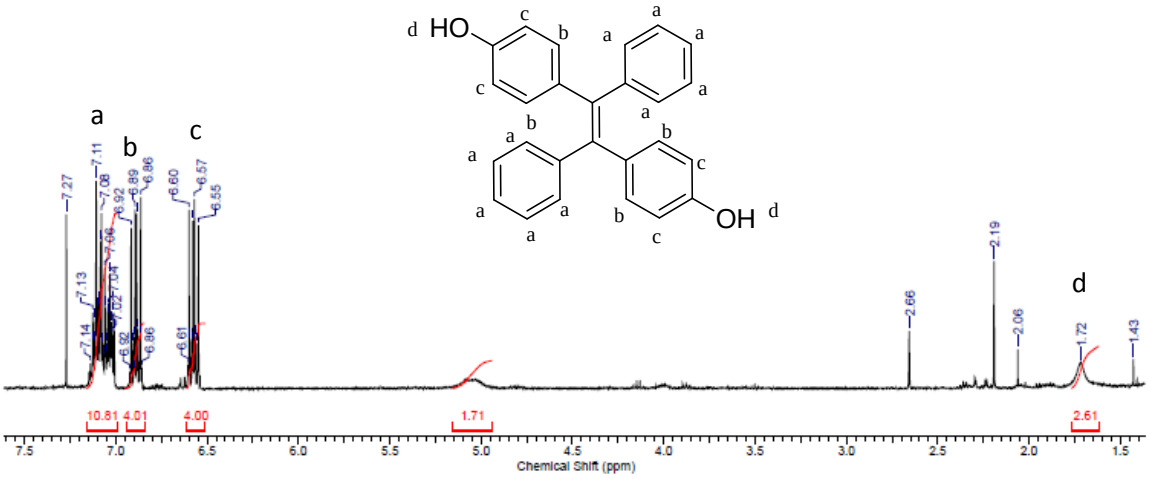

CARBON 13 NMR FOR MONOMER 2 AND POLYMER P-Ac (from chapter 5)